

# Final Report for AFOSR Grant: F49620-99-1-0277 : Activities, Findings, Publications and Products

M. R. Flannery (PI)

April 23, 2001

## Contents

<b>1</b>	<b>Collision Dynamics of Stretched Atoms</b>	<b>2</b>
<b>2</b>	<b>Importance</b>	<b>2</b>
2.1	Antihydrogen Formation . . . . .	2
2.2	Electron-Ion Recombination . . . . .	3
2.3	Basic Collision Problems . . . . .	3
<b>3</b>	<b>Present Results from AFOSR support</b>	<b>4</b>
3.1	Ultralow energy Three-body electron-ion recombination . . . . .	4
3.2	Sub-Projects . . . . .	4
<b>4</b>	<b>List of Publications</b>	<b>5</b>
4.1	Referee Reports . . . . .	5
<b>5</b>	<b>Classical and Quantal Form Factors</b>	<b>7</b>
5.1	Publications: Classical and Quantal Form Factors . . . . .	7
<b>6</b>	<b>Collisional Stark Mixing in Rydberg Atoms</b>	<b>8</b>
6.1	Collisional Stark Mixing: Research Performed . . . . .	9
6.2	Publications: Collisional Stark Mixing . . . . .	12
6.3	Publication: $nl \rightarrow n'l'$ Collisional Transitions . . . . .	13
<b>7</b>	<b>Invited Papers Presented at Scientific Conferences</b>	<b>14</b>
<b>8</b>	<b>Conclusion</b>	<b>14</b>
<b>9</b>	<b>Appendix: Copies of (7) papers published under AFOSR grant</b>	<b>16</b>

# 1 Collision Dynamics of Stretched Atoms

The abstract of the original proposal awarded 6/99 is: "The theoretical study of collisions with stretched (excited and Rydberg) atoms is proposed. Classical and semiclassical expressions for the inelastic form factor will be developed in such a way that they will form the basis of new theories for the cross sections of ( $n\ell \rightarrow n'\ell'$ ) collision processes involving excited atoms. Stark  $\ell$ -mixing ( $n\ell \rightarrow n\ell'$ ) will also be investigated by classical techniques. Collisions involving planetary atoms will be studied by adiabatic invariance methods."

This report will furnish the huge successes and achievements accomplished under AFOSR funding.

## 2 Importance

Collision Dynamics of Stretched atoms is of key importance in several classes of problems, such as the following

- (A) Three-Body Recombination of positron  $e^+$  with antiprotons  $\bar{p}$ ,



to form antihydrogen  $\bar{H}$  at positron (cryogenic) temperatures 4K.

- (B) Electron - ion recombination process



at electron temperatures of  $T_e \sim 5$  mK. The theory to be developed for the above processes is important in that it must be derived from "first principles" and will therefore provide a fundamental understanding of two quite different examples of recombination at ultracold energies.

The theory and computational techniques under development for (A) and (B) are also important for understanding current experiments at NIST on recombination and for trapping experiments to be performed at CERN in the near future.

### 2.1 Antihydrogen Formation

At the Low Energy Antiproton Ring (LEAR) at CERN, antiprotons have been captured in specially designed Penning traps, cooled to meV energies and stored for hours in a small volume of space. Positrons have also been similarly accumulated.

The current problem is how to arrange them to recombine efficiently into  $\bar{H}$  and then controlling  $\bar{H}$  in such a way that permits spectroscopic measurements. Trapped atom technology can then be applied to  $\bar{H}$ . Since the sharp ( $2s \rightarrow 1s$ ) double photon transition in H can be measured to an accuracy of 1 in  $10^{15}$ , then, by comparing the measured values of the

Rydberg and anti-Rydberg wavenumbers,  $\bar{H}$  becomes a fundamental physical system ideal for new tests of fundamental symmetries under combined operations of C (charge conjugation) P (parity) and T (time reversal). CPT invariance is minimal condition for the existence of antiparticles within quantum field theory. Moreover, by comparing the gravitational red shift of the ( $2s \rightarrow 1s$ ) transition for  $H$  and  $\bar{H}$ , the first test of the gravitational Weak Equivalence Principle (WEP) for antimatter would then be possible. New basic theory on (1) at ultracold temperatures is required.

## 2.2 Electron-Ion Recombination

The theory under development for anti-hydrogen recombination (1) will also be applicable to the electron-ion recombination process



and

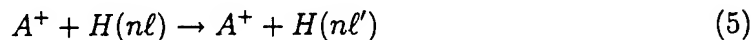


at electron temperatures of  $T_e \sim 5$  mK. Accurate experiments on these systems are currently under investigation by S. Rolston at NIST and by P. Gould at University of Connecticut. The eventual comparison with our theory under development is of key significance and importance since it will be the first accurate comparison of ultracold recombination. As has been shown in our current investigation [1], the mechanisms of recombination at ultracold energies are quite different from those for recombination at room and higher temperatures.

## 2.3 Basic Collision Problems

Within the general theory of the three-body recombination processes above, there are several key collision mechanisms, operating at ultralow energies, which are addressed in this proposal. On changing antimatter signs to matter signs, these are:

1. Theory of Stark Mixing collisions



2. Theory of  $n\ell - n'\ell'$  ultracold collisional transitions



where projectile  $P$  can be electrons or ions. These are important to (1), (3) and (4).

### 3 Present Results from AFOSR support

#### 3.1 Ultralow energy Three-body electron-ion recombination

Three-body electron-ion recombination is described [1] at ultralow electron temperatures  $T_e$ . At  $4K$ , the initial stage involves extremely rapid collisional capture into high Rydberg states  $n > 100 - 400$  with high angular momentum  $l \approx n - 1$  at a rate  $\sim T_e^{-4.5}$ . This is followed by extremely slow collisional-radiative decay. The key collisional mechanism appears to be collisional  $l$ -mixing of the Rydberg atoms  $A(n)$  by ions and electrons until sufficiently low  $l$ 's are attained so as to permit relatively rapid radiative decay to the lowest electronic levels. This sequence is in direct contrast to the sequence of much slower collisional capture at higher  $T_e$  followed by the much faster decay of  $A(n)$  by electron collisions to lower levels where radiative decay completes the recombination. At ultra-low temperatures, the rate limiting sequence is therefore collisional  $l$ -mixing followed by radiative decay in contrast to recombination at much higher energies and electron densities  $N_e \sim 10^8 \text{ cm}^{-3}$ , where the rate limiting step is the initial collisional or radiative capture at intermediate  $T_e (\sim 1 \text{ eV})$  and higher  $T_e (\sim 10 \text{ eV})$ , respectively.

#### 3.2 Sub-Projects

We therefore had to investigate (a) dynamical properties of Rydberg atoms, (b) Stark Mixing  $nl \rightarrow n'l'$  collisional transitions and (c)  $nl \rightarrow n'l'$  collisional transitions in Rydberg atoms in levels  $n \approx 100 - 400$ , for which fully quantal calculations were prohibitively difficult. Highlights of these investigations are:

1. We defined, formulated and developed the concept of a *classical* inelastic form factor.
2. By appeal to the dynamical  $SO(4)$  symmetry of  $H(n, \ell)$ , we were able to provide the first exact classical and quantal solutions for the Stark Mixing problem for the whole array of  $nl \rightarrow n'l'$  transitions in Rydberg atoms. This has been a long outstanding problem in Atomic Physics for the past 40 years.
3. By exploiting the classical form factor, we were able to formulate the first classical impulse theory for  $nl \rightarrow n'l'$  collisional transitions in Rydberg atoms.

All of this work resulted in the following seven publications in Peer Reviewed Scientific Journals



## 4 List of Publications

1. *Classical Atomic Form Factor*, by D. Vrinceanu and M. R. Flannery, Physical Review Letters, **82**, (1999), pp. 3412-3415.
2. *Classical and Quantal Atomic Form Factors for arbitrary transitions*, by D. Vrinceanu and M. R. Flannery, Phys. Rev. A **60**, (1999), pp. 1053-1069.
3. *Quantal-Classical Correspondence Impulse Theory*, by M. R. Flannery and D. Vrinceanu Physical Review Letters, **85**, (2000), pp. 1-5.
4. *Quantal Stark Mixing at ultralow energies*, by D. Vrinceanu and M. R. Flannery, J. Phys. B: At. Mol. Opt. Phys. **33** (2000), pp. L721-8.
5. *Classical Stark Mixing at ultralow energies*, by D. Vrinceanu and M. R. Flannery, Physical Review Letters, **85**, (2000), pp. 4880-3.
6. *Analytical quantal collisional Stark Mixing Probabilities*, by D. Vrinceanu and M. R. Flannery, J. Phys. B: At. Mol. Opt. Phys. **34** (2001), pp. L1-L8.
7. *Classical and Quantal Collisional Stark Mixing at ultralow collision energies*, by D. Vrinceanu and M. R. Flannery, Phys. Rev. A **63** (2001) 032701-(1-22).

### 4.1 Referee Reports

1. The referee's report on paper #1, *Classical Atomic Form Factor*, Phys. Rev. Letts, **82**, (1999), 3412 reads:

".... This is a very nice example of how classical mechanics can be used to understand the behavior of quantum mechanical observables, even for comparatively small quantum numbers. The present work is new and simple. It is important because it makes a significant contribution to advancing our understanding of the relation between classical and quantum mechanics. This is a subject of substantial and growing interest in almost all fields of modern physics, so there is no doubt that the criterion of "broad interest" is fulfilled. The manuscript is concisely and well written; it should be easily understandable by a broad audience. I do not hesitate to recommend publication in Physical Review Letters."

2. The referee's report on Paper #2, *Classical and Quantal Atomic Form Factors for arbitrary transitions*, Phys. Rev. A **60**, (1999), 1053 reads:

"This is a remarkable paper with a great deal of physical insight combined with systematic analyses of the numerical results. The unified classical/quantal treatment is both interesting and useful. I recommend publication in the Physical Review A."

3. In the referee report on paper #3 *Quantal-Classical Correspondence Impulse Theory* Phys. Rev. Letts, 85, (2000).1. the referee wrote:

" In this paper a new way of formulating the quantal impulse approximation is presented which allows one to obtain its classical limit in a natural and rather simple way. The presented approach which involves the Wigner functions of initial and final states exhibits in a lucid way the quantitative relationship between this quantum impulse approximation and the binary encounter approach. So far this connection has been rather obscure. As far as inelastic collisions are concerned, the presented results have a great potential in inspiring new semiclassical approaches.

In my opinion, the main result of this paper is of topical significance in two respects. Firstly, the quantal impulse approximation is of central importance in general scattering theory. Secondly, recently there has been a general strong interest in the power of classical dynamics and in its connection with quantum dynamics (Compare with Refs. 10-15). As a minor remark, in this context it might be worth not only to refer to time-independent problems but also to some semiclassical work dealing with explicitly time dependent problems (e.g. G. Alber and O. Zobay, PRA 59, R3174 (1999)). Furthermore, the presentation of the material is clear and scientifically sound. I recommend publication."

4. In a referee report on paper #4, "Quantal Stark Mixing at ultralow energies", J. Phys. B: Atom. Mol. Opt. Phys. 33 (2000) L721, the referee wrote:

"The article presents an elegant derivation, based on group theoretical arguments, of angular mixing transition probabilities between  $\ell$  and  $\ell'$  states in hydrogen induced by low energy collisions with charged particles..."

5. In a referee report on paper #5 "Classical Stark mixing at ultralow collision energies", Phys. Rev. Letts, 85, (2000), 4880, the referee wrote:

"The paper presents an elegant solution to a long-standing problem in atomic physics, but the method of approach is of interest to a much wider community because the authors show how to exploit the classical/quantum correspondence in a system with a rich dynamical symmetry. It is rare to find so comprehensive a solution to a difficult problem...."

6. In a referee report on paper #6, *Analytical quantal collisional Stark Mixing Probabilities*, J. Phys. B: At. Mol. Opt. Phys. 34 (2001), L1, the referee writes:

"The authors present interesting analytical and numerical results on collision-induced Stark mixing probabilities for hydrogen and, more generally, for Rydberg atoms. These results are more compact and easier to use than the authors' corresponding findings in previous publications.."

7. In two referee reports on our paper #7, "Classical and Quantal Collisional Stark Mixing at low energies", to be published in Phys. Rev. A 63 (2001) 032701-(1-22), the referees wrote:

(A) "The paper under consideration makes an important advancement in the theory of collisional l-mixing. These new results are given by Eqs. (28) and further by Eq. (34). The authors succeeded in presenting the formulae in rather compact form reflecting mathematical beauty of the problem, in addition to its pragmatic value. This material and analysis of the results certainly deserve publication."

(B) It is quite clear that this manuscript meets the requirements for publication in Physical Review A. The authors have presented a uniform approach to the problem of collisional Stark mixing in slow collisions between Rydberg-atoms and charged particles, and have obtained analytic solutions, both classical and quantal, for the full array of intrashell nl-nl' transitions. Previous work on this problem was restricted to initial s-states; the present work achieves a significant generalization for arbitrary initial values of the angular momentum. This manuscript could well have formed the basis of three separate papers, one on the classical solution, one on the quantum mechanical treatment and a third on the Monte Carlo simulations. However, by using the SO(4) isomorphism to exploit the rich symmetry of the problem, the authors have achieved a uniform approach that points out important insights and connections between the classical and quantum results.

The present uniform approach evidently allows an elegant and complete solution to the problem that had not been previously achieved.

## 5 Classical and Quantal Form Factors

The first breakthrough came from our definition of a "classical" form factor, in classical correspondence to the quantal form factor

$$\mathcal{F}_{fi} = \langle \Psi_f | e^{i\mathbf{q} \cdot \mathbf{r} / \hbar} | \Psi_i \rangle$$

The physical significance of the form factor is that  $P_{if}(\mathbf{q}) = |\mathcal{F}|^2$  is the probability [2] of an internal transition arising from any external impulsive perturbation (whether due to collision with particles or exposure to electromagnetic radiation) which induces a sudden change  $\mathbf{q}$  to the internal momentum of the target system. This work resulted in two published papers [1] and [2] above.

### 5.1 Publications: Classical and Quantal Form Factors

1. *Classical Atomic Form Factor*, by

D. Vranceanu and M. R. Flannery, Phys. Rev. Letts, 82 (1999) pp. 3412-3415.

Here, the general trends exhibited in the variation of the inelastic form factor in collisional transitions  $nl \rightarrow n'l'$ , when  $l'$  is changed and  $n, l$  and  $n'$  are kept fixed were explained solely in

terms of classical mechanics. Previous quantal results were reproduced from purely classical mechanics principles. Our conclusions are valid not only for large quantum numbers (which provide the usual classical correspondence) but also for other cases, which, up to now have only been described by quantal or semiclassical methods. The interesting trends exhibited in the form factor are directly reflected in experimental and theoretical treatments of collisions involving excited atoms.

2. *Classical and Quantal Atomic Form Factors for arbitrary transitions.* by D. Vrinceanu and M. R. Flannery, Phys. Rev. A, **60** (1999) pp. 1053-1069.

Here, the classical form factor was deduced from exact correspondence with a phase space representation of the quantal form factor. Analytical expressions were provided for  $nl \rightarrow n'l'$ ,  $nl \rightarrow n'$  and  $n \rightarrow n'$  transitions in hydrogenic systems and for  $n \rightarrow n'$  in the one dimensional harmonic oscillator. An efficient procedure for calculation of quantal form factors as analytical functions of momentum transfer, for arbitrary quantum numbers, was presented. The classical approach has the ability to explain quite succinctly interesting trends and various important aspects which remain hidden within the quantal treatment of form factors. The classical/quantal comparison ranges from being qualitatively good for  $nl \rightarrow n'l'$  transitions to close agreement for  $nl \rightarrow n'$  and  $n \rightarrow n'$  transitions. Excellent agreement is obtained for the integrated form factor for all transitions.

## 6 Collisional Stark Mixing in Rydberg Atoms

In the original proposal awarded 6/99, we mentioned in the section on Theoretical Method that "By appeal to scattering theory, theories for Stark mixing of Rydberg atoms initially in high  $\ell$ -states must first be developed. The mixing will occur by collisions mainly with the heavy particles as in

$$\bar{p} + \bar{H}(n, \ell) \rightarrow \bar{p} + \bar{H}(n, \ell')$$

and by microfields in plasma. The theory must account for large angular momenta changes  $\Delta\ell = \ell - \ell'$  and occurs from large  $\ell \approx n - 1$ ."

During the past 24 months (12/15/98-12/14/2000) of the grant, research was conducted by the PI (M. R. Flannery) and Daniel Vrinceanu, a Ph. D graduate student in the School of Physics, working under the PI's supervision as Thesis Advisor. It was discovered [1] that the first stage in recombination at ultralow temperatures  $T_e$  is a very rapid collisional capture into high (circular) Rydberg states  $n\ell$ , with high angular momentum  $\ell \sim n - 1$ , and large radiative lifetimes, at a rate proportional to  $T_e^{-4.5}$ . Stark Mixing occurs when the electron of a Rydberg atom (in a state with principal quantum number  $n$ ) changes its angular momentum, without changing its energy, as a result of a collision, at large impact parameter  $b$ , with a slow massive particle of charge  $Z_1e$  moving with velocity  $v$ . The  $\ell$ -mixing collisions are essential in producing the low angular momentum states required to radiatively decay at relatively high rate to low  $n$ -levels, thereby stabilizing the recombination. This sequence is in direct contrast to the sequence of much slower collisional capture at higher  $T_e$  followed by the much faster decay of  $A(n)$  by electron collisions to lower levels where radiative decay

completes the recombination. The  $\ell$ -mixing was caused mainly by collisions with ions rather than by light electrons. A full theoretical treatment of  $nl \rightarrow n\ell'$  transitions by collisions with ions at ultralow energies was therefore initiated.

## 6.1 Collisional Stark Mixing: Research Performed

On considering the Rydberg atom in a frame rotating with the internuclear axis, the Stark Mixing problem can be reduced to the problem of the Rydberg atom in mixed *static fields*: electric, provided by the projectile ion and magnetic, produced by the non-inertial (Coriolis) forces. In this way, the well known equations, in both classical [4] and quantum [5, 6] mechanics, for the problem of interaction between weak fields and an atom can be adopted to provide, in principle, a solution for the Stark Mixing problem. Both quantal and classical [7] versions of this approach have succeeded only for  $\ell = 0$  to higher angular momentum  $\ell'$  transitions, appropriate to the experiments[8].

Since three-body collisional capture produces the Rydbergs in high  $\ell$  states, a new theory for the full array  $n\ell \rightarrow n\ell'$  of collisional transitions in  $H(n, \ell)$  was required. The present new treatment [9] developed during the grant period is not an extension of any previous theory and is capable of providing the first comprehensive classical and quantal solutions for Stark Mixing. Our research has resulted in formulating and developing a unified theory for the general time dependent solution of Collisional Stark Mixing. The exceptional rich dynamic symmetry of the hydrogen atom provided the key foundation which enabled both exact classical [9, 10] and exact quantal [9, 11] solutions to be constructed in a unified way by using group representation theory. This classical-quantal correspondence transcends the well known Ehrenfest's theorem just because of the  $SO(4)$  dynamical group symmetry of the energy shell of the hydrogen atom. New classical and quantal solutions applicable to transitions between arbitrary angular momentum states have been derived. A new expression [10] for the classical transition probability  $P_{\ell\ell'}$  is defined in a language which exploits the dynamical symmetry. The derived classical probability for the general array  $\ell \rightarrow \ell'$  of transitions has a very simple functional form, can be easily calculated for any principal quantum number and provides physical insight and simple geometrical explanations for the behavior of the transition probabilities. Monte Carlo simulations [9] were also performed to yield results in agreement with both the exact quantal and classical probabilities. Representative quantal, classical and Monte Carlo probabilities  $P_{\ell\ell'}$  are shown in Figs. [1-5]. Many similar results are contained in Refs.[9, 10, 11]. Here, the Stark parameter  $\alpha$  is  $3Za_n v_n / 2vb$  and the classically allowed and forbidden regions correspond to positive and negative values, respectively, of the parameter  $\mathcal{B}(\ell, \ell')$ , defined in Ref. [9]. A step discontinuity in the classical  $P_{\ell\ell'}$  and an exponential behavior in the quantal  $P_{\ell\ell'}$  occurs as  $\ell'$  increases through this region. Within the classical region, the quantal  $P_{\ell\ell'}$  oscillate about the classical background. Also, cusp-type singularities occur in the classical  $P_{\ell\ell'}$  when the parameter  $\mathcal{A}(\ell, \ell')$  of Ref. [9] passes through zero. By revealing essential characteristics which remain obscured within the quantal treatment, the classical results complement the quantal results.

This work on Collisional Stark Mixing has resulted in four papers [9, 10, 11, 12].

Summaries are as follows:

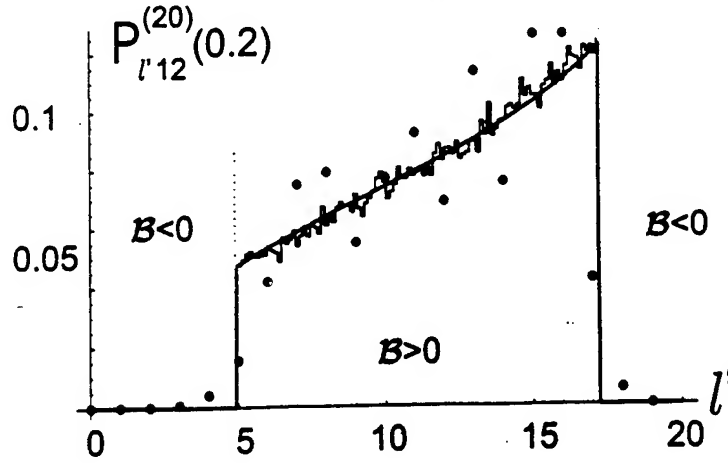


Figure 1: The Monte-Carlo simulation (step-like lines), the classical (solid line) and quantal (dots) transition probabilities  $P_{l'\ell}(\alpha)$  for a given Stark parameter  $\alpha = 0.2$  and initial  $\ell = 12$  within the  $n = 20$  shell.  $\mathcal{A} < 0$  for all  $\ell'$ .

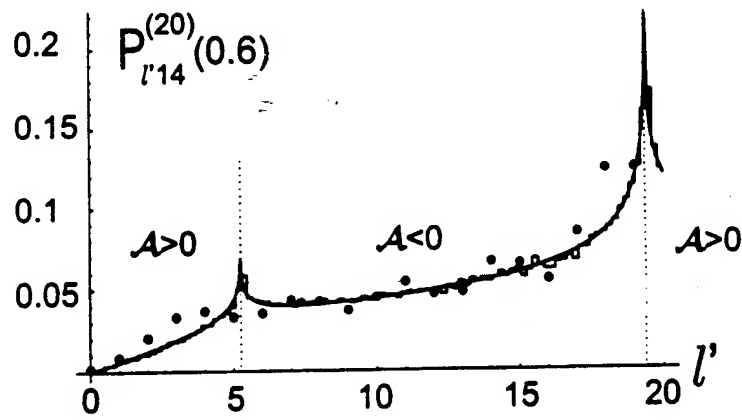


Figure 2: The Monte-Carlo simulation (step-like lines), the classical (solid line) and quantal (dots) transition probabilities  $P_{l'\ell}(\alpha)$  for a given Stark parameter  $\alpha = 0.6$  and initial  $\ell = 14$  within the  $n = 20$  shell.  $\mathcal{B} > 0$  for all  $\ell'$ .

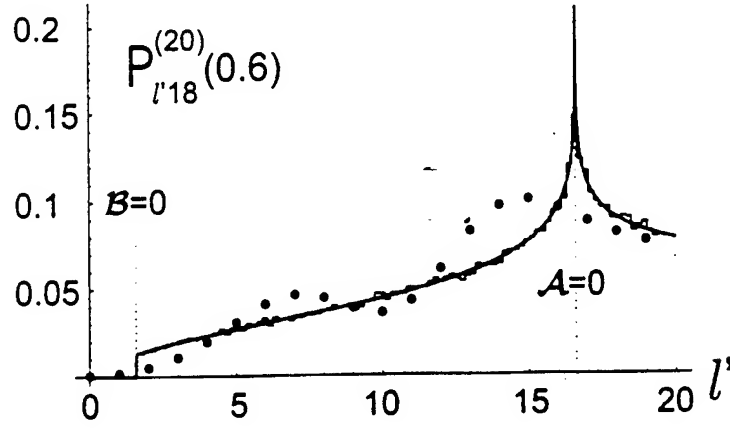


Figure 3: The Monte-Carlo simulation (step-like lines), the classical (solid line) and quantal (dots) transition probabilities  $P_{l'\ell}(\alpha)$  for a given Stark parameter  $\alpha = 0.6$  and initial  $\ell = 18$  within the  $n = 20$  shell. Across the first dotted line  $B$  changes sign and  $A$  is negative in both sides of this line.  $A$  changes sign across the second line while  $B$  remain positive.

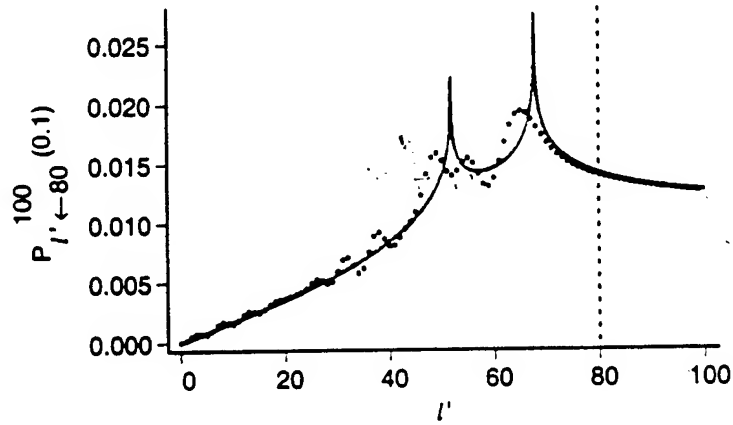


Figure 4: Stark Mixing probability for transitions within the energy shell  $n = 100$  from the initial state  $\ell = 80$ , with angle  $\eta$  given by  $\cos \eta/2 = 0.1$ , as a function of the final angular momentum  $l'$ . Exact quantal result is represented by the dots, Classical limit is represented by the solid line and the initial state is indicated by the dotted line.

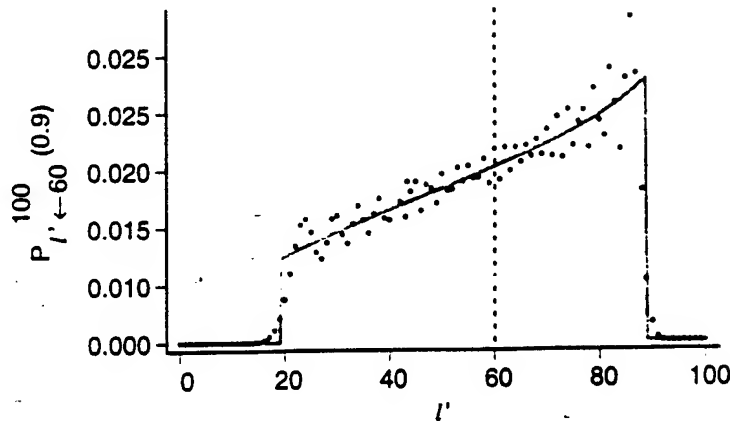


Figure 5: Stark Mixing probability for transitions within the energy shell  $n = 100$  from the initial state  $\ell = 60$ , with angle  $\eta$  given by  $\cos \eta/2 = 0.9$ , as a function of the final angular momentum  $\ell'$ . Exact quantal result is represented by the dots, classical limit is represented by the solid line and the initial state is indicated by the dotted line.

## 6.2 Publications: Collisional Stark Mixing

3. *Quantal Stark mixing at ultralow collision energies*, by  
D. Vrinceanu and M. R. Flannery, J. Phys. B **33**, L721 (2000).

Here, a new exact solution of the time-dependent quantal equation was obtained for the full array of angular momentum mixing transitions  $n\ell \rightarrow n\ell'$  in atomic hydrogen induced by collisions with charged particles at ultralow energies. Based on this new solution, efficient numerical procedures were devised. It was proven that the present (fixed frame) solution is equivalent to the rotating frame approach described by Kozansky and Ostrovsky [6, 7] and that it overcomes the difficulties therein. Analytic expressions for low quantum numbers  $n$  were presented. Numerical results for the transition array with  $n = 28$  were reported.

4. *Classical Stark Mixing at ultralow collision energies*, by  
D. Vrinceanu and M. R. Flannery, Phys. Rev. Letts (**85**, 4880 (2000))

Here, exact solutions of the time-dependent classical equations were obtained for the full array of angular momentum mixing transitions  $n\ell \rightarrow n\ell'$  in atomic hydrogen induced by collisions with charged particles at ultralow energies. A novel classical expression for the transition probability  $P_{\ell'\ell}$  was presented. The exact classical results for  $P_{\ell'\ell}(\alpha)$  as a function of  $\ell$ ,  $\ell'$  and the Stark parameter  $\alpha$  agreed exceptionally well with (exact) quantal results. They complement the quantal results by revealing essential characteristics which remain obscured in the quantal treatment.

5. *Analytical Quantal Collisional Stark Mixing probabilities* by  
by D. Vrinceanu and M. R. Flannery, J. Phys. B: At. Mol. Opt. Phys. **34** (2001), pp. L1-L8.



Exact expression for the probability  $P_{\ell'\ell}^{(n)}$  of Stark Mixing transitions between arbitrary angular momentum states  $\ell$  and  $\ell'$  within the same energy shell  $n$ , as a result of a collision with a slow charged projectile at large impact parameters is presented. The formula obtained is compact and easy to use for numerical evaluations even for very large quantum numbers ( $n \sim 100$ ). A classical approximation is directly obtained and compared with the exact quantal result in the limit of large  $n$ . Two distinct sets of quantal oscillations are predicted.

6. *Classical and Quantal Collisional Stark Mixing at low energies*, by D. Vrinceanu and M. R. Flannery, Phys. Rev. A **63**, (2001, March issue)

Here, exact classical and quantal solutions were presented for the full array of intrashell transitions  $n\ell \rightarrow n\ell'$ , between any angular momentum states, induced by slow distant collisions with a charged particles. The collisions considered are adiabatic with respect to orbital frequency and sudden with respect to Stark precessional frequency. The rich symmetry of the problem allows a unified approach and is the source of the excellent agreement, beyond the usual Ehrenfest's correspondence principle, between the classical and quantal treatments. A classical transition probability is defined. Probabilities for transition between any angular momentum states within a high Rydberg energy level are derived in exact analytic forms and are analyzed for a large number of numerical examples. The transition probabilities obtained from the three methods - quantal and classical formulations and Monte-Carlo classical simulations - are directly compared to provide excellent agreement. The common  $SO(4)$  symmetry provides this classical-quantal correspondence at a level, more fundamental than Ehrenfest's theorem and the Heisenberg correspondence. The classical method is also complementary in that it reveals very succinctly essential and valuable characteristics which remain obscured within the quantal treatment. This reflects the essential power of classical dynamics when applied to collision problems.

### 6.3 Publication: $n\ell \rightarrow n'\ell'$ Collisional Transitions

A successful formulation [13] of a classical version of the quantal impulse treatment was made and applied to  $n\ell \rightarrow n'\ell'$  Collisional Transitions in Rydberg atoms. The summary is as follows:

7. *Quantal-Classical Correspondence Impulse Theory*, by M. R. Flannery and D. Vrinceanu, Phys. Rev. Letts, **85** (2000) pp. 1-5.

Here, the quantal impulse cross section was derived in a novel form appropriate for direct classical correspondence. The classical impulse cross section is then uniquely defined and yields the first classical expression for  $n\ell - n'\ell'$  collisional transitions. The derived cross sections satisfy the optical theorem and detailed balance. Direct connection with the classical binary encounter approximation is also firmly established. The unified method introduced is general in its application to various collision and recombination processes and enables new directions of enquiry to be pursued quite succinctly.

## 7 Invited Papers Presented at Scientific Conferences

The following four papers were invited papers presented at the following conferences.

1. *The Recombination Era from the Big Bang to Modern Astrophysics, Aeronomy and the New State ( Bose-Einstein Condensate) of Matter*, M. R. Flannery, **Invited Discourse**, presented at **The Royal Irish Academy, Dublin, Ireland, April 26, 1999.**
2. *Dissociative Recombination*, M. R. Flannery, **Invited Paper**, presented at the Fourth International Conference on Dissociative Recombination, Nasslingen, Stockholm, Sweden, June 16-20, 1999.
3. *Three-Body Collisional Ion-Ion Recombination*, M. R. Flannery, **Invited Paper**, presented at the Gordon Conference on Simple Systems in Chemistry and Physics, Newport, RI, July 11-16, 1999.

In addition, various research papers were presented at:

1. DAMOP in 1999
2. 17th *International Conference on Atomic Physics*, Florence, June 4-9, 2000.
3. *Atoms, Molecules and Quantum Dots in Laser Fields: Fundamental Processes*, Pisa, June 12-16, 2000.

Also an Invited Colloquium: "Recombination", was presented to the Department of Physics and Astronomy, University of Nebraska, Lincoln, September 30, 1999.

## 8 Conclusion

During the period (6/12/99-present) of our current AFOSR grant, we have been successful, as described herein, in providing (a) an exact classical and quantal theory of collisional Stark Mixing and (b) the definition and development of a classical form factor which we have shown is basic to our formulation of (c) a classical impulse theory of  $n\ell - n'\ell'$  collisional transitions. Much more work needs to be done along the lines proposed in my Renewal Proposal to AFOSR and which, is felt will lead to many more fundamental breakthroughs as those described in the present report.

## References

- [1] M. R. Flannery and D. Vrinceanu. in *Atomic Processes in Plasmas: 11<sup>th</sup> APS Topical Conference*, edited by E. Oks and M. S. Pindzola (AIP Press, New York, 1998), pp. 317-333.
- [2] D. Vrinceanu and M. R. Flannery, Phys. Rev. Lett. **82**, 3412 (1999).
- [3] D. Vrinceanu and M. R. Flannery, Phys. Rev. A, **60**, 1053 (1999).
- [4] M. Born, *The Mechanics of the Atom* (Ungar, New York, 1960), p. 235.
- [5] Yu. N. Demkov, B. S. Monozon, and V. N. Ostrovskii, Sov. Phys. JETP **30**, 775 (1970).
- [6] A. K. Kazansky and V. N. Ostrovsky, J. Phys. B **29**, L855 (1996).
- [7] A. K. Kazansky and V. N. Ostrovsky, Sov. Phys. JETP **83**, 1095 (1996).
- [8] X. Sun and K. B. MacAdam, Phys. Rev. A **47**, 3913 (1993).
- [9] D. Vrinceanu and M. R. Flannery, Phys. Rev. A **63** (2001) 032701-(1-22).
- [10] D Vrinceanu and M R Flannery, Phys. Rev. Lett. **85**, 4880(2000).
- [11] D. Vrinceanu and M. R. Flannery, J. Phys. B **33**, L721 (2000).
- [12] D. Vrinceanu and M. R. Flannery, J. Phys. B: At. Mol. Opt. Phys. **34** (2001), pp. L1-L8.
- [13] M. R. Flannery and D. Vrinceanu, Phys. Rev. Lett. **85**, 1 (2000).

## 9 Appendix: Copies of papers published under AFOSR grant

Copies of the following papers published under the AFOSR grant are attached in this Appendix:

1. *Classical Atomic Form Factor*, by D. Vrinceanu and M. R. Flannery, Physical Review Letters, **82**, (1999), pp. 3412-3415.
2. *Classical and Quantal Atomic Form Factors for arbitrary transitions*, by D. Vrinceanu and M. R. Flannery, Phys. Rev. A **60**, (1999), pp. 1053-1069.
3. *Quantal-Classical Correspondence Impulse Theory*, by M. R. Flannery and D. Vrinceanu, Physical Review Letters, **85**, (2000), pp. 1-5.
4. *Quantal Stark Mixing at ultralow energies*, by D. Vrinceanu and M. R. Flannery, J. Phys. B: At. Mol. Opt. Phys. **33** (2000), pp. L721-8.
5. *Classical Stark Mixing at ultralow energies*, by D. Vrinceanu and M. R. Flannery, Physical Review Letters, **85**, (2000), pp. 4880-3.
6. *Analytical quantal collisional Stark Mixing Probabilities*, by D. Vrinceanu and M. R. Flannery, J. Phys. B: At. Mol. Opt. Phys. **34** (2001), pp. L1-L8.
7. *Classical and Quantal Collisional Stark Mixing at ultralow collision energies*, by D. Vrinceanu and M. R. Flannery, Phys. Rev. A **63** (2001) 032701-(1-22).

# Classical Atomic Form Factor

D. Vrinceanu and M. R. Flannery

School of Physics, Georgia Institute of Technology, Atlanta, Georgia 30332

(Received 25 November 1998)

The general trends exhibited in the variation of the inelastic form factor in collisional transitions  $nl \rightarrow n'l'$ , when  $l'$  is changed and  $n, l$ , and  $n'$  are kept fixed, are explained solely in terms of classical mechanics. Previous quantal results are reproduced from purely classical mechanics principles. Our conclusions are valid not only for large quantum numbers (which provide the usual classical correspondence) but also for other cases, which, up to now have been described only by quantal or semiclassical methods. The interesting trends exhibited in the form factor are directly reflected in experimental and theoretical treatments of collisions involving excited atoms. [S0031-9007(99)09037-7]

PACS numbers: 32.80.Cy, 31.15.Gy, 34.50.-s

With the advent of new technology which facilitates the accurate measurement [1] of electron-excited atom collision cross section there has also been renewed interest in the theory [2] of collisions involving Rydberg atoms. Recent experiment [1], in particular, has confirmed that the cross section for the quadrupole  $2^3S \rightarrow 3^3D$  transition in  $e - \text{He}(2^3S)$  collisions is much higher than that for the pure dipole  $2^3S \rightarrow 3^3P$  transition at low and intermediate energies, in accord with the theoretical predictions of Ref. [3] (Born and multichannel eikonal approximations). Flannery and McCann [4] have noted that this unexpected behavior is only part of a more general systematic trend in that (a) the  $2^3S \rightarrow n^3D$  collisional transitions are predominant over all other transitions to the same  $n$  value, even for transitions to the electronic continuum, and (b) there is a unique value  $l'_{\max}$  of the final angular momentum  $l'$  that is preferentially populated in  $nl \rightarrow n'l'$  transitions ( $n' \gg n$ ) in collisions between Rydberg atoms and electrons or atoms.

The origin of this general behavior was traced [4] to the variation with  $l'$  of the quantum mechanical inelastic form factor

$$\mathcal{F}_{fi}(\mathbf{q}) = \langle \psi_f(\mathbf{r}) | e^{i\mathbf{q}\cdot\mathbf{r}/\hbar} | \psi_i(\mathbf{r}) \rangle = \langle \phi_f(\mathbf{p} + \mathbf{q}) | \phi_i(\mathbf{p}) \rangle \quad (1)$$

for  $i(n, l) \rightarrow f(n', l')$  transitions between atomic states;  $\psi_{i,f}(\mathbf{r})$  are the wave functions in position space and  $\phi_{i,f}(\mathbf{p}) = (2\pi\hbar)^{-3/2} \int \psi_{i,f}(\mathbf{r}) \exp(-i\mathbf{p}\cdot\mathbf{r}/\hbar) d\mathbf{r}$ , the wave functions in momentum space.

When an instantaneous impulse applied at  $t = t_0$  transfers momentum  $\mathbf{q}$  to an atomic electron, the exact solution of Schrödinger's equation under Hamiltonian

$$H(\mathbf{p}, \mathbf{r}, t) = \mathbf{p}^2/2m - e^2/r - \mathbf{r} \cdot \mathbf{q}\delta(t - t_0) \quad (2)$$

is

$$\Psi(\mathbf{r}, t) = [1 + (e^{i\mathbf{q}\cdot\mathbf{r}/\hbar} - 1)\theta(t - t_0)]\psi_{nlm}(\mathbf{r}),$$

where  $\theta$  is the Heaviside step function. The probability for  $i = |nl\rangle \rightarrow f = |n'l'\rangle$  transitions from the  $(2l + 1)$  initial sublevels is then

$$P_{nl,n'l'}(\mathbf{q}) = |\langle \psi_{n'l'} | \Psi \rangle|^2 = \sum_{m,m'} |\langle n'l'm' | e^{i\mathbf{q}\cdot\mathbf{r}/\hbar} | nlm \rangle|^2 \quad (3)$$

also deduced in [5]. The probability of any impulsive  $i \rightarrow f$  transition, whether due to particle collisions or electromagnetic field, is therefore

$$P_{if}(\mathbf{q}) = |\mathcal{F}_{fi}(\mathbf{q})|^2, \quad (4)$$

which provides physical significance to the inelastic form factor, a fundamental property of the atom. For impulsive collisions between a particle 1 and a Rydberg electron 2 bound to a core 3, the overall transition matrix element  $T$  decomposes as [5]

$$T_{if}(\mathbf{q}) = \mathcal{F}_{fi}(\mathbf{q})T_{12}(\mathbf{q}), \quad (5)$$

where  $T_{12}$ , the matrix element for (1-2) free-free elastic scattering in the (1-2) center of mass, is a function only of  $\mathbf{q}$ , as for Coulomb scattering  $T_{12} = 4\pi\hbar^2 e^2/q^2$ , or for Born's approximation,  $T_{12} = \int V(\mathbf{r}_{12}) \exp(i\mathbf{q}\cdot\mathbf{r}/\hbar) d\mathbf{r}_{12}$ . The probability of transition in the target atom per each (1-2) impulsive encounter is  $P_{if} = |T_{if}|^2/|T_{12}|^2$ , in agreement with (4).

The cross section is obtained by the following integration of the form factor (5) over momentum change,

$$\sigma_{if} = \left( \frac{2\pi}{M_{12}^2 v_i^2} \right) \int_{|k_i - k_f|}^{k_i + k_f} |\mathcal{F}_{fi}(\mathbf{q})|^2 |f_{12}(\mathbf{q})|^2 q d\mathbf{q}, \quad (6)$$

where  $k_{i,f}$  are the initial and final wave numbers of relative motion of the projectile-target system of reduced mass  $M$  and  $q = \hbar|\mathbf{k}_i - \mathbf{k}_f|$  is the momentum change. The scattering amplitude for (1-2) collisions of reduced mass  $M_{12}$  is  $f_{12} = (2M_{12}/4\pi\hbar^2)T_{12}$ . For (1-2) slow collisions with scattering length  $a$ , the Fermi interaction  $V(\mathbf{r}_{12}) = [4\pi a(\hbar^2/M_{12})]\delta(\mathbf{r}_1 - \mathbf{r}_2)$  also yields decomposition (5) with  $f_{12} = a$ .

The inelastic quantal form factor therefore not only exerts primary importance in collision studies, but also has a deep physical reality. In recent experimental studies

of excitation of Rydberg atoms by short unipolar half-cycle electromagnetic pulses the transition amplitude is determined directly by the inelastic form factor [6].

Analytical quantal [7,8] and semiclassical [9] form factors are available, although general systematic trends cannot be easily extracted from them. A classical form factor for  $n \rightarrow n'$  has been deduced [10] from binary encounter impulse theory and from a microcanonical distribution in energy space. A key point of this paper is that a complementary classical approach for  $nl \rightarrow n'l'$  transitions can also be developed in a way which reveals, quite succinctly, important aspects which remain hidden within the quantal treatment.

Consider a Rydberg atom in a stationary  $(n, l)$  state with energy  $E$  and angular momentum  $L$ . If the atom is perturbed by any general impulsive field [as in Eq. (2) or the Fermi interaction], then the transition probability to the final state  $(n', l')$  (of energy  $E'$  and angular momentum  $L'$ ) is the inelastic form factor.

The quantal probability density for finding the electron in the radial interval  $(r, r + dr)$  is

$$\rho_{nl}^q(r) = r^2 |R_{nl}|^2, \quad (7)$$

where  $R_{nl}$  is the hydrogenic radial wave function expressed in terms of the generalized Laguerre polynomial.

The phase space of a classical atom, with Hamiltonian  $H(\mathbf{r}, \mathbf{p}) = p^2/2m + V(r)$ , angular momentum  $\mathbf{L}(\mathbf{r}, \mathbf{p}) = \mathbf{r} \times \mathbf{p}$ , and period  $\tau_{nl} = \nu_{nl}^{-1}$  in stationary state  $(n, l)$  is populated according to the microcanonical distribution [8,10]

$$\rho_{nl}^c d\mathbf{r} d\mathbf{p} = \{h \nu_{nl} \hbar \delta(H - E) \delta(|\mathbf{L}| - L)\} \frac{d\mathbf{r} d\mathbf{p}}{(2\pi\hbar)^3} \quad (8)$$

normalized to  $(2l+1)$  states in all of phase space. On integrating over the momentum space  $\mathbf{p}$  and angular part  $\hat{\mathbf{r}}$  of the configuration space  $\mathbf{r}$ , the classical distribution is

$$\rho_{nl}^c(r) dr = \frac{2l+1}{\tau_{nl}} \frac{2}{r} dr,$$

where the radial speed is given by  $m\dot{r}^2/2 = E - V(r) - (l+1/2)^2 \hbar^2/2mr^2$ . For the Kepler atom ( $\tau_{nl} = 2\pi n^3$  a.u.) and  $\rho_{nl}^c$  (in a.u.) is

$$\begin{aligned} \rho_{nl}^c(r) &= \frac{1}{\pi n^3} \left[ \frac{2}{r} - \frac{1}{n^2} - \frac{(l+1/2)^2}{r^2} \right]^{-1/2} \\ &= \frac{1}{\pi n^3} \frac{1}{\dot{r}(r)}. \end{aligned} \quad (9)$$

The quantal (7) and classical (9) radial probability densities are illustrated in Fig. 1. As in the textbook example of the harmonic oscillator, the classical distribution has singularities at the corresponding turning points given by the radii (in a.u.)

$$R^\pm = n^2 \{1 \pm \epsilon\} = n^2 \{1 \pm [1 - (l+1/2)^2/n^2]^{1/2}\}. \quad (10)$$

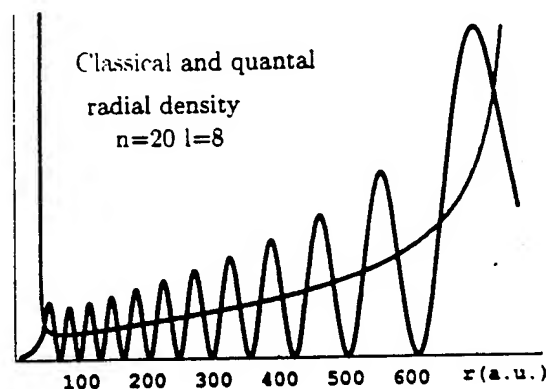


FIG. 1. Classical and quantal radial densities of probability of localization for the stationary state of the hydrogen atom [ $E = -1/(2 \times 20^2)$  and  $l = 8$ ].

The classical distribution is zero outside the accessible region, bounded by  $R^\pm$ .

By using definition (1) the transition probability (3) can be converted to the new form

$$P_{if}(q) = (2\pi\hbar)^3 \int \rho_{nl}(\mathbf{r}, \mathbf{p}) \rho_{n'l'}^*(\mathbf{r}, \mathbf{p} + \mathbf{q}) d\mathbf{r} d\mathbf{p}, \quad (11)$$

where the quantal distributions in phase space are given by  $\rho^q(\mathbf{r}, \mathbf{p}) = (2\pi\hbar)^{-3/2} \psi(\mathbf{r}) \exp(-i\mathbf{p} \cdot \mathbf{r}/\hbar) \phi^*(\mathbf{p})$ . This form is now suitable for classical correspondence obtained by replacing densities  $\rho^q$  by the phase space distributions (8). The basic definition of the classical form factor is therefore given by (8) and (11). The physical significance is that the initial and final states correspond to definite regions in phase space, populated according to the microcanonical distribution (8), and that the transition probability is given, in a geometric sense, by the amount of overlap of these regions. In configuration space alone, the regions are spherical shells with inner and outer radii given by Eq. (10), the pericenter ( $R^-$ ) and apocenter ( $R^+$ ) of the Kepler orbit.

Analytical expressions with explicit dependence on  $q$  for quantal and classical probabilities for  $nl \rightarrow n'l'$ ,  $nl \rightarrow n'$ ,  $n \rightarrow n$  transitions are developed in a separate paper [8]. Rather than examining the  $l'$  variation of (11) for a given  $q$ , the key results are more readily deduced and are easily transparent by investigating the probability for all momentum transfers

$$F_{nl \rightarrow n'l'}^c = \int P_{if}(q) dq = (2\pi\hbar)^3 \int_{\mathcal{R}} d\mathbf{r} \rho_{nl}^c(\mathbf{r}) \rho_{n'l'}^c(\mathbf{r}), \quad (12)$$

where  $\mathcal{R}$  is the overlapping region in configuration space defined by intersection of  $(R_i^-, R_i^+)$  and  $(R_f^-, R_f^+)$  intervals.

Inserting  $\rho(r) = 4\pi\rho^c(r)r^2$  with (9) in (12) gives the classical form factor (CFF)

$$F_{nl \rightarrow n'l'}^c = 2 \frac{(2l' + 1)}{n^3 n'^3} \int_{R_{\min}}^{R_{\max}} \frac{dr/r^2}{\dot{r}_i(r)\dot{r}_f(r)}, \quad (13)$$

where  $R_{\min} = \max(R_i^-, R_f^-)$  and  $R_{\max} = \min(R_i^+, R_f^+)$  define the bounds of the overlapping region  $\mathcal{R}$ . Different overlap situations are illustrated in Fig. 2 for a representative case. The gray region is the accessible region for the initial state and the curves are possible final state trajectories. Transitions occur only when the final state trajectory penetrates the initial state accessible region. The longer time spent by the electron on the final state trajectory within the initial state accessible region, the bigger is the transition probability.

As  $l$  increases from zero to its maximum value for circular orbits,  $R^-$  increases from zero to  $n^2$ , while  $R^+$  decreases from  $2n^2$  to the same value  $n^2$ . For final states  $n' > \sqrt{2}n$ , then  $R_{\max} = R_i^+$  for all values of  $l'$ . Three regions of overlap are then apparent and are, respectively, accessed as  $l'$  is increased.

**Region I,  $R_f^- < R_i^-$ .**—Here the overlap region  $\mathcal{R} = (R_i^-, R_i^+)$  is determined solely by the initial state and has spatial extent which remains constant as  $l'$  is varied from zero to some value  $l_1$  where  $R_f^- = R_i^-$ . There is always an orientation of the final orbit which will then intersect the initial orbit, as exhibited in Fig. 2, for  $(n = 3, l = 2)$  and  $(n' = 8, l' = 0 - 2)$  orbits. The  $l'$  variation of (13) is contained solely within the increasing integrand  $(\dot{r}_f)^{-1}$ .

**Region II,  $R_i^- < R_f^-$ .**—Here the overlap region  $\mathcal{R} = (R_f^-, R_i^+)$  includes the  $f$  pericenter and has spatial extent which decreases, as  $l'$  increases, eventually to zero when  $R_f^- = R_i^+$ . In this region, the initial and final orbits can intersect each other, as for the  $(n' = 8, l' = 4)$  orbit in Fig. 2. The  $l'$  variation of (13) results from variation of both the increasing lower limit  $R_f^-$  and the increasing integrand  $(\dot{r}_f)^{-1}$ .

**Region III,  $R_f^- > R_i^+$ .**—Here the initial and final trajectories no longer intersect, since the pericenter of the final state is greater than the apocenter of the initial state. This region where  $(i \rightarrow f)$  transitions do not occur, as illustrated by  $(n' = 8, l' = 5, 6, 7)$  orbits in Fig. 2, is the classically inaccessible region.

The boundaries between regions I and II and between regions II and III occur, respectively, at  $l' = l_1$  where  $R_f^-(n', l') = R_i^-(n, l)$  and at  $l' = l_2$  where  $R_f^-(n', l') = R_i^+(n, l)$ . Thus  $l_1$  and  $l_2$  are given by

$$\left(l_{1,2} + \frac{1}{2}\right)^2 = n^2(1 \mp \epsilon)[2 - (1 \mp \epsilon)n^2/n'^2], \quad (14)$$

where  $\epsilon$  is the eccentricity  $[1 - (l + 1/2)^2/n^2]^{1/2}$  of the initial orbit.

Variation of the CFF (13), with final angular momentum  $l'$  is then determined both by the lower integration limit  $R_{\min}$  (which is a constant  $R_i^-$  in region I and increases as  $R_f^-$  in region II) and by the integrand  $(\dot{r}_f)^{-1}$ . Figure 3 illustrates the general pattern. As  $l'$  is increased from 0 to  $l_1$  (region I), the increase in CFF originates purely from the increasing integrand  $(\dot{r}_f)^{-1}$ . As  $l'$  is varied from  $l_1$  to  $l_2$ , the increasing integrand is offset by the decreasing range  $(R_f^-, R_i^+)$  of integration (region II). For  $l_2 < l' < n - 1$ , CFF is zero because transitions are not classically allowed in region III.

At  $l' = l_1$  the trajectories touch only at their corresponding pericenters and CFF has a turning point singularity characteristic of classical descriptions. The zero radial speed of the electron at the contact point of both initial and final orbits causes the infinite CFF (transition probability).

As is evident from Figs. 3–5, the agreement between the classical and quantal results is excellent in region I, even for small quantum numbers. In region II, the quantal results oscillate about CFF. Since classical motion is confined to a definite region, the dramatic fall for large  $l'$  is steeper than that for the quantal case where states

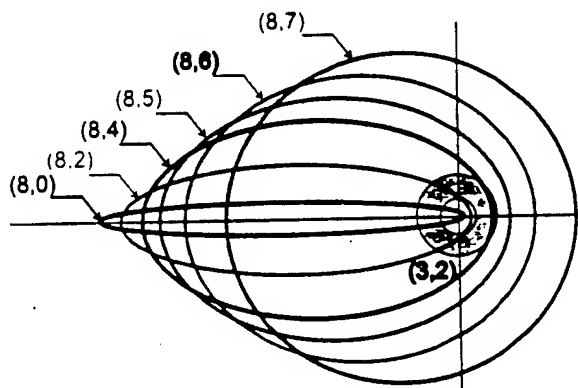


FIG. 2. Various final state ( $n' = 8, l' = 1-7$ ) trajectories and the initial accessible region corresponding to  $(n = 3, l = 2)$ .

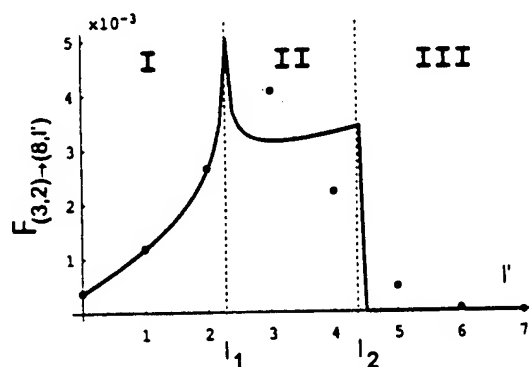


FIG. 3. Characteristic dependence of the inelastic form factor on the final angular momentum  $l'$ , for fixed  $n (= 3)$ ,  $l (= 2)$ , and  $n' (= 8)$ . Classical calculations: solid line; quantal results: dots.

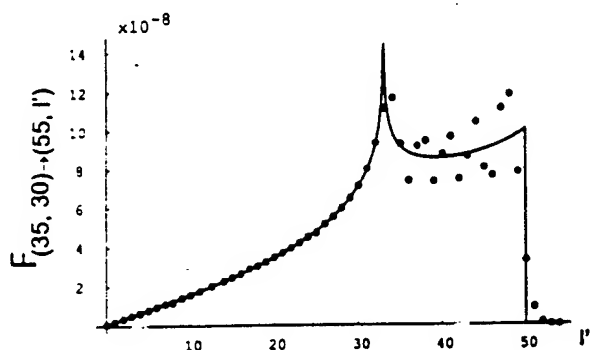


FIG. 4. Classical (solid line) and quantal (dots) inelastic form factor for transitions from state  $(n = 35, l = 30)$  to  $(n' = 55, l' = 0 \rightarrow 54)$  states.

have exponential tails within the classical inaccessible region III. As expected from correspondence principles, for the larger quantum numbers, the quantum form factor tends to CFF, even in the regions II and III, as shown in Fig. 4. For quasielastic transitions  $nl \rightarrow n'l'$  the classical and quantal results are in excellent agreement for all angular momenta (Fig. 5). The quantal results exhibit maxima in the neighborhood of  $l' = l_1, l_2$  where CFF has the classical singularities. The position of  $l_1$  defined by (14) in the limit of large  $l$ , where the eccentricity  $\epsilon \rightarrow 0$ , is  $l_1(l \rightarrow n - 1) = n\sqrt{2}[1 - 1/2(n/n')^2]^{1/2} - 1/2$ , an exquisite result for initial circular orbits. For  $n' \gg n$ ,  $l_1$  tends from the bottom to  $l_1(l \rightarrow n - 1, n' \gg n) = n\sqrt{2} - 1/2$ , a key result in detailed agreement with that previously derived from consideration of the quantal momentum-space overlap [4].

For small initial angular momentum  $l$ ,  $\epsilon \rightarrow 1$  and  $l_1$  is then zero so that the maximum CFF is given by  $l_2(l \rightarrow 0) = 2n[1 - (n/n')^2]^{1/2} - 1/2$ , appropriate to highly eccentric initial orbits. In the  $n' \gg n$  limit then  $l_2(l \rightarrow 0, n' \gg n) = 2n - 1/2$ . As the initial  $l$  increases, there is therefore a slow variation ( $2n \rightarrow \sqrt{2}n$ ) in the position  $l_2$  of the maximum of CFF, which is

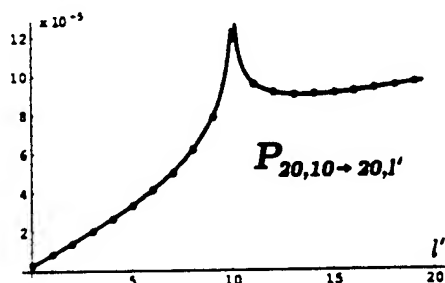


FIG. 5. Classical (solid line) and quantal (dots) inelastic form factor for quasielastic transitions from  $n = 20, l = 10$  state.

pushed slightly to lower values. This theoretical prediction is also confirmed by the quantal results [4].

When the energy  $E'$  of the final orbit is not sufficient to accommodate the value of  $l_2$  deduced above ( $n' < \sqrt{2}n$ ), the peak in CFF (as in Fig. 5) is given by  $l_1$ , provided the initial  $l$  is large enough. When the final  $n'$  is sufficiently small so that the lower  $l_1$  cannot be accommodated, i.e.,  $l_1 > n' - 1$ , CFF and the quantal result exhibit a monotonic increase confined to region I, which is always characterized by excellent agreement between quantal and classical results.

In summary, the pattern exhibited by the  $l'$  variations (Figs. 3–5) is essentially identical with the quantal pattern. The positions of maxima of the  $l'$  variation of CFF depend strongly on the initial  $n$  and only weakly on the initial  $l$ , in agreement with the quantal calculations [4], which were restricted to certain cases. Excellent quantitative agreement between classical and quantal results makes the classical form factor a very useful tool particularly at large quantum numbers (Rydberg atoms) where exact quantal results are not easy to obtain (either analytically or numerically) and to use, due to the highly oscillatory nature of the wave function. Although the emphasis here is on the electron form factors, the present analysis is applicable also to form factors for transitions between rovibrational states of molecules.

This work was supported by AFOSR Grant No. F49620-96-1-0142 and NSF Grant No. 98-02622. One of us (D.V.) thanks Motorola and Gil Amelio for support.

- [1] A.R. Filipelli, C.C. Lin, L.W. Anderson, and J.W. McConkey, *Adv. At. Mol. Opt. Phys.* **33**, 1 (1994); M.E. Lagos, J.B. Boffard, L.W. Anderson, and C.C. Lin, *Phys. Rev. A* **53**, 1505 (1996).
- [2] V.S. Lebedev and I.I. Fabrikant, *Phys. Rev. A* **54**, 2888 (1996); M.I. Syrkin, *Phys. Rev. A* **53**, 825 (1996); V.S. Lebedev and V.S. Marchenko, *Sov. Phys. JETP* **64**, 251 (1986).
- [3] M.R. Flannery and K.J. McCann, *Phys. Rev. A* **12**, 846 (1975).
- [4] M.R. Flannery and K.J. McCann, *J. Phys. B* **12**, 427 (1979); *Astrophys. J.* **236**, 300 (1980).
- [5] M.R. Flannery, *Phys. Rev. A* **22**, 2408 (1980).
- [6] C.O. Reinhold, J. Burgdörfer, R.R. Jones, C. Raman, and P.H. Bucksbaum, *J. Phys. B* **28**, L457 (1995).
- [7] I. Bersons and A. Kulsh, *Phys. Rev. A* **55**, 1674 (1997).
- [8] D. Vrinceanu and M.R. Flannery (to be published).
- [9] F. Gounand and L. Petitjean, *Phys. Rev. A* **30**, 61 (1984).
- [10] L. Vriens, *Case Studies in Atomic Collision Physics I*, edited by E.W. McDaniel and M.R.C. McDowell (North-Holland, Amsterdam, 1969), p. 364; V. Borodin, A.K. Kazanski, and V.I. Ochkur, *J. Phys. B* **25**, 445 (1992).



# Classical and quantal atomic form factors for arbitrary transitions

D. Vrinceanu and M. R. Flannery

*School of Physics, Georgia Institute of Technology, Atlanta, Georgia 30332*

(Received 24 February 1999)

The classical form factor is deduced from exact correspondence with a phase-space representation of the quantal form factor. Analytical expressions are provided for  $nl \rightarrow n'l'$ ,  $nl \rightarrow n'$ , and  $n \rightarrow n'$  transitions in hydrogenic systems and for  $n \rightarrow n'$  in the one-dimensional harmonic oscillator. An efficient procedure for calculation of quantal form factors as analytical functions of momentum transfer, for arbitrary quantum numbers, is presented. The classical approach has the ability to explain quite succinctly interesting trends and various important aspects which remain hidden within the quantal treatment of form factors. The classical-quantal comparison ranges from being qualitatively good for  $nl \rightarrow n'l'$  transitions to close agreement for  $nl \rightarrow n'$  and  $n \rightarrow n'$  transitions. Excellent agreement is obtained for the integrated form factor for all transitions. [S1050-2947(99)09107-6]

PACS number(s): 32.80.Cy, 34.50.-s, 31.15.Gy

## I. INTRODUCTION

The inelastic form factor

$$\mathcal{F}_i = \langle \Psi_f | e^{i\mathbf{q} \cdot \mathbf{r}/\hbar} | \Psi_i \rangle = \langle \Psi_f | e^{i\mathbf{K} \cdot \mathbf{r}_{\text{a.u.}}} | \Psi_i \rangle$$

is a very basic quantity. It can accurately describe the overall response and dynamics of an atom or molecule involved in various processes or external interactions. It is also common in various schemes of approximation.

The study of the hydrogen atom form factor serves as a pivotal starting point for the general study of electronic transitions between highly excited states of atoms and molecules. The additional effects of the nonhydrogenic core may be incorporated via use of quantum defect theory. Inelastic transitions between the ro-vibrational states of molecules can be studied by appeal to the inelastic form factor for the harmonic oscillator.

Inelastic scattering of incident (neutral or charged) particles or of photons (or short bursts of electromagnetic radiation [1]) by a structured target can be decomposed into an internal structure part, provided by the form factor of the target, and a dynamic part which depends on details of the external projectile-target interaction. Bound-bound, bound-continuum, continuum-continuum, and ionization transitions are treated on the same footing by using the form factor.

The quantal impulse, semiclassical impact parameter, first Born approximation, and binary encounter methods of collision theory [2] focus on the transition probability as a dynamic response of the target in the field of the projectile. The physical significance of the form factor  $\mathcal{F}$  is that  $P_i(\mathbf{q}) = |\mathcal{F}|^2$  is the probability of an internal transition arising from any external impulsive perturbation (whether due to collision with particles or exposure to electromagnetic radiation) which induces a sudden change  $\mathbf{q}$  to the internal momentum of the target system [3]. Since any interaction can be decomposed as a series of sudden interactions, the scattering cross section or other observables are determined by integrating the form factor, multiplied by some weighting factor characteristic of the interaction, over momentum transfer  $\mathbf{q}$ . For

example, the generalized oscillator strength  $f$  is written in terms of the inelastic form factor as

$$f = \frac{2\Delta E_{\text{a.u.}}}{K^2} |\mathcal{F}|^2,$$

where  $\mathbf{K} = \mathbf{q}(a_0/\hbar)$  is dimensionless, and where  $\Delta E_{\text{a.u.}}$  is the change in energy between the initial and final states. The first Born approximation for the inelastic scattering of structureless ions of charge  $Ze$ , of speed  $v$ , by a hydrogenlike ion of charge  $Z'e$ , is

$$\sigma(v) = \frac{8\pi ZZ' a_0^2}{(v/v_0)^2} \int_{K_{\min}}^{K_{\max}} |\mathcal{F}(K)|^2 K^{-3} dK,$$

which can emphasize small momentum transfers  $K$  occurring at high energies. The inelastic scattering of an ultraslow neutral particle by a Rydberg atom is

$$\sigma(v) = \frac{2\pi a^2}{(v/v_0)^2} \int_{K_{\min}}^{K_{\max}} |\mathcal{F}(K)|^2 K dK,$$

where  $a$  is the scattering length of the projectile-Rydberg-electron interaction and  $v_0 = e^2/\hbar$  is the atomic unit for velocity. This expression emphasizes intermediate and larger  $K$  occurring within the interaction distance  $a$ .

Classical mechanics provides a good quantitative description of excited states via the correspondence principles [4]. Classical mechanics also promotes physical insight into the process by transparent causality, and provides scaling laws and elucidation of the dynamics. A phase-space description combined with statistical properties (microcanonical distribution in most cases) are the basis for an alternative or complementary view of quantal phenomena.

Based on the recognition of the above fundamental aspects of the form factor, this paper presents results for quantal form factors, and defines the classical form factor for the highly excited hydrogen atom and harmonic oscillator. Classical mechanics is advantageous here (a) in revealing essential details of the dynamics for inelastic transitions, (b) in

explaining the interesting trends in the behavior of the form factor (as a function of the various variables), and (c) in predicting quantitative results inaccessible to rigorous quantal calculations because of the formidable numerical restrictions imposed by the highly oscillatory wave functions.

Some analytical quantal [5,6], semiclassical [7,8] and classical [9,6] form factors are available, but general systematic trends cannot be easily extracted from them. A key point of this paper is that a complementary classical approach for general  $nl \rightarrow n'l'$  transitions is developed in such a way that reveals quite succinctly important aspects which remain hidden within the quantal treatment. The consistency of this approach is verified by applying it to  $nl \rightarrow n'$  and  $n \rightarrow n'$  transitions. The known results [6] are then rederived in a unified way.

The simple example of the one-dimensional harmonic oscillator is treated in Sec. II. The correspondence between the quantal and classical form factor for inelastic transitions in this system is apparent. On this ground, a generalization for three-dimensional systems (like the hydrogen atom) becomes feasible. A definition of the classical form factor interpreted as a transition probability between two states described by microcanonical distributions in the phase space, is proposed in Sec. III. The classical form factor for  $nl \rightarrow n'l'$  is introduced in Sec. IV, and compared with the quantal counterpart. Various summations, over the momentum transfer and initial and final quantum numbers are obtained within the same theoretical framework. The classical calculation are based on the microcanonical distributions presented in Appendix A. In Appendix B the classical calculations are detailed. An efficient algorithm for calculation of the various quantal form factors is introduced in Appendix C.

## II. FORM FACTOR FOR THE HARMONIC OSCILLATOR

The simple example of the one-dimensional harmonic oscillator with the Hamiltonian

$$H = p^2/2m + m\omega^2 r^2/2$$

is considered in this section. The quantized energy levels are  $E_n = (n + 1/2)\hbar\omega$ , and the corresponding wave functions  $u_n(r)$  have the generating function

$$F(t, r) = \sum_{n=0}^{\infty} \frac{u_n(r) t^n}{\sqrt{n!}} = \pi^{-1/4} r_0^{-1/2} \times \exp[-(r/r_0)^2/2 + \sqrt{2}tr/r_0 - t^2/2],$$

where  $r_0 = \sqrt{\hbar/m\omega}$  is the natural length of the oscillator.

The inelastic form factor for the transition from level  $n$  to level  $n'$  when the momentum  $q$  is transferred is defined as

$$\mathcal{F}_{nn'}(q) = \langle u_{n'} | e^{iqr/\hbar} | u_n \rangle,$$

and has the generating function, in terms of the dimensionless variable  $Q = qr_0/\sqrt{2\hbar}$

$$\begin{aligned} I(t, z; Q) &= \sum_{n, n'=0}^{\infty} \mathcal{F}_{nn'} \frac{t^n z^{n'}}{\sqrt{n!n'!}} \\ &= \exp(-Q^2/2) \exp[tz + i(t+z)Q]. \end{aligned}$$

This function provides an easy way to compute the form factor by using

$$\mathcal{F}_{nn'} = \frac{1}{\sqrt{n!n'!}} \left. \frac{\partial^{n+n'} I(t, z; Q)}{\partial^n t \partial^{n'} z} \right|_{t, z=0} \quad (1)$$

and reveals the following analytical structure of the quantal form factor for the harmonic oscillator:

$$\mathcal{F}_{nn'} = \exp(-Q^2/2) W_{n+n'}(Q),$$

where  $W_{nn'}$  is a polynomial of order  $n+n'$ .

The square of the absolute value of the form factor can be interpreted as the transition probability of the harmonic oscillator when an impulsive interaction imparts momentum  $q$  [3]. Based on this observation, a classical analog of the form factor can be defined. Consider the phase space to be populated according to the microcanonical distribution. The transition probability is then given, in a geometric sense, by the volume of that region in phase space where both initial and final states can coexist.

The density of probability in phase space for a given state of the harmonic oscillator is

$$\rho_n(r, p) = N \delta(H(r, p) - (n + \frac{1}{2})\hbar\omega),$$

where the normalization factor  $N = \omega/2\pi$  ensures one particle in all of the phase space. The transition probability is then given by the conditional probability that the system in the initial state  $n$  is in the phase-space volume element  $dr dp$ , and the  $q$ -displaced final state has quantum number  $n'$  within the same volume element. Hence

$$\begin{aligned} P_{nn'}(q) &= \frac{\hbar\omega^2}{2\pi} \int dr dp \delta(H(r, p) - (n + \frac{1}{2})\hbar\omega) \\ &\quad \times \delta(H(r, p + q) - (n' + \frac{1}{2})\hbar\omega) \end{aligned}$$

Phase space integration yields

$$P_{nn'}(Q) = \frac{1}{\pi} [-Q^4 + 2(n+n'+1)Q^2 - (n-n')^2]^{-1/2}, \quad (2)$$

where the dimensionless parameter  $Q^2 = (q^2/2m)/\hbar\omega$  is, again,  $q^2 r_0^2 / 2\hbar^2$ . Then

$$P_{nn'}(Q) = \frac{1}{\pi} [(Q_+^2 - Q^2)(Q^2 - Q_-^2)]^{-1/2},$$

which shows that  $q$  is restricted to those values for which the square root is a real number; otherwise the transition is classically forbidden, and  $P_{nn'}$  is zero. The limiting values of  $Q = Q_{\pm}$  are given by

$$Q_{\pm}^2 = (n+n'+1) \pm \sqrt{(2n+1)(2n'+1)},$$

where the probability  $P_{nn'}$  exhibits characteristic classical singularities. The classical transition probability (2) satisfies detailed balance. The transition probability for elastic collision ( $n=n'$ ) is

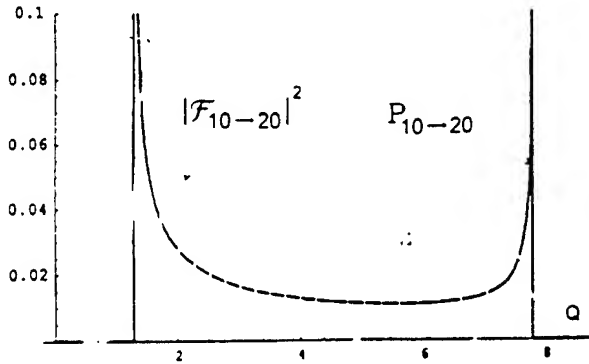


FIG. 1. Classical and quantal transition probabilities for the  $(n=10) \rightarrow (n'=20)$  transition in the harmonic oscillator vs momentum transfer  $Q$ .

$$P_{nn}(Q) = \frac{1}{\pi Q} [2(2n+1) - Q^2]^{-1/2}. \quad (3)$$

The advantage of using the classical transition probability is illustrated by the following example. Consider the  $10 \rightarrow 20$  transition. The quantal expression deduced from Eq. (1),

$$\begin{aligned} \mathcal{F}_{10 \rightarrow 20}(Q) = & \frac{e^{-Q^2/2} Q^{10}}{5225472000 \sqrt{323323}} (-670442572800 \\ & + 609493248000 Q^2 - 228559968000 Q^4 \\ & + 46884096000 Q^6 - 5860512000 Q^8 \\ & + 468840960 Q^{10} - 24418800 Q^{12} \\ & + 820800 Q^{14} - 17100 Q^{16} + 200 Q^{18} - Q^{20}) \end{aligned}$$

is rather large, and is numerically inefficient due to the oscillations in the wave functions. The classical transition probability (2), however, has the simpler form

$$P_{10,20}(Q) = \frac{1}{\pi} \frac{1}{\sqrt{-Q^4 + 62Q^2 - 100}}$$

within the classically allowed range  $31 - \sqrt{861} \leq Q^2 \leq 31 + \sqrt{861}$ .

The classical  $P_{nn'}$  and quantal  $|\mathcal{F}_{nn'}|^2$  are compared in Fig. 1. The comparison exhibits excellent "background" agreement within the classically allowed region of  $Q$ , the characteristic classical singularities at  $Q_{\pm}$ , and the characteristic exponential quantal tails in the forbidden region. The number of quantal oscillations in  $\mathcal{F}_{nn'}$  is given by  $\min(n, n') + 1$  which occur within the extent  $[(2n+1)(2n'+1)]^{1/2}$  centered on the median value  $(n+n'+1)$  of the  $Q^2$  range.

The classical transition probability for any momentum transfer (or the integrated form factor) is

$$\begin{aligned} P_{if} &= \int_{-\infty}^{\infty} P_{if}(Q) dQ \\ &= \frac{2}{\pi} \int_{Q_-}^{Q_+} [(Q^2 - Q_-^2)(Q_+^2 - Q^2)]^{-1/2} dQ, \end{aligned}$$

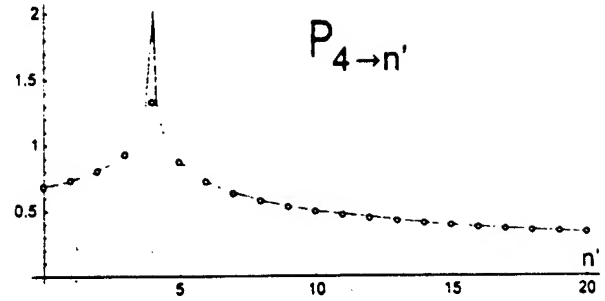


FIG. 2. Classical (solid line) and quantal (dots) transition probabilities for any momentum transfer  $q$  from the state  $n=4$  to states  $n'=0-20$ .

which reduces to

$$P_{nn'} = \frac{2}{\pi Q_-} \left[ F\left(\frac{\pi}{4} \middle| \frac{-s}{1-s}\right) + \sqrt{\frac{1-s}{s}} F\left(\arcsin \sqrt{\frac{s}{2}} \middle| \frac{1}{s}\right) \right]$$

$$\text{where } s = 1 - Q_-^2/Q_+^2$$

in terms of the incomplete elliptic function  $F$ .

Figure 2 shows that there is an excellent agreement between the quantal and classical transition probabilities for general  $n \rightarrow n'$  transitions in the harmonic oscillator for any momentum transfer. The singularity at  $n'=n$  arises from Eq. (3). The characteristic agreement is displayed in Fig. 2.

### III. PHASE-SPACE EXPRESSION FOR THE FORM FACTOR

The quantal amplitude

$$\mathcal{F}_{if}(q) = \langle \Psi_f(r) | e^{iq \cdot r/\hbar} | \Psi_i(r) \rangle_r = \langle \Phi_f(p+q) | \Phi_i(p) \rangle_p \quad (4)$$

is expressed as the above integrations over either configuration space or over momentum space, where the momentum wave functions are defined as

$$\Phi(p) = (2\pi\hbar)^{-3/2} \int \Psi(r) \exp(-iq \cdot r/\hbar) dr.$$

The transition probability

$$P_{if}(q) = |\langle \Psi_f(r) | e^{iq \cdot r/\hbar} | \Psi_i(r) \rangle|^2 \quad (5)$$

can therefore be expressed as

$$\begin{aligned} & \langle \Psi_f(r) | e^{iq \cdot r/\hbar} | \Psi_i(r) \rangle_r \langle \Phi_f(p+q) | \Phi_i(p) \rangle_p \\ &= \int dr dp [\Psi_f^*(r) e^{i(p+q) \cdot r/\hbar} \Phi_f(p+q)] \\ & \quad \times [\Psi_i(r) e^{-ip \cdot r/\hbar} \Phi_i^*(p)]. \end{aligned}$$

The quantal phase-space distribution may be defined by

$$\rho(r, p) = (2\pi\hbar)^{-3/2} \Psi(r) e^{-ip \cdot r/\hbar} \Phi^*(p)$$

since the probability densities  $\rho(r)$  in configuration space and  $\rho(p)$  in momentum space (obtained by integrating the

quantal phase-space distribution over momentum or configuration space) yield  $\rho(\mathbf{r}) = \int \rho(\mathbf{r}, \mathbf{p}) d\mathbf{p} = |\Psi(\mathbf{r})|^2$  and  $\rho(\mathbf{p}) = |\Phi(\mathbf{p})|^2$ , respectively. This distribution is the standard ordered version [10] of the Wigner distribution [11].

The transition probability is therefore

$$P_{if}(\mathbf{q}) = (2\pi\hbar)^3 \int d\mathbf{r} d\mathbf{p} \rho_i(\mathbf{r}, \mathbf{p}) \rho_f^*(\mathbf{r}, \mathbf{p} + \mathbf{q}). \quad (6)$$

This expression for the transition probability is now in a form appropriate for classical correspondence, obtained by replacing the quantal densities  $\rho_{i,f}$  (even though  $\rho_{i,f}$  have no direct physical interpretation) by the classical phase-space distributions  $\rho^c(\mathbf{r}, \mathbf{p})$ . Thus

$$P_{if}(\mathbf{q}) = (2\pi\hbar)^3 \int d\mathbf{r} d\mathbf{p} \rho_i^c(\mathbf{r}, \mathbf{p}) \rho_f^c(\mathbf{r}, \mathbf{p} + \mathbf{q}) \quad (7)$$

is the basic expression for the classical probability for impulsive transitions. The number of initial states in the phase-space element  $d\mathbf{r} d\mathbf{p}$  is  $\rho_i d\mathbf{r} d\mathbf{p}$ , and  $(2\pi\hbar)^3 \rho_f$  is the probability that the final state is in the same phase-space element.

Two fundamental properties, corresponding to similar properties of the quantal result (5), can be readily proven for the classical transition probability (7). The classical distributions satisfy

$$\rho(\mathbf{r}, \mathbf{p}) = \sum_n \rho_n(\mathbf{r}, \mathbf{p}) = (2\pi\hbar)^{-3},$$

which means that the total number states in the phase volume element is  $d\mathbf{r} d\mathbf{p} / (2\pi\hbar)^3$ , the number of elementary phase-space cells. The probability of transition from initial state  $i$  to all states  $f$  is then

$$\sum_f P_{if}(\mathbf{q}) = \int \rho_i(\mathbf{r}, \mathbf{p}) d\mathbf{r} d\mathbf{p} = g_i,$$

the statistical weight  $g_i$  of the initial state. The second property provides the transition probability for all momentum transfers  $\mathbf{q}$ . Integration of Eq. (7) over all possible values of the momentum transfer  $\mathbf{q}$  involves

$$\begin{aligned} \int \rho(\mathbf{r}, \mathbf{p} + \mathbf{q}) d\mathbf{q} &= \int \rho(\mathbf{r}, \mathbf{p}') d\mathbf{p}' \int \delta(\mathbf{p} + \mathbf{q} - \mathbf{p}') d\mathbf{q} \\ &= \rho(\mathbf{r}), \end{aligned}$$

where  $\rho(\mathbf{r})$  is the classical distribution in configuration space. Then

$$\int P_{if}(\mathbf{q}) d\mathbf{q} = (2\pi\hbar)^3 \int \rho_i(\mathbf{r}) \rho_f(\mathbf{r}) d\mathbf{r}. \quad (8)$$

This classical property is again in correspondence with the quantal result

$$\int |\mathcal{F}_{if}(\mathbf{q})|^2 d\mathbf{q} = (2\pi\hbar)^3 \int |\Psi_i(\mathbf{r})|^2 |\Psi_f(\mathbf{r})|^2 d\mathbf{r}, \quad (9)$$

which can be derived from Eq. (4).

In the action-angle representation for bound states, the classical distribution is

$$\rho_a(J, w) dJ dw = \delta(J/\hbar - n) dJ dw / (2\pi\hbar)^D$$

for a general  $D$ -dimensional system with a set of action-angle variables  $(J, w)$  in a state specified by the set of quantum numbers  $n$ . The classical probability for  $n \rightarrow n'$  transitions is therefore

$$\begin{aligned} P_{in}(\mathbf{q}) &= (2\pi\hbar)^{-D} \int \int \delta(J/\hbar - n) \delta(J'/\hbar - n') \\ &\times \delta(\mathbf{p} + \mathbf{q} - \mathbf{p}') \delta(\mathbf{r} - \mathbf{r}') d\mathbf{z} dw dJ' dw', \quad (10) \end{aligned}$$

which provides a more general classical correspondence with the quantal expression (6), rewritten as

$$\begin{aligned} P_{if}(\mathbf{q}) &= (2\pi\hbar)^3 \int \int d\mathbf{r} d\mathbf{p} d\mathbf{r}' d\mathbf{p}' \rho_i(\mathbf{r}, \mathbf{p}) \rho_f(\mathbf{r}', \mathbf{p}') \\ &\times \delta(\mathbf{r} - \mathbf{r}') \delta(\mathbf{p} + \mathbf{q} - \mathbf{p}'). \end{aligned}$$

These expressions emphasize the impulsive nature of the momentum transferred.

#### IV. FORM FACTOR FOR THE HYDROGENIC ATOM

##### A. Form factor for $nI \rightarrow n'I'$ transitions

The classical distribution for an atom with given energy  $E$  and angular momentum  $L$ , in  $(\mathbf{r}, \mathbf{p})$  phase space is (Appendix A)

$$\begin{aligned} \rho(E, L; \mathbf{r}, \mathbf{p}) dE dL d\mathbf{r} d\mathbf{p} \\ = dE \delta(H - E_n) dL \delta(|L| - L) \frac{d\mathbf{r} d\mathbf{p}}{(2\pi\hbar)^3}, \quad (11) \end{aligned}$$

where both the Hamiltonian  $H(\mathbf{r}, \mathbf{p}) = p^2/2m + V(r)$  and angular momentum  $|L(\mathbf{r}, \mathbf{p})| = rp \sin \theta_p$  are constants of motion. The classical transition probability for the case of a central field one-electron atom, between the states, or bands of states centered at  $(E, L)$  and  $(E', L')$ , due to momentum transfer  $\mathbf{q}$ , is then

$$\begin{aligned} P(E, L; E', L'; \mathbf{q}) dE dL dE' dL' \\ = dE dL dE' dL' \int \frac{d\mathbf{r} d\mathbf{p}}{(2\pi\hbar)^3} \delta(H(\mathbf{r}, \mathbf{p}) - E) \\ \times \delta(|L(\mathbf{r}, \mathbf{p})| - L) \delta(H(\mathbf{r}, \mathbf{p} + \mathbf{q}) - E') \\ \times \delta(|L(\mathbf{r}, \mathbf{p} + \mathbf{q})| - L'). \quad (12) \end{aligned}$$

The quantity  $P(\Gamma; \Gamma'; \mathbf{q})$  is the transition probability density (per unit intervals  $d\Gamma d\Gamma'$ ). When  $E$ ,  $E'$ ,  $L$ , or  $L'$  are quantized, the transition probability between corresponding states are obtained by the formal replacements  $dE \rightarrow \hbar \nu_{nI}$  and  $dL \rightarrow \hbar$  on the right-hand side of Eq. (12). The transition probability between bound states with given quantum numbers  $(n, l)$  and  $(n', l')$  is then

$$P_{nl,n'l'}(q) = h \nu_{nl} h \nu_{n'l'} \hbar^2 \times P(E_{nl}, (l+1/2)\hbar; E_{n'l'}, (l'+1/2)\hbar), \quad (13)$$

where  $\nu_{nl} = \tau_{nl}^{-1}$  is the radial frequency of the classical orbit.

Since the densities used in Eq. (13) are already normalized to  $(2l+1)$  particles in all of the phase space (see Appendix A), Eq. (13) represents the basic definition of the classical form factor, in direct correspondence with the (symmetrical) quantal form factor

$$F_{nl,n'l'}(q) = \sum_m \sum_{m'} |\langle nlm | e^{iq \cdot r / \hbar} | n'l'm' \rangle|^2. \quad (14)$$

The physical significance of the basic expression (7) is that the initial and final states correspond to definite regions in phase space populated according to the microcanonical distributions (11). Transitions can only occur if these two regions overlap, and the amount of overlap is a measure of the transition probability. The classical form factor (13) which has been developed in detail in Appendix B, will be directly compared with the quantal result of Eq. (14), developed in Appendix C as a function of  $q$  for arbitrary  $nl \rightarrow n'l'$  transitions.

The result of the classical calculation (13) (see Appendix B for details) is

$$P_{nl,n'l'}(q) = \left[ \frac{2(2l+1)(2l'+1)\hbar^3}{\tau_{nl}\tau_{n'l'}} \right] \times \int_{\mathcal{R}} \frac{dr/r^2}{\dot{r}\dot{r}'} \left[ \frac{G_{if}^+(r,q) + G_{if}^-(r,q)}{q} \right] \Theta(r,q), \quad (15)$$

where  $\Theta(r,q)$  is the step function having value unity within  $r < r^*$  (given in Appendix B), and zero otherwise, and the function

$$G_{if}^{\pm}(r,q) = \frac{1}{\sqrt{(q^2 - A_{\pm}^2)(B_{\pm}^2 - q^2)}} \quad (16)$$

must be real, so that  $q$  must be within the classically accessible range  $\mathcal{R}$  given by

$$A_{\pm}^2 = m^2(\dot{r} \pm \dot{r}')^2 + (L - L')^2 / r^2 \leq q^2 \leq B_{\pm}^2 = m^2(\dot{r} \pm \dot{r}')^2 + (L + L')^2 / r^2.$$

The radial velocity  $\dot{r}$  ( $\dot{r}'$ ) is a function only of  $r$  for a given  $nl$  (or  $n'l'$ ) state. For a given momentum transfer  $q$ , the  $r$  integration proceeds over the radial ranges within which the square roots in Eq. (16) are real. This situation is illustrated in Fig. 3 for the  $(4,3) \rightarrow (8,2)$  transition in the hydrogen

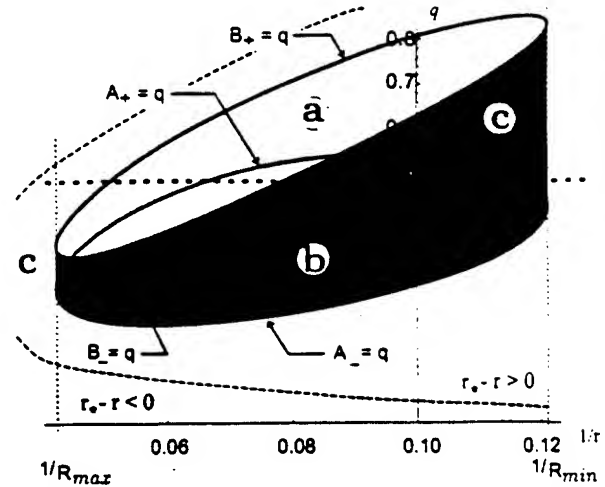


FIG. 3. Integration region for a typical  $(4,3) \rightarrow (8,2)$  transition.

atom. The dotted curve is the boundary ( $r_* - r = 0$ ) of the region within which the function  $\Theta$  is unity, and which encompasses the physical accessible region  $A_- \leq q \leq B_+$ . When  $q$  is small (below the  $A_-$  curve) or large (above the  $B_+$  curve),  $G_{if}$  has complex values and the transition probability is necessarily zero. In the shaded regions only  $G_{if}^+$  (a) or  $G_{if}^-$  (b) or both  $G_{if}^{\pm}$  (c) can contribute to the integral for a given  $q$ . The range  $\mathcal{R}$  of radial integration always lies within the region specified by  $A_+ = A_- = \text{real}$  and  $B_+ = B_- = \text{real}$ . The boundaries of this region are then given by  $R_{\min} = \max(R_i^-, R_f^-)$  and  $R_{\max} = \min(R_i^+, R_f^+)$ , where  $R^-$  and  $R^+$  are the pericenter and the apocenter of the Kepler orbit. The three situations possible (details in Ref. [3]) for the overlap of initial and final orbits are illustrated in Fig. 4 as  $L'$  of the final orbit is increased. Region I gives the maximum overlap when region  $\mathcal{R} = (R_i^-, R_i^+)$  is specified only by the initial state. In Region II the overlap is partial, because the lower limit of  $\mathcal{R}$  is given by the pericenter of the final orbit  $R_f^-$ . In Region III the pericenter  $R_f^-$  has moved outside  $R_i^+$ , so that there is no overlap, the transition is classically forbidden.

The quantal transition probability for bound-bound transitions, for hydrogenic atoms, is a rational function in the momentum transfer  $q$ . The proof of this statement and the algorithm for quantal calculations are presented in Appendix C. The form factor for the  $(4,3) \rightarrow (8,2)$  transition, as a function of  $q$ , is

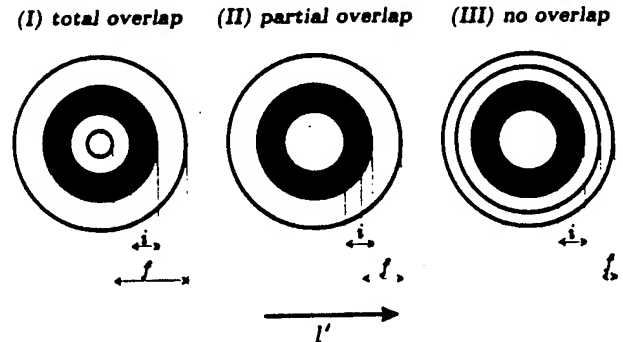


FIG. 4. Overlap situations for fixed initial  $n, l$ , and  $n'$  and varying  $l'$ .

$$\begin{aligned}
 P_{4,3 \rightarrow 8,2}(q) = & \frac{34359738368q^2}{(9+64q^2)^{24}} (1977006755367 - 84352288228992q^2 - 52980973020131328q^4 + 914957411105636352q^6 \\
 & + 557017745580707807232q^8 + 49144600326376878243840q^{10} + 1304678925402985186983936q^{12} \\
 & - 12446991865892540818391040q^{14} + 839683843672479677596827648q^{16} \\
 & + 5269768456130999660417384448q^{18} + 226149481324737121139390676992q^{20} \\
 & - 3490013454414646748315148877824q^{22} + 22442701774022980630594896003072q^{24} \\
 & - 63431755657397448352885433696256q^{26} + 66458636923717615551358326276096q^{28}).
 \end{aligned}$$

The results of calculations for the quantal and classical probabilities (form factors) are compared in Fig. 5. The four singularities in the classical transition probability, which indicates maxima in quantal results, correspond with those values of the momentum transfer for which the ( $q = \text{const}$ ) line is tangent to one of the curves  $A \pm q$  or  $B \pm q$  in Fig. 3. One of these equations has then a double root in  $r$ , which eventually yields after integration a logarithmic singularity.

In Fig. 6 the quantum numbers  $n, l$ , and  $n'$  are fixed and the transition probability versus the momentum transfer  $q$  is plotted for various final angular momenta  $l'$ . As  $l'$  increases, the quantal and classical transition probabilities increase, and attain a maximum for some value of  $l'$ . This value is roughly given by  $l' \sim n\sqrt{2}$ , in agreement with the results derived in Ref. [3]. Further increasing  $l'$  produces a sharp decrease in the quantal transition probability. The classical transition probability is forbidden for  $l' = 6$  and 7, since there is no overlap at all between the phase-space regions occupied by the initial and the final states, for any momentum transfer  $q$ . This situation corresponds to region III of Fig. 4. The quantal results for  $l' = 6$  and 7 are therefore classically inaccessible.

When the final principal quantum number  $n'$  is varied, keeping  $n, l$ , and  $l'$  fixed, the shape of the transition probability versus momentum transfer is preserved and the magnitude rapidly decreases as  $n'$  increases. This observation, valid for both quantal and classical cases, is demonstrated in Fig. 7 for a specific case. Because the transition probability (14) contains the factor  $1/r' \sim 1/n'^3$ , the classical form factor provides an explanation for this behavior.

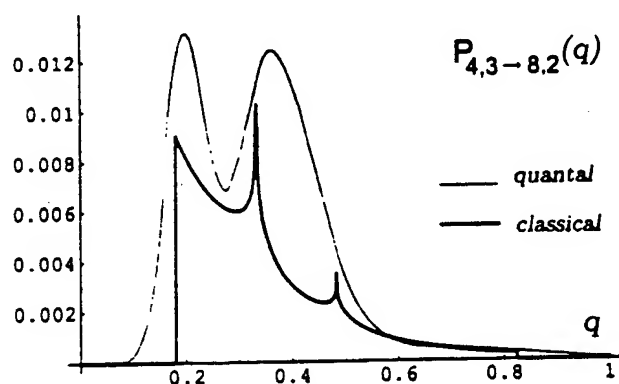


FIG. 5. Quantal and classical transition probabilities for the  $(4,3) \rightarrow (8,2)$  transition.

When the final state is in the continuum with energy between  $E'$  and  $E' + dE'$ , result (15) is still valid provided  $h\nu_{n',l'}$  is replaced by  $dE'$ . The probability for a bound-free transition is then

$$\begin{aligned}
 P_{n,l,l'}(E'; q) dE' = & \left[ \frac{(2l+1)(2l'+1)\hbar^2 dE'}{\pi \tau_{nl}} \right] \\
 & \times \int \frac{dr/r^2}{\pi \dot{r}_1 \dot{r}_2} \left[ \frac{G_{if}^+(r, q) + G_{if}^-(r, q)}{q} \right].
 \end{aligned}$$

### B. Integrated $nl \rightarrow n'l'$ form factor

The integrated form factor or the transition probability for any momentum transfer is the integral of the  $q$ -dependent transition probability over the  $q$  space. The quantal calculation gives

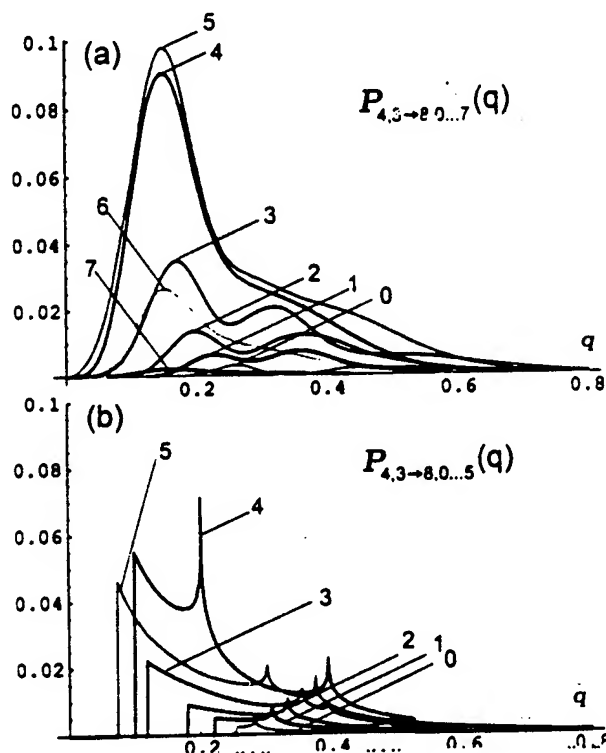


FIG. 6. Quantal (a) and classical (b) transition probabilities for the  $(4,3) \rightarrow (8,l')$  transitions, with  $l' = 0, \dots, 7$ .

$$\int |F_{nl,n'l'}^q(\mathbf{q})|^2 d\mathbf{q} \\ = (2\pi\hbar)^3 \int d\mathbf{q} \sum_m |\Psi_{nlm}(\mathbf{r})|^2 \sum_{m'} |\Psi_{n'l'm'}(\mathbf{r})|^2,$$

which, with  $\Psi(\mathbf{r}) = (R_{nl}/r)Y_{lm}(\hat{\mathbf{r}})$ , reduces to

$$\int |F_{nl,n'l'}^q(\mathbf{q})|^2 d\mathbf{q} \\ = 2\pi^2(2l+1)(2l'+1)\hbar^3 \int \rho_{nl}^q(r)\rho_{n'l'}^q(r)dr/r^2, \quad (17)$$

where  $\rho^q(r)dr = R_{nl}^2(r)dr$  is the radial probability.

Integration of the corresponding classical transition probability (8) gives

$$\int P_{nl,n'l'}(\mathbf{q}) d\mathbf{q} = \frac{8\pi^2(2l+1)(2l'+1)\hbar^3}{\tau_1\tau_2} \int_{\mathcal{R}} \frac{(dr/r^2)}{r_1 r_2}. \quad (18)$$

Upon integration, Eq. (18) yields

$$P_{nl,n'l'} = \frac{8}{n^3 n'^3} F(\arcsin \sqrt{s} | 1/s) [(x_3 - x_2)(x_4 - x_1)]^{-1/2} \\ \text{with } s = \frac{(x_3 - x_2)(x_4 - x_1)}{(x_3 - x_1)(x_4 - x_2)},$$

where  $F$  is the incomplete elliptic function and  $x_i$  ( $i = 1, 2, 3$ , and  $4$ ) is the sorted set  $(R_i^-, R_i^+, R_j^-, R_j^+)$ . When there is no overlap between the initial and final states ( $R_i^+ < R_j^-$ ) the transition is of course classically forbidden (situation III in Fig. 4). Comparison between the quantal and classical expressions reveals the definition of the classical radial probability:  $\rho^c(r)dr = 2dt/\tau$ , in agreement with the customary correspondence (deduced in Appendix A). The  $q$  integrated transition probabilities for fixed initial quantum numbers  $n$  and  $l$  and final  $n'$  as function of the final angular momentum  $l'$  are shown in Fig. 8. There is excellent agreement between the quantal and classical calculations before the first singularity in  $l'$ , which marks the transition from region I to region II in Fig. 4. For larger  $l'$ , the quantal transition probabilities oscillate about the classical transition probabilities. As proven in Ref. [3], there is a limiting value  $l'_*$  of  $l'$  after which the quantal transition probability exponentially decays while the classical form factor is zero. This situation corresponds with region III in Fig. 4, where the transition is classically forbidden. If this special value of  $l'$  cannot be accommodated, because  $l'_* \geq n' - 1$ , the transition is classically always permitted and the quantal transition probability has no exponential tail. This is the case of quasi elastic transitions (between the same principal quantum numbers), as presented in Fig. 9. For this case, the agreement

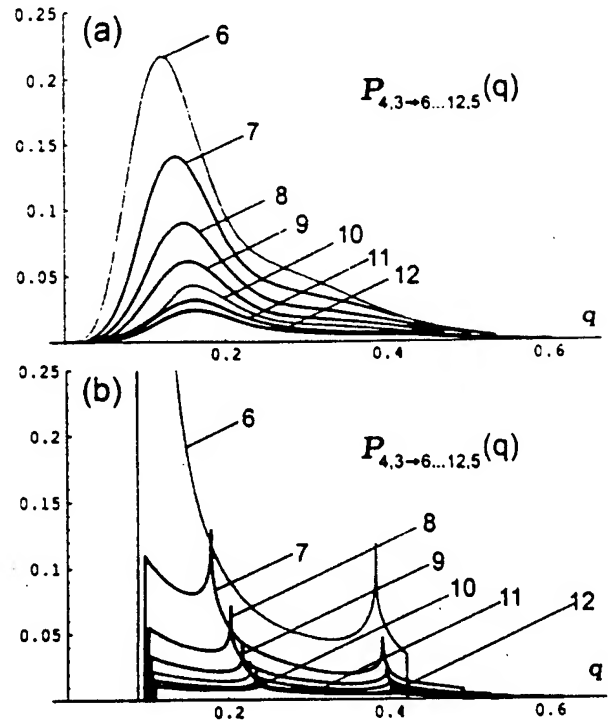


FIG. 7. Quantal (a) and classical (b) transition probabilities for the  $(4,3) \rightarrow (n',5)$  transitions, with  $n' = 6, \dots, 12$ .

between quantal and classical calculations is excellent for any  $l'$ . The  $q$ -integrated form factors were discussed in Ref. [3].

### C. Form factor for $nl \rightarrow n'$ transitions

Summation over the final angular momentum number  $l'$  provides the form factor

$$P_{nl,n'}(\mathbf{q}) = \sum_{l'=0}^{n'-1} \sum_{m,m'} | \langle nlm | e^{i\mathbf{q} \cdot \mathbf{r}/\hbar} | n'l'm' \rangle |^2. \quad (19)$$

The basic definition (7) gives the classical analog for this form factor:

$$P_{nl,n'}(\mathbf{q}) = (2\pi\hbar)^3 \int d\mathbf{r} d\mathbf{p} \rho_{nl}(\mathbf{r}, \mathbf{p}) \rho_{n'}(\mathbf{r}, \mathbf{p} + \mathbf{q}),$$

where the densities  $\rho_{nl}$  and  $l$ -averaged  $\rho_{n'}$  are described in Appendix A. Using  $V(r) = E - p^2/2m$ , the final distribution is rewritten in the  $r$  independent form as

$$\rho_{n'}(\mathbf{r}, \mathbf{p} + \mathbf{q}) = (h\nu_{n'}) \delta[(\mathbf{p} + \mathbf{q})^2/2m - p^2/2m + E - E'] / (2\pi\hbar)^3,$$

where  $\dagger$  means "not  $\mathbf{r}$ ." The classical transition probability for impulsive  $nl \rightarrow n'$  transitions is then

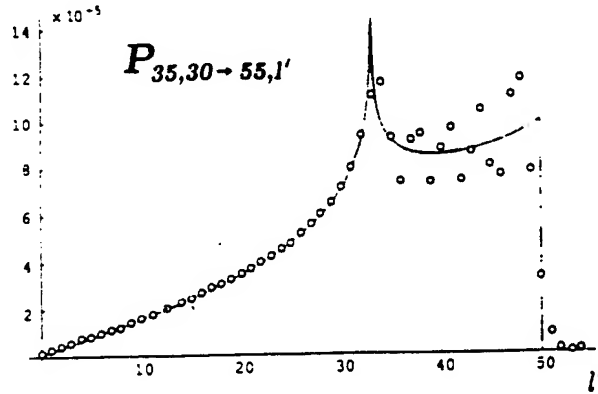


FIG. 8. Quantal (dots) and classical (solid line) transition probabilities for the  $(35,30) \rightarrow (55,l')$  transitions, with  $l' = 0, \dots, 54$ .

$$P_{nl,n'}(q) = \int dp \rho_{nl}(p) \rho_{n'}(p+q),$$

which is the classical overlap only of the momentum space distributions, rather than the full phase-space distributions, as in Eq. (12) for  $nl \rightarrow n'l'$  transitions. Since

$$\int \delta(pq \cos \theta_{pq} / m + q^2/2m + E - E') d\hat{p} = 2\pi m / pq$$

for  $p > p_0 = |2m(E' - E) - q^2|/2q$ , and zero otherwise, this transition probability reduces to

$$P_{nl,n'}(q) = \frac{2\pi m}{q} (h\nu_{n'}) \int_{p_0}^{\infty} \rho_{nl}(p) p dp,$$

which involves only the momentum distribution of the initial state. The same result is also obtained in Appendix B by

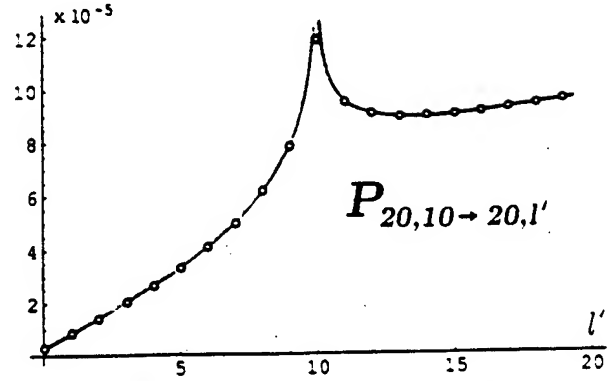


FIG. 9. Quantal (dots) and classical (solid line) transition probabilities for the  $(20,10) \rightarrow (20,l')$  transitions, with  $l' = 0, \dots, 19$ .

(summing) integrating the original probability  $P_{nl,n'l'}$  over all possible final angular momenta. The probability for  $n,l \rightarrow n'$  transitions in hydrogen is

$$P_{nl,n'}(q) = \frac{2(2l+1)}{\pi q n'^3} \int_{p_{\min}}^{p_+} \frac{n}{p} (1+n^2 p^2)^{-2} \times \left[ 1 - \left( \frac{L(1+n^2 p^2)}{2n^2 p} \right)^2 \right]^{-1/2} dp, \quad (20)$$

where all quantities are in atomic units, and  $L = l + 1/2$ . The limits of integration are given by  $p_{\min} = \max[p_0, |q^2 + 1/n'^2 - 1/n^2|/2q, p_-]$ , where  $p_{\pm} = (1 \pm (1 - L^2/n^2)^{1/2})/L$  are the extreme values (at pericenter and apocenter) of the momentum of the electron on a given orbit. As a specific example, consider the  $4,3 \rightarrow 8$  transition. The quantal form factor is (cf. Appendix C)

$$P_{4,3 \rightarrow 8}(q) = \frac{34359738368 q^2}{5(9 + 64 q^2)^{17}} (9721215 + 4498478208 q^2 + 471603326976 q^4 + 6554684489728 q^6 - 451062079160320 q^8 + 6344423684177920 q^{10} - 12676750592966656 q^{12} - 12899470417068032 q^{14} + 535928355657089024 q^{16} + 450359962737049600 q^{18}).$$

The classical and quantal form factors, are compared in Fig. 10. The insets show the  $p$  integration range as a function of the momentum transfer  $q$ . Three special cases are presented: (a) excitation, (b) quasielastic transition, and (c) deexcitation. For  $q$  sufficiently small that  $p_0 > p_+$ , the transition is classically forbidden [cases (a) and (c)]. As  $q$  increases, the integration limits of Eq. (20) are  $(p_0, p_+)$ . The increase of  $P$  in cases (a) and (c) is due to the effect of increasing range of integration overwhelming the background  $q^{-1}$  decrease. With a further increase in  $q$ , the inte-

gration limits change to  $(p_-, p_+)$  which are independent of  $q$ . Here  $P$  decreases purely as  $q^{-1}$ , as in (a) and (b). For larger  $q$ , the more rapid decrease in  $P$  results from a  $q^{-1}$  variation combined with the effect of a decreasing range of integration, as exhibited for all cases. The transition is again classically forbidden, for all cases, in the limit of large  $q$  when  $p_0 > p_+$ . These three overlap situations described above are illustrated in Fig. 11. For deexcitation ( $E' < E$ ),  $p_0$  has always one minimum value  $p_0^* = [2m(E - E')]^{1/2}$ . When  $p_0^* > p_-$ , then the pattern of case (c), with momentum



limits ( $p_0, p_-$ ), is established. This occurs for de-excitation to levels  $n' < n_+(n, L) = (L/\sqrt{2})[1 - (1 - L^2/n^2)^{1/2}]^{-1/2}$ . De-excitation to levels  $n' > n_+$  is characterized by the pattern of case (c). When  $p_0^* > p_+$ , transitions are classically forbidden. This occurs for de-excitation to final states,  $n' < n_-(n, L) = (L/\sqrt{2})[1 + (1 - L^2/n^2)^{1/2}]^{-1/2}$ , whose orbits are fully within the orbit of the initial  $(n, L)$  state. The  $n_-$  limit therefore delineates the classically allowed from classically forbidden de-excitation transitions. The  $n_{\pm}$  demarcations are illustrated in Fig. 11. For excitation,  $p_0$  can be zero at  $q^* = [2m(E' - E)]^{1/2}$ , so that there is always a range of transition momenta  $q$  for which  $p_0 < p_-$  i.e.  $n' > n_+(n, L)$ . Excitation is therefore always characterized by the pattern of case (a). The quantal-classical agreement for  $nl \rightarrow n'$  transitions is overall very good.

#### D. Form factor for $n \rightarrow n'$ transitions

The classical probability of transition between states specified only by their principal quantum numbers as function of the dimensionless parameter  $Q = qa_0/Z\hbar$  (as derived in Appendix B) is

$$P_{n,n'}(Q) = \frac{2^9}{3\pi(nn')^3} Q^5 \left[ Q^4 + 2 \left( \frac{1}{n^2} + \frac{1}{n'^2} \right) Q^2 + \left( \frac{1}{n^2} - \frac{1}{n'^2} \right)^2 \right]^{-3},$$

which is the classical correspondence of

$$P_{n,n'}(q) = \sum_{l=0}^{n-1} \sum_{l'=0}^{n'-1} \sum_{m,m'} |\langle nlm | e^{i\mathbf{q} \cdot \mathbf{r}/\hbar} | n'l'm' \rangle|^2. \quad (21)$$

This quantal form factor (as derived in Appendix C) is again a rational function in the momentum transfer  $q$  since it is a summation of  $P_{nl,n'l'}$  form factors. The classical result is in agreement with the result deduced by Vriens [9] from comparison of binary-encounter and Bethe treatments of electron-atom collisions, and by Borodin [12] from the microcanonical phase space distribution  $\delta(H-E)$ .

Exact quantal and classical form factors for  $6 \rightarrow 40$  transitions are compared in Fig. 12. The expression for the quantal form factor for this specific transition

$$\begin{aligned} P_{6 \rightarrow 40}(q) = & \frac{382205952 \cdot 10^7 q^2 (289 + 14400 q^2)^{32}}{(529 + 14400 q^2)^{48}} (609748651778452988718867471792636791 \\ & + 1411176845994965835001817764524075792 \times 10^2 q^2 - 184318171941496097624317093441846656 \\ & \times 10^5 q^4 + 93670997716818370857325330958800896 \times 10^7 q^6 - 2400432080403014981637748114489344 \\ & \times 10^{10} q^8 + 34865881226093843259112916256817152 \times 10^{10} q^{10} - 2927694744198493018588901567102976 \\ & \times 10^{12} q^{12} + 14387567274612996874680196399104 \times 10^{15} q^{14} - 395454399288571654223098281984 \\ & \times 10^{17} q^{16} + 5 \cdot 10746343048968862171136 \times 10^{22} q^{18} - 396176923859529631650545664 \times 10^{20} q^{20} \\ & + 1656184316737309252780032 \times 10^{22} q^{22}) \end{aligned}$$

is an application of the general expression for transitions  $6 \rightarrow n'$  presented in Table I. These results are derived in Appendix B (classical form factor) and Appendix C (quantal form factor). Due to the correspondence principle, there is excellent agreement between the quantal and more compact classical expressions  $n' \gg n \gg 1$ . The agreement is also expected because the characteristic classical singularities in the form factor are "smoothed" after the  $l, l', m$ , and  $m'$  summations.

#### V. SUMMARY AND CONCLUSIONS

Based on the phase-space description of an atomic system, classical expressions for the inelastic form factor have been derived. The formulas obtained are the exact classical correspondences of the quantal form factors. The classical methods quite succinctly reveals important aspects which remain hidden in the quantum treatment. An efficient algorithm for calculation of quantal form factors as analytical

functions of momentum transfer  $q$ , for arbitrary initial and final states, has also been developed.

For  $nl \rightarrow n'l'$  transitions, the classical method provides both the qualitative behavior of the quantum results and its physical interpretation. The classical-quantal agreement is particularly noteworthy for the integrated form factors (cf. Figs. 8 and 9) for inelastic and quasielastic transitions. This is because both classical and quantal form factors depend only on the overlap of the initial and final distributions in configuration space [cf. Eqs. (17) and (18)], so that the classical singularities apparent in Fig. 5 are averaged to produce the smooth results in Figs. 8 and 9.

The increasing accuracy obtained upon  $l'$  integration is due to the absence of the multiple delineation of the phase space associated with  $nl \rightarrow n'l'$  transitions (see Fig. 3). Again the classical picture not only provides the physical explanation for the quantal behavior when the momentum transfer  $q$  and quantum numbers are varied, but also identifies the patterns associated with each type (excitation, quasi-

elastic, and de-excitation) of transition (cf. Fig. 10). The agreement between classical and quantal integrated form factors is again excellent. In the limit of summing over all final states, the total transition probability is  $\sum_f P_{if}(q) = g_i$ , the same result for both quantal and classical cases, which ensures full agreement in this limit.

On integrating over angular momentum quantum number  $l$  for  $n \rightarrow n'$  transitions, the agreement is excellent for all  $q$  even for small quantum numbers. This is due to the fact that the phase-space region common to the both initial and final states (a sphere in configuration space with of radius  $r_*$ ) is densely and continuously populated.

The classical form factors represent an attractive approach for classical collision theory. The form factor is a collision kernel to be convoluted according to the dynamics of the external interaction causing the transition. Due to the oscillatory nature of the wave functions, quantal calculations for processes involving highly excited states are still computationally expensive (in terms of precision, memory, and/or

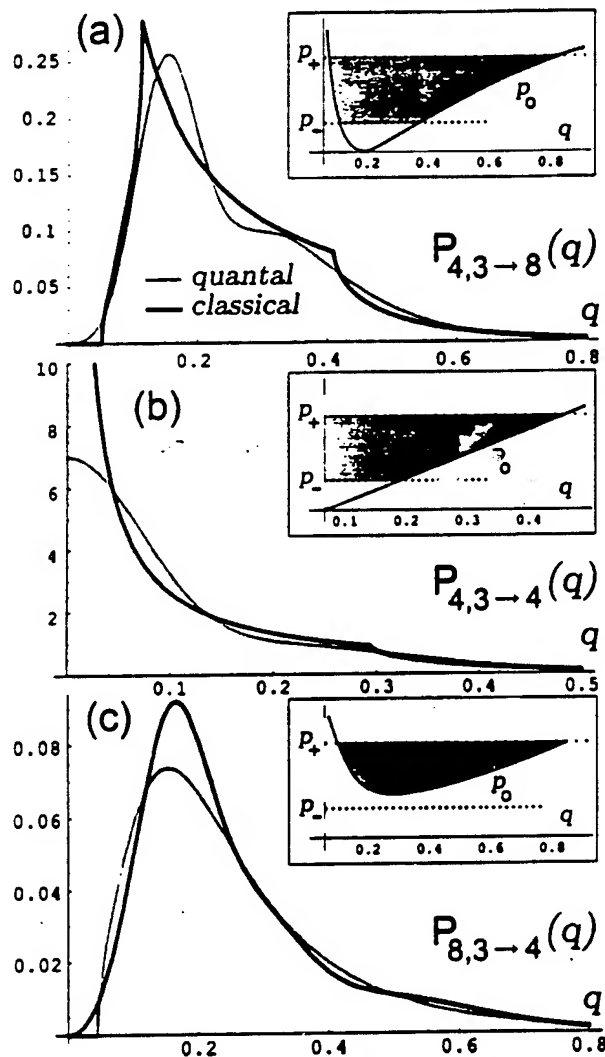


FIG. 10. Quantal and classical transition probabilities for (a)  $(4,3) \rightarrow 8$ , (b)  $(4,3) \rightarrow 4$ , and (c)  $(8,3) \rightarrow 4$  transitions as a function of the momentum transfer. Insets: the gray area is the integration range.

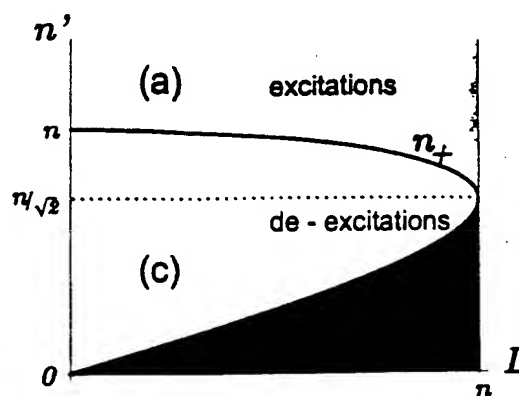


FIG. 11. The three overlap situations in momentum space: in region (a) there is a value of  $q$  for which  $p_0 < p_-$ ; in region (c)  $p_0 > p_-$  for any  $q$ , even though  $p_0 < p_+$  for some  $q$ ; in shaded region transitions are classically forbidden,  $p_0 > p_+$ .

time), while classical models are capable of exact results, according to the correspondence principles [4]. Although classical-quantal comparisons have been made to the one-dimensional harmonic oscillator and to hydrogenic systems, classical form factors can be useful for other atomic and molecular systems. The present method would also be valuable in determining the response of the three-dimensional Rydberg atom to a train of unidirectional short pulses of electromagnetic radiation [1]. The classical form factor methods would be also useful for excited-atom collisions [13].

#### ACKNOWLEDGMENTS

This work was supported by AFOSR Grant No. 49620-96-1-0142 and NSF Grant No. 98-02622. One of us (D.V.) thanks Motorola for generous support.

#### APPENDIX A: MICROCANONICAL DISTRIBUTIONS

The basic classical probability density for a particle moving in a symmetrical potential  $V(r)$  is given by the microcanonical distribution

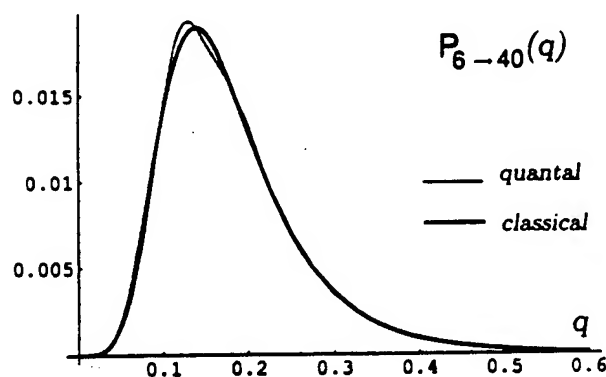


FIG. 12. Quantal and classical transition probabilities for the  $6 \rightarrow 40$  transition as a function of the momentum transfer.

TABLE I. Quantal form factor [Eq. (21) from text] for  $n' \rightarrow n$  transitions.

$n'$	$P_{nn'}(q) = \frac{2^8 n^7 q^2 [(n/n') - 1]^2 + q^2 n^2)^{n-n'-2}}{3 n'^3 [(n/n' + 1)^2 + q^2 n^2]^{n-n'-2}} \times$
1	$-1 - n^2 + 3 n^2 q^2$
2	$3 q^6 n^6 - 5 q^4 n^4 + q^2 n^2 + 9 n^2/4 - 23 n^4/16 + 15 n^6/64 - 9 n^4 q^2/2 + 65 n^6 q^2/16 - 11 n^6 q^4/4 - 1$
3	$3 q^{10} n^{10} + 11 q^8 n^8 + 14 q^6 n^6 + 6 q^4 n^4 - q^2 n^2 + 71 n^2/27 - 62 n^4/27 + 1790 n^6/2187 - 2431 n^8/19683$ $+ 377 n^{10}/59049 - 4 n^4 q^2/9 + 290 n^6 q^2/81 - 1460 n^8 q^2/729 + 143 n^{10} q^2/6561 - 122 n^6 q^4/9 + 310 n^8 q^4/27$ $- 442 n^{10} q^4/243 - 412 n^8 q^6/27 + 518 n^{10} q^6/81 - 43 n^{10} q^8/9 - 1$
4	$3 q^{14} n^{14} + 17 q^{12} n^{12} + 39 q^{10} n^{10} + 45 q^8 n^8 + 25 q^6 n^6 + 3 q^4 n^4 - 3 q^2 n^2 + 45 n^2/16 - 2131 n^4/768 + 5093 n^6/4096$ $- 167011 n^8/589824 + 35231 n^{10}/1048576 - 32899 n^{12}/16777216 + 106183 n^{14}/2415919104 + 41 n^4 q^2/8 - 269 n^6 q^2/256$ $- 3475 n^8 q^2/3072 + 107449 n^{10} q^2/196608 - 128581 n^{12} q^2/1572864 + 201047 n^{14} q^2/50331648 - 217 n^6 q^4/16$ $+ 2691 n^8 q^4/128 - 59239 n^{10} q^4/6144 + 333157 n^{12} q^4/196608 - 290087 n^{14} q^4/3145728 - 197 n^8 q^6/4 + 16273 n^{10} q^6/384$ $- 34543 n^{12} q^6/3072 + 188555 n^{14} q^6/196608 - 917 n^{10} q^8/16 + 8027 n^{12} q^8/256 - 16035 n^{14} q^8/4096 - 239 n^{12} q^{10}/8$ $+ 2119 n^{14} q^{10}/256 - 95 n^{14} q^{12}/16 - 1$
5	$3 q^{18} n^{18} + 23 q^{16} n^{16} + 76 q^{14} n^{14} + 140 q^{12} n^{12} + 154 q^{10} n^{10} + 98 q^8 n^8 + 28 q^6 n^6 - 4 q^4 n^4 - 5 q^2 n^2 + 73 n^2/25$ $- 28828 n^4/9375 + 24084 n^6/15625 - 1475182 n^8/3515625 + 29028838 n^{10}/439453125 - 4495228 n^{12}/732421875$ $+ 90535316 n^{14}/274658203125 - 12906833 n^{16}/1373291015625 + 1251587 n^{18}/11444091796875 + 56 n^4 q^2/5$ $- 13876 n^6 q^2/1875 + 75224 n^8 q^2/46875 + 319042 n^{10} q^2/3515625 - 7425752 n^{12} q^2/87890625 + 9110956 n^{14} q^2/732421875$ $- 8239208 n^{16} q^2/10986328125 + 4510567 n^{18} q^2/274658203125 - 4 n^6 q^4/5 + 6836 n^8 q^4/375 - 673004 n^{10} q^4/46875$ $+ 3108484 n^{12} q^4/703125 - 18475444 n^{14} q^4/29296875 + 2024596 n^{16} q^4/48828125 - 54614636 n^{18} q^4/54931640625$ $- 1912 n^8 q^6/25 + 178396 n^{10} q^6/1875 - 672976 n^{12} q^6/15625 + 10191692 n^{14} q^6/1171875 - 22581416 n^{16} q^6/29296875$ $+ 18069764 n^{18} q^6/732421875 - 914 n^{10} q^8/5 + 59212 n^{12} q^8/375 - 2347228 n^{14} q^8/46875 + 1541158 n^{16} q^8/234375$ $- 2802002 n^{18} q^8/9765625 - 5272 n^{12} q^{10}/25 + 1233332 n^{14} q^{10}/9375 - 1272296 n^{16} q^{10}/46875 + 2099902 n^{18} q^{10}/1171875$ $- 676 n^{14} q^{12}/5 + 6996 n^{16} q^{12}/125 - 17868 n^{18} q^{12}/3125 - 232 n^{16} q^{14}/5 + 6076 n^{18} q^{14}/625 - 167 n^{18} q^{16}/25 - 1$
6	$3 q^{22} n^{22} + 29 q^{20} n^{20} + 125 q^{18} n^{18} + 315 q^{16} n^{16} + 510 q^{14} n^{14} + 546 q^{12} n^{12} + 378 q^{10} n^{10} + 150 q^8 n^8 - 70 q^6 n^6 + 15 q^4 n^4$ $- 15 q^2 n^2 + 323 n^2/108 - 1417 n^4/432 + 1230149 n^6/699840 - 6667507 n^8/12597120 + 43800179 n^{10}/453496320$ $- 33636707 n^{12}/3023308800 + 805306763 n^{14}/979552051200 - 8183128999 n^{16}/211583243059200$ $+ 8488861159 n^{18}/7616996750131200 - 4894595653 n^{20}/274211883004723200 + 398746151 n^{22}/3290542596056678400$ $+ 35 n^4 q^2/2 - 18907 n^6 q^2/1296 + 157637 n^8 q^2/29160 - 781087 n^{10} q^2/839808 + 1290871 n^{12} q^2/25194240$ $- 167865689 n^{14} q^2/27209779200 - 57381211 n^{16} q^2/48977662560 + 5399280829 n^{18} q^2/70527747686400$ $- 117424517 n^{20} q^2/50779978334208 + 2465858993 n^{22} q^2/403961001574400 + 905 n^6 q^4/36 + 7 n^8 q^4/108$ $- 43949 n^{10} q^4/3888 + 4792471 n^{12} q^4/839808 - 188652173 n^{14} q^4/151165440 + 4792471 n^{16} q^4/839808$ $- 188652173 n^{18} q^4/151165440 + 77931593 n^{20} q^4/544195584 - 32278661 n^{22} q^4/3627970560$ $+ 264468259 n^{20} q^6/940369969152 - 594305017 n^{22} q^6/169266594447360 + 43385 n^{10} q^6/324 - 1458407 n^{12} q^6/17496$ $- 60952999 n^{14} q^6/2519424 - 82299863 n^{16} q^6/22674816 + 470998955 n^{18} q^6/1632586752$ $- 111918155 n^{20} q^6/9795520512 + 166167173 n^{22} q^6/940369969152 - 6335 n^{10} q^8/18 + 258155 n^{12} q^8/648$ $- 4222535 n^{14} q^8/23328 + 11088691 n^{16} q^8/279936 - 43657751 n^{18} q^8/10077696 + 1017419 n^{20} q^8/4478976$ $- 58621799 n^{22} q^8/13060694016 - 6167 n^{12} q^{10}/9 + 128209 n^{14} q^{10}/216 - 2015063 n^{16} q^{10}/9720 + 141006431 n^{18} q^{10}/4199040$ $- 61592369 n^{20} q^{10}/25194240 + 13034627 n^{22} q^{10}/201553920 - 14035 n^{14} q^{12}/18 + 170017 n^{16} q^{12}/324$ $- 23723233 n^{18} q^{12}/174960 + 12337645 n^{20} q^{12}/839808 - 27182041 n^{22} q^{12}/50388480 - 5030 n^{16} q^{14}/9 + 90701 n^{18} q^{14}/324$ $- 93505 n^{20} q^{14}/1944 + 737941 n^{22} q^{14}/279936 - 8995 n^{18} q^{16}/36 + 36175 n^{20} q^{16}/432$ $- 37405 n^{22} q^{16}/5184 - 3455 n^{20} q^{18}/54 + 14045 n^{22} q^{18}/1296 - 259 n^{22} q^{20}/36 - 1$

$$\rho(E, L, L_z; \mathbf{r}, \mathbf{p}) dE dL dL_z d\mathbf{r} d\mathbf{p}$$

$$= \{ \delta(H - E) \delta(|\mathbf{L}| - L) dL \delta(\mathbf{L} \cdot \hat{\mathbf{z}} - L_z) dL_z \} \frac{d\mathbf{r} d\mathbf{p}}{(2\pi\hbar)^3}, \quad (\text{A1})$$

where the Hamiltonian  $H$ , angular momentum  $|\mathbf{L}|$ , and the projection of the angular momentum on  $z$  axis  $\mathbf{L} \cdot \hat{\mathbf{z}}$  are conserved quantities, and specify the state of the system. Various other less restrictive [14] distributions are directly de-

duced from Eq. (A1) by dropping from Eq. (A1) those  $\delta$  functions which correspond with the restrictions on the state of the system to be relaxed. For example, when the projection  $L_z$  of the angular momentum is arbitrary, the distribution is

$$\rho(E, L; \mathbf{r}, \mathbf{p}) dE dL d\mathbf{r} d\mathbf{p} = \{ \delta(H - E) \delta(|\mathbf{L}| - L) dL \} \frac{d\mathbf{r} d\mathbf{p}}{(2\pi\hbar)^3}, \quad (\text{A2})$$

and describes a population of  $2L$  states in all of phase space. The physical interpretation is that Eq. (A2) is the number of states (phase-space cells) compatible with energy and angular momentum conservation. The  $\{ \}$  factor is a fractional number of states in the interval  $dE dL dL_z$  of about  $(E, L, L_z)$ .

If the system is described in terms of discrete quantum numbers, e.g., the motion is bounded within a finite spatial region, the classical distribution is defined in the action-angle representation by

$$\rho_{nlm} dJ d\omega = \delta(J_1/h - n) \delta(J_2/h - (l + 1/2)) \\ \times \delta(J_3/h - m) \frac{dJ d\omega}{(2\pi\hbar)^3}.$$

Upon action-angle variables  $(J, \omega)$  integration, this distribution corresponds to a single particle in all of phase space. Also  $\sum_{nlm} \rho_{nlm} = (2\pi\hbar)^{-3}$  is the number of particles in all states occupying the unit phase-space element. The phase-space distribution for state  $nl$  is

$$\rho_{nl} dJ d\omega = \delta(J_1/h - n) \delta(J_2/h - (l + 1/2)) \\ \times \frac{dJ_1 dJ_2 dJ_3 d\omega_1 d\omega_2 d\omega_3}{(2\pi\hbar)^3}.$$

Since  $J_3 = J_2 \cos \hat{L} \cdot \hat{z}$ , the  $J_3$  integration gives  $2J_2$ , so that the above  $\rho_{nl}$  distribution corresponds to a population of  $(2l + 1)$  states in all of phase space. The corresponding distribution in  $(r, p)$  phase space is then, by changing variables

$$\rho_{nl} dr dp = \hbar^2 \left[ \frac{\partial H(J_1, J_2)}{\partial J_1} \right] \left[ \frac{\partial L(J_2)}{\partial J_2} \right] \delta(H(r, p) - E_{nl}) \\ \times \delta(|L(r, p)| - L) \frac{dr dp}{(2\pi\hbar)^3}.$$

Since  $\partial H / \partial J_1 = \nu_{nl} = \tau_{nl}^{-1}$ , the frequency (or inverse period) for radial bounded motion, then

$$\rho_{nl}(r, p) dr dp = \{ \hbar \nu_{nl} \delta(H - E_{nl}) \hbar \delta(|L| - L) \} \frac{dr dp}{(2\pi\hbar)^3}. \quad (A3)$$

This result can be obtained, formally, from Eq. (A2), by replacing  $dE$  and  $dL$  by  $\hbar \nu_{nl}$  and  $\hbar$ , respectively. The separation between highly excited neighboring energy levels  $n$  and  $n \pm 1$  is  $\hbar \nu_{nl}$ , the Bohr correspondence, and  $\hbar$  is the separation between neighboring angular momentum levels  $n, l$  and  $n, l \pm 1$ .

By noting that

$$\int_{-1}^1 \delta(rp \sin \theta - L) d(\cos \theta) = \frac{2L}{rp} (r^2 p^2 - L^2)^{-1/2},$$

$$p \gtrsim L/r = p_0$$

and

$$\int_{p_{\min}}^{\infty} \delta(p^2/2m + V(r) - E_{nl}) \frac{p dp}{(r^2 p^2 - L^2)^{1/2}} \\ = \frac{m}{(r^2 p_+^2 - L^2)^{1/2}} = 1/(r\dot{r})$$

for  $p_+^2 = 2m(E_{nl} - V(r)) \geq p_{\min}^2$ , which ensures real radial speeds  $\dot{r}$ , then

$$\int \delta(H - E_{nl}) \delta(|L| - L) dr dp = 8\pi^2 L \oint \frac{dr}{r} = 8\pi^2 L / \nu_{nl}.$$

Distribution (A3) is thus confirmed as being normalized to  $(2l + 1)$  states.

Since  $dr dp / (2\pi\hbar)^3$  is the total number of bound and continuum states, with all quantum numbers, in the phase-space volume element  $dr dp = dJ d\omega$ , then the  $\{ \}$  factor in (A3) represents the fractional number of states with specific quantum numbers.

For the particular case of Coulomb attraction the energy levels are degenerate. The phase-space distribution for an hydrogenic atom in the energy level  $E_n$ , corresponding with the principal quantum number  $n$ , is

$$\rho_n(r, p) dr dp = \hbar \nu_n \delta(H - E_n) \frac{dr dp}{(2\pi\hbar)^3} \quad (A4)$$

for bound states of degeneracy  $n^2$ . The same expression holds for states in the continuum if  $\hbar \nu_n$  is replaced by  $dE$ .

The classical distribution  $\rho_{nl}(r) = \int \rho_{nl}(r, p) dp$  in configuration space is

$$\rho_{nl}(r) r^2 dr d\hat{r} = \frac{g_l}{\tau_{nl}} \frac{2 dr}{r} \frac{d\hat{r}}{4\pi}$$

where  $g_l = 2l + 1$  is the statistical weight of the  $nl$  level. For Coulombic attraction,  $V(r) = -Ze^2/r$ ,  $\tau_n = 2\pi n^3$  a.u., and

$$4\pi \rho_{nl}(r) r^2 dr = R_{nl}(r) dr \\ = \frac{1}{\pi n^3} \left( \frac{2Z}{r_{\text{a.u.}}} - \frac{Z^2}{n^2} - \frac{(l + 1/2)^2}{r_{\text{a.u.}}^2} \right)^{-1/2} dr$$

for one  $nl$  state ( $g_l = 1$ ).

Integration of Eq. (A2) over the configuration space yields the momentum space distribution  $\rho(E, L; p) = \int \rho(E, L; r, p) dr$ . Then

$$\rho(E, L; p) p^2 dp d\hat{p} \\ = \frac{g_l}{2\pi\hbar^2} \left[ \sum_i \frac{2 p dp}{(p^2 - L^2/r_i^2)^{1/2}} \frac{1}{|V'(r_i)|} \right] \frac{d\hat{p}}{4\pi}, \quad (A5)$$

where  $r_i$  are the roots of  $p^2 = 2m[E - V(r)]$  for a given  $p$  and  $V' = dV/dr$ . The radial momentum distribution,  $\rho_{nl} = \rho(E, L) \hbar \nu_{nl} \hbar$ , for bound hydrogenic states, reduces with  $g_l = 1$  to

$$\rho_{nl}(p) 4\pi p^2 dp = \left( \frac{2Ze^2 dp}{\tau_n |E|^2} \right) (1+x^2)^{-2} \\ \times \left( 1 - \frac{2m|E|L^2}{(2mZe^2)^2} \frac{(x^2+1)^2}{x^2} \right)^{-1/2},$$

where  $x = p/(2m|E|)^{1/2}$ . Since  $E = -Z^2(e^2/a_0)/2n^2$ , then  $x = p/p_n$  where  $p_n = Zp_0/n$  is the characteristic momentum in the Rydberg orbit  $n$ ,  $p_0 = \hbar/a_0$  is the atomic unit for linear momentum, and  $a_0$  the Bohr radius is the atomic unit for distance. With  $L = (l+1/2)\hbar$ , the hydrogenic momentum distribution is

$$\rho_{nl}(p) 4\pi p^2 dp = \frac{4}{\pi} n \frac{dP}{(1+n^2P^2)^2} \left\{ 1 - \left[ \frac{l+1/2}{n} \right] \right. \\ \left. \times \left( \frac{1+n^2P^2}{2nP} \right)^2 \right\}^{-1/2},$$

where  $P = p/Zp_0$ . This compares formally with the quantal results and is useful for the  $nl \rightarrow n'$  classical form factor. Another formulation of classical momentum distributions was recently presented in Ref. [15].

## APPENDIX B: CALCULATIONS OF CLASSICAL FORM FACTORS

The classical form factor for transitions between energy and angular momentum bands  $(E, E+dE; L, L+dL)$  is

$$P_{if}(\mathbf{q}) = P(E, L; E', L'; \mathbf{q}) dE dE' dL dL' \\ = (2\pi\hbar)^{-3} \Delta_{if}(\mathbf{q}) dE dE' dL dL'$$

in terms of the phase-space integral

$$\Delta_{if}(\mathbf{q}) = \int d\mathbf{r} d\mathbf{p} \delta(H(\mathbf{r}, \mathbf{p}) - E) \delta(|\mathbf{L}(\mathbf{r}, \mathbf{p})| - L) \\ \times \delta(H(\mathbf{r}, \mathbf{p} + \mathbf{q}) - E') \delta(|\mathbf{L}(\mathbf{r}, \mathbf{p} + \mathbf{q})| - L')$$

of  $\delta$  functions involving states  $i = (E, L)$  and  $f = (E', L')$ . For transitions between bound states the transition probability is obtained simply by the replacements  $dE \rightarrow h\nu$  and  $dL \rightarrow \hbar$ . The integral can be recast in terms of the radial integral

$$\hat{R}_{if}(\mathbf{p}_1, \mathbf{p}_2; r) = \frac{1}{4\pi} \int_{-1}^1 \delta(rp_1 \sin \theta - L) \\ \times d(\cos \theta) \int_0^{2\pi} \delta(rp_2 \sin \bar{\theta} - L') d\phi, \quad (B1)$$

where  $\theta$  and  $\bar{\theta}$  are the angles between  $\hat{r}$  and  $\hat{p}_1$  and  $\hat{p}_2$ , respectively, as

$$\Delta_{if}(\mathbf{q}) = \int d\mathbf{p}_1 d\mathbf{p}_2 \delta(\mathbf{q} + \mathbf{p}_1 - \mathbf{p}_2) \delta(H(\mathbf{r}, \mathbf{p}_1) - E) \\ \times \delta(H(\mathbf{r}, \mathbf{p}_2) - E') (4\pi \hat{R}_{if}(\mathbf{p}_1, \mathbf{p}_2; r) r^2 dr). \quad (B2)$$

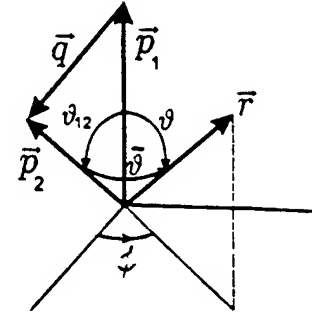


FIG. 13. The basic geometry for calculation of  $\hat{R}_{if}$ .

When  $\hat{R}_{if}$  is summed (integrated) over all  $L$  states, then  $\int \hat{R}_{if} dL dL' = 1$  and

$$\int \hat{R}_{if} dL' = \frac{1}{2} \int_{-1}^1 \delta(rp_1 \sin \theta - L) d(\cos \theta) = L/(mr^2 p_1 \dot{r}). \quad (B3)$$

### 1. Form factor for $EL \rightarrow E'L'$ transitions

Evaluation of  $\hat{R}_{if}$  for fixed  $L$  and  $L'$  is facilitated by noting, from Fig. 13, that

$$\cos \bar{\theta} = \cos \theta_{12} \cos \theta + \sin \theta_{12} \sin \theta \cos \phi$$

in terms of  $\hat{r}(\theta, \phi)$  and the fixed angle  $\theta_{12}$  between  $\hat{p}_1$  and  $\hat{p}_2$ .

On changing the  $\phi$  variable to  $\bar{\theta}$  in Eq. (B1), the  $\phi$  integral, for  $\theta$  fixed, is

$$\int_0^{2\pi} \delta(rp_2 \sin \bar{\theta} - L') d\phi = 2 \int_{|\theta - \theta_{12}|}^{\theta + \theta_{12}} S^{-1}(\bar{\theta}, \theta, \theta_{12}) \\ \times \delta(rp_2 \sin \bar{\theta} - L') d(\cos \bar{\theta}).$$

The factor 2 originates from the fact that, as  $\phi = 0 \rightarrow \pi \rightarrow 2\pi$ , the range  $(|\theta - \theta_{12}|, \theta + \theta_{12})$  in  $\bar{\theta}$  is covered twice. The function

$$S = \sin \theta_{12} \sin \theta \sin \phi$$

is expressed as a function of  $\bar{\theta}$  and  $\theta$  variables by

$$S^2(\bar{\theta}, \theta; \theta_{12}) = \sin^2 \theta \sin^2 \bar{\theta} - (\cos \theta_{12} - \cos \theta \cos \bar{\theta})^2.$$

Subsequent integrations are facilitated by noting that

$$\delta(F(x)) = \sum_n \frac{(x - x_n)}{|F'(x_n)|}, \quad F(x_n) = 0.$$

Hence

$$(\sin \bar{\theta}) \delta(rp_2 \sin \bar{\theta} - L') = \left[ \frac{L'}{mp_2 r^2 \dot{r}} \right] \sum_{i=1}^2 \delta(\bar{\theta} - \bar{\theta}_i),$$

where the roots,  $\bar{\theta}_1 < \pi/2$  and  $\bar{\theta}_2 = \pi - \bar{\theta}_1$ , are given by

$$\sin \bar{\theta}_1 = L'/rp_2, \quad \cos \bar{\theta}_1 = -\cos \bar{\theta}_2.$$

The  $\phi$  integral therefore reduces to

$$\int_0^{2\pi} \delta[rp_2 \sin \bar{\theta} - L'] d\phi = \left[ \frac{L'}{mp_2 r^2 \dot{r}'} \right] \\ \times [S_-^{-1}(\bar{\theta}_1, \theta) + S_+^{-1}(\bar{\theta}_1, \theta)],$$

where

$$S_{\pm}^2(\bar{\theta}_1, \theta) = \sin^2 \theta \sin^2 \bar{\theta}_1 - (\cos \theta_{12} \pm \cos \theta \cos \bar{\theta}_1)^2.$$

Upon  $\theta$  integration,

$$4\pi \hat{R}_{if}(\mathbf{p}_1, \mathbf{p}_2; r) = \left[ \frac{2L'}{mp_2 r^2 \dot{r}'} \right] \int_{-1}^1 [S_-^{-1}(\bar{\theta}_1, \theta) \\ + S_+^{-1}(\bar{\theta}_2, \theta)] \delta(rp_1 \sin \bar{\theta} - L) d(\cos \theta) \\ = \left[ \frac{2LL'}{m^2 p_1 p_2 r^4 \dot{r} \dot{r}'} \right] [S_-^{-1}(\bar{\theta}_1, \theta_1) \\ + S_-^{-1}(\bar{\theta}_1, \theta_2) + S_+^{-1}(\bar{\theta}_1, \theta_1) \\ + S_+^{-1}(\bar{\theta}_1, \theta_2)],$$

where  $\sin \theta_1 = \sin \theta_2 = L_1/rp_1$ , and  $\cos \theta_2 = -\cos \theta_1$ . From these relations and from the above definitions of the  $S_{\pm}$  functions, then

$$S_-(\bar{\theta}_1, \theta_1) = S_+(\bar{\theta}_1, \theta_2),$$

$$S_-(\bar{\theta}_1, \theta_2) = S_+(\bar{\theta}_1, \theta_1),$$

with the result that the radial integral is

$$4\pi \hat{R}_{if}(\mathbf{p}_1, \mathbf{p}_2; r) = \left[ \frac{4LL'}{m^2 p_1 p_2 r^4 \dot{r} \dot{r}'} \right] [S_+^{-1}(\bar{\theta}_1, \theta_1; \theta_{12}) \\ + S_-^{-1}(\bar{\theta}_1, \theta_1; \theta_{12})].$$

Upon  $\mathbf{p}_2$  integration in Eq. (B2)

$$\hat{R}_{if}(\mathbf{p}_1; r) = \int \hat{R}_{if}(\mathbf{p}_1, \mathbf{p}_2; r) \delta(\mathbf{p}_2 - (\mathbf{p}_1 + \mathbf{q}_1)) d\mathbf{p}_2,$$

$S_{\pm}$  are evaluated using the substitutions

$$\sin \theta = L/rp_1, \quad \cos \theta = mr/p_1,$$

$$\sin \bar{\theta} = L'/rp_2, \quad \cos \bar{\theta} = m\dot{r}'/p_2,$$

and

$$\cos \theta_{12} = (p_1^2 + p_2^2 - q^2)/2p_1 p_2$$

to give, simply,

$$2p_1 p_2 S_{\pm}(\bar{\theta}_1, \theta_1) = \sqrt{(q^2 - A_{\pm}^2)(B_{\pm}^2 - q^2)},$$

expressed in terms of the momentum-change limits

$$A_{\pm}^2 = m^2(\dot{r} \pm \dot{r}')^2 + (L - L')^2/r^2$$

and

$$B_{\pm}^2 = m^2(\dot{r} \pm \dot{r}')^2 + (L + L')^2/r^2.$$

The integral  $\hat{R}_{if}(\mathbf{p}_1; r)$  is then

$$4\pi \hat{R}_{if}(\mathbf{p}_1; r) = \left[ \frac{8LL'}{m^2 r^4 \dot{r} \dot{r}'} \right] [G_{if}^+(r, q) + G_{if}^-(r, q)], \quad (B4)$$

where

$$G_{if}^{\pm}(r, q) = \frac{1}{\sqrt{(q^2 - A_{\pm}^2)(B_{\pm}^2 - q^2)}}.$$

Since

$$mr^2/2 = E - V(r) - L^2/2mr^2$$

holds for the initial and final states, the  $S$ ,  $A$ , and  $B$  functions, and hence integral (B1), are all independent of  $\mathbf{p}_1$ . The transition integral (B2) is then

$$\Delta_{if}(\mathbf{q}) = \int_0^{\infty} 4\pi \hat{R}_{if}(r, q) \Pi(r, q) r^2 dr, \quad (B5)$$

where the only  $\mathbf{p}$  integral is

$$\Pi(r, q) = \int \delta(H(\mathbf{r}, \mathbf{p}) - E) \delta(H(\mathbf{r}, \mathbf{p} + \mathbf{q}) - E') d\mathbf{p}.$$

Hence

$$\Pi(r, q) = 2\pi \int_0^{\infty} p^2 dp \delta[p^2/2m + V(r) - E] \\ \times \int_{-1}^{+1} \delta[pq \cos \theta/m - E' - E - q^2/2m] d(\cos \theta),$$

where  $\theta$  is the angle between  $\mathbf{p}$  and  $\mathbf{q}$ . There is only one root provided that

$$p \geq p_0 = m/q|E - E' + q^2/2m|.$$

The  $\mathbf{p}$  integrations therefore yield

$$\Pi(r, q) = \frac{2\pi m^2}{q} \Theta(r, q),$$

where  $\Theta$  is the step function having a value 1 if  $V(r) \leq E - p_0^2/2m$  is satisfied, and zero otherwise. The final expression for the classical transition probability density (13) for  $E, L \rightarrow E', L'$  impulsive transitions is therefore

$$P(E, L; E', L'; q) = \frac{1}{(2\pi\hbar)^3} \frac{2\pi m^2}{q} \\ \times \int 4\pi \hat{R}_{if}(r, q) \Theta(r, q) r^2 dr, \quad (B6)$$

where  $\hat{R}_{if}$  is given by Eq. (B4). Hence

$$P(E, L; E', L'; q) = \frac{16\pi LL'}{(2\pi\hbar)^3 q} \int_{\mathcal{R}} \frac{dr/r^2}{\dot{r} \dot{r}'} [G_{if}^+(r, q) + G_{if}^-(r, q)] \Theta(r, q).$$

For hydrogenic systems, the condition  $V(r) \leq E - p_0^2/2m$  is satisfied for any  $q$  and all  $r$  within the radial region  $\mathcal{R}$  (cf. Fig. 3). Thus the step function  $\Theta$  is always unity.

The probability of  $n, l \rightarrow n', l'$  transitions due to an impulsive momentum change is then

$$P_{nl, n'l'}(q) = (\hbar \nu_{nl})(\hbar \nu_{n'l'}) \hbar^2 \times P(E_n, (l+1/2)\hbar; E_{n'}, (l'+1/2)\hbar; q).$$

## 2. Form factor for $EL \rightarrow E'$ transitions

On using Eq. (B3) in Eq. (B6) the probability density for  $E, L \rightarrow E'$  transitions is

$$P(E, L; E'; q) = \frac{L}{\pi\hbar^3 q} \int_0^\infty (vr)^{-1} \Theta(r, q) dr,$$

where  $v(r)$  is the speed along the initial trajectory. Since  $p^2 = 2m[E - V(r)]$ , integration over  $r$  may be replaced by  $p$  integration and  $dr/v = dp/V'(r)$  so that

$$P(E, L; E'; q) = \frac{L}{\pi\hbar^3 q} \sum_j \int_{p_0}^\infty |\dot{r}_j V'(r_j)|^{-1} dp,$$

where  $r_j$  is the root of  $p^2 = 2m[E - V(r)]$ . In terms of the momentum distribution (A5), then

$$P(E, L; E'; q) = \frac{mL}{g_l \hbar^3 q} \int_{p_0}^\infty \rho(E, L; p) 4\pi p dp,$$

which for bound  $nl$  states is in agreement with previous results [8,16,6].

The classical form factor for  $nl \rightarrow n'$  transitions in hydrogenic systems is, in atomic units,

$$P_{nl, n'}(q) = \frac{2(2l+1)}{\pi q n'^3} \int_{p_{\min}}^{p_{\max}} \frac{n}{p} (1+n^2 p^2)^{-2} \times \left[ 1 - \left( \frac{L(1+n^2 p^2)}{2n^2 p} \right)^2 \right]^{-1/2} dp,$$

where the integration limits are given by two conditions: the integrand is real and  $p \geq p_0 = |q^2 + 1/n'^2 - 1/n^2|/2q$ .

## 3. Form factor for $E \rightarrow E'$ transitions

Using Eq. (B6) with  $\hat{R}_{if} = 1$ , the probability density for  $E \rightarrow E'$  transitions is

$$P(E, E'; q) = \frac{2\pi m^2}{q(2\pi\hbar)^3} \left( \frac{4}{3} \pi r_*^3 \right),$$

where  $r_*$  is the largest  $r$  which satisfy the condition

$$p(r) = 2m[E - V(r)] \geq p_0 = \frac{m}{q} |E' - E - q^2/2m|.$$

This probability density is exact for all  $V(r)$  and has a simple physical interpretation. The transition probability is given by  $V\Delta p/(2\pi\hbar)^3$ , which is the number of states in the "reaction" volume  $V = 4/3\pi r_*^3$  multiplied by the volume of momentum space  $\Delta p$  consistent with energy conservation. The initial-final-state energy conservation equations are  $E = p^2/2m + V(r)$  and  $E' = E + q \cdot p/m + q^2/2m$ , respectively. Then

$$\Delta p = \int_{\phi=0}^{2\pi} d\mathbf{p} = 2\pi p^2 dp d(\cos \theta) = \frac{2\pi m^2}{q} dE dE',$$

where the  $z$  axis is along  $\hat{q}$ .

The classical form factor for  $n \rightarrow n'$  transitions is

$$P_{nn'}(q) = (\hbar \nu_n)(\hbar \nu_{n'}) P(E_n, E_{n'}; q).$$

For Coulomb attraction  $V(r) = -Ze^2/r$ , then

$$r_*(q) = 8(Ze^2 m) q^2 [q^4 - 4m(E + E')q^2 + 4m^2(E - E')^2]^{-1}$$

so that the transition probability, with the substitution  $q = Q(Z\hbar/a_0)$  now becomes

$$P_{nn'}(Q) = \frac{2^9}{3\pi(nn')^3} Q^3 \left[ Q^4 + 2 \left( \frac{1}{n^2} + \frac{1}{n'^2} \right) Q^2 + \left( \frac{1}{n^2} - \frac{1}{n'^2} \right)^2 \right]^{-3/2}.$$

## APPENDIX C: CALCULATIONS OF QUANTAL FORM FACTORS

The quantal transition probability (5) for the hydrogen atom is in general a rational function of the momentum transfer  $q$  because Eq. (5) with  $\Psi(\mathbf{r}) = R_{nl}(r)Y_{lm}(\hat{r})$  can be decomposed as

$$F_{nl, n'l'}(q) = (2l+1)(2l'+1) \sum_{L=|l-l'|}^{l+l'} f_{n'l'}^L(q)^2 (2L+1) \times \begin{Bmatrix} L & l & l' \\ 0 & 0 & 0 \end{Bmatrix}^2$$

where  $\{\dots\}$  is the Wigner  $3j$  symbol, and  $f_{n'l'}^L(q)$  is the radial integral:

$$f_{n'l'}^L(q) = \int_0^\infty R_{nl}(r) R_{n'l'}(r) j_L(qr) r^2 dr, \quad (C1)$$

where  $j_L$  is the modified Bessel function. Because the radial wave function  $R_{nl}$  has the simple structure  $e^{-r/n} r^l Q(r)$ ,

where  $Q$  is a polynomial of order  $n-l-1$ , integral (C1) contains only terms with the form

$$I_{k,L}(\alpha, q) = \int_0^\infty e^{-\alpha r} r^k j_L(qr) dr,$$

where  $\alpha$  is  $1/n + 1/n'$  and  $k$  is an integer number ( $k = l + l' + 2, \dots, n + n'$ ) greater than  $L$ . This integral is the following rational function in  $q$ :

$$I_{k,L}(\alpha, q) = \frac{q^L \alpha^{k-L-1}}{(2L+1)(2L-1)!!} \frac{(L+k)!}{(\alpha^2 + q^2)^k} \times {}_2F_1\left(-\frac{k-L}{2} + 1, -\frac{k-L}{2} + \frac{1}{2}, L + \frac{3}{2}; -\frac{q^2}{\alpha^2}\right),$$

since the hypergeometric function  ${}_2F_1$  is a polynomial when either the first or second argument is an integer. This proves that integral (C1), and hence the quantal form factor (14), are rational function in  $q$ . It also provides the practical procedure to calculate the quantal probability (14) in an analytical form.

The quantal transition probability (21) can be written in terms of the density matrix element,  $\rho_n(\mathbf{r}, \mathbf{r}')$   $= \sum_{l,m} \psi_{nlm}^*(\mathbf{r}) \psi_{nlm}(\mathbf{r}')$ , as

$$P_{nn'}(q) = \int \int d\mathbf{r} d\mathbf{r}' e^{iq\mathbf{r} \cdot \mathbf{r}'} \rho_n(\mathbf{r}, \mathbf{r}') \rho_{n'}^*(\mathbf{r}, \mathbf{r}').$$

The density  $\rho_n$  is the residue of the Coulomb Green's function [17] and can be calculated from

$$\rho_n(\mathbf{r}, \mathbf{r}') = \lim_{E \rightarrow E_n} (E - E_n) \mathcal{G}_E(\mathbf{r}, \mathbf{r}') = \frac{1}{\pi n a_0^3} \frac{P_n}{x - y}$$

in the spatial variables  $(x, y)$  given by

$$x = Z/a_0(r + r' + \rho), \quad y = Z/a_0(r + r' - \rho)$$

where  $\rho = |\mathbf{r} - \mathbf{r}'|$ . The function  $P_n$  has a simple structure. Because

$$P_n = \left( \frac{\partial}{\partial x} - \frac{\partial}{\partial y} \right) [M_{n,1/2}(x/n) M_{n,1/2}(y/n)],$$

where  $M$  is Whittaker's function, then  $P_n$  is simply  $\exp[-(x+y)/2n] \times$  polynomial in  $x$  and  $y$ . Thus

$$P_n(x, y) = -\frac{e^{-(x+y)/2n}}{2n^3} [2n(x-y)f_n(x)g_n(x) + (n-1)xy(f_n(x)g_n(y) - g_n(x)f_n(y))],$$

where the polynomials

$$f_n(x) = {}_1F_1(1-n, 2x/n), \quad g_n(x) = {}_1F_1(2-n, 3x/n)$$

are given by the degenerate hypergeometric function  ${}_1F_1$ , where the first argument is a negative integer. Finally,  $P_{nn'}$  is the integral in  $x, y$  variables:

$$P_{nn'}(q) = \frac{1}{24nn'} \int_0^\infty \int_0^\infty dx dy \sin(q(x-2)/2) \times (x^2 + 4xy + y^2) P_n(x, y) P_{n'}(x, y)/(x-y).$$

The observation that  $P_n(x, x) = 0$ , means that  $x - y$  is a divisor for  $P_n(x, y)$ . On writing  $\sin$  in exponential form, the integral contains only primitive terms of the form  $x^m(f \text{ or } g)(x)e^{-\alpha x}$ , with various positive integer powers  $m$  and  $\alpha_\pm = (1/n + 1/n' \pm i q)/2$ . The elementary integrals

$$\int_0^\infty x^m f_n(x) e^{-\alpha x} dx = \left( \frac{\alpha n - 1}{\alpha n} \right)^n \frac{m!}{\alpha} \left( \frac{n}{\alpha n - 1} \right)^m \times {}_2F_1(n+1, 1-m, 2, 1/\alpha n)$$

and

$$\int_0^\infty x^m g_n(x) e^{-\alpha x} dx = \left( \frac{\alpha n - 1}{\alpha n} \right)^n \frac{m!}{\alpha} \left( \frac{n}{\alpha n - 1} \right)^m \times {}_2F_1(n+1, 2-m, 3, 1/\alpha n)$$

are rational functions in  $\alpha$  which is linear in  $q$ . The form factor  $P_{nn'}$  is therefore a rational function of  $q$ . The procedure described is remarkably efficient since it reduces the multiple integrations to a finite number of symbolic operations by (a) recognizing the primitive terms, and (b) replacing them with the appropriate elementary integrals. Based on this procedure, the results of calculations for the transition probabilities for  $n' = 1, 2, 3, 4, 5$ , and 6 and arbitrary  $n$  are presented in Table I. This illustrates the power of the method. The form factors for transitions from  $K, L$ , and  $M$  shells were obtained by Bethe and Walske [18]. The form factors for transitions to continuum states with wave number  $k$  are obtained by analytical continuation replacing  $n$  with  $i/k$ . The dipole oscillator strengths for  $n - n'$  transitions,

$$f_{nn'} = 2\Delta E_{n,n'} \lim_{q \rightarrow 0} \frac{P_{nn'}(q)}{q^2},$$

can be readily deduced from the results presented in Table I.



- [1] M.T. Frey, F.B. Dunning, C.O. Reinhold, S. Yoshida, and J. Burgdörfer, *Phys. Rev. A* **59**, 1434 (1999).
- [2] See, e.g., N. F. Mott and H. S. W. Massey, *The Theory of Atomic Collisions* (Oxford University Press, London, 1965).
- [3] D. Vrinceanu and M. R. Flannery, *Phys. Rev. Lett.* **82**, 3412 (1999).
- [4] M. R. Flannery, in *Rydberg States of Atoms and Molecules*, edited by R. F. Stebbings and F. B. Dunning (Cambridge University Press, Cambridge, 1983), p. 393.
- [5] I. Bersons and A. Kulsh, *Phys. Rev. A* **55**, 1674 (1997); **59**, 1399 (1999).
- [6] I.L. Beigman and V.S. Lebedev, *Phys. Rep.* **250**, 95 (1995); V. S. Lebedev and I. L. Beigman, *Physics of Highly Excited Atoms and Ions* (Springer-Verlag, Berlin, 1998).
- [7] Y. Fang, A.N. Vasil'ev, and V.V. Mukhailin, *Phys. Rev. A* **58**, 3683 (1998).
- [8] F. Gounand and L. Petitjean, *Phys. Rev. A* **30**, 61 (1984).
- [9] L. Vriens, in *Case Studies in Atomic Collision Physics I*, edited by E. W. McDaniel and M. R. C. McDowell (North-Holland, Amsterdam, 1969), p. 364.
- [10] M.V. Berry, *Philos. Trans. R. Soc. London* **287**, 30 (1977); C.L. Mehta, *J. Math. Phys.* **5**, 677 (1964).
- [11] E.P. Wigner, *Phys. Rev.* **40**, 749 (1932).
- [12] V. Borodin, A.K. Kazanski, and V.I. Ochkur, *J. Phys. B* **25**, 445 (1992).
- [13] A.R. Filipelli, C.C. Lin, L.W. Anderson, and J.W. McConkey, *Adv. At., Mol., Opt. Phys.* **33**, 1 (1994); M.E. Lagus, J.B. Boffard, L.W. Anderson, and C.C. Lin, *Phys. Rev. A* **53**, 1505 (1996).
- [14] E. M. Lifshitz and L. P. Pitaevski, *Physical Kinetics* (Pergamon Press, Oxford, 1981), p. 104.
- [15] Inés Samengo, *Phys. Rev. A* **58**, 2767 (1998).
- [16] M. Matsuzawa, *Phys. Rev. A* **9**, 241 (1974).
- [17] L. Hostler, *J. Math. Phys.* **5**, 591 (1964).
- [18] H.A. Bethe, *Ann. Phys. (Leipzig)* **5**, 325 (1930); M.C. Walske, *Phys. Rev.* **101**, 940 (1956).

# PHYSICAL REVIEW LETTERS

VOLUME 85

3 JULY 2000

NUMBER 1

## Quantal-Classical Correspondence Impulse Theory

M. R. Flannery and D. Vranceanu

*School of Physics, Georgia Institute of Technology, Atlanta, Georgia 30332*

(Received 10 January 2000)

The quantal impulse cross section is derived in a novel form appropriate for direct classical correspondence. The classical impulse cross section is then uniquely defined and yields the first general classical expression for  $n\ell - n'\ell'$  collisional transitions. The derived cross sections satisfy the optical theorem and detailed balance. Direct connection with the classical binary encounter approximation is also firmly established. The unified method introduced is general in its application to various collision and recombination processes and enables new directions of enquiry to be pursued quite succinctly.

PACS numbers: 03.65.Sq, 31.15.Gy, 32.80.Cy, 34.60.+z

The quantal impulse approximation (QIA) is an established and productive cornerstone in general scattering theory [1]. It is based on the assumption that an inelastic collision of incident particle  $i$  with a two-particle subsystem (2,3) results from each binary ( $i-j$ ) scattering under the two-body interaction  $V_{ij}$  alone, leaving the "spectator" particle  $k$  unaffected. The internal interaction  $V_{jk}$  between the "active" particle  $j$  and the spectator particle  $k$  is ignored during the ( $i-j$ ) collision except insofar as it generates a distribution  $\rho(\mathbf{p}_{jk})d\mathbf{p}_{jk}$  over the relative momentum  $\mathbf{p}_{jk}$  of particles  $j$  and  $k$ . This approach has been invaluable in nuclear physics for high-energy neutron scattering by complex nuclei [1] and in atomic physics for atom-Rydberg atom collisions at thermal energies [2-7] and for electron (ion)-atom and atom-atom collisions [8,9] at high energies. It is also valuable, for example, in the study of three-body recombination,  $\text{Li} + \text{Li} + \text{Li} \rightarrow \text{Li}_2 + \text{Li}$  which limits the density and lifetimes of Bose-Einstein condensates at ultralow energy, and  $e^+ + \bar{p} + e^+ \rightarrow \bar{H} + e^+$  for the formation of antihydrogen.

A classical binary-encounter approximation (BEA) has also been formulated for Rydberg collisions [3] and for high-energy collisional ionization [8-10]. Although QIA and BEA are conceptually connected, the formal interrelationship between them is quite complex and has never been firmly established. Previous studies [6,8,11] have depended on fairly complicated theoretical analysis in an effort to reduce QIA to BEA.

In this Letter, the quantal impulse approximation is presented in a new form which provides quite naturally "the royal road" to classical correspondence. A classical impulse approximation can then be uniquely defined. The novel expression yields the first general classical cross section for  $n\ell - n'\ell'$  transitions and the standard result for  $n\ell - n'$  transitions. The derived cross sections satisfy the optical theorem (which implies probability conservation) and detailed balance. The method introduced then permits BEA formulas to be derived quite succinctly and in a unified way. There is substantial renewed [7,10-15] interest in the power of classical dynamics in almost all fields of modern physics, attributed to the desire [15] to obtain a more thorough understanding of the classical-quantal correspondence. This present development provides a profound and important quantal-classical connection in collision physics. The new formulation also provides a natural origin for development of new semiclassical methods.

The transition T-matrix for the free-free ( $\mathbf{p}_{ij} \rightarrow \mathbf{p}'_{ij}$ ) scattering under the two-particle ( $i-j$ ) potential  $V_{ij}$  alone is

$$T_{ij}(\mathbf{p}_{ij}, \mathbf{p}'_{ij}) = \langle \exp(i\mathbf{p}'_{ij} \cdot \mathbf{r}_{ij}/\hbar) | V_{ij}(\mathbf{r}_{ij}) | \Psi(\mathbf{p}_{ij}, \mathbf{r}_{ij}) \rangle_{\mathbf{r}_{ij}},$$

where  $\Psi(\mathbf{p}_{ij}, \mathbf{r}_{ij})$  is the exact wave function for  $i-j$  scattering in the ( $i-j$ ) center-of-mass frame  $\text{CM}(i,j)$ . The momentum transferred from  $i$  to  $j$  is

$$\mathbf{q}_j = \mathbf{p}_i - \mathbf{p}'_i = \mathbf{p}'_j - \mathbf{p}_j = \mathbf{p}_{ij} - \mathbf{p}'_{ij},$$

where the momentum of particle  $i$  is  $\mathbf{p}_i$  in the fixed  $\text{CM}(ijk)$  frame of all three particles, and is  $\mathbf{p}_{ij}$  in the

CM( $i, j$ ) frame. The primed ( $'$ ) and unprimed momenta denote postcollision and precollision values.

The quantal impulse T-matrix for  $i - (j, k)$  scattering decomposes as the sum  $T_{if} = T_{if}^{(i2)} + T_{if}^{(i3)}$  of binary collision matrices  $T_{if}^{(ij)}$ , with  $j = 2$  or  $3$ . Each  $T_{if}^{(ij)}$  in the momentum-space representation (MS) is the overlap [1,6,7],

$${}^{\text{MS}}T_{if}^{(ij)}(\mathbf{p}_i, \mathbf{p}_i') = \langle \phi_f(\mathbf{p}_{jk} + \mathbf{q}_{jk}) \times |T_{ij}(\mathbf{p}_{ij}, \mathbf{p}_{ij}')| \phi_i(\mathbf{p}_{jk}) \rangle_{\mathbf{p}_{jk}}, \quad (1)$$

of the free-free  $T_{ij}$  matrix with the initial and final momentum wave functions

$$\phi(\mathbf{p}_{jk}) = (2\pi\hbar)^{-3/2} \int \psi(\mathbf{r}_{jk}) \exp(-i\mathbf{p}_{jk} \cdot \mathbf{r}_{jk}/\hbar) d\mathbf{r}_{jk},$$

for the  $(j, k)$  subsystem. The momentum transferred to  $j - k$  relative motion is

$$\mathbf{q}_{jk} = \mathbf{p}_{jk}' - \mathbf{p}_{jk} = \frac{M_k}{M_j + M_k} \mathbf{q}_j,$$

where  $p_{jk}$  is the relative momentum in the initial CM( $j, k$ ) frame. After the  $(i - j)$  collision, CM( $j, k$ ) moves with the residual momentum  $M_j \mathbf{q}_j / (M_j + M_k)$ . The binary  $T_{if}^{(ij)}$  matrix has also the configuration space (CS) representation

$${}^{\text{CS}}T_{if}^{(ij)}(\mathbf{p}_i, \mathbf{p}_i') = \langle \exp(i\mathbf{p}_i' \cdot \mathbf{r}_i/\hbar) \psi_f(\mathbf{r}_{jk}) \times |V_{ij}(\mathbf{r}_{ij})| \Psi_i^+(\mathbf{p}_i; \mathbf{r}_i, \mathbf{r}_{jk}) \rangle_{\mathbf{r}, \mathbf{r}_{jk}}. \quad (2)$$

The impulse approximation [6] for the initial total system wave function in (2) is

$$\Psi_i^+ \approx \Psi_{\text{imp}}(\mathbf{p}_i; \mathbf{r}_i, \mathbf{r}_{jk}) \\ = (2\pi\hbar)^{-3/2} \int \phi_i(\mathbf{p}_{jk}) \Phi(\mathbf{p}_{ij}, \mathbf{p}_{ij}'; \mathbf{r}_{ij}, \mathbf{r}_{jk}) d\mathbf{p}_{jk},$$

where the active and spectator particles are  $j$  and  $k$ , respectively. The free-free  $(i - j)$  scattering wave function is  $\Psi(\mathbf{p}_{ij}, \mathbf{r}_{ij})$  in the CM( $i, j$ ) frame and is

$$\Phi(\mathbf{p}_{ij}, \mathbf{p}_k; \mathbf{r}_{ij}, \mathbf{r}_k) = \exp(i\mathbf{p}_k \cdot \mathbf{r}_k/\hbar) \Psi(\mathbf{p}_{ij}, \mathbf{r}_{ij})$$

in the fixed CM( $ijk$ ) frame. With the aid of the  $(\mathbf{r}_{jk}, \mathbf{r}_i) \rightarrow (\mathbf{r}_{ij}, \mathbf{r}_k)$  transformation equations for the integration variables in Eq. (2), of the identity  $\mathbf{p}_i \cdot \mathbf{r}_i + \mathbf{p}_{jk} \cdot \mathbf{r}_{jk} = \mathbf{p}_k \cdot \mathbf{r}_k + \mathbf{p}_{ij} \cdot \mathbf{r}_{ij}$ , and of  $\psi(\mathbf{r}_{jk}) = (2\pi\hbar)^{-3/2} \int \phi(\mathbf{p}_{jk}) \exp(i\mathbf{p}_{jk} \cdot \mathbf{r}_{jk}/\hbar) d\mathbf{p}_{jk}$ , it can be shown that the momentum-space and configuration-space representations (1) and (2) of  $T_{if}$  are equivalent.

The quantal differential cross section is

$$\frac{d\sigma_{if}}{d\mathbf{p}_i'} = \frac{v_i'}{v_i} \left( \frac{1}{4\pi} \frac{2\mathcal{M}_i}{\hbar^2} \right)^2 |T_{if}(\mathbf{p}_i, \mathbf{p}_i')|^2, \quad (3)$$

where  $\mathcal{M}_i = M_i(M_j + M_k)/(M_i + M_j + M_k)$  is the reduced mass of the  $i - (j + k)$  collision system and  $\mathbf{p}_i^{(i)}$

are the momenta of  $i$  with  $\mathbf{v}_i^{(i)}$  measured with respect to initial CM( $j, k$ ). Although QIA assumes that each scattering is a *separate* event, the cross section (3) involves  $|T_{if}|^2 = |T_{if}^{(i2)} + T_{if}^{(i3)}|^2$  which exhibits *interference* between the two-body  $(i - j)$  scattering amplitudes. For three identical particles  $|T_{if}|^2 = 4|T_{if}^{(ij)}|^2$ . The classical representation of Eq. (3), however, involves only  $|T_{if}|^2 = |T_{if}^{(i2)}|^2 + |T_{if}^{(i3)}|^2$  which is valid for binary and independent scattering (as, e.g., in Rydberg collisions).

The key idea of this paper is to find a phase-space representation for  $|T_{if}^{(ij)}|^2$ . This is accomplished by writing

$$|T_{if}^{(ij)}(\mathbf{p}_i, \mathbf{p}_i')|^2 = \{ {}^{\text{CS}}T_{if}^{(ij)} \} \{ {}^{\text{MS}}T_{if}^{(ij)*} \} \quad (4)$$

as the product of the momentum-space (1) and the configuration-space (2) representations. It can be shown that Eq. (4) with Eqs. (1) and (2) for  $(i - j)$  scattering *alone* reduces to

$$|T_{if}^{(ij)}(\mathbf{p}_i, \mathbf{p}_i')|^2 = (2\pi\hbar)^3 \int d\mathbf{p} \int d\mathbf{r} \rho_f^*(\mathbf{r}, \mathbf{p} + \mathbf{q}) \times |T_{ij}(\mathbf{p}_{ij}, \mathbf{p}_{ij}')|^2 \rho_i(\mathbf{r}, \mathbf{p}), \quad (5)$$

where  $(\mathbf{r}_{jk}, \mathbf{p}_{jk}, \mathbf{q}_{jk})$  are now denoted by  $(\mathbf{r}, \mathbf{p}, \mathbf{q})$ . The internal  $(j - k)$  quantal distribution in phase space is

$$\rho(\mathbf{r}, \mathbf{p}) = (2\pi\hbar)^{-3/2} \psi(\mathbf{r}) e^{-i\mathbf{p} \cdot \mathbf{r}/\hbar} \phi^*(\mathbf{p}), \quad (6)$$

in agreement with that [12] previously defined. The standard probability densities  $\rho(\mathbf{r}) = \int \rho(\mathbf{r}, \mathbf{p}) d\mathbf{p} = |\psi(\mathbf{r})|^2 = R_{\ell\ell}^2(r) |Y_{\ell m}(\hat{\mathbf{r}})|^2$  in configuration space and  $\rho(\mathbf{p}) = \int \rho(\mathbf{r}, \mathbf{p}) d\mathbf{r} = |\phi(\mathbf{p})|^2 = \phi_{\ell\ell}^2(p) |Y_{\ell m}(\hat{\mathbf{p}})|^2$  in momentum space are recovered directly from (6), which is the standard ordered version [12] of the Wigner distribution [16]. In terms of the phase-space distributions for the initial and final internal  $j - k$  states, the differential cross section (3), with Eq. (5) for independent scattering, separates into  $(i-2)$  and  $(i-3)$  components, each given by

$$\frac{d\sigma_{if}^{(ij)}}{d\mathbf{p}_i'} = \frac{v_i'}{v_i} \left( \frac{\mathcal{M}_i}{M_{ij}} \right)^2 (2\pi\hbar)^3 \int d\mathbf{p} \int d\mathbf{r} \times \{ \rho_f^*(\mathbf{r}, \mathbf{p} + \mathbf{q}) |f_{ij}(\mathbf{p}_{ij}, \mathbf{p}_{ij}')|^2 \rho_i(\mathbf{r}, \mathbf{p}) \}, \quad (7)$$

where the  $(i - j)$  and  $i - (j + k)$  reduced masses are  $M_{ij}$  and  $\mathcal{M}_i$ , respectively. The scattering amplitude,  $f_{ij}(\mathbf{p}_{ij}, \mathbf{p}_{ij}') = f_{ij}[g(\mathbf{p}), q_j]$ , for free-free  $(i - j)$  collisions is a general function of momentum change  $q_j$  and of the  $i - j$  relative velocity  $\mathbf{g} = \mathbf{v}_i - \mathbf{v}_j$ . It therefore depends implicitly via  $g$  on the  $j - k$  relative momentum  $\mathbf{p}$ . Thus, (5) and (7) are the free-free transition probabilities/differential cross sections, respectively, averaged over the initial and final phase space distributions.

The above novel expression (7) for the quantal impulse cross section (3) has the phase-space representation appropriate for direct classical correspondence, obtained by

replacing the quantal densities  $\rho_{i,f}$  of (6) by the corresponding classical phase-space distributions [12]:

$$\rho^c(E, L; \mathbf{r}, \mathbf{p}) d\mathbf{r} d\mathbf{p} = \{\delta(p^2/2m + V(r) - E) dE\} \times \{\delta(|\mathbf{r} \times \mathbf{p}| - L) dL\} \frac{d\mathbf{r} d\mathbf{p}}{(2\pi\hbar)^3}, \quad (8)$$

for a  $(j-k)$  symmetric interaction  $V(r)$ . The internal Hamiltonian  $H(r, p) = p^2/2m + V(r)$  of the  $j-k$  subsystem (with relative momentum  $\mathbf{p}_{jk} \equiv \mathbf{p}$  and reduced mass  $M_{jk} \equiv m$ ) and the internal angular momentum  $\mathbf{L}(\mathbf{r}, \mathbf{p}) = \mathbf{r} \times \mathbf{p}$  are conserved quantities in phase space. The distribution (8) holds also for bound states  $(n, \ell)$  but with  $dE$  and  $dL$  replaced [12] by  $\hbar \nu_{nl}$  and  $\hbar$ , respectively, where the frequency (or inverse period) for bounded radial motion is  $\nu_{nl} = \tau_{nl}^{-1}$ . The distribution (8) is normalized to  $\int \rho_{n,\ell}^c d\mathbf{r} d\mathbf{p} = (2\ell + 1)$  states over all of phase space.

(a)  $n\ell \rightarrow n'\ell'$  transitions.—The angular  $\hat{\mathbf{r}}(\theta_r, \phi_r)$  integration, resulting from Eq. (8) in Eq. (7), involves the angular momentum overlap integral,

$$\hat{R}_{if}(r, q) = \frac{(2\pi\hbar)^{-3}}{4\pi} \int_{-1}^1 \delta(rp \sin\theta_r - L) d(\cos\theta_r) \times \int_0^{2\pi} \delta(rp' \sin\bar{\theta}_r - L') d\phi_r, \quad (9)$$

where  $\cos\theta_r = \hat{\mathbf{p}} \cdot \hat{\mathbf{r}}$  and  $\cos\bar{\theta}_r = \hat{\mathbf{p}}' \cdot \hat{\mathbf{r}}$  with  $\mathbf{p}$  along the  $Z$  axis and with  $\mathbf{p}' = \mathbf{p} + \mathbf{q}$  fixed in the  $XZ$  plane. Integration via the techniques outlined in [12] yields

$$\hat{R}_{if}(r, q) dE dL dE' dL' = \frac{\hbar^3}{m^2} \rho_{n,\ell}^c(r) \rho_{n',\ell'}^c(r) \times [G_{if}^+(r, q) + G_{if}^-(r, q)], \quad (10)$$

$$\sigma_{n\ell, n'\ell'}^{(ij)}(\mathbf{p}_i) = \frac{2\pi}{M_{ij}^2 v_i^2} \int_{q_-}^{q_+} q_j dq_j \int_{\mathcal{R}(q)} P_{n\ell, n'\ell'}(r, q) dr \left\{ \frac{1}{\pi} \int_{g^2(r, q)}^{g^{*2}(r, q)} \frac{|f_{ij}(g, q_j)|^2 dg^2}{[(g^2 - g_-^2)(g_+^2 - g^2)]^{1/2}} \right\}. \quad (12)$$

The classical probability that the  $i-j$  impulsive transition transfers momentum  $q$  to the  $j-k$  system with internal separation  $r$  in the interval  $r, r + dr$  is

$$P_{n\ell, n'\ell'}(r, q) dr = \left( \frac{2\pi m^2}{q} \right) [4\pi \hat{R}_{if} r^2 dr dE dL dE' dL'] = (4\pi)^2 \rho_{n,\ell}^c(r) \rho_{n',\ell'}^c(r) r^2 \frac{\hbar^3}{2q} [G_{if}^+(r, q) + G_{if}^-(r, q)] \Theta(r, q). \quad (13)$$

The classical limits to the  $g^2$  integral in Eq. (12) for fixed  $(r, q)$  are

$$g_{\pm}^2(r, q) = v_i^2 + v_j^2(r) - 2v_i v_j(r) \times \cos[\bar{\theta}^*(r, q) \pm \theta_i(q)],$$

where, for given transfers  $\mathcal{E} = E' - E$  and  $q$  in energy and momentum, the angles that  $\mathbf{p}_i$  and  $\mathbf{p}$  each make with  $q$  are, respectively, determined by

The classical radial density and the classical radial probability for continuum states of energy  $E$  are

$$\rho_{E\ell}^c(r) = \int \rho_{n,\ell}^c(\mathbf{r}, \mathbf{p}) d\mathbf{p} = 4\pi L dE dL / [(2\pi\hbar)^3 r^2 \dot{r}],$$

and  $4\pi \rho_{E\ell}^c r^2 dr = (2L dL / \hbar^2) (2dE dt / \hbar)$ , respectively. The bound state distribution is  $\rho_{n,\ell}^c = [(2\ell + 1)/4\pi] (2\dot{r} / \tau_{n,\ell})$ . Each of the contributions,

$$G_{if}^{\pm}(r, q) = [(q^2 - A_{\pm}^2)(B_{\pm}^2 - q^2)]^{-1/2}, \quad (11)$$

must be real, so that  $q$  must then lie within the classically accessible range given by

$$A_{\pm}^2(r) = m^2(\dot{r} \pm \dot{r}')^2 + (L - L')^2/r^2 \leq q^2 \leq B_{\pm}^2(r) = m^2(\dot{r} \pm \dot{r}')^2 + (L + L')^2/r^2.$$

For a given momentum transfer  $q$ , the  $r$  integration proceeds over the various [12] radial ranges  $\mathcal{R}(q)$  within which the  $G_{if}^{\pm}$  are real. The initial and final radial speeds  $\dot{r}$  and  $\dot{r}'$  determined by

$$\frac{1}{2} m \dot{r}^{(n)\ell} = E^{(n)} - V(r) - L^{(n)\ell}/2mr^2$$

are functions only of  $r$  for given initial  $n\ell$  and final  $n'\ell'$  states. Hence,  $G_{if}^{\pm}(r, q)$  and the angular integral  $\hat{R}_{if}(r, q)$  depend only on  $r$  and  $q$  and not on  $\mathbf{p}$ . The remaining  $\mathbf{p}$  integration in Eq. (7) therefore involves only the overlap,

$$\int \delta[H(r, \mathbf{p}) - E] |f_{ij}(g(\mathbf{p}), q_j)|^2 \times \delta[H(r, \mathbf{p} + \mathbf{q}) - E'] d\mathbf{p},$$

of the  $i-j$  free-free differential cross section with the initial and final energy distributions at a fixed  $r$ . When integrated [17] and combined with the angular momentum overlap integral (9), the cross section for  $n\ell - n'\ell'$  transitions resulting from  $(i-j)$  collisions is

$$\cos\theta_i(q, \mathcal{E}) = (2\mathcal{M}_i \mathcal{E} + q_j^2)/2p_i q_j,$$

$$\cos\bar{\theta}^*(q, \mathcal{E}) = (2m\mathcal{E} - q^2)/2pq,$$

in accord with energy and momentum conservation, implicit in the  $\delta$  function and impulse conditions. Since  $|\cos\bar{\theta}| \leq 1$ , the  $(j, k)$  relative momentum  $p > p_0 = |2m\mathcal{E} - q^2|/2q$  so that the step function  $\Theta$  in  $P_{n\ell, n'\ell'}$  has value 1 for  $p(r) \geq p_0$  and zero

otherwise. Since  $|\cos\theta_i| \leq 1$ , then  $q_- = |p_i - p'_i| \leq q_j \leq p_i + p'_i = q_+$ , as expected.

The integrated probability for the impulsive ( $n\ell - n'\ell'$ ) transition,

$$P_{n\ell, n'\ell'}(q) = \int_{\mathcal{R}} P_{n\ell, n'\ell'}(r, q) dr, \quad (14)$$

is simply the classical form factor as defined in Ref. [12]. Equation (12) therefore illustrates the interesting manner in which  $P_{n\ell, n'\ell'}$  becomes deconvoluted over  $r$  when the general ( $i - j$ ) scattering cross section  $\sigma(g, q_j)$  depends additionally on the ( $i - j$ ) relative speed  $g$ . For  $g$ -independent  $\sigma$ , (12) reduces to the standard impulse result [1,6] involving the full form factor (14).

Since the integration limits and  $P_{i,f}$  are symmetrical in  $i$  and  $f$ , the basic cross section (12) satisfies the detailed balance relation  $p_i^2 \sigma_{n\ell, n'\ell'}(\mathbf{p}_i) = p_i'^2 \sigma_{n'\ell', n\ell}(\mathbf{p}_i')$ . "Semi-

quantal" probabilities may now be defined by replacing either or both of the classical radial densities  $\rho_{n\ell}^c$  in (13) by their  $\hbar$ -independent quantal equivalents,

$$\rho_{n\ell}^q(r) = \sum_m |\psi_{n\ell m}(r)|^2 = (2\ell + 1)R_{n\ell}^2(r)/4\pi,$$

for both bound  $n\ell$  and continuum  $\epsilon\ell$  states.

(b)  $n\ell \rightarrow n'\ell'$  transitions.—On integrating Eq. (9) over all final angular momenta  $L'$ , then

$$\begin{aligned} \hat{R}'_{ij} dE dL &= \left\{ \frac{1}{2} \int_{-1}^1 \delta[r p \sin\theta_r - L] d(\cos\theta_r) \right\} \frac{dE dL}{(2\pi\hbar)^3} \\ &= \frac{1}{4\pi m p} \rho_{n\ell}^c(r). \end{aligned} \quad (15)$$

The classical probability for the  $n\ell - (E', E' + dE')$  impulsive transitions in the ( $j, k$ ) subsystem with internal momenta in the interval  $(p, p + dp)$  is then

$$P_{n\ell, E'}(p, q) dp = \left( \frac{2\pi m^2}{q} \right) [4\pi \hat{R}'_{ij} r^2 dr dE dL dE'] = \frac{mdE'}{2pq} [4\pi \rho_{n\ell}^c(p) p^2 dp],$$

since  $4\pi \rho_{n\ell}^c(p) p^2 dp = 4\pi \rho_{n\ell}^c(r) r^2 dr$  under the energy constraint  $p^2(r) = 2m[E - V(r)]$  for the initial classical distribution. Note that  $m/q = M_j/q_j$ . The classical impulse cross section for  $n\ell - (E', E' + dE')$  transitions is therefore

$$\sigma_{n\ell, E'}^{(ij)}(\mathbf{p}_i) = \frac{2\pi}{M_{ij}^2 v_i^2} \int_{q_-}^{q_+} q_j dq_j \int_{p_0(q)}^{\infty} P_{n\ell, E'}(p, q) dp \left\{ \frac{1}{\pi} \int_{g_-^2(p, q)}^{g_+^2(p, q)} \frac{|f_{ij}(g, q_j)|^2 dg^2}{[(g^2 - g_-^2)(g_+^2 - g^2)]^{1/2}} \right\}. \quad (16)$$

The cross section for  $n\ell - n'$  transitions is obtained by substituting  $\hbar\nu_{n'}$  for  $dE'$  in  $P_{n\ell, E'}$ . By adopting the quantal distribution  $(2\ell + 1)\phi_{n\ell}^2(p)$  for  $4\pi \rho_{n\ell}^c(p)$ , then Eq. (16) provides semiclassical cross sections [6].

(c) *Relationship with Optical Theorem and Classical Binary Encounter Theory.*—Integration of Eq. (16) over all possible final  $E'$  states is facilitated by recognizing that the required integral,

$$\int_{g_-^2}^{g_+^2} \frac{2g/q_j dE'}{[(g^2 - g_-^2)(g_+^2 - g^2)]^{1/2}} = \int_{\mathcal{E}_-}^{\mathcal{E}_+} \frac{d\mathcal{E}}{[(\mathcal{E} - \mathcal{E}_-)(\mathcal{E}_+ - \mathcal{E})]^{1/2}},$$

is simply  $\pi$ . The classical limits  $\mathcal{E}_{\pm}(q_i, \hat{\mathbf{r}}_i \cdot \hat{\mathbf{v}}_j; v_i, v_j)$  to the energy transfer  $\mathcal{E}$ , for the prescribed fixed arguments, need not then be specified. The cross section for all elastic and inelastic transitions is then

$$\begin{aligned} \sigma_{n\ell}^{(ij)}(v_i) &= \sum_{n'} \sigma_{n\ell, n'}(v_i) + \int_0^{\infty} \sigma_{n\ell, \epsilon}(v_i) d\epsilon \\ &= \frac{1}{v_i} \int \rho_{n\ell}^c(\mathbf{p}) d\mathbf{p} \int \left\{ g \frac{d\sigma_{ij}}{d\hat{\mathbf{p}}_{ij}} \right\} d\hat{\mathbf{p}}_{ij}. \end{aligned} \quad (17)$$

i.e., the rate  $v_i \sigma_{n\ell}$  for transitions to all states is therefore the rate for all  $i - j$  binary encounters, averaged over the initial momentum function for  $j$  in the field of  $k$ . Expression (17) simply restates the optical theorem, which, when applied to (1), provides (17) directly.

Expression (17) is the original basis [8] of the standard classical *binary-encounter approximation* (BEA) for energy-changing collisions, where the  $\hat{\mathbf{p}}'_{ij}$ -region of integration is constrained by the required energy change. Previous BEA semiclassical results [3,6] for  $n\ell - n'$  collisional transitions can then be shown [17] to be identical with (16). Generalization [17] of BEA to cover the an-

gular momentum changes in  $n\ell - n'\ell'$  collisional transitions is made simply by replacing  $\int \rho_{n\ell}(\mathbf{p}) d\mathbf{p}$  in (17) by the integral  $\int \rho_{n\ell}(\mathbf{p}, \mathbf{r}) d\mathbf{p} d\mathbf{r}$  over phase space. See also Refs. [13,14].

In summary, the quantal impulse cross section (3) has been presented in a valuable new form (7) which is the appropriate representation for direct classical correspondence. The classical impulse cross section has been defined by (7) with (8) which yields, in quite a succinct fashion, the first general expression (12) for the classical impulse cross section for  $n\ell - n'\ell'$  and  $n\ell - \epsilon\ell'$  electronic transitions. The cross section satisfies the optical theorem and detailed balance. Direct connection with the classical binary encounter approximation (17) has been established and the derived  $n\ell - n'$  and  $n\ell - \epsilon$  cross sections (16) reproduce the standard BEA cross sections [3,7]. The present unified method can also furnish semiclassical impulse cross sections, obtained simply by adopting semiclassical phase-space distributions (at present, unknown) within Eq. (7). Although applied here to a time-independent formulation of collisional

electronic transitions in an atom, the prescribed method is general in that it can be applied, where appropriate, to atom-molecule rovibrational collisions, to three-body recombination, and to explicit time-dependent problems as laser-pulse excitation [18]. The method presented also helps elucidate, quite succinctly, the role played by the quantal-classical correspondence in collision dynamics.

This work is supported by grants from AFOSR: F 49620-99-1-0277 and NSF: 98-02622.

- 
- [1] M. L. Goldberger and K. M. Watson, *Collision Theory* (Wiley, New York, 1964), pp. 683–865.
  - [2] E. Fermi, *Nuovo Cimento* **11**, 157 (1934).
  - [3] M. R. Flannery, *Ann. Phys. (N.Y.)* **61**, 465 (1970); **79**, 480 (1973).
  - [4] *Rydberg States of Atoms and Molecules*, edited by R. F. Stebbings and F. B. Dunning (Cambridge University Press, New York, 1983).
  - [5] T. F. Gallagher, *Rydberg Atoms* (Cambridge University Press, Cambridge, England, 1994).
  - [6] M. R. Flannery, *Phys. Rev. A* **22**, 2408 (1980).
  - [7] V. S. Lebedev and I. L. Beigman, *Physics of Highly Excited Atoms and Ions* (Springer-Verlag, Berlin, 1998).
  - [8] L. Vriens, *Case Studies in Atomic Collision Physics I*, edited by E. W. McDaniel and M. R. C. McDowell (North-Holland, Amsterdam, 1969), p. 364.
  - [9] M. R. Flannery, *J. Phys. B* **4**, 892 (1971).
  - [10] M. Gryzinski and J. A. Kunc, *J. Phys. B* **32**, 5789 (1999).
  - [11] V. S. Lebedev, *J. Phys. B* **24**, 1977 (1991).
  - [12] D. Vrinceanu and M. R. Flannery, *Phys. Rev. Lett.* **82**, 3412 (1999); *Phys. Rev. A* **60**, 1053 (1999).
  - [13] A. Haffad and M. R. Flannery, *Phys. Rev. A* **50**, 429 (1994).
  - [14] G. Ivanovski, R. K. Janev, and E. A. Solov'ev, *J. Phys. B* **28**, 4799 (1995).
  - [15] K. G. Kay, *Phys. Rev. Lett.* **83**, 5190 (1999).
  - [16] E. P. Wigner, *Phys. Rev.* **40**, 749 (1932).
  - [17] M. R. Flannery (to be published).
  - [18] G. Alber and O. Zobay, *Phys. Rev. A* **59**, R3174 (1999).

## LETTER TO THE EDITOR

# Quantal Stark mixing at ultralow collision energies

D Vrinceanu and M R Flannery

School of Physics, Georgia Institute of Technology, Atlanta, GA 30332, USA

Received 9 June 2000, in final form 11 September 2000

**Abstract.** A new exact solution of the time-dependent quantal equation is obtained for the full array of angular momentum mixing transitions  $n\ell \rightarrow n\ell'$  in atomic hydrogen induced by collisions with charged particles at ultralow energies. Based on this new solution, efficient numerical procedures are devised. It is proven that the present (fixed-frame) solution is equivalent to the rotating-frame approach described by Kazansky and Ostrovsky (Kazansky A K and Ostrovsky V N 1996 *Phys. Rev. Lett.* 77 3094) and that it overcomes the difficulties therein. Analytic expressions for low quantum numbers  $n$  are presented. Numerical results for the transition array with  $n = 28$  are reported.

Stark mixing occurs when the electron of a Rydberg atom (in a state with principal quantum number  $n$ ) changes its angular momentum  $\ell$ , without changing its energy, as a result of a collision, at large impact parameter  $b$ , with a slow massive particle of charge  $Z_1e$  moving with velocity  $v$ . It is important in many areas of atomic physics, as in the Auger (or autoionization) process which follows the collision between ions and atoms (Miraglia and Macek 1990), in ZEKE spectroscopy (Merk and Zare 1994), in astrophysics (e.g. Percival 1983), in recent efforts (Mensh'ikov and Fedichev 1995) to produce anti-hydrogen at 4 K and for general three-body recombination (Flannery and Vrinceanu 1998) at ultralow energies. The first stage in ultralow energy electron-ion recombination (Flannery and Vrinceanu 1998) at temperature  $T_e$  is a very rapid collisional capture into high Rydberg states with high angular momentum  $\ell$  and large radiative lifetimes at a rate proportional to  $T_e^{-4.5}$ . Thus the  $\ell$ -mixing is an essential step in producing the low-angular-momentum states required to radiatively decay at a relatively high rate to low levels, thereby stabilizing the recombination.

On considering the Rydberg atom in a frame rotating with the internuclear axis, the Stark mixing problem can be reduced to the problem of the Rydberg atom in mixed *static fields*: electric, provided by the projectile ion, and magnetic, produced by the non-inertial (Coriolis) forces. In this way, the well known equations, in both classical (Born 1960) and quantum (Demkov *et al* 1970) mechanics, for the problem of interaction between weak fields and an atom, can be adopted to provide, in principle, a solution for the Stark mixing problem. Both quantal (Kazansky and Ostrovsky 1996a, b) and classical (Kazansky and Ostrovsky 1996b, c) versions of this approach have succeeded only for  $\ell = 0$  to higher angular momentum  $\ell'$  transitions, appropriate to the experiments described in a paper by Sun and MacAdam (1993).

This letter presents a new exact solution for the Stark mixing process, valid for transitions  $n\ell \rightarrow n\ell'$  between *any states* within the shell of energy  $E_n$ . The present theory in the fixed-frame representation is shown to be formally equivalent to the rotating-frame approach (Kazansky and Ostrovski 1996a, b), but, in contrast to it, the full array of transition amplitudes can be obtained at once by efficient numerical procedures. Results for transitions within the

$n = 28$  energy shell are presented. Analytical formulae for the transition probabilities are possible for low  $n$ .

The trajectory of the projectile, initially moving along the positive  $Z$  direction, is assumed to be confined in the  $YOZ$  plane. In addition to the Hamiltonian  $H_0 = p^2/2m_e - e^2/r$ , the angular momentum  $L = r \times p$  of the unperturbed Rydberg electron and the Runge-Lenz (or eccentricity) vector,

$$A = \left[ p^2 r - (p \cdot r)p - m_e e^2 \frac{r}{r} \right] / p_n, \quad (1)$$

directed toward the pericentre and normalized to angular momentum units, are also conserved. Here  $p_n = \sqrt{-2m_e E_n}$ . These quantities define the dynamic  $SO(4)$  symmetry of the hydrogen atom. Because the  $SO(4)$  group is isomorphic with the direct product  $SO(3) \oplus SO(3)$  of two rotation groups, a special decomposition,  $L = M + N$  and  $A = M - N$ , permits the dynamics of the hydrogen atom to be separated into two decoupled motions. The generators  $M$  and  $N$  act independently as angular momenta and are also conserved quantities for the unperturbed Rydberg atom.

The orbital electron interacts with the time-dependent electric field  $\tilde{E}(t)$  generated by the passing projectile of charge  $Z_1 e^2$ . In the weak-field approximation, this field is constant over the spatial extension of the atom. In this approximation, which is the same as the dipole approximation, the interaction potential  $V = e\tilde{r} \cdot \tilde{E}$  is

$$V(r, R) = -Z_1 e^2 \frac{R \cdot r}{R^3} = \frac{Z_1 e^2}{vb} \frac{d\Phi}{dt} \hat{R} \cdot r = \frac{Z_1 e^2}{vb} \frac{d\Phi}{dt} (y \sin \Phi + z \cos \Phi) \quad (2)$$

where  $R$  is the internuclear vector and  $\Phi$  is the angle between  $R$  and the  $OZ$ -axis. The angular momentum of relative motion  $L_{rel} = \mu R^2 \dot{\Phi} = \mu vb$ , where  $\mu$  is the reduced mass of the projectile-target system, remains conserved since  $L_{rel} \gg L$ , so  $L_{rel}$  and  $L$  are effectively decoupled. A classical trajectory for the relative motion is then valid.

If the projectile moves very slowly, the orbital electron adjusts itself adiabatically to the ion perturbation and no energetic transitions occur. In this limit, Pauli's replacement rule  $r \approx \langle r \rangle = -3A/2p_n$  is valid within the  $n$  energy shell (see Vranceanu and Flannery (2000) for a detailed explanation). The perturbing potential (2) can then be written in terms of the components  $A_2$  and  $A_3$  as

$$V(\alpha) = -\alpha \frac{d\Phi}{dt} (A_2 \sin \Phi + A_3 \cos \Phi)$$

where the Stark parameter  $\alpha = 3Z_1 a_n v_n / 2bv$  and  $a_n$  and  $v_n$  are the average electron-orbit radius and velocity.

The Schrödinger equation for the time evolution operator  $U(t, t_0)$  is

$$i\hbar \frac{\partial U}{\partial t} = (H_0 + V)U \quad (3)$$

where  $H_0$  is the free atom Hamiltonian and  $V$  is the interaction potential (2). The position operator and hence the perturbation potential (2) commute with the unperturbed Hamiltonian, as one can prove directly from the matrix elements of the commutator  $[r, H_0]$  between any states within the energy  $E_n$  shell. The potential in the interaction representation

$$V_I = e^{iH_0 t/\hbar} V e^{-iH_0 t/\hbar}$$

is then identical with the potential in the Schrödinger representation ( $V_I = V$ ). The equation to be solved, in the interaction representation, is

$$i\hbar \frac{\partial U_I}{\partial t} = -\alpha \frac{d\Phi}{dt} (A_2 \sin \Phi + A_3 \cos \Phi) U_I \quad (4)$$



where  $U_1(t, t_0) = \exp(iH_0t/\hbar)U\exp(-iH_0t_0/\hbar)$ . Because the set of operators  $\{L_1, A_2, A_3\}$  is closed under the commutation operation and generates the rotation group  $SO(3)$ , the solution of equation (4) is obtained in terms of elements of this group as

$$U_1(t, t_0) = e^{i\Phi L_1/\hbar} \exp[-i(\Phi - \Phi_0)(L_1 - \alpha A_3)/\hbar] e^{-i\Phi_0 L_1/\hbar}. \quad (5)$$

Impact angles  $\Phi$  and  $\Phi_0$  correspond to the position of the projectile at times  $t$  and  $t_0$ , respectively. The above solution (5) can be easily verified with the aid of the relations

$$\begin{aligned} e^{i\lambda A_2/\hbar} L_1 e^{-i\lambda A_2/\hbar} &= L_1 \cos \lambda + A_3 \sin \lambda \\ e^{i\lambda A_2/\hbar} A_3 e^{-i\lambda A_2/\hbar} &= A_3 \cos \lambda - L_1 \sin \lambda \\ e^{i\lambda L_1/\hbar} A_3 e^{-i\lambda L_1/\hbar} &= A_3 \cos \lambda + A_2 \sin \lambda \end{aligned}$$

which are derived from the basic identity

$$e^{\lambda A} B e^{-\lambda A} = B + \frac{\lambda}{1!} [A, B] + \frac{\lambda^2}{2!} [A, [A, B]] + \dots \quad (6)$$

and the commutation relations  $[L_1, A_2] = i\hbar A_3$ ,  $[L_1, A_3] = -i\hbar A_2$  and  $[A_2, A_3] = i\hbar L_1$ . The initial condition  $U(t_0, t_0) = 1$  is automatically satisfied. Note, in the limit as  $\alpha \rightarrow 0$ , that  $U(t_0, t) = 1$  for all time and no  $(l, m)$  transitions can then occur.

The transition amplitude for a Stark mixing process is

$$a_{\beta\alpha}^{(n)} = \langle n\beta | U_1(\infty, -\infty) | n\alpha \rangle \quad (7)$$

where the initial unperturbed state  $|n\alpha\rangle$ , at  $t = -\infty$ , evolves to the final states  $|n\beta\rangle$ , at  $t = \infty$ . Since  $\alpha$  and  $\beta$  label the states within the same energy shell, the superscript  $n$  can be omitted and all dynamics is restricted to the energy shell defined by quantum number  $n$ . The full array of transition amplitudes is given by equation (5) in (7) and is feasible and efficient for practical numerical applications since it requires only matrix operations.

The core of solution (5) is the exponential of the operator  $L_1 - \alpha A_3$ . By using basic commutator algebra, Pauli's replacement and equation (6), this operator can be diagonalized as

$$e^{-iyq/\hbar} (L_1 - \alpha A_3) e^{iyq/\hbar} = \gamma L_1$$

where  $q = (2p_n/3) \arctan \alpha$  and  $\gamma = \sqrt{1 + \alpha^2}$ . The solution (5) has therefore the alternative form

$$U_1(t, t_0) = e^{i\Phi L_1/\hbar} e^{-iyq/\hbar} e^{-iy(\Phi - \Phi_0)L_1/\hbar} e^{iyq/\hbar} e^{-i\Phi_0 L_1/\hbar} \quad (8)$$

which illustrates quite nicely how the action of the slow distant encounter charged projectile incident along the negative  $Z$ -axis can be decomposed into successive rotations about the  $X$ -axis and alternating impulsive momentum transfers  $\pm q(\alpha)$  along the  $Y$ -axis. In the limit of zero impulse  $q$ , (8) is unitary and no transitions occur. In the limit of small Stark parameter  $\alpha$  the above solution (8), for undeflected collisions  $\Delta\Phi \equiv (\Phi - \Phi_0) = -\pi$ , reduces to

$$U_1 = e^{-2iq\gamma/\hbar} + O(\alpha^2)$$

in agreement with the impulsive result (Vrinceanu and Flannery 2000).

It is however interesting to note that by introducing the Pauli replacement directly in the potential (2) and by writing the Runge-Lenz vector as  $A = M - N$ , the potential decomposes as

$$V = V_M + V_N$$

where  $V_M = -\alpha(M_2 \sin \Phi + M_3 \cos \Phi)\Phi$  and  $V_N = \alpha(N_2 \sin \Phi + N_3 \cos \Phi)\Phi$ . Because the commutators  $[M_i, N_j]$ ,  $[M_i, H_0]$  and  $[N_i, H_0] = 0$  (for any  $i, j = 1, 2, 3$  combination), the

Table 1. The four bases useful for describing the quantal states of the hydrogen atom.

Basis	Quantum numbers	Complete set of commuting observables	Origin
Orbital	$ nlm\rangle_O$	$H_0, L^2, L_3$	Standard for spherical coordinates; describes correctly the states of the field-free atom
Parabolic	$ n_1 n_2 m\rangle_P$	$H_1, H_2, L_3$	Separation of Hamiltonian $H = H_1 + H_2$ in parabolic coordinates. $\xi = r + z, \eta = r - z, \tan \varphi = y/x; n = n_1 + n_2 +  m  + 1$
Stark	$ nqm\rangle_S$	$H_0, A_3, L_3$	Parabolic basis; describes the Stark states for small electric field $\mathcal{E}$ , when the interaction $-e\mathcal{E}z$ is diagonal; $q = n_1 - n_2$
Algebraic	$ n\mu\nu\rangle_A$	$H_0, M_3, N_3$	The two rotation groups in which the dynamic symmetry group $SO(4) = SO(3) \oplus SO(3)$ decomposes; the equivalent angular momentum for both $SO(3)$ representations is $j = (n-1)/2$ ; $\mu = (m+q)/2$ and $\nu = (m-q)/2$

problem (3) becomes separable, in exactly the same way as the classical Stark mixing equations can be decoupled (Vrinceanu and Flannery 2000). The time evolution operator then factorizes as

$$U = U_{H_0} U_M U_N \quad (9)$$

where, of course,  $U_{H_0} = \exp(-iH_0(t-t_0)/\hbar)$  and both  $U_M$  and  $U_N$  are solutions of equations  $i\hbar\partial U_M/\partial t = V_M U_M$  and  $i\hbar\partial U_N/\partial t = V_N U_N$ , similar to equation (3). With the aid of the group theoretical result (5), the solutions for the operators  $U_M$  and  $U_N$  are then

$$U_M = e^{i\Phi M_1/\hbar} \exp[-i/\hbar(\Phi - \Phi_0)(M_1 - \alpha M_3)] e^{-i\Phi_0 M_1/\hbar} \quad (10)$$

and

$$U_N = e^{i\Phi N_1/\hbar} \exp[-i/\hbar(\Phi - \Phi_0)(N_1 + \alpha N_3)] e^{-i\Phi_0 N_1/\hbar}. \quad (11)$$

In calculating the amplitude (7), four interesting basis sets can be chosen for the one-electron hydrogen-like atom. Table 1 summarizes key properties of these bases. The orbital basis is useful for describing the field-free atom, before and after the collision, whereas the algebraic basis appears naturally as a basis where  $M_3$  and  $N_3$  are diagonal. The solution (9) has the simplest expression in this algebraic basis. All four bases in table 1 span the  $n^2$  degenerate energy shell and can be equally adopted to characterize the hydrogen atom. The algebraic basis spans a tensorial product of two spaces ( $|\mu\rangle \otimes |\nu\rangle$ ) corresponding to spaces used for matrix representation of the product  $SO(3) \oplus SO(3)$ . The two spaces have the same dimension because  $M^2 = N^2 = L^2 + A^2 = (n^2 - 1)\hbar^2$  and are associated with two angular momenta with  $j = (n-1)/2$ .

The transition amplitude between the two algebraic states is then the product  $a_{\mu'\nu'}^{(\mu\nu)} = a_{\mu'\mu} a_{\nu'\nu}$  of two amplitudes for  $M$  and  $N$  independent actions. Each factor is the matrix element of a  $j = (n-1)/2$ -dimensional representation of the rotations represented by equations (10) and (11). For example, from (10), one obtains  $a_{\mu'\mu} = F(\alpha)_{\mu'\mu}$ , with

$$F(\alpha) = \mathcal{D}^{(j)}[-\Phi, (1, 0, 0)] \mathcal{D}^{(j)}\left[\gamma \Delta\Phi, \left(\frac{1}{\gamma}, 0, -\frac{\alpha}{\gamma}\right)\right] \mathcal{D}^{(j)}[\Phi_0, (1, 0, 0)]$$

where  $\mathcal{D}[\phi, (n_1, n_2, n_3)]$  is the Wigner matrix representation for the rotation  $\mathcal{R}(\phi, \mathbf{n})$  with angle  $\phi$  about direction  $\mathbf{n}$  (see Louck (1996) for the explicit expression).  $\Delta\Phi$  is the polar angle  $\Phi - \Phi_0$  swept out during the interaction. The transition probability in the space of  $N$  is the element  $\nu'\nu$  of the matrix  $F(-\alpha)$ .

Calculation of the transition probability between orbital states requires the explicit unitary transformation between the orbital and algebraic bases. This can be obtained by direct scalar

products of the orbital and parabolic states for which explicit coordinate representations are known. The result may be written in terms of hypergeometric functions (Tarter 1970). However, an equivalent result is provided by the  $SO(4) \approx SO(3) \oplus SO(3)$  isomorphism. The orbital state, as a combination of two angular momentum states, is

$$|n\ell m\rangle = \sum_{\mu, \nu=-j}^j C_{\mu\nu}^{(\ell m)} |n\mu\nu\rangle$$

where the transformation matrix  $C^{(\ell m)}$  is given by the standard Clebsch–Gordan coefficients  $(j\mu j\nu|\ell m)$ . The transition probability for the  $\ell m \rightarrow \ell' m'$  transition then becomes

$$a_{\ell' m' \ell m} = \sum_{\mu\nu\mu'\nu'} C_{\mu'\nu'}^{(\ell' m')} C_{\mu\nu}^{(\ell m)} F_{\mu'\mu}(\alpha) F_{\nu'\nu}(-\alpha) \quad (12)$$

which can be expressed in matrix form as

$$a_{\ell' m' \ell m} = \text{Trace}[C^{(\ell' m')} F(-\alpha) C^{(\ell m)T} F^T(\alpha)]$$

where  $C^T$  is the transpose of matrix  $C$ . This result (12) is in exact agreement with the solution obtained by Kazansky and Ostrovsky (1996a, b), who used the rotating-frame approach.

The quantal development above is exquisite in that it follows exactly the same reasoning within the exact classical mechanics solution (Vrinceanu and Flannery 2000). This result exhibits the essential power of the  $SO(4)$  symmetry group for the energy shell of the hydrogen atom. The common  $SO(4)$  symmetry therefore transcends the chosen formulation (classical or quantal) and provides a classical–quantal correspondence at a level more fundamental than Ehrenfest's theorem and the Heisenberg correspondence.

In practice, the fourfold summation (12) and the use of the Wigner rotation matrices  $D$  in  $F(\alpha)$  are not very efficient and the difficulty of calculation increases dramatically with  $n$ . Instead, the solution (5) provides a much simpler approach, because the matrix elements of the argument in the exponential have simple expressions directly in the orbital basis. The array of transitions is obtained at once, all within one matrix exponentiation of a band diagonal matrix for which efficient algorithms are available (see e.g. Golub and Loan 1983).

When the projection of the initial and final angular momentum is not determined, the transition probability is

$$P_{\ell\ell'}(\alpha) = \frac{1}{2\ell+1} \sum_{m=-\ell}^{\ell} \sum_{m'=-\ell'}^{\ell'} |a_{\ell' m' \ell m}|^2.$$

The present theory is now applied in the following paragraphs for low  $n = 2$  and 3, when analytic results can be derived, and for  $n = 28$ , when accurate numerical results can be obtained. A matrix representation for the operator  $L_1 - \alpha A_3$  is required. Instead of the spherical basis  $|\ell m\rangle$ , which is difficult to use in this case, we define a new linear basis obtained by mapping the  $(\ell, m)$  quantum numbers to a unique index  $k = \ell^2 + \ell + m + 1$ , in such a way that  $(0, 0) \rightarrow 1$ ,  $(1, -1) \rightarrow 2$ ,  $(1, 0) \rightarrow 3$ ,  $(1, 1) \rightarrow 4$ ,  $(2, -2) \rightarrow 5$  and so on. The inverse mapping is given by  $\ell = \text{floor}(\sqrt{k-1})$  and  $m = k - \ell^2 - \ell - 1$ . The index  $k$  counts the degeneracy of the energy shell, and runs from 1 to  $n^2$ . The matrix element

$$(L_1)_{\ell m}^{\ell' m'} = \sqrt{(\ell+m)(\ell-m+1)}/2\delta_{\ell\ell'}\delta_{m',m-1} + \sqrt{(\ell-m)(\ell+m+1)}/2\delta_{\ell\ell'}\delta_{m',m+1}$$

of  $L_1$  is non-zero only for  $\Delta\ell = 0$  and  $\Delta m = \pm 1$ , which reflects the fact that the cylindrical symmetry of the Rydberg atom is broken by the precession of  $L$  about the field of the projectile. These  $m$ -changing transitions are however conditioned by the full structure of solution (5)

		$\ell$		$1$		$2$						
$\ell$	$m$	$m'$	$0$	$-1$	$0$	$1$	$-2$	$-1$	$0$	$1$	$2$	
0	0	0	0	$2\alpha\sqrt{2/3}$	0	0	0	0	0	0	0	1
	-1	0	0	$1/\sqrt{2}$	0	0	$\alpha$	0	0	0	0	2
1	0	$2\alpha\sqrt{2/3}$	$1/\sqrt{2}$	0	$1/\sqrt{2}$	0	0	$2\alpha\sqrt{3}$	0	0	0	3
	1	0	0	$1/\sqrt{2}$	0	0	0	0	$\alpha$	0	0	4
	-2	0	0	0	0	0	1	0	0	0	0	5
	-1	0	$\alpha$	0	0	1	0	$\sqrt{3/2}$	0	0	0	6
2	0	0	0	$2\alpha\sqrt{3}$	0	0	$\sqrt{3/2}$	0	$\sqrt{3/2}$	0	0	7
	1	0	0	0	$\alpha$	0	0	$\sqrt{3/2}$	0	1	0	8
	2	0	0	0	0	0	0	0	1	0	0	9
		1	2	3	4	5	6	7	8	9		

Figure 1. Matrix representation of  $L_1 - \alpha A_3$  for  $n = 3$ .

which shows that such transitions are only in evidence for non-zero  $\alpha$ . The matrix element

$$(A_3)_{\ell m}^{\ell' m'} = -\sqrt{\frac{(\ell^2 - m^2)(n^2 - \ell^2)}{(2\ell + 1)(2\ell - 1)}} \delta_{\ell' \ell - 1} \delta_{m' m} \\ - \sqrt{\frac{[(\ell + 1)^2 - m^2][n^2 - (\ell + 1)^2]}{(2\ell + 3)(2\ell + 1)}} \delta_{\ell' \ell + 1} \delta_{m' m}$$

of the component  $A_3 = -(2/3n)z$  along the fixed  $Z$ -axis of quantization is non-zero for  $\Delta\ell = \pm 1$  and  $\Delta m = 0$  transitions. These dipole transitions only contribute for non-zero  $\alpha$ . The matrix  $L_1 - \alpha A_3$  has therefore the band diagonal structure, as illustrated in figure 1 for the special case of  $n = 3$ . The transition amplitude for transition  $k \rightarrow k'$  is the  $kk'$  matrix element of the exponential of the matrix  $-i\Delta\Phi(L_1 - \alpha A_3)$ , sandwiched between the rotations implied by (5). When  $\alpha \approx 0$ , the dipole-forbidden transitions are not possible because the transition matrix  $\approx \exp -i\Delta\Phi L_1$  still has a band diagonal structure. When  $\alpha$  increases, more and more off-diagonal elements become populated, resulting in an increasing number of dipole-forbidden transitions with  $\Delta\ell = \ell' - \ell$  and  $\Delta m = m' - m$ . Efficient algorithms, using Padé approximations, are available (Golub and Loan 1983) for matrix exponentiation. The whole array of transition probabilities for all  $\ell$  and  $\ell'$  is then obtained at once.

Analytical probabilities for  $\ell \rightarrow \ell'$  transitions within the  $n = 2$  shell are listed below:

$$P_{00}^{(2)} = \left(\frac{1}{\gamma^4}\right) [1 + \alpha^2 \cos(\gamma \Delta\Phi)]^2 \\ P_{01}^{(2)} = \left(\frac{2\alpha^2}{3\gamma^4}\right) [2 + \alpha^2 + \alpha^2 \cos(\gamma \Delta\Phi)] \sin^2\left(\frac{\gamma \Delta\Phi}{2}\right) \\ P_{11}^{(2)} = \left(\frac{1}{6\gamma^4}\right) [6 + 8\alpha^2 + 5\alpha^4 + 4\alpha^2 \cos(\gamma \Delta\Phi) + \alpha^4 \cos(2\gamma \Delta\Phi)].$$

The following transition probabilities for the  $n = 3$  shell are also obtained:

$$P_{00}^{(3)} = \left(\frac{1}{9\gamma^4}\right) [3 - 2\alpha^2 + \alpha^4 + 8\alpha^2 \cos(\gamma \Delta\Phi) + 2\alpha^4 \cos(2\gamma \Delta\Phi)]^2$$

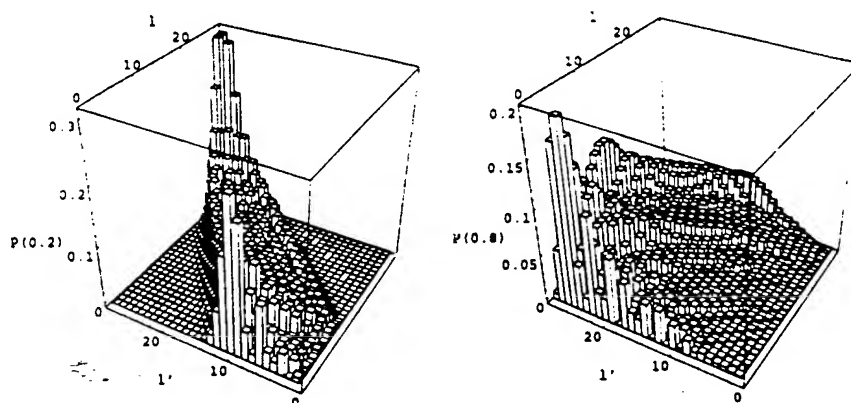


Figure 2. Stark mixing transition probabilities for the  $28\ell \rightarrow 28\ell'$  transition array, with  $\alpha = 0.2$  (left) and  $\alpha = 0.8$  (right).

$$\begin{aligned}
 P_{01}^{(3)} &= \left( \frac{16\alpha^2}{9\gamma^8} \right) [1 + \alpha^2 \cos(\gamma \Delta \Phi)]^2 [2 + \alpha^2 + \alpha^2 \cos(\gamma \Delta \Phi)] \sin^2 \left( \frac{\gamma \Delta \Phi}{2} \right) \\
 P_{02}^{(3)} &= \left( \frac{32\alpha^4}{45\gamma^8} \right) [2 + \alpha^2 + \alpha^2 \cos(\gamma \Delta \Phi)]^2 \sin^4 \left( \frac{\gamma \Delta \Phi}{2} \right) \\
 P_{11}^{(3)} &= \left( \frac{1}{6\gamma^8} \right) [(6 + 30\alpha^4 + 4\alpha^6 + 3\alpha^8) + 8\alpha^2(3 - 2\alpha^2 + 2\alpha^4) \cos(\gamma \Delta \Phi) \\
 &\quad + 2\alpha^4(11 - 2\alpha^2 + \alpha^4) \cos(2\gamma \Delta \Phi) + 8\alpha^6 \cos(3\gamma \Delta \Phi) + \alpha^8 \cos(4\gamma \Delta \Phi)] \\
 P_{12}^{(3)} &= \left( \frac{2\alpha^2}{15\gamma^8} \right) [(20 + 34\alpha^2 + 32\alpha^4 + 8\alpha^6) + \alpha^2(26 + 20\alpha^2 + 9\alpha^4) \cos(\gamma \Delta \Phi) \\
 &\quad + 2\alpha^4(4 + \alpha^2) \cos(2\gamma \Delta \Phi) + \alpha^6 \cos(3\gamma \Delta \Phi)] \sin^2 \left( \frac{\gamma \Delta \Phi}{2} \right) \\
 P_{22}^{(3)} &= \left( \frac{1}{90\gamma^8} \right) [(90 + 240\alpha^2 + 318\alpha^4 + 196\alpha^6 + 63\alpha^8) \\
 &\quad + 8\alpha^2(15 + 22\alpha^2 + 14\alpha^4) \cos(\gamma \Delta \Phi) + 2\alpha^4(23 + 22\alpha^2 + 13\alpha^4) \cos(2\gamma \Delta \Phi) \\
 &\quad + 8\alpha^6 \cos(3\gamma \Delta \Phi) + \alpha^8 \cos(4\gamma \Delta \Phi)].
 \end{aligned}$$

The detailed balance relation

$$(2\ell + 1)P_{\ell'\ell}^{(n)} = (2\ell' + 1)P_{\ell\ell'}^{(n)}$$

is satisfied by the present treatment, so the  $P_{\ell'\ell}^{(n)}$  probabilities for transitions with  $\ell' > \ell$  can be obtained.

Figure 2 displays the results for calculation of the transition probabilities inside the  $n = 28$  energy shell. An undeflected path ( $\Delta \Phi = -\pi$ ) is assumed. For small  $\alpha = 0.2$  only elastic or transitions with small angular momentum transfer  $\Delta \ell$  have significant probabilities; a band along the diagonal is exhibited. As  $\ell$  increases,  $\Delta \ell$  increases and then decreases as  $\ell \rightarrow n - 1$ . As  $\alpha$  increases, the band broadens and larger angular momentum transfers become possible for all  $\ell$ .

The present treatment is valid (a) for weak fields, in evidence for impact parameters  $b > b^* = (3Z_1/2)^{1/2}a_n$ , which implies Stark parameters  $\alpha < \alpha^* = (3Z_1/2)^{1/2}(v_n/v)$ , and

(b) for adiabatic collisions when the collision frequency  $\phi$  is less than the orbital frequency  $\omega_n = v_n/a_n$  of the Rydberg electron, so the Pauli replacement holds. These two conditions combine to yield the partitioning  $v < v^* = (3Z_1/2)^{1/2}v_n$  and  $b > b^*$  in  $(v, b)$ -space for Stark mixing collisions (Flannery and Vranceanu 1998) for a slow encounter in a dipole field. The limit  $v < v^*$  defines our meaning of *ultralow* collision energies. The cross section for Stark mixing is

$$\sigma_{nt \rightarrow n' t'} = 2\pi \int_0^\infty P_{t't}^{(n)} b \, db = 2\pi \left( \frac{3Z_1 a_n}{2v/v_n} \right)^2 \int_0^\infty P_{t't}^{(n)}(\alpha, \Delta\Phi) \frac{d\alpha}{\alpha^3}. \quad (13)$$

When  $v < v^*$  and  $b < b^*$ , the Stark parameter  $\alpha > 1$ . Since the transition probabilities are bounded for large  $\alpha$ , the contribution to the  $\alpha$ -integration is vanishingly small for large  $\alpha$ , decreasing as  $\alpha^{-3}$ , and can, in practice, be neglected for  $\alpha > 1$ . This implies that the *lower* limit to  $b$  is  $b_r = \frac{3}{2}Z_1(v_n/v)a_n$ . At ultralow energies, this limit is always much greater than the weak-field limit  $b^*$ . At the upper limit  $v = v^*$  of ultralow energies,  $b_r$  approaches from above the weak-field limit  $b^*$ . In practical calculations of (13), various physical effects such as Debye screening in a plasma, quantum defects and spin-orbit coupling determine an *upper* limit to  $b$  and hence a lower limit  $\alpha_{\min}$  to  $\alpha$ . For trajectories with zero deflection ( $\Delta\Phi = -\pi$ ), (13) varies universally as  $(Z_1 a_n v_n/v)^2$ . Departure from this variation is governed by  $\Delta\Phi(b, v)$  and by the physical limits imposed upon the  $\alpha$ -integration.

In summary, this letter has presented a new form (5) of the exact quantal solution for the Stark mixing probabilities. Based on this new solution for the whole array of transitions, analytical expressions for small quantum numbers  $n$  and accurate numerical results even for large  $n$  can be obtained. Using the rich symmetry group of the hydrogen atom, the relation with previously published results (Kazansky and Ostrovsky 1996a, b) has been developed in an exquisite fashion. The symmetry group also provides a complete exact classical solution (Vranceanu and Flannery 2000), capable of explaining the main features of the quantal results and of providing a quantal-classical (dynamical) correspondence at a level, more fundamental than Ehrenfest's theorem and the Heisenberg correspondence.

This research is supported by grants from AFOSR: F 49620-99-1-0277 and NSF: 98-02622.

## References

- Born M 1960 *The Mechanics of the Atom* (New York: Ungar) p 235  
 Demkov Yu N, Monozon B S and Ostrovskii V N 1970 *Sov. Phys.-JETP* **31** 173  
 Flannery M R and Vranceanu D 1998 *Atomic Processes in Plasmas: 11th APS Topical Conf.* ed E Oks and M S Pindzola (New York: AIP) pp 317-33  
 Golub G H and Loan C F V 1983 *Matrix Computation* (Baltimore, MD: John Hopkins University Press) p 384  
 Kazansky A K and Ostrovsky V N 1996a *Phys. Rev. Lett.* **77** 3094  
 ——— 1996b *Sov. Phys.-JETP* **83** 1095  
 ——— 1996c *J. Phys. B: At. Mol. Opt. Phys.* **29** 3651  
 Louck J D 1996 *Atomic, Molecular, and Optical Physics Handbook* ed G W F Drake (New York: AIP) p 15  
 Men'shikov L I and Fedichev P O 1995 *Sov. Phys.-JETP* **81** 78  
 Merkt F and Zare R N 1994 *J. Chem. Phys.* **101** 3495  
 Miraglia J E and Macek J 1990 *Phys. Rev. A* **42** 3971  
 Percival I 1983 *Atoms in Astrophysics* ed P G Burke, W B Eissner, D G Hummer and I C Percival (New York: Plenum) p 96  
 Sun X and MacAdam K B 1993 *Phys. Rev. A* **47** 3913  
 Tarter C B 1970 *J. Math. Phys.* **11** 3192  
 Vranceanu D and Flannery M R 2000 *Phys. Rev. A* submitted

# Classical Stark Mixing at Ultralow Collision Energies

D. Vrinceanu and M. R. Flannery

*School of Physics, Georgia Institute of Technology, Atlanta, Georgia 30332*

(Received 15 May 2000)

Exact solutions of the time-dependent classical equations are obtained for the full array of angular momentum mixing transitions  $n\ell \rightarrow n\ell'$  in atomic hydrogen induced by collisions with charged particles at ultralow energies. A novel classical expression for the transition probability  $P_{\ell\ell'}$  is presented. The exact classical results for  $P_{\ell\ell'}(\alpha)$  as a function of  $\ell, \ell'$  and the Stark parameter  $\alpha$  agree exceptionally well with (exact) quantal results. They complement the quantal results by revealing essential characteristics which remain obscured in the quantal treatment.

PACS numbers: 34.50.Pi, 34.10.+x, 34.60.+z

Stark mixing occurs when the electron of a Rydberg atom (in a state with principal quantum number  $n$ ) changes its angular momentum, without changing its energy, as a result of a collision, at large impact parameter  $b$ , with a slow massive particle of charge  $Z_1e$  moving with velocity  $v$ . It is a subject of broad interest and importance in many areas of modern physics [1] and chemistry [2], astrophysics [3], line broadening [4], Auger processes [5], and for anti-hydrogen formation by three-body recombination [6,7] at ultracold temperatures. Although remarkable effort has been devoted to obtaining theoretical solutions for Stark mixing in Rydberg atoms to various levels of approximation [1–13], the purpose of this Letter is to point out that the problem is capable of an exact solution in the classical formulation. The exceptionally rich dynamical  $SO(4)$  symmetry of  $H(n, \ell)$  is the key foundation which allows both classical and quantal exact solutions to be constructed [14] in a similar and unified way. There is substantial renewed [1,15–19] interest in the power of classical dynamics in almost all fields of modern physics, attributed to the desire [15,19] to obtain a more thorough understanding of the classical-quantal correspondence. Stark mixing by ion impact is probably the last problem in collision physics which is capable of an exact solution.

The present new treatment is not an extension of any previous theory and is capable of providing the first comprehensive classical solution for the full array  $n\ell \rightarrow n\ell'$  of collisional transitions in  $H(n, \ell)$ . A new expression for the classical transition probability  $P_{\ell\ell'}$  is defined in a language which exploits the dynamical symmetry. The derived probability for the general array  $\ell \rightarrow \ell'$  of transitions has a very simple functional form, can be easily calculated for any principal quantum number, and provides physical insight and simple geometrical explanations for the behavior of the transition probabilities. Stark mixing probabilities are calculated and compared with the (exact) quantal results [14,20]. Considering the Rydberg atom in a frame which rotates together with the internuclear axis, the Stark mixing problem can in principle be reduced [11,12] to the problem of the Rydberg atom in mixed static electric and magnetic fields. This approach is successful only for the

particular case of  $\ell = 0$ , which is fully recovered by the present general fixed frame formulation.

The target Rydberg atom (with averaged electron orbit radius  $a_n$ , velocity  $v_n$ , momentum  $p_n$ , and angular frequency  $\omega_n = v_n/a_n$ ) is centered at the origin  $O$  of a fixed coordinate frame. The trajectory of the projectile, initially moving with impact parameter  $b$  along the positive  $Z$  direction, is assumed to be confined in the  $YOZ$  plane. In addition to the energy  $E$ , constant along the Hamiltonian  $H_0 = p^2/2m_e - e^2/r$ , the angular momentum  $\mathbf{L} = \mathbf{r} \times \mathbf{p}$  of the unperturbed Rydberg electron and the Runge-Lenz (or eccentricity) vector,

$$\mathbf{A} = p_n^{-1} \left[ \mathbf{p} \times \mathbf{L} - m_e e^2 \frac{\mathbf{r}}{r} \right], \quad (1)$$

directed toward the pericenter and normalized to angular momentum units, are also conserved. These quantities define the dynamic  $SO(4)$  symmetry of the hydrogen atom. Because the  $SO(4)$  group is isomorphic with the direct product  $SO(3) \oplus SO(3)$  of two rotation groups, a special decomposition,  $\mathbf{L} = \mathbf{M} + \mathbf{N}$  and  $\mathbf{A} = \mathbf{M} - \mathbf{N}$ , permits the dynamics of the hydrogen atom to be separated into two decoupled motions. The generators  $\mathbf{M}$  and  $\mathbf{N}$  act independently as angular momenta and are also conserved quantities for the unperturbed Rydberg atom. They evolve independently [21] with time on application of a constant electric field  $\vec{E}$  and precess about  $\vec{E}$  with the Stark frequencies  $\tilde{\omega}_S = \mp(3/2)a_nv_n(\vec{E}/e)$ . For weak fields, the Stark splitting  $\Delta E_S = \hbar\omega_S < \hbar\omega_n = \Delta E_n$ , the  $(n \rightarrow n \pm 1)$  energy splitting. For constant fields, the vectors  $\mathbf{L}$  and  $\mathbf{A}$  vary periodically with frequency  $\omega_S$ .

The weak field approximation assumes that the time-dependent electric field  $\vec{E}(t)$  generated by the passing projectile of charge  $Z_1e$  is constant over the atom's spatial extent and the dipole approximation for interaction potential  $V = e\vec{r} \cdot \vec{E}$  is valid. Hence

$$\vec{E}(t) = -\frac{Z_1e\hat{R}}{R^2} = \frac{Z_1e}{vb} \frac{d\Phi}{dt} \hat{R},$$

where  $\Phi$  is the polar angle between the internuclear vector  $\mathbf{R}$  and the  $Z$  axis.

On assuming that the collision is orbital adiabatic ( $\dot{\Phi} < \omega_n$ ),  $\vec{E}$  is constant over one period so that the slow rate of variation  $\Delta L/T$  of the angular momentum over one orbital period  $T = 2\pi/\omega_n$ , is the classical average

$$\frac{dL}{dt} = -\frac{e}{T} \int_0^T (\mathbf{r} \times \vec{E}) dt = -e\langle \mathbf{r} \rangle \times \vec{E}(t).$$

Since the weak field approximation ( $\omega_S < \omega_n$ ) also holds, the vectors  $\mathbf{L}$  and  $\mathbf{A}$  change very little over one orbital period and  $\langle \mathbf{r} \rangle \approx -3A/2p_n = -3A(a_n v_n/2e^2)$ . The following set [3],

$$\frac{dL}{dt} = -\omega_S \hat{R} \times \mathbf{A}, \quad \frac{dA}{dt} = -\omega_S \hat{R} \times \mathbf{L},$$

of coupled equations can then be deduced, where both  $\hat{R}$  and  $\omega_S = \alpha\Phi$  now vary with time. The Stark parameter  $\alpha$  is  $3Z_1 a_n v_n/2bv$ . The weak field ( $\omega_S < \omega_n$ ) and adia-

batic ( $\dot{\Phi} < v_n/a_n$ ) conditions combine to yield the partitioning  $b \geq (v/v_n)a_n$ , when  $v \geq v^* = (3Z_1/2)^{1/2}v_n$ , and  $b \geq (3Z_1/2)^{1/2}a_n$ , when  $v \leq v^*$ , of  $(v, b)$  space for validity of the present solutions. For  $v \geq v^*$ ,  $\alpha$  remains  $\leq 1$ . For  $v < v^*$ ,  $\alpha$  can exceed unity. When written in terms of vectors  $\mathbf{M}$  and  $\mathbf{N}$ , the above set of differential equations yields the set of decoupled equations,

$$\frac{dM}{d\Phi} = -\alpha \hat{R} \times \mathbf{M}, \quad \frac{dN}{d\Phi} = +\alpha \hat{R} \times \mathbf{N}. \quad (2)$$

Since the magnitudes  $M^2 = N^2 = (L^2 + A^2)/4 = n^2 \hbar^2/4$  remain constant throughout the collision, exact solutions of Eqs. (2) can then be obtained [14] at general angle  $\Phi$  in terms of finite rotations from the initial values  $\mathbf{M}(\Phi_0)$  and  $\mathbf{N}(\Phi_0)$ , via the orthogonal transformations  $\mathbf{M}(\Phi) = U_M(\Phi, \Phi_0)\mathbf{M}(\Phi_0)$  and  $\mathbf{N}(\Phi) = U_N(\Phi, \Phi_0)\mathbf{N}(\Phi_0)$ . For example, if the initial state is specified by the vectors  $(\mathbf{L}, \mathbf{A})$  at  $\Phi_0 = \pi$ , then the final state  $(\mathbf{L}', \mathbf{A}')$ , at  $\Phi = 0$ , is determined by the rule

$$\begin{aligned} L'_1 &= \gamma^{-2}[1 + \alpha^2 \cos(\pi\gamma)]L_1 + \alpha\gamma^{-1} \sin(\pi\gamma)A_2 + \alpha\gamma^{-2}[1 - \cos(\pi\gamma)]A_3, \\ L'_2 &= -\cos(\pi\gamma)L_2 - \gamma^{-1} \sin(\pi\gamma)L_3 + \alpha\gamma^{-1} \sin(\pi\gamma)A_1, \\ L'_3 &= \gamma^{-1} \sin(\pi\gamma)L_2 - \gamma^{-2}[\alpha^2 + \cos(\pi\gamma)]L_3 + \alpha\gamma^{-2}[\cos(\pi\gamma) - 1]A_1, \\ A'_1 &= \gamma^{-2}[1 + \alpha^2 \cos(\pi\gamma)]A_1 + \alpha\gamma^{-1} \sin(\pi\gamma)L_2 + \alpha\gamma^{-2}[1 - \cos(\pi\gamma)]L_3, \\ A'_2 &= -\cos(\pi\gamma)A_2 - \gamma^{-1} \sin(\pi\gamma)A_3 + \alpha\gamma^{-1} \sin(\pi\gamma)L_1, \\ A'_3 &= \gamma^{-1} \sin(\pi\gamma)A_2 - \gamma^{-2}[\alpha^2 + \cos(\pi\gamma)]A_3 + \alpha\gamma^{-2}[\cos(\pi\gamma) - 1]L_1. \end{aligned} \quad (3)$$

Here  $\gamma = \sqrt{1 + \alpha^2}$  and the components of the initial and final vectors are defined in the fixed coordinate frame considered. The above exact solutions (3) are easily verified and satisfy the invariant relations

$$\mathbf{L}' \cdot \mathbf{A}' = \mathbf{L} \cdot \mathbf{A} = 0 \quad (4)$$

and

$$L'^2 + A'^2 = L^2 + A^2 = n^2 \hbar^2. \quad (5)$$

The orbit of the final state  $(n, \mathbf{L}')$  is confined to a plane perpendicular to the final  $\mathbf{L}'$  and the energy is preserved (since  $n$  does not change). The above constraints, Eqs. (4) and (5), define in the  $(\mathbf{L}, \mathbf{A})$  space a hypersurface on which the initial state, defined by the initial angular momentum quantum number  $\ell$ , is uniformly distributed. The volume of this hypersurface is therefore given by

$$\mathcal{V}_{n\ell} = \iint \delta(|\mathbf{L}| - \hbar\ell) \delta(|\mathbf{A}| - \hbar\sqrt{n^2 - \ell^2}) \delta(\mathbf{L} \cdot \mathbf{A}) d\mathbf{L} d\mathbf{A}. \quad (6)$$

Each point from this manifold evolves during the collision according to the rule (3), so that only a fraction of possible initial states can produce the final state with angular momentum quantum number  $\ell'$ , after the collision. The volume of  $(\mathbf{L}, \mathbf{A})$  space which overlaps the initial and final states is

$$\mathcal{V}_{n\ell\ell'} = \iint \delta(|\mathbf{L}| - \hbar\ell) \delta(|\mathbf{L}'| - \hbar\ell') \delta(|\mathbf{A}| - \hbar\sqrt{n^2 - \ell^2}) \delta(\mathbf{L} \cdot \mathbf{A}) d\mathbf{L} d\mathbf{A}. \quad (7)$$

The  $\ell \rightarrow \ell'$  transition probability is then, in a geometric sense, the ratio of the two volumes

$$P_{\ell'\ell}^{(n)} = \frac{\mathcal{V}_{n\ell\ell'}}{\mathcal{V}_{n\ell}}. \quad (8)$$

This is a novel result in that Eq. (8) is defined in terms of the new  $(\mathbf{L}, \mathbf{A})$  representative space, being more appropriate, than the customary  $(\mathbf{r}, \mathbf{p})$  phase space, for direct expression of the dynamical  $SO(4)$  symmetry of  $H(n, \ell)$ .

The six-dimensional integral (6) can be calculated directly, while the integral (7) eventually reduces to yield the one-dimensional integral [14]

$$P_{\ell'\ell}^{(n)} = \frac{2\ell'}{\pi \hbar n^2} \frac{1}{1 - \cos\chi} \int \frac{dz}{\sqrt{(z^2 - \mathcal{A})(\mathcal{B} - z^2)}}$$

for the transition probability. This, in turn, may be expressed in terms of the complete elliptic integral,



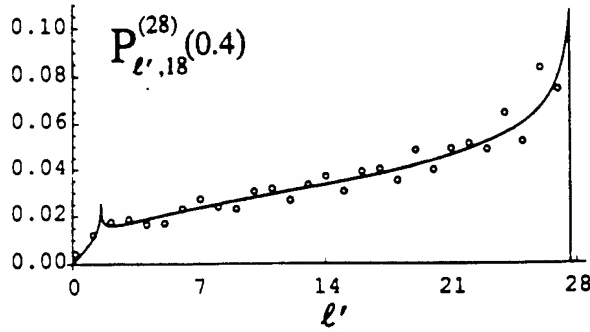


FIG. 1. Probability for the  $18 \rightarrow \ell'$  transition, within the  $n = 28$  energy shell, for a given Stark parameter  $\alpha = 0.4$ . Exact quantal results are denoted by dots.

$$K(m) = \int_0^{\pi/2} (1 - m \sin^2 x)^{-1/2} dx, \text{ as}$$

$$P_{\ell\ell'}^{(n)}(\chi) = \frac{2\ell'/n^2}{\pi \hbar \sin^2(\chi/2)} \begin{cases} 0, & \mathcal{B} < 0, \\ \frac{K(\mathcal{B}/(\mathcal{B}-\mathcal{A}))}{\sqrt{\mathcal{B}-\mathcal{A}}}, & \mathcal{B} > 0, \mathcal{A} < 0, \\ \frac{K((\mathcal{B}-\mathcal{A})/\mathcal{B})}{\sqrt{\mathcal{B}}}, & \mathcal{B} > 0, \mathcal{A} > 0, \end{cases} \quad (9)$$

where

$$\mathcal{A}(\ell/n, \ell'/n; \chi) = \frac{\cos(u_1 + u_2) - \cos \chi}{1 - \cos \chi}, \quad (10)$$

$$\mathcal{B}(\ell/n, \ell'/n; \chi) = \frac{\cos(u_1 - u_2) - \cos \chi}{1 - \cos \chi}.$$

The angles  $u_1$  and  $u_2$  depend only on the initial and final states via  $\cos u_1 = 2\ell^2/n^2 - 1$  and  $\cos u_2 = 2\ell'^2/n^2 - 1$ . The rotation angle  $\chi$ , which depends only on the Stark parameter  $\alpha$  and the polar angle  $\Delta\Phi = \Phi - \Phi_0$  swept out during the collision time interval  $(t_0, t)$ , is determined by

$$\cos \frac{\chi}{2} = [1 + \alpha^2 \cos(\sqrt{1 + \alpha^2} \Delta\Phi)] / (1 + \alpha^2).$$

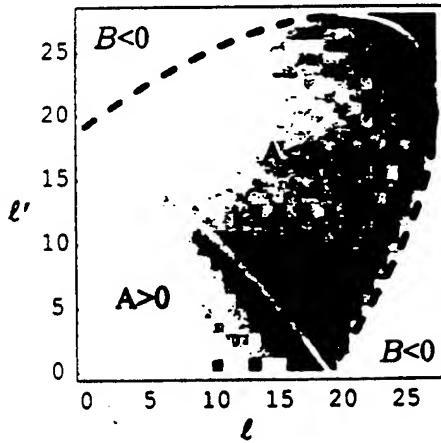


FIG. 2. Density plots of the  $\ell \rightarrow \ell'$  transition probabilities, calculated within the quantal treatment for  $\alpha = 0.4$  and  $n = 28$ . The probabilities increase as the color becomes darker. The continuous and broken lines represent the classical  $\mathcal{A} = 0$  and  $\mathcal{B} = 0$  ridges.

The condition  $\mathcal{B} < 0$  defines the classical inaccessible region. Two types of singular points are apparent from the solution (9). At  $\mathcal{B} = 0$ , the transition probability  $P_{\ell\ell'}(\alpha)$  has a finite jump (step discontinuity) and at  $\mathcal{A} = 0$  it has a logarithmic (cusp) singularity. These features are displayed in Figs. 1–5 for representative transitions. For a given Stark parameter  $\alpha$  and initial angular momentum  $\ell$ , the solutions of the equations  $\mathcal{A} = 0$  and  $\mathcal{B} = 0$  provide the critical values

$$\ell'_{\pm} = \ell \left| \cos \frac{\chi}{2} \pm \left( \frac{n^2}{\ell^2} - 1 \right)^{1/2} \sin \frac{\chi}{2} \right|$$

of the final angular momentum, where the cusp or step singularities are located. The inequality  $\mathcal{A} < \mathcal{B}$  is strictly fulfilled except for the limiting cases of  $\ell$  or  $\ell' \rightarrow 0$  or  $n$  when  $\mathcal{A} = \mathcal{B}$ . These limits are readily deduced from Eq. (9) to provide the following probabilities:

$$P_{\ell'0}^{(n)}(\alpha) = \frac{\ell' / (\hbar n^2)}{\sin(\chi/2) \sqrt{\sin^2(\chi/2) - (\ell'/n)^2}},$$

$$P_{\ell'n}^{(n)}(\alpha) = \frac{\ell' / (\hbar n^2)}{\sin(\chi/2) \sqrt{(\ell'/n)^2 - \sin^2(\chi/2)}},$$

$$P_{n\ell}^{(n)}(\alpha) = \frac{1 / (\hbar n)}{\sin(\chi/2) \sqrt{(\ell/n)^2 - \sin^2(\chi/2)}}.$$

The  $\ell \rightarrow \ell' = 0$  transitions have zero classical probability. The specific case [12] of  $0 \rightarrow \ell'$  transitions is therefore directly recovered from our general result (9).

Figure 1 shows the classical probability  $P_{\ell', 18}^{(28)}$  for the representative array  $\ell = 18 \rightarrow \ell'$  transitions. The quantal results [14,20] oscillate about the classical background. Figure 1 also displays the  $\mathcal{A} = 0$  cusp at  $\ell'_-$  followed by the  $\mathcal{B} = 0$  downward step at  $\ell'_+$ , as  $\ell'$  is increased from 0 to  $n$ . In the central region  $\mathcal{A} < 0$  and  $\mathcal{B} > 0$ .

Figure 2 provides the density map of the quantal probabilities [14,20] for the full array of  $\ell \rightarrow \ell'$  transitions at  $\alpha = 0.4$ . In the classical forbidden regions (where  $\mathcal{B} < 0$ ), the upper left and lower right corners, the quantal probabilities decrease exponentially. The lines of singularities  $\mathcal{A} = 0$  and  $\mathcal{B} = 0$  are also shown. Along these,

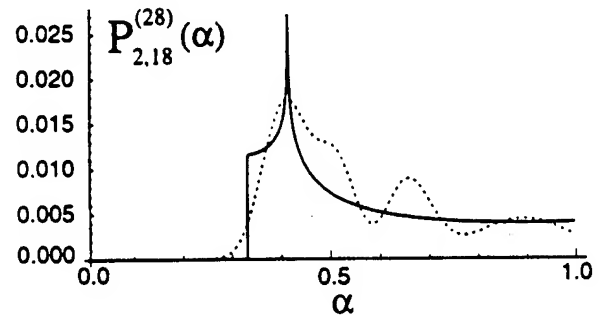


FIG. 3. Probability for the  $18 \rightarrow 2$  transition, within the  $n = 28$  energy shell, as a function of the Stark parameter  $\alpha$ . Exact quantal results: dotted line.

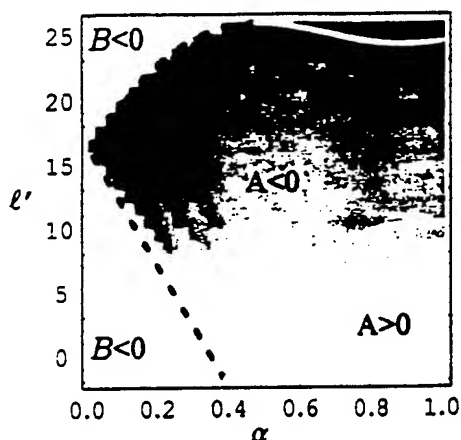


FIG. 4. Density plots of the  $\ell = 18 \rightarrow \ell'$  transition probabilities, calculated within the quantal treatment for  $n = 28$ , as a function of  $\alpha$ .

the classical transition probabilities display cusp and step-like behavior, respectively, and, in their vicinity, the quantal results have local maxima. Figure 1 follows from a vertical line drawn through the plot at  $\ell = 18$ , showing a cusp-step variation. Figure 2 predicts step-step and step-cusp variations for transitions from  $\ell > 19$ .

In Fig. 3, the classical and quantal transition probabilities for the  $18 \rightarrow 2$  transition are plotted as a function of the Stark parameter  $\alpha$ . This plot can also be obtained by following the variation of the transition probability along a horizontal line with  $\ell' = 2$  in Fig. 4.

Figure 4 presents a density map for the quantal probabilities for transition from the initial angular momentum  $\ell = 18$  to any  $\ell'$  and for any value of  $\alpha$ . As  $\alpha \rightarrow 0$  the span of possible final angular momenta is reduced, such that only elastic transitions are possible at  $\alpha = 0$ . The classical singularity lines  $\mathcal{A} = 0$  and  $\mathcal{B} = 0$  illustrate again the correspondence with the quantal results. The cusp-step pattern of Fig. 1 is also explained by a vertical line at  $\alpha = 0.4$  of Fig. 4. For low  $\alpha < 0.4$ , a step-step variation is predicted, i.e., the accessible  $\ell'$  lie within the range  $\ell'_- < \ell' < \ell'_+$ . The results in Fig. 5 confirm this prediction. Cusp-cusp patterns occur at higher  $\alpha \geq 0.5$ .

In conclusion, the exact solution (3) of the classical equations (2) has been obtained, by exploiting the SO(4) dynamical symmetry of  $H(n, \ell)$ . The novel expression (8) provides the general result (9) for the classical probability  $P_{\ell\ell'}^{(n)}$  for the full array of Stark mixing transitions  $n\ell \rightarrow n\ell'$ . Since  $\mathcal{A}$  and  $\mathcal{B}$  are symmetrical in  $(\ell, \ell')$  the probability (9) satisfies the detailed balance relation  $2\ell P_{\ell\ell'}^{(n)} = 2\ell' P_{\ell'\ell}^{(n)}$ . Probability conservation  $\int_0^1 P_{\ell\ell'}^{(n)} d\alpha = 1$  is also satisfied. Cross sections [14] may be calculated from Eq. (9). Exceptional agreement is obtained between the classical and quantal  $P_{\ell\ell'}^{(n)}(\alpha)$  as a function of  $\ell, \ell'$  and the Stark parameter  $\alpha$ . The common SO(4) symmetry provides this classical-quantal correspondence at a level more fundamental than Ehrenfest's theorem and the

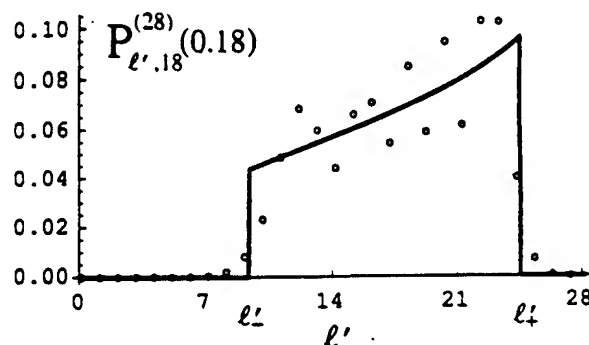


FIG. 5. As in Fig. 1, but for Stark parameter  $\alpha = 0.18$ .

Heisenberg correspondence. The classical method is also complementary in that it reveals very succinctly essential and valuable characteristics which remain obscured within the quantal treatment. This reflects the essential power of classical dynamics when applied to collision problems.

This work has been supported by AFOSR Grant No. 49620-99-1-0277 and NSF Grant No. 98-02622.

- [1] V. S. Lebedev and I. L. Beigman, *Physics of Highly Excited Atoms and Ions* (Springer-Verlag, Berlin, 1998).
- [2] F. Merkt and R. N. Zare, *J. Chem. Phys.* **101**, 3495 (1994).
- [3] I. Percival, *Atoms in Astrophysics* (Plenum, New York, 1983), pp. 75–102.
- [4] D. Hoang-Binh and H. Van Regemorter, *J. Phys. B* **28**, 3147 (1995).
- [5] J. E. Miraglia and J. Macek, *Phys. Rev. A* **42**, 3971 (1990).
- [6] L. I. Men'shikov and P. O. Fedichev, *Sov. Phys. JETP* **81**, 78 (1995).
- [7] M. R. Flannery and D. Vranceanu, in *Proceedings of the 11th APS Topical Conference*, edited by E. Oks and M. S. Pindzola (AIP Press, New York, 1998), pp. 317–333.
- [8] I. Percival and D. Richards, *J. Phys. B* **12**, 2051 (1979).
- [9] R. M. Pengelly and M. J. Seaton, *Mon. Not. R. Astron. Soc.* **127**, 165 (1964).
- [10] Yu. N. Demkov, B. S. Monozon, and V. N. Ostrovskii, *Sov. Phys. JETP* **30**, 775 (1970).
- [11] P. Bellomo, D. Farrelly, and T. Uzer, *J. Chem. Phys.* **107**, 2499 (1995).
- [12] A. Kazansky and V. Ostrovsky, *J. Phys. B* **29**, 3651 (1996).
- [13] A. K. Kazansky and V. N. Ostrovsky, *Phys. Rev. Lett.* **77**, 3094 (1996); *Sov. Phys. JETP* **83**, 1095 (1996).
- [14] D. Vranceanu and M. R. Flannery, *Phys. Rev. A* (to be published).
- [15] M. R. Flannery and D. Vranceanu, *Phys. Rev. Lett.* **85**, 1 (2000).
- [16] M. Gryzinski and J. A. Kunc, *J. Phys. B* **32**, 5789 (1999).
- [17] V. S. Lebedev, *J. Phys. B* **24**, 1977 (1991).
- [18] D. Vranceanu and M. R. Flannery, *Phys. Rev. Lett.* **82**, 3412 (1999); *Phys. Rev. A* **60**, 1053 (1999).
- [19] K. G. Kay, *Phys. Rev. Lett.* **83**, 5190 (1999).
- [20] D. Vranceanu and M. R. Flannery, *J. Phys. B* **33**, L721 (2000).
- [21] M. Born, *The Mechanics of the Atom* (Ungar, New York, 1960), p. 235.

## LETTER TO THE EDITOR

## Analytical quantal collisional Stark mixing probabilities

D Vrinceanu and M R Flannery

School of Physics, Georgia Institute of Technology, Atlanta, GA 30332, USA

Received 27 September 2000

### Abstract

An exact expression for the probability  $P_{\ell\ell'}^{(n)}$  of Stark mixing transitions between arbitrary angular momentum states  $\ell$  and  $\ell'$  within the same energy shell  $n$ , as a result of a collision with a slow charged projectile at large impact parameters is presented. The formula obtained is compact and easy to use for numerical evaluations even for very large quantum numbers ( $n \sim 100$ ). A classical approximation is directly obtained and compared with the exact quantal result in the limit of large  $n$ . Two distinct sets of quantal oscillations are predicted.

(Some figures in this article are in colour only in the electronic version; see [www.iop.org](http://www.iop.org))

In a previous letter, Vrinceanu and Flannery (2000a) provided a new quantal theory in a fixed reference frame for the probabilities  $P_{\ell\ell'}^{(n)}$  for the full array  $n\ell \rightarrow n\ell'$  of transitions induced by collisions between  $H(n\ell)$ , or any Rydberg atom, and an ion of charge  $Ze$  at ultralow energies. The conventional approach to this problem consists in solving a coupled-channel system of  $n^2$  differential equations. For large  $n$ , this task becomes prohibitively difficult even when some simplification can be introduced, such as that, for example, by Beigman and Syrkin (1985). A time-evolution operator method (Pfennig 1971) depends on the roots of an algebraic equation of degree  $n^2$  so that, in general, it is not possible to obtain analytical results and it was only applied to transitions between the parabolic states of the  $n = 2$  shell. The alternative method proposed by Vrinceanu and Flannery (2000a) exploits the rich dynamical  $SO(4)$  symmetry of  $H(n\ell)$  to solve the problem exactly in the fixed-frame representation. A similar approach by Kazansky and Ostrovsky (1996a, b) was successful only for the special case of  $n0 \rightarrow n\ell'$  transitions. The solution presented by Vrinceanu and Flannery (2000a) has the advantage that the full array  $P_{\ell\ell'}^{(n)}$  of transition probabilities is obtained at once for a given velocity and impact parameter of the projectile. Moreover, analytical expressions were obtained for low  $n$ . Numerical results were possible for low to intermediate  $n \approx 30$ .

The present letter reports a significant advance to what was previously obtained. An exact analytical expression for the quantal probabilities  $P_{\ell\ell'}^{(n)}$  is now presented for any  $n$ . The remarkable simplicity of the result allows both accurate numerical results for very large  $n \approx 100$ , and an immediate classical limit.

The target Rydberg atom is described by the Pauli–Lenz vector operator  $A$  and the angular momentum vector operator  $L$ . The projectile with velocity  $v$  along the  $z$ -axis, internuclear

vector  $R$  and impact parameter  $b$  is characterized by the Stark parameter  $\alpha = 3Za_n v_n / 2bv$ , where  $a_n$  and  $v_n$  are the average electron-orbit radius and velocity. The adiabatic dipole interaction is  $V(R) = -Ze^2(r) \cdot \hat{R}/R^2$ , where the averaged vector position of the Rydberg electron of mass  $m_e$  is  $\langle r \rangle = -3A/(2m_e v_n)$ . Under the adiabatic, dipole and classical path assumptions, the Schrödinger equation for the evolution operator in the interaction picture is (Vrinceanu and Flannery 2000a)

$$i\hbar \frac{\partial U_I}{\partial \Phi} = -\alpha(A_2 \sin \Phi + A_3 \cos \Phi)U_I$$

when time  $t$  is replaced, via the relation  $R^2 \Phi = -vb$ , by the angle  $\Phi$  between  $R$  and the (positive)  $z$ -axis of a fixed frame. The previous work of Vrinceanu and Flannery (2000a) used the exact solution for  $U_I$  directly to provide the full array of transition probabilities. However, upon the decomposition  $L = M + N$  and  $A = M - N$ , the solution separates as

$$U_I = U_M \otimes U_N$$

where the operators  $U_M$  and  $U_N$  are defined by

$$U_M = e^{i\Phi M_1/\hbar} e^{-i\Delta\Phi(M_1 - \alpha M_3)/\hbar} e^{-i\Phi_0 M_1/\hbar}$$

and

$$U_N = e^{i\Phi N_1/\hbar} e^{-i\Delta\Phi(N_1 + \alpha N_3)/\hbar} e^{-i\Phi_0 N_1/\hbar}$$

and where  $\Delta\Phi(t) = \Phi(t) - \Phi(t_0)$  is the polar angle swept out by  $R$  within the time interval  $(t - t_0)$ . Since the angular momentum-like operators  $M$  and  $N$  commute, the corresponding evolution operators  $U_M$  and  $U_N$  act independently as rotations in carrier spaces of dimension  $2j + 1 = n$ .

The probability for transition  $\ell \rightarrow \ell'$  between states with given angular momentum is defined by

$$P_{\ell\ell'}^{(n)} = \frac{1}{2\ell + 1} \sum_{m=-\ell}^{\ell} \sum_{m'=-\ell'}^{\ell'} |a_{\ell'm'-\ell m}^{(n)}|^2 \quad (1)$$

where the  $(\ell, m) \rightarrow (\ell', m')$  transition amplitude between angular momentum states within the energy shell of quantum number  $n$  is

$$a_{\ell'm'-\ell m}^{(n)} = \langle n\ell'm' | U_M \otimes U_N | n\ell m \rangle = \sum_{\mu\nu\mu'\nu'} C_{j\mu j\nu}^{\ell m} C_{j\mu' j\nu'}^{\ell' m'} D_{\mu'\mu}^{(j)}(U_M) D_{\nu\nu'}^{(j)}(U_N) \quad (2)$$

and where  $D^{(j)}(R)$  is Wigner's  $(2j + 1)$ -dimensional matrix representation of the finite rotation  $R$ .

The tenfold summation within equation (1) can be contracted to yield the following result:

$$P_{\ell\ell'}^{(n)} = \frac{2\ell' + 1}{n} \sum_{L=|\ell'-\ell|}^{n-1} (2L + 1) \left\{ \begin{matrix} \ell' & \ell & L \\ j & j & j \end{matrix} \right\}^2 H_{jL}^2(\eta) \quad (3)$$

which is compact and involves only one summation. Here  $\{\dots\}$  is the 6- $j$  symbol for coupling of three angular momenta and  $H_{jL}$  is a special matrix element of the irreducible representation of the group  $O(4)$ . This function (also called the generalized character  $\chi_L^j$ , associated with the irreducible representation of the rotation group) is well studied (for example, see the books

by Talman (1968) and Varshalovich *et al* (1988)). It can be written in terms of ultraspherical polynomials  $C_n^{(\alpha)}$  as

$$H_{jL}(\eta) = (2L)!! \sqrt{\frac{(2j+1)(2j-L)!}{(2j+L+1)!}} \left(\sin \frac{\eta}{2}\right)^L C_{2j-L}^{(1+L)}\left(\cos \frac{\eta}{2}\right).$$

The angle  $\eta$  is the proper angle of the rotation produced by the successive rotations  $U_N^{-1}$  and  $U_M$ , and is determined from the two-dimensional representation of the product  $U_N^{-1}U_M$  by

$$\cos \frac{\eta}{2} = \frac{1}{2} \text{Trace}_2 [U_M U_N^{-1}] = \frac{1 + \alpha^2 \cos \sqrt{1 + \alpha^2} \Delta \Phi}{1 + \alpha^2}. \quad (4)$$

The formula given by equation (3) is capable of providing exact numerical results even for large quantum numbers  $n$ , in contrast to equation (1) where the number of terms to be summed increases dramatically with  $n$ . Moreover, a classical limit of equation (3) can be directly and easily obtained. Note that the capacity of the projectile to produce angular momentum changes is governed solely by the key parameter  $\eta$ , the argument of  $H_{jL}$  in equation (3). Since  $\Delta \Phi$  varies with time  $t$ , expression (3) furnishes  $P_{\ell' \ell}^{(n)}$  as a function of  $t$  and the Stark parameter  $\alpha$ , absorbed within parameter  $\eta$ . It can be shown that both detailed balance  $(2\ell + 1)P_{\ell' \ell}^{(n)} = (2\ell' + 1)P_{\ell \ell'}^{(n)}$  and probability conservation  $\sum_{\ell'} P_{\ell' \ell}^{(n)} = 1$  are satisfied. For the special case of zero initial angular momentum, the 6- $j$  symbol is (Varshalovich *et al* 1988, p 299)

$$\left\{ \begin{array}{ccc} \ell' & 0 & L \\ j & j & j \end{array} \right\} = (-1)^{\ell' + \ell + 1} \frac{\delta_{\ell' L}}{\sqrt{n(2\ell' + 1)}}.$$

The probability for  $0 \rightarrow \ell'$  transitions is then

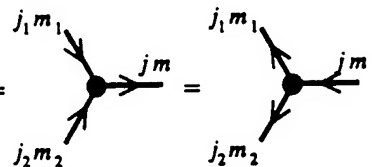
$$P_{\ell' 0}^{(n)}(X) = \frac{2\ell' + 1}{n^2} H_{j \ell'}^2(X)$$

in agreement with Kazansky and Ostrovsky (1996a, b). Equation (3) may be recast into the interesting form

$$P_{\ell' \ell}^{(n)}(X) = n(2\ell' + 1) \sum_{L=|\ell' - \ell|}^{n-1} \left\{ \begin{array}{ccc} \ell' & \ell & L \\ j & j & j \end{array} \right\}^2 P_{L0}^{(n)}(X).$$

Since the square of the 6- $j$  symbol is the probability of coupling three angular momenta, a physical interpretation may be given for the above formula. The Stark mixing transition can therefore be seen as a multi-step process involving partial waves of angular momentum  $L$ .

The proof of equation (3) is based on standard analytical techniques of rotation algebra. The main steps are represented by the diagrams in figure 1. The conventions adopted are similar to those described in detail by Zare (1988) and by Varshalovich *et al* (1988). Only the basic rules are explained here. Every internal line represents a summation over the magnetic quantum number of an angular momentum with the quantum number attached to the line. A double line represents the summation ( $\sum_j (2j + 1) \dots$ ) over the angular momentum quantum numbers. The coupling of two angular momenta is represented by a vertex with two incoming and one outgoing lines and has associated Clebsch-Gordan coefficient

$$C_{j_1 m_1 j_2 m_2}^{j m} = (j_1 m_1 j_2 m_2 | j m) =$$


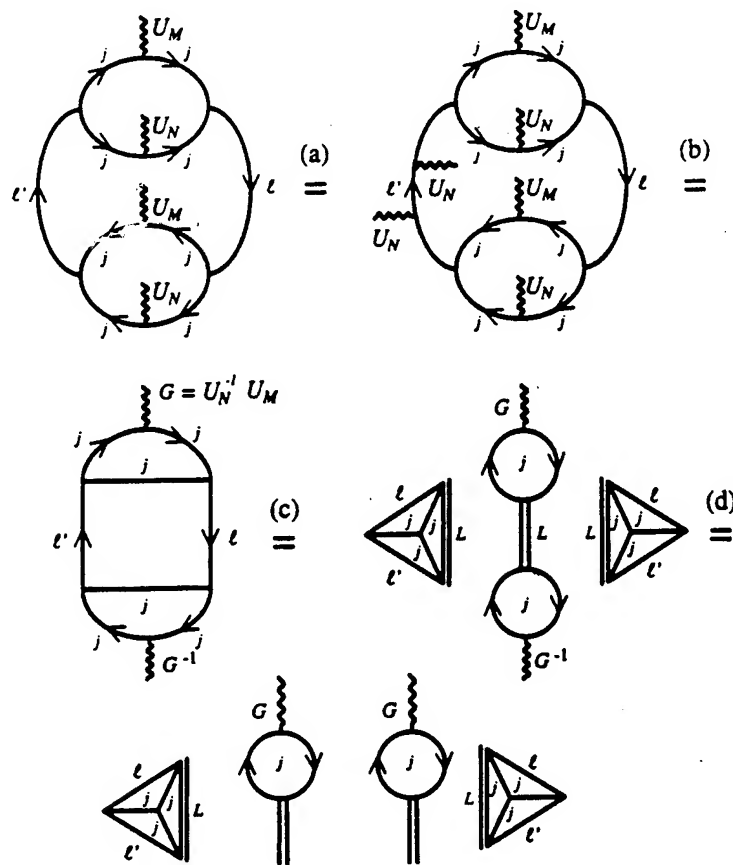


Figure 1. Schematic proof of the main result.

Since the Clebsch-Gordan coefficient is real, the conjugate symbol with one incoming and two outgoing lines also represents the same coefficient. The  $m_1 m_2$  matrix element of the  $2j+1$ -representation of rotation  $R$  is represented by a directed line with a wavy line attached

$$\mathcal{D}_{m_1 m_2}^{(j)}(R) = \langle jm_1 | R | jm_2 \rangle =$$

The matrix element associated with the inverse rotation  $R^{-1}$  has the same representation but with the direction reversed. Under this simple notation, the amplitude equation (2), for example, has the following representation:

$$a_{\ell' m' \leftarrow \ell m}^{(n)} = \langle n \ell' m' | U_I | n \ell m \rangle =$$

Table 1. Exact expressions for the Stark mixing transition probabilities inside the shell  $n = 1, 2, 3, 4$  and  $5$ .

$n$	$\ell$	$\ell'$	$f$	$(2\ell+1)P_{\ell\ell'}^{(n)}(x) = f \times (1-x^2)^{(\ell-\ell')/2} \times \dots$ ( $x = \cos \eta/2$ )
1	0	0	1	1
2	0	0	1	$x^2$
	0	1	1	1
	1	1	1	$2+x^2$
3	0	0	$\frac{1}{9}$	$(-1+4x^2)^2$
	0	1	$\frac{8}{3}$	$x^2$
	0	2	$\frac{8}{9}$	1
	1	1	1	$1-2x^2+4x^4$
	1	2	$\frac{2}{3}$	$3+2x^2$
	2	2	$\frac{1}{9}$	$19+22x^2+4x^4$
4	0	0	1	$(-x+2x^3)^2$
	0	1	$\frac{1}{3}$	$(-1+6x^2)^2$
	0	2	1	$4x^2$
	0	3	$\frac{4}{3}$	1
	1	1	$\frac{1}{25}$	$2+145x^2-396x^4+324x^6$
	1	2	$\frac{4}{3}$	$1+9x^4$
	1	3	$\frac{12}{25}$	$4+3x^2$
	2	2	1	$2-5x^2+4x^4+4x^6$
	2	3	$\frac{1}{3}$	$11+20x^2+4x^4$
	3	3	$\frac{1}{25}$	$52+75x^2+44x^4+4x^6$
5	0	0	$\frac{1}{25}$	$(1-12x^2+16x^4)^2$
	0	1	$\frac{8}{25}$	$(-3x+8x^3)^2$
	0	2	$\frac{8}{35}$	$(-1+8x^2)^2$
	0	3	$\frac{128}{25}$	$x^2$
	0	4	$\frac{128}{175}$	1
	1	1	$\frac{1}{25}$	$9-162x^2+996x^4-1792x^6+1024x^8$
	1	2	$\frac{2}{35}$	$3+114x^2-384x^4+512x^6$
	1	3	$\frac{16}{25}$	$1+4x^2+16x^4$
	1	4	$\frac{64}{175}$	$5+4x^2$
	2	2	$\frac{1}{25}$	$27+240x^2-284x^4-768x^6+1024x^8$
	2	3	$\frac{16}{35}$	$4-13x^2+28x^4+16x^6$
	2	4	$\frac{32}{245}$	$17+38x^2+8x^4$
	3	3	$\frac{1}{25}$	$59-52x^2-184x^4+288x^6+64x^8$
	3	4	$\frac{4}{175}$	$95+246x^2+168x^4+16x^6$
	4	4	$\frac{1}{1225}$	$2509+3644x^2+3624x^4+1184x^6+64x^8$

The main steps (a)–(d) in the proof of equation (3), illustrated in figure 1, are outlined briefly below.

- The upper left-hand diagram is just the transition probability equation (1). The next diagram is obtained by inserting the identity operation  $U_N U_N^{-1}$  on line  $\ell'$ .
- The rotation matrix element from one branch of the Clebsch–Gordan coefficient can be

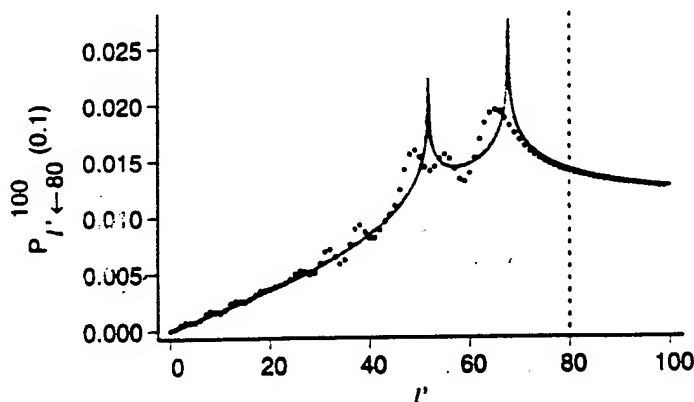


Figure 2. Stark mixing probability for transitions within the energy shell  $n = 100$  from the initial state  $\ell = 80$ , with angle  $\eta$  given by  $\cos \eta/2 = 0.1$ , as a function of the final angular momentum  $\ell'$ . The exact quantal result is represented by the dots, the classical limit is represented by the full curve and the initial state is indicated by the dotted line.

'redistributed' to the other two branches. As an effect of this, the matrix elements of the rotations  $U_N$  on branches with angular momentum  $j$  are annihilated and the  $U_M$ s are multiplied by  $U_N^{-1}$  to give the rotation  $G = U_N^{-1}U_M$ . The angle of this rotation is  $\eta$  of equation (4).

- (c) This step involves the identity provided by Varshalovich *et al* (1988) in equation (22), p 260. This formula gives the summation of products of four Clebsch–Gordan coefficients in terms of a double summation over the angular quantum number and the magnetic quantum number of two Clebsch–Gordan coefficients multiplied by two  $6-j$  coefficients represented as tetrahedrons.
- (d) It is easy to prove that the central object, which has two loops linked by the  $L$ -summation (and implicitly an  $M$  summation), is a rotational invariant. Therefore, one can choose the direction of the  $z$ -axis along the direction of the rotation  $G$ . As a rotation about the  $z$ -axis, the matrix representation of  $G$  is diagonal and the line that links the two loops disappears, since only terms with  $M = 0$  are allowed in the summation represented by this line. The transition probability is then obtained as an  $L$ -summation of products of two identical  $6-j$  symbols and two objects which depend only on the angle  $\eta$ , the principal quantum number  $n$  and the angular momentum index  $L$ . These objects are identical to  $H_{jL}(\eta)$  because, by definition,

$$H_{jL}(\eta) = \sum_m C_{jmL0}^{jm} e^{-im\eta}.$$

A detailed analytical proof of equation (3) has also been derived without utilizing the diagrammatic techniques presented here. The transition probability equation (3) is a polynomial in the variable  $x = \cos \eta/2$ . Only even powers occur in this polynomial and, because the  $L$ -summation in equation (3) starts with  $|\ell - \ell'|$ , this polynomial has the factor  $(1 - x^2)^{|\ell - \ell'|}$ . Table 1 provides the exact analytical probabilities for transitions within the states with principal quantum number  $n = 1, 2, 3, 4$  and  $5$ . They agree with the expressions obtained previously by Vrinceanu and Flannery (2000a) for  $n = 2, 3$ . Expressions for larger values of  $n$  have a similar structure and the corresponding polynomials can be easily calculated.



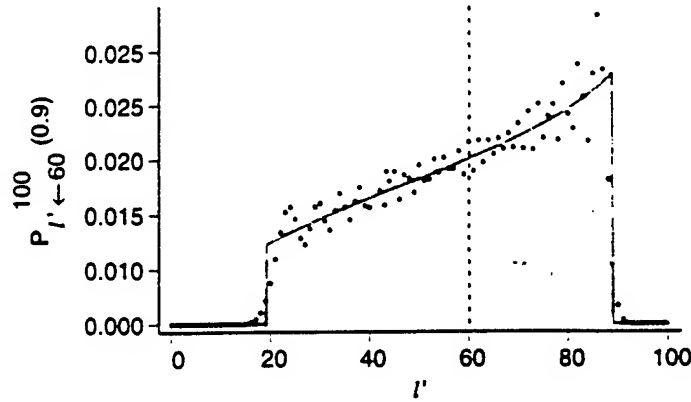


Figure 3. Stark mixing probability for transitions within the energy shell  $n = 100$  from the initial state  $\ell = 60$ , with angle  $\eta$  given by  $\cos \eta/2 = 0.9$ , as a function of the final angular momentum  $\ell'$ . The exact quantal result is represented by the dots, the classical limit is represented by the full curve and the initial state is indicated by the dotted line.

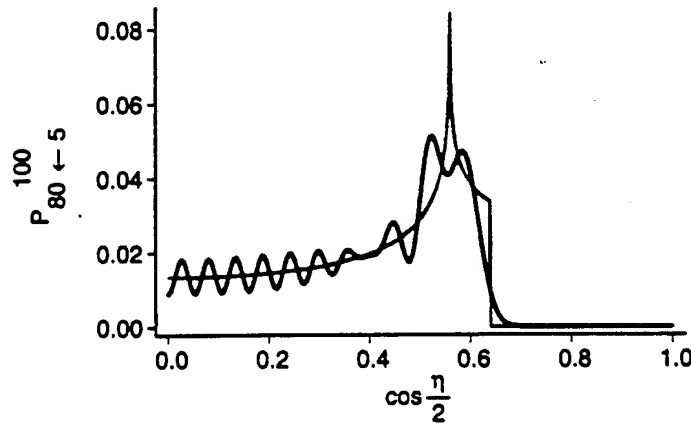


Figure 4. Stark mixing probability for transitions within the energy shell  $n = 100$  from the initial state  $\ell = 5$  to the final state  $\ell' = 80$ , as a function of  $\cos \eta/2$ . The exact quantal result is represented by the darker (wavy) curve. The classical limit is represented by the lighter curve.

In the limit of very large quantum numbers the square of the 6- $j$  symbol reduces (cf Zare, 1988) to  $1/(24\pi V)$ . In this case, the volume  $V$  of the tetrahedron formed by the angular momentum vectors with magnitudes  $\ell$ ,  $\ell'$ ,  $L$  and three vectors of magnitude  $j$  as indicated graphically in figure 1, is determined by

$$V^2 = \frac{1}{144} [L^2 (2j^2 \ell^2 + 2j^2 \ell'^2 - \ell^2 \ell'^2) - j^2 (\ell^2 - \ell'^2)^2 - j^2 L^4].$$

The square of the generalized character function  $H_{jL}(\eta)$  has the classical limit obtained by Kazansky and Ostrovsky (1996a) as

$$H_{jL}^2(\eta) \approx \frac{1}{2 \sin \eta/2} \frac{1}{[\sin^2 \eta/2 - (L/2j)^2]^{1/2}}.$$

Using these two approximations and transforming the  $L$ -summation in equation (3) to an integration, the classical limit of the transition probability is obtained. This limit is identical to the probability derived by Vrinceanu and Flannery (2000b) from the classical equations. Figures 2–4 demonstrate that the classical limit is effective for large quantum numbers. All the examples considered pertain to  $n = 100$  and took a few minutes to produce on a PC. Figures 2 and 3, for small and large  $bv$ , respectively, illustrate that the quantal results oscillate about the classical background. Figure 3 further shows that the quantal result exhibits the characteristic exponential decay in the classical forbidden regions ( $\ell' < 20$  and  $\ell' > 90$ ). The classical singularities are related to the fact that the volume  $V \rightarrow 0$  for certain combinations of angular momenta. A detailed analysis of the various possible classical patterns is a subject explored elsewhere (Vrinceanu and Flannery 2000b). Figure 4 illustrates the variation of the probability for large momentum transfer with the angle  $\eta$ . For large  $bv$ , when  $\cos \eta/2 \rightarrow 1$ , the transition is classically forbidden and the quantal probability decays exponentially. Small  $bv$  implies  $\cos \eta/2 \rightarrow 0$  and the quantal results oscillate about the classical background. The present theory therefore predicts two distinct sets of oscillations in  $P_{\ell\ell'}^{(n)}(\eta)$ —one set evident in the variations with  $\ell'$  (or  $\ell$ ) and the other in the variation with  $\eta$ , i.e. with  $bv$  and  $\Delta\Phi$ . An approximation for the 6- $j$  symbol and  $H_{jL}$ , more refined than the classical limits given here, should provide closer agreement with the quantal transition probabilities.

The probabilities  $P_{\ell\ell'}^{(n)}$  are valid in the regions,  $[v \leq v^* = (3Z_1/2)^{1/2}v_n, b \geq b^* = (3Z_1/2)^{1/2}a_n]$  and  $[v \geq v^*, b \geq b_c = (v/v_n)a_n]$ , of  $(v, b)$ -space where both the adiabatic and weak field conditions are simultaneously satisfied.

What is possibly the last remaining problem in collision physics, capable of an exact solution, has now been solved exactly in closed form. Not only does the present solution reflect the intrinsic mathematical beauty of the problem, it can easily be applied even for large  $n$ .

This research is supported by grants from AFOSR: F 49620-99-1-0277 and NSF: 98-02622.

## References

- Beigman I L and Syrkin M I 1985 *Sov. Phys.-JETP* **62** 226
- Golub G H and Loan C F V 1983 *Matrix Computation* (Baltimore: Johns Hopkins University Press) p 384
- Kazansky A K and Ostrovsky V N 1996a *Sov. Phys.-JETP* **83** 1095
- 1996b *Phys. Rev. Lett.* **77** 3094
- Pfennig H 1972 *J. Quant. Spectrosc. Radiat. Transfer* **12** 821
- Talman J D 1968 *Special Functions: a Group Theoretic Approach* (New York: Benjamin) p 176
- Varshalovich D A, Moskalev A N and Khersonskii V K 1988 *Quantum Theory of Angular Momentum* (Singapore: World Scientific)
- Vrinceanu D and Flannery M R 2000a *J. Phys. B: At. Mol. Opt. Phys.* **33** L721
- 2000b *Phys. Rev. Lett.* **85** 4880
- Zare R N 1988 *Angular Momentum* (New York: Wiley)

## Classical and quantal collisional Stark mixing at ultralow energies

D. Vranceanu and M. R. Flannery

*School of Physics, Georgia Institute of Technology, Atlanta, Georgia 30332*

(Received 6 June 2000; published 2 February 2001)

Exact classical and quantal solutions are presented for the full array of intrashell transitions  $n\ell \rightarrow n'\ell'$ , between any angular momentum states, induced by slow distant collisions with a charged particle. The collisions are adiabatic with respect to the orbital frequency of the atomic electron and the transitions are induced by the weak ion-atom dipole field generated by the ion moving along a classical path. The rich symmetry of the problem allows a unified approach and is the source of the excellent agreement, beyond the usual Ehrenfest's correspondence principle, between the classical and quantal treatments. A classical transition probability is defined. Probabilities for transition between any angular momentum states within a high Rydberg energy level are derived in exact analytic forms and are analyzed for a large number of numerical examples. The transition probabilities obtained from the three methods—quantal and classical formulations and Monte Carlo classical simulations—are directly compared to provide excellent agreement.

DOI: 10.1103/PhysRevA.63.032701

PACS number(s): 34.50.Pi, 34.60.+z, 34.10.+x

## I. INTRODUCTION

The collision of a slow heavy charged particle with an excited atom at large impact parameters induces transitions between neighboring angular momentum states of the excited atom. For very low velocity of the projectile, the transitions with change in principal quantum number are much less probable than the quasielastic angular momentum changing collisions at large impact parameters. Because these states are very close in energy, or are even degenerate as for hydrogen and Rydberg atoms, the process is very efficient since little or no energy transfer is required. In fact, the cross sections increase as the energy of the incoming particle is decreased. This process is called Stark mixing and is important in many problems in atomic physics. For example, Bethe [1] analyzed the absorption of low-energy negative  $K^-$  mesons in liquid hydrogen on the recognition that the Stark mixing is essential in such processes. Also, Stark mixing is included in the calculation of the Auger (or autoionization) process, which follows the collision between ions and atoms [2] and in zero-electron-kinetic-energy (ZEKE) photoelectron spectroscopy [3]. Stark mixing has also been important in astrophysics (e.g., [4]), in recent efforts to produce antihydrogen at 4 K [5] and for general three-body recombination at ultralow energies [6]. The first stage in recombination at ultralow temperatures  $T_e$  [6] is a very rapid collisional capture into high Rydberg states with high angular momentum and large radiative lifetimes, at a rate proportional to  $T_e^{-4.5}$ . Since the  $n$ -changing collisions are relatively unimportant at ultralow energies, the  $\ell$ -mixing collisions are essential in producing the low angular momentum states required to radiatively decay at relatively high rate to low  $n$  levels, thereby stabilizing the recombination.

Experiments [7] on single ion collisions with alkali-metal Rydberg atom have measured large  $\ell$ -mixing cross sections for slow projectiles, including dipole-forbidden transitions. Various theoretical models have been developed to reproduce the experimental data. Even though a set of coupled-channel equations can be written, their solution becomes impractical for the large quantum numbers considered in the

experiment ( $n \approx 28$ ). On averaging over the azimuthal quantum number  $m$ , the size of the problem becomes much reduced and satisfactory results have been obtained [8]. Considering the Rydberg atom in a frame that rotates together with the internuclear axis, the Stark mixing problem is reduced to the problem of the Rydberg atom in mixed *static fields*: electric, provided by the projectile ion, and magnetic, produced by the noninertial (Coriolis) forces. In this way, the well known results (in both classical [9] and quantum [10,11] mechanics) for the problem of interaction between weak fields and an atom can be adopted [12] to provide a solution for the Stark mixing problem. In a remarkable series of papers, both classical [13–15] and quantal [15,16] versions of this approach have been successfully applied for the zero to higher angular momentum transitions, by including the quantum defect appropriate to the experiments [7]. Classical trajectory Monte Carlo simulations [17] were also in agreement with the experiments [7].

All theoretical efforts rely on the impact parameter formalism, in which the projectile is a classical particle moving along a definite trajectory. The dipole interaction has been proven to be a good approximation for the projectile-target potential because of the long-range Coulomb interactions and the decisive role of large impact parameters. For slow moving ions, Stark mixing can occur without energy transfer. The dynamics of the Rydberg atom is therefore adiabatic. The orbit of the Rydberg electron can still be considered elliptical, but its shape and orientation change slowly during the collision time, which is very much longer than the orbital time. This classical mechanics picture translates into the quantal description by restricting the dynamics to the energy shell, as prescribed by adiabatic perturbation theory.

In this paper, a unified theory for the general time-dependent solution of collisional Stark mixing is presented, both in the classical and quantal formulations. The exceptional rich dynamic symmetry of the hydrogen atom provides the key foundation that enables both the classical and quantal solutions to be constructed in a unified way (Sec. II) by using group representation theory. This classical-quantal correspondence transcends the well known Ehrenfest's theorem

(as observed in the general case of weak field-atom interaction [15,18]) just because of the  $SO(4)$  dynamical group symmetry<sup>1</sup> of the energy shell of the hydrogen atom. The agreement, as expected, is very good. It is shown that the present quantal solution (developed in Sec. III A) can be formulated (Sec. III B) so as to provide the rotating coordinate frame formal result obtained in [12,15,16]. The efficiency of the present quantal solution is demonstrated in Sec. VI. A new classical solution applicable to transitions between arbitrary angular momentum states is derived in Sec. IV A. We define the classical transition probability, in a language designed to exploit the dynamical symmetry, as the normalized volume of phase space accessible to both initial and final states in Sec. IV B. Monte Carlo simulations (Sec. V) are also performed to yield results in agreement with the classical expression for the Stark mixing probabilities.

## II. KINEMATICS OF STARK MIXING

Stark mixing occurs when the electron of a Rydberg atom changes its angular momentum, without changing its energy, as a result of a collision, at large impact parameters, with a slow massive particle of charge  $Z_1 e$ . In addition to the energy, given by the constant Hamiltonian

$$H_0 = \frac{p^2}{2m_e} - \frac{e^2}{r},$$

the angular momentum  $L = r \times p$  of the unperturbed Rydberg electron and the Runge-Lenz (or eccentricity) vector

$$A = \left[ p^2 r - (p \cdot r)p - m_e e^2 \frac{r}{r} \right] / \sqrt{-2m_e E}, \quad (1)$$

which is directed toward the pericenter and normalized to angular momentum units, are also conserved. These quantities define the dynamic  $SO(4)$  symmetry of the hydrogen atom with given energy  $E$ , which is a subgroup of the global  $SO(4,2)$  symmetry group. Because the  $SO(4)$  group is isomorphic with the direct product  $SO(3) \oplus SO(3)$  of two rotation groups, a special decomposition

$$L = M + N, \quad A = M - N \quad (2)$$

permits the dynamics of the hydrogen atom to be separated into two decoupled motions. The generators  $M$  and  $N$  act independently as angular momenta and are also conserved quantities for the unperturbed Rydberg atom. They evolve independently [9] with time on application of an electric field.

The orbital electron interacts with the time-dependent electric field  $\tilde{E}(t)$  generated by the passing projectile of charge  $Z_1 e$ . In the weak-field approximation, this field is constant over the spatial extent of the atom. In this approxi-

<sup>1</sup>This group contains sufficient generators to enable one to formulate the dynamics of the system solely in terms of operations of irreducible representations of the group [19].

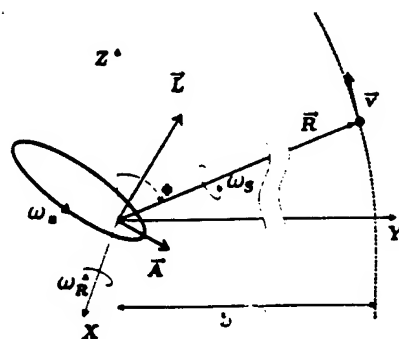


FIG. 1. Geometry of the Stark mixing collision.

mation, which is the same as the dipole approximation, the interaction potential  $V = e\tilde{r} \cdot \tilde{E}$  is

$$\begin{aligned} V(r, R) &= -Z_1 e^2 \frac{R \cdot r}{R^3} = \frac{Z_1 e^2}{vb} \frac{d\Phi}{dt} \hat{R} \cdot r \\ &= \frac{Z_1 e^2}{vb} \frac{d\Phi}{dt} (y \sin \Phi + z \cos \Phi). \end{aligned} \quad (3)$$

The impact parameter  $b$ , the impact angle  $\Phi$ , and internuclear vector  $R$  are displayed in Fig. 1. The angular momentum of relative motion  $L_{rel} = \mu R^2 \dot{\Phi} = -\mu vb$  (where  $\mu$  is the reduced mass of the projectile-target system) remains conserved since  $L_{rel} \gg L$  (so that  $L_{rel}$  and  $L$  are effectively decoupled).

Various frequencies or time scales are important to the present discussion of the collision, and are as follows.

(i) The projectile rotation (collision) frequency

$$\omega_R = -\frac{d\Phi}{dt} = \frac{bv}{R^2} \approx \frac{bv}{b} \approx \frac{1}{\tau_{coll}}$$

from which the collision time  $\tau_{coll}$  can be defined.

(ii) The transition frequency

$$\omega_{ij} = \frac{E_i - E_j}{\hbar}$$

of the Rydberg electron. For transitions  $n \rightarrow n \pm 1$  between neighboring levels,  $\omega_{n, n \pm 1}$  is simply  $\omega_0/n^3 = \omega_n = v_n/a_n$ , the orbital frequency (the Bohr correspondence principle). Here  $a_n = n^2 a_0$  and  $v_n = v_0/n$  are the averaged orbital radius and velocity.

(iii) The Stark precession frequency

$$\omega_S = \frac{3}{2} a_n v_n (E/e) = \frac{3}{2} \frac{Z_1 a_n v_n}{R^2}$$

for the precession of  $A$  about  $R$  provides the precessional frequency of the Runge-Lenz (eccentricity) vector  $A$  of the Rydberg orbit about the field direction  $\tilde{E}$ .

(iv) The spin-orbit coupling frequency  $\omega_{SO}$  corresponds with the maximum fine-structure splitting and is approximately  $[20] \alpha_{FS}^2 \omega_n / n$ , where  $\alpha_{FS}$  is the fine structure constant.

(v) The quantum defect frequency  $\omega_{\text{QD}}$  is the precessional frequency of the electron orbit due to its interaction with the polarizable core. This frequency is important when one-electron atoms are considered other than hydrogen. The combined polarization of the core due to the orbital electron and the charged projectile has to be taken into account. Given the quantum defect  $\delta_l$ , the quantum defect frequency is

$$\omega_{DD} \approx 5 \delta \omega_n / \ell$$

when  $\ell$  is sufficiently large such that the core penetration and relativistic corrections can be ignored [21].

By considering the  $\exp(i\omega t)$  factor in time-dependent perturbation theory, several types of collisions can be classified, as in [22], by comparing the above frequencies.

The Stark mixing parameter  $\alpha$  is defined as the following ratio between the Stark and collision frequencies:

$$\alpha = \frac{\omega_s}{\omega_p} = \frac{3Z_1}{2} \left( \frac{a_n v_n}{b v} \right) = \frac{3Z_1}{2} \frac{\mu}{m_e} \frac{n \hbar}{L_{\perp}}. \quad (4)$$

When  $\alpha \ll 1$ , then  $\omega_S \tau_{\text{coll}} \ll 1$  and the collision time is much shorter than the Stark precessional time so that  $\ell$ -changing or *Stark sudden* transitions are favored. This is in contrast to *Stark adiabatic* transitions where  $\alpha \gg 1$ ; the electronic angular momentum does not change since the atom has sufficient time to relax to the Stark effect.

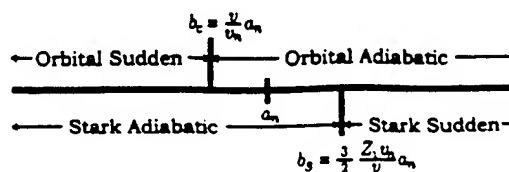
The orbital parameter  $\beta$  is the ratio

$$\beta = \omega_R / \omega_n = \frac{v}{v_n} \frac{a_n}{b} = \frac{b_c}{b}.$$

For an *orbital adiabatic* collision, when  $\beta \ll 1$  or  $b \gg b_c$ , the orbital electron adjusts itself adiabatically to the slow ion perturbation. Since  $\omega_n \tau_{\text{coll}} \gg 1$ , no energetic transitions occur. The *orbital sudden* regime,  $\beta \gg 1$  or  $b \ll b_c$ , is associated with  $\omega_n \tau_{\text{coll}} \ll 1$  and impulsive  $n \rightarrow n'$  transitions.

The product of the  $\alpha$  and  $\beta$  parameters defines the ratio  $\omega_s/\omega_n = (3Z/2)(a_n/b)^2$ , which depends only on  $b$  (and not  $v$ ). For *weak fields* the Stark mixing splitting  $\Delta E_s = \hbar \omega_s \ll \hbar \omega_n$ , the  $(n \rightarrow n \pm 1)$  energy gap. This also means that the internuclear distance  $R$  is much greater than the mean orbital radius  $a_n$ . In this approximation, the electron's orbital time is then much shorter than any characteristic collisional time to cause  $\ell$  changes to the elliptical orbit. The vectors  $\mathbf{A}$  and angular momentum  $\mathbf{L}$ , which are constant for the unperturbed motion, then become good dynamical variables for the description of the perturbed motion, within the weak-field approximation.

With respect to orbital motion, the collision is sudden or adiabatic according to  $b < b_C$  and  $b > b_C$ , respectively, where  $b_C = (v/v_n)a_n$ . With respect to the Stark frequency, the collision is adiabatic or sudden according to  $b < b_S$  and  $b > b_S$ , respectively, where  $b_S = (v_n/v)a_n$ . The impact parameter  $b$  space can then be partitioned as in Fig. 2. As  $v$

FIG. 2. Partitioning the impact parameter space  $b$ .

decreases,  $b_S$  increases outward and  $b_C$  increases inward, thereby limiting the extent of the two sudden regions where  $n$  changes and  $\ell$  mixing occurs. The variation with  $v$  can be represented by a  $(v, b)$  phase-space diagram partitioned into the characteristic regions as illustrated in Fig. 3. For  $v > v^* = (3Z/2)^{1/2} v_n$ , the  $(n, \ell)$  changing and  $\ell$  changing (orbital and Stark sudden) shaded regions overlap and expand, in direct contrast to ultracold speeds  $v \leq v^*$ , where the orbital and Stark adiabatic (clear) regions increase and the shaded regions diminish and do not overlap, thereby indicating few collisional changes. The region of interest here is the overlap of the orbital adiabatic ( $\omega_R < \omega_n$ ) region,  $b > b_C = (v/v_n) a_n$ , with the weak-field ( $\omega_S < \omega_n$ ) region,  $b > b^* = (3Z/2)^{1/2} a_n$ , i.e., the region in Fig. 3 defined by  $b > b_C$  for  $v \geq v^* = (3Z/2)^{1/2} v_n$  and by  $b > b^*$  for  $v \leq v^*$ .

The following formulation assumes that the Rydberg atom, during the collision, occupies the same degenerate energy shell. The main element of the perturbation potential (3) is the electron position vector  $\mathbf{r}$ , which by Pauli's replacement rule [23]

$$\mathbf{r} \sim \langle \mathbf{r} \rangle = -\frac{3}{2} \frac{\mathbf{A}}{p_n} \quad (5)$$

is replaced by its average  $\langle r \rangle$ , a procedure valid for orbital adiabatic collisions (see Appendix A for a detailed explanation).

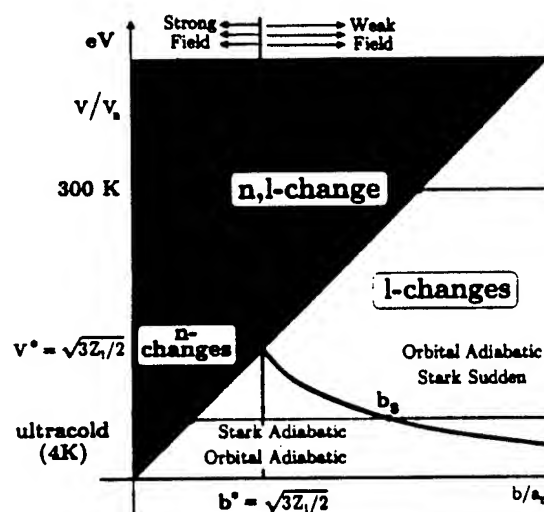


FIG. 3. Partitioning the  $v$ - $b$  phase-space map into regions characterized mainly by (a) energy changes, (b) energy and angular momentum changes, (c) angular momentum changes, and (d) no changes. Regions for strong and weak field collisions are also shown.

tion). Since  $Z_1 e^2 r/bv$  is then  $\alpha A$ , the perturbing potential (3) can be written in terms of the components  $A_2$  and  $A_3$  as

$$V(\alpha) = e\langle \vec{r} \rangle \cdot \vec{E}(t) = -\alpha \frac{d\Phi}{dt} (A_2 \sin \Phi + A_3 \cos \Phi),$$

under the adiabatic, dipole and classical path assumptions. Moreover, the components  $\{L_1, A_2, A_3\}$  generate a subgroup of the original symmetry group. The solution of the problem can then be written in terms of these symmetry-group generators and the Stark parameter  $\alpha$ , which acts as a coupling constant. Under the above approximations, the collision parameters  $v$ ,  $b$ , and  $Z_1$  become combined into one parameter  $\alpha$ .

The cross section for Stark mixing is

$$\begin{aligned} \sigma_{n'l-n'l'} &= 2\pi \int_0^\infty P_{l'l'}^{(n)} b db \\ &= 2\pi \left( \frac{3Z_1 a_n}{2v/v_n} \right)^2 \int_0^\infty P_{l'l'}^{(n)}(\alpha, \Delta\Phi) \frac{d\alpha}{\alpha^3}. \end{aligned} \quad (6)$$

The probabilities  $P_{l'l'}^{(n)}$  obtained here are defined only in the full orbital adiabatic region  $b > b_c$  for  $v \geq v^*$  and in the adiabatic region restricted by the weak-field condition  $b > b^*$  for  $v \leq v^*$  (see Fig. 3). When  $v < v^*$  and  $b < b^*$ , the Stark parameter  $\alpha > 1$ . Since the transition probabilities are bounded for large  $\alpha$ , the contribution to the  $\alpha$  integration is vanishingly small for large  $\alpha$ , decreasing as  $\alpha^{-3}$ , and can be neglected for  $\alpha > 1$ . Cross section (6) can then be defined at ultralow speeds  $v \leq v^*$ , when the lower limit  $b_{min}$  to the  $b$ -integration is taken as the weak-field limit  $b^*$ . For higher speeds  $v > v^*$ , the probabilities determined here are valid only in the full adiabatic region  $b > b_c$  and do not hold in the (orbital sudden) region  $b^* < b < b_c$  required in (6). In practical calculations of Eq. (6), various physical effects such as quantum defect, spin-orbit coupling, and Debye screening in a plasma determine an upper limit to the  $b$  integration and hence a lower limit  $\alpha_{min}$  to the  $\alpha$  integration. For example, the spin-orbit splitting overlaps with the Stark splitting when  $b > b_{max}$ , where  $b_{max} \approx n^{5/2} \alpha_{FS}^{-1} (3Z_1/2)^{1/2} a_0$ . Similarly, the quantum defect comes into effect for the critical  $b_{max} \approx n^{5/2} \delta^{1/2} (3Z_1/10)^{1/2} a_0$ . The Debye radius  $R_D = (kT/4\pi^2 Z_1 e^2 N)^{1/2}$ , where  $T$  and  $N$  are the temperature and number density of the projectiles, is another viable upper limit to the impact parameter [4]. Stray electric fields in the collision region can also impose an upper limit to the impact parameter. The decision of which limit should be adopted in the definition (6) depends, of course, on the specific problem considered. These cutoff procedures are crucial for low angular momentum transfers where the transition probability  $P(\alpha)$  cannot offset the  $1/\alpha^3$  singularity (cf. Ref. [4]) as  $b \rightarrow \infty$ . The initial and final angles  $\Phi_0$  and  $\Phi$ , between which the Stark mixing is effective, are also dependent on the specific cutoff procedure [14]. For trajectories with zero deflection ( $\Delta\Phi = -\pi$ ), then Eq. (6) varies universally as

$(Z_1 a_n/v)^2$ . Departure from this variation is governed by  $\Delta\Phi(b, v)$  and by the physical limits imposed upon the  $\alpha$  integration.

The discussion above is valid for both quantal and classical descriptions of Stark collisional mixing, since both involve only kinematics and general dynamical symmetry arguments. It is shown below (in Secs. III A and IV A) that both quantal and classical dynamics are governed by the following generic equation:

$$i \frac{\partial U}{\partial t} = \pm \alpha \frac{d\Phi}{dt} (J_2 \sin \Phi + J_3 \cos \Phi) U \quad (7)$$

for the time evolution operator  $U$  within the rotation Lie group  $SO(3)$ . The generators  $\{J_1, J_2, J_3\}$  of this group have the commutators  $[J_j, J_k] = i \epsilon_{jkn} J_n$ , where  $\epsilon_{jkn}$  is the Levi-Civita antisymmetric permutation symbol for any  $j, k = 1, 2, 3$ . The required solution of Eq. (7) is

$$U(t, t_0) = e^{i\Phi J_1} \exp[-i\Delta\Phi(J_1 \pm \alpha J_3)] e^{-i\Phi_0 J_1}. \quad (8)$$

This can be easily verified with the aid of the relations

$$e^{i\lambda J_2} J_1 e^{-i\lambda J_2} = J_1 \cos \lambda + J_3 \sin \lambda,$$

$$e^{i\lambda J_2} J_3 e^{-i\lambda J_2} = J_3 \cos \lambda - J_1 \sin \lambda,$$

$$e^{i\lambda J_1} J_3 e^{-i\lambda J_1} = J_3 \cos \lambda + J_2 \sin \lambda,$$

which are derived from the basic identity

$$e^{\lambda A} B e^{-\lambda A} = B + \frac{\lambda}{1!} [A, B] + \frac{\lambda^2}{2!} [A, [A, B]] + \dots \quad (9)$$

and the above commutation relations. The net polar angle  $\Delta\Phi$  swept during the collision between  $t_0$  and  $t$  is  $\Phi - \Phi_0$ . The initial condition  $U(t_0, t_0) = 1$  is automatically satisfied. If no cutoff radius is considered,  $\Phi_0 \rightarrow \pi$  as  $t_0 \rightarrow -\infty$  and  $\Phi \rightarrow \Phi_D$  (the classical deflection angle) as  $t \rightarrow \infty$ . For the simplest case of distant straight line trajectories  $\Phi_D = 0$ , and the evolution operator is then

$$U(\infty, -\infty) = \exp[i\pi(J_1 \pm \alpha J_3)] e^{-i\pi J_1}$$

or, in terms of finite angle rotations  $\mathcal{R}[\varphi, \mathbf{n}]$  by angle  $\varphi$  about direction  $\mathbf{n}$  and the parameter  $\gamma = \sqrt{1 + \alpha^2}$ , is

$$U(\infty, -\infty) = \mathcal{R}[-\gamma\pi, (1/\gamma, 0, \pm \alpha/\gamma)] \mathcal{R}[\pi, (1, 0, 0)].$$

### III. QUANTAL THEORY

#### A. Quantal intrashell dynamics

The Schrödinger equation for the time evolution operator  $U(t, t_0)$  is

$$i\hbar \frac{\partial U}{\partial t} = (H_0 + V)U, \quad (10)$$

where  $H_0$  is the free atom Hamiltonian and  $V$  is the interaction potential (3). If the projectile is moving sufficiently slowly, adiabatic perturbation theory can be applied and then

the whole dynamics of the target atom becomes restricted to the initial degenerate energy shell (the orbital adiabatic region in Fig. 3). This simple fact has two major consequences. First, the position operator and hence the perturbation potential (3) commute with the unperturbed Hamiltonian, as one can prove directly from the matrix elements of the commutator  $[r, H_0]$  between any states within the energy  $E_n$  shell. The potential in the interaction representation

$$V_I = e^{iH_0 t/\hbar} V e^{-iH_0 t/\hbar}$$

is then identical with the potential in the Schrödinger representation ( $V_I = V$ ), and the equation to be solved, in the interaction representation, is

$$i\hbar \frac{\partial U_I}{\partial t} = V U_I, \quad (11)$$

where  $U_I(t, t_0) = \exp(iH_0 t/\hbar) U(t, t_0) \exp(-iH_0 t_0/\hbar)$ . Second, the components  $x, y, z$  of the position operator do not commute between themselves when restricted to the energy shell. This follows from the well known Pauli "replacement" [23]  $\mathbf{r} \rightarrow -3n\mathbf{A}/2$  (see Appendix A for details). This shows that the position vector  $\mathbf{r}$  behaves, within the intrashell dynamics, like an angular momentum and is denoted by  $\{\mathbf{r}\}$  when operating only within the  $n$ -shell. In fact, the set of operators  $\{L_x, -2\{y\}p_n/3, -2\{z\}p_n/3\}$  generates a rotation group and Eqs. (11) and (7) are identical when  $J_1 = L_x$ ,  $J_2 = -2\{y\}p_n/3$  and  $J_3 = -2\{z\}p_n/3$ . Using the solution (8) of Eq. (7), the exact solution of Eq. (10) of Sec. II for the evolution operator, within the adiabatic approximation, is then

$$U_I(t, t_0) = e^{i\Phi L_1/\hbar} \exp\left[-\frac{i}{\hbar} \Delta\Phi \left(L_1 - \frac{2\alpha}{3} p_n \{z\}\right)\right] e^{-i\Phi_0 L_1/\hbar}. \quad (12)$$

This can also be directly verified by substituting Eq. (12) in Eq. (10) and using Eq. (9) with the appropriate commutator algebra.

The transition probability for a general  $i \rightarrow f$  transition at time  $t$  is

$$a_{fi}(t) = \langle \Phi_f(\mathbf{r}, t) | \Psi_i(\mathbf{r}, t) \rangle = \langle \Phi_f(\mathbf{r}, t) | U(t, t_0) | \Psi_i(\mathbf{r}, t_0) \rangle \\ = \langle \Phi_f(\mathbf{r}) | U_I(t, t_0) | \Phi_i(\mathbf{r}) \rangle,$$

where  $\Psi_i$  is the target wave function, which tends in the asymptotic limits ( $t \rightarrow \pm\infty$ ) to the unperturbed basis set  $\Phi_i(\mathbf{r}, t) = \phi_i(\mathbf{r}) \exp(-iE_i t/\hbar)$ . The transition amplitude for a Stark mixing process is

$$a_{\beta\alpha}^{(n)} = \langle n\beta | U_I(\infty, -\infty) | n\alpha \rangle, \quad (13)$$

where the initial state  $i = |n\alpha\rangle$  at  $t = -\infty$  evolves to the final states  $f = |n\beta\rangle$  at  $t = \infty$ ;  $\alpha$  and  $\beta$  now label the states within the same energy shell. The superscript  $n$  will be omitted, since all dynamics is restricted to the energy shell described by quantum number  $n$ . When  $\alpha$  and  $\beta$  label states with a given magnitude and projection of the angular momentum, the transition amplitude is given by Eq. (12) in Eq. (13) and is feasible and efficient for practical numerical applications.

The core of solution (12) is the exponential of the operator  $L_1 - 2\alpha p_n z/3$ . By using basic commutator algebra and Eq. (9), this operator is diagonalized as

$$e^{-iyq/\hbar} \left( L_1 - \frac{2\alpha}{3} p_n \{z\} \right) e^{iyq/\hbar} = \gamma L_1,$$

where  $q = 2p_n \arctan(\alpha)/3$  and  $\gamma = \sqrt{1 + \alpha^2}$ . The solution (12) has therefore the alternative form

$$U_I(t, t_0) = e^{i\Phi L_1/\hbar} e^{-i\{y\}q/\hbar} e^{-i\gamma\Delta\Phi L_1/\hbar} e^{i\{y\}q/\hbar} e^{-i\Phi_0 L_1/\hbar}, \quad (14)$$

which illustrates very effectively how the action of the slow distant encounter charged projectile coming from the negative  $z$  axis is decomposed into successive rotations about the  $x$  axis and alternating impulsive momentum transfers ( $\pm q$ ) along the  $y$  axis.

It is interesting to compare the solution (14) obtained in this orbital adiabatic limit with the purely impulsive solution presented in sec. III C. The evolution operator (14), for undeflected collisions, yields

$$U_I(\infty, -\infty) = e^{-i\{y\}q/\hbar} e^{i\pi\gamma L_1/\hbar} e^{i\{y\}q/\hbar} e^{-i\pi L_1/\hbar}.$$

In the limit that  $\alpha \rightarrow 0$ ,  $q \rightarrow 2\alpha p_n/3 = \Delta q/2$  and  $\exp(i\pi\gamma L_1/\hbar) \rightarrow \exp(i\pi L_1/\hbar)$ . Then

$$U_I(\infty, -\infty) \\ = \left[ 1 + \frac{(-i)}{1!} \left( \frac{\{y\}\Delta q}{2\hbar} \right) + \frac{(-i)^2}{2!} \left( \frac{\{y\}\Delta q}{2\hbar} \right)^2 + \dots \right] e^{i\pi L_1/\hbar} \\ \times \left[ 1 + \frac{i}{1!} \left( \frac{\{y\}\Delta q}{2\hbar} \right) + \frac{i^2}{2!} \left( \frac{\{y\}\Delta q}{2\hbar} \right)^2 + \dots \right] e^{-i\pi L_1/\hbar},$$

which reduces, with the aid of  $\exp(i\pi L_1/\hbar) y^n \exp(-i\pi L_1/\hbar) = y^n (\cos \pi)^n = (-y)^n$ , to

$$U_I = e^{-2iq\{y\}/\hbar} + O(\alpha^2). \quad (15)$$

This limit merges with the impulsive result Eq. (20) below.

### B. Formal development

It is interesting, however, to note that by introducing Pauli's replacement directly in the potential (3) and by writing the Runge-Lenz vector as  $\mathbf{A} = \mathbf{M} - \mathbf{N}$ , the potential decomposes as

$$V = V_M + V_N,$$

where

$$V_M = -\alpha(M_2 \sin \Phi + M_3 \cos \Phi)\Phi$$

and

$$V_N = \alpha(N_2 \sin \Phi + N_3 \cos \Phi)\Phi.$$

Because the commutators  $[M_i, N_j] = 0$ ,  $[M_i, H_0] = 0$ , and  $[N_i, H_0] = 0$  (for any  $i, j = 1, 2, 3$  combination), the problem (10) becomes separable, exactly in the same way as the classical Stark mixing equations become decoupled (see the next section). The time evolution operator then factorizes as

TABLE I. The four bases useful for describing the quantal states of the hydrogen atom.

Basis	Quantum numbers	Complete set of commuting observable	Origin
orbital	$ n\ell m\rangle_O$	$H_0, L^2, L_3$	Standard for spherical coordinates; describes correctly the states of the field-free atom
parabolic	$ n_1 n_2 m\rangle_P$	$H_1, H_2, L_3$	Separation of Hamiltonian $H = H_1 + H_2$ in parabolic coordinates, $\xi = r + z$ , $\eta = r - z$ , $\tan \varphi = y/x$ ; $n = n_1 + n_2 +  m  + 1$
Stark	$ nqm\rangle_S$	$H_0, A_3, L_3$	Parabolic basis; describes the Stark states for small electric field $\mathcal{E}$ , when the interaction $-e\mathcal{E}z$ is diagonal; $q = n_1 - n_2$
algebraic	$ n\mu\nu\rangle_A$	$H_0, M_3, N_3$	The two rotation groups in which the dynamic symmetry group $SO(4) = SO(3) \oplus SO(3)$ decomposes using Eq. (2); the equivalent angular momentum for both $SO(3)$ representations is $j = (n-1)/2$ ; $\mu = (m+q)/2$ and $\nu = (m-q)/2$

$$U = U_{H_0} U_M U_N, \quad (16)$$

where, of course,  $U_{H_0} = \exp[-iH_0(t-t_0)/\hbar]$ , and  $U_M$  and  $U_N$  are the solutions of the equations  $i\hbar \partial U_M / \partial t = V_M U_M$  and  $i\hbar \partial U_N / \partial t = V_N U_N$ , respectively. Using the group-theoretical result Eq. (8) of Sec. II, the solutions for the operators  $U_M$  and  $U_N$  are then

$$U_M = e^{i\Phi M_1/\hbar} \exp[-i/\hbar(\Phi - \Phi_0)(M_1 - \alpha M_3)] e^{-i\Phi_0 M_1/\hbar} \quad (17)$$

and

$$U_N = e^{i\Phi N_1/\hbar} \exp[-i/\hbar(\Phi - \Phi_0)(N_1 + \alpha N_3)] e^{-i\Phi_0 N_1/\hbar} \quad (18)$$

In calculating the amplitude (13), four interesting basis sets can be chosen for the one electron hydrogenlike atom. Table I summarizes key properties of these bases. The orbital basis is useful for describing the field-free atom, before and after the collision, whereas the algebraic basis appears naturally as a basis where  $M_3$  and  $N_3$  are diagonal. The solution (16) has the simplest expression in this algebraic basis. All four bases in Table I span the  $n^2$  degenerate energy shell and can be equally adopted to characterize the hydrogen atom. The algebraic basis spans a tensorial product of two spaces  $(|\mu\rangle \otimes |\nu\rangle)$  corresponding with spaces used for a matrix representation of the product  $SO(3) \oplus SO(3)$ . The two spaces have the same dimension because  $M^2 = N^2 = (L^2 + A^2)/4 = (n^2 - 1)\hbar^2/4$  and are associated with two angular momenta with  $j = (n-1)/2$ .

The transition amplitude between the two algebraic states is then the product of two amplitudes for  $M$  and  $N$  independent actions, exactly in the same way in which the classical  $M$  and  $N$  vectors evolve independently in time, i.e.,  $a_{(\mu'\nu'),(\mu\nu)} = a_{\mu'\mu} a_{\nu'\nu}$ . Each factor is the matrix element of a  $j = (n-1)/2$  dimensional representation of the rotations represented by Eq. (16). For example, from Eq. (17), one gets  $a_{\mu'\mu} = F_{\mu'\mu}(\alpha)$  with

$$F(\alpha) = \mathcal{D}^{(j)} \left[ -\gamma\pi, \left( \frac{1}{\gamma}, 0, -\frac{\alpha}{\gamma} \right) \right] \mathcal{D}^{(j)}[\pi, (1, 0, 0)],$$

where  $\mathcal{D}[\phi, (n_1, n_2, n_3)]$  is the Wigner matrix representation for the rotation  $\mathcal{R}[\phi, \mathbf{n}]$  by angle  $\phi$  about direction  $\mathbf{n}$  (see [24] for the explicit expression). The transition probability in the space of  $N$  is the element  $\nu'\nu$  of the matrix  $F(-\alpha)$ .

Calculation of the transition probability between orbital states requires the explicit unitary transformation between the orbital and algebraic bases. This can be obtained by direct scalar products of orbital and parabolic states for which explicit coordinate representations are known. The result can be written in terms of hypergeometric functions [25]. However, an equivalent result is provided by the  $SO(4) \sim SO(3) \oplus SO(3)$  isomorphism. The orbital state, as a combination of two angular momentum states, is (see [26] for example)

$$|n\ell m\rangle = \sum_{\mu, \nu=-j}^j C_{\mu\nu}^{(\ell m)} |n\mu\nu\rangle,$$

where the transformation matrix  $C^{(\ell m)}$  is given by the standard Clebsch-Gordan coefficients  $\langle j\mu j\nu | \ell m \rangle$ . The transition amplitude for the  $\ell m \rightarrow \ell' m'$  transition is then

$$a_{\ell' m', \ell m} = \sum_{\mu\nu\mu'\nu'} C_{\mu'\nu'}^{(\ell' m')} C_{\mu\nu}^{(\ell m)} F_{\mu'\mu}(\alpha) F_{\nu'\nu}(-\alpha), \quad (19)$$

which can be expressed in matrix form as

$$a_{\ell' m', \ell m} = \text{Tr}[C^{(\ell' m')} F(-\alpha) C^{(\ell m)T} F^T(\alpha)],$$

where  $C^T$  is the transpose of matrix  $C$ . The above result Eq. (19) is in exact agreement with the solution obtained in [12,15,16] using the rotating frame approach. The quantal development here in the fixed frame is exquisite in that it follows exactly the same reasoning basic to the exact classi-



cal mechanics solution (Sec. IV A). This result exhibits the essential power of the  $SO(4)$  symmetry group for the energy shell of the hydrogen atom. The common  $SO(4)$  symmetry therefore transcends the chosen formulation (classical or quantal) and provides a classical-quantal correspondence at a level more fundamental than Ehrenfest's theorem and the Heisenberg correspondence. In practice, the fourfold summation (19) and the use of the Wigner rotation matrices  $\mathcal{D}$  for  $F(\alpha)$  are not very efficient and the difficulty of calculation increases dramatically with  $n$ . Instead, the solution (12) provides a simpler approach, since the matrix elements of the argument in the exponential have simple expressions directly in the orbital basis. The array of transitions is obtained at once, within one matrix exponentiation of a band diagonal matrix for which efficient algorithms are available [27].

When the projection of the initial and final angular momentum is not determined, the transition probability is

$$P_{fi}(\alpha) = \frac{1}{2\ell+1} \sum_{m=-\ell}^{\ell} \sum_{m'=-\ell'}^{\ell'} |a_{\ell' m' \ell m}|^2.$$

The exact quantal solution can therefore be derived directly without making use of unnecessary complications of a rotating frame and a fictitious magnetic field. The structure of the present solution Eq. (14) represents a sequence of alternating momentum transfers (in the  $y$  direction) and rotations about the  $x$  axis. This recognition motivates the following section.

### C. Impulsive limit

In the other extreme situation (the orbital sudden-Stark sudden region in Fig. 3, where  $\alpha \ll 1$ ), the impulsive limit, the collision is very fast and the collision time  $\tau_{\text{coll}}$  is much smaller than the orbital time. The potential has again the same form in both Schrödinger and interaction representations,  $V = V_I$ , since, in the equality  $\langle f|V|i \rangle = \langle f|V_I|i \rangle e^{i\omega_{fi}t}$ , the exponent  $\omega_{fi}t \ll 1$  [with  $\omega_{fi} = (E_f - E_i)/\hbar$ ] can be replaced by zero. Now the position operator has the normal behavior, in that its components commute between themselves. The impulsive transition amplitude is

$$a_{fi}^{\text{imp}} = \langle \phi_f(\mathbf{r}) | \exp - \frac{i}{\hbar} \int_{t_0}^t V(\mathbf{r}, t') dt' | \phi_i(\mathbf{r}) \rangle,$$

as may be directly verified upon using the closure relation. Since the force  $\mathbf{F} = -\nabla_r V(\mathbf{r}, t)$  acting on the Rydberg electron is impulsive and imparts momentum  $\Delta \mathbf{q}$ , then

$$\begin{aligned} \exp - \frac{i}{\hbar} \int_{t_0}^{t=\infty} V(\mathbf{r}, t') dt' &= \exp - \frac{i}{\hbar} \int d\mathbf{r} \cdot \int_{-\infty}^{\infty} \mathbf{F}(\mathbf{r}, t) dt \\ &= \exp - \frac{i}{\hbar} \Delta \mathbf{q} \cdot \mathbf{r} \end{aligned}$$

so that the probability amplitude for an impulsive collision is simply

$$a_{fi}^{\text{imp}}(\mathbf{q}) = \langle \phi_f | \exp - \frac{i}{\hbar} \Delta \mathbf{q} \cdot \mathbf{r} | \phi_i \rangle, \quad (20)$$

the inelastic form factor amplitude. This agrees with other alternative derivations [28,29] for the probability of an impulsive transition. The momentum transferred in an (impulsive) rectilinear collision is

$$\Delta \mathbf{q} = (2Z_1 e^2 / b v) \hat{\mathbf{y}} = (4 \alpha \hbar / 3 n a_0) \hat{\mathbf{y}}.$$

The transition amplitude, valid in the orbital and Stark sudden region (cf. Fig. 3), is therefore

$$a_{fi}^{\text{imp}}(\alpha) = \langle \phi_f | \exp - i \frac{4}{3} \frac{\alpha}{n} \frac{y}{a_0} | \phi_i \rangle,$$

which connects with the  $\alpha \rightarrow 0$  limit Eq. (15) of the adiabatic result Eq. (14). Even though this approximation is appropriate for the amplitude for transitions  $n\ell \rightarrow n'\ell'$  between different energy shells, it is a good approximation, in particular for very small  $\alpha$  [see Eq. (15)], if the normalized

$$\bar{P}_{\beta\alpha}^{\text{imp}} = |a_{\beta\alpha}^{\text{imp}}|^2 / \sum_{\beta} |a_{\beta\alpha}^{\text{imp}}|^2$$

transition probability is adopted for the problem of intrashell transitions. This normalization is a consequence of the difference between the operators  $\{\mathbf{r}\}$ , appropriate only to intrashell transitions, and  $\mathbf{r}$  for all transitions.

## IV. CLASSICAL THEORY

### A. Classical intrashell dynamics

The angular momentum vector  $\mathbf{L}$  and the Runge-Lenz vector defined by

$$\mathbf{A} = p_n^{-1} \left[ \mathbf{p} \times \mathbf{L} - m_e e^2 \frac{\mathbf{r}}{r} \right]$$

are constant for the unperturbed classical Rydberg atom. Moreover,  $\mathbf{A} \cdot \mathbf{L} = 0$  and  $A^2 + L^2 = m_e a_n = n^2 \hbar^2$ . In the presence of an electric field of intensity  $\tilde{\mathbf{E}}$ , the angular momentum  $\mathbf{L}$  changes at the rate

$$\frac{d\mathbf{L}}{dt} = -e \tilde{\mathbf{r}} \times \tilde{\mathbf{E}}.$$

On assuming that the collision is orbital adiabatic ( $\Phi \ll \omega_n$  and  $\tilde{\mathbf{E}}$  is constant over one period), the slow change of  $\mathbf{L}$  during the collision is the classical average

$$\frac{\Delta \mathbf{L}}{T} = \left\langle \frac{d\mathbf{L}}{dt} \right\rangle_T = -\frac{e}{T} \int_{t-T/2}^{t+T/2} (\tilde{\mathbf{r}} \times \tilde{\mathbf{E}}) dt = -e \langle \tilde{\mathbf{r}} \rangle \times \tilde{\mathbf{E}}(t)$$

over one orbital period  $T$ . Since the weak-field approximation ( $\omega_S \ll \omega_n$ ) also holds, the vectors  $\mathbf{L}$  and  $\mathbf{A}$  then change very little over one orbital period. Using Pauli's replacement rule  $\langle \mathbf{r} \rangle \approx -3\mathbf{A}/2p_n$ , the following set of coupled equations can then be deduced [9,22]:

$$\frac{d\mathbf{A}}{dt} = -\omega_S \hat{\mathbf{R}} \times \mathbf{L}, \quad \frac{d\mathbf{L}}{dt} = -\omega_S \hat{\mathbf{R}} \times \mathbf{A},$$

where both  $\omega_S = \alpha\Phi$  and  $\hat{\mathbf{R}}$  vary with time. Under the substitution

$$\mathbf{M} = \frac{\mathbf{L} + \mathbf{A}}{2}, \quad \mathbf{N} = \frac{\mathbf{L} - \mathbf{A}}{2}, \quad (21)$$

the above set of differential equations becomes decoupled to yield

$$\frac{d\mathbf{M}}{dt} = -\omega_S \hat{\mathbf{R}} \times \mathbf{M}, \quad \frac{d\mathbf{N}}{dt} = +\omega_S \hat{\mathbf{R}} \times \mathbf{N}, \quad (22)$$

where the magnitudes  $M^2 = N^2 = (L^2 + A^2)/4 = n^2 \hbar^2/4$  remain constant throughout the collision. The classical analysis for constant electric fields is given by Born [9]. For time-independent  $\omega_S$ , both  $\mathbf{M}$  and  $\mathbf{N}$  precess with constant frequency  $\omega_S$  about the (fixed) direction of internuclear axis  $\hat{\mathbf{R}}$ . For general time-varying  $\omega_S$ , the system of differential equations (22) does not have an exact solution. Percival and Richards [22] have used classical perturbation theory to solve Eqs. (22) and then provided a diffusional theory of angular momentum mixing. Bellomo *et al.* [17] approached the same problem by proceeding via the time evolution propagator  $U_{\alpha\alpha}^{\pm}(t, t_0)$  for  $\mathbf{M}$  and  $\mathbf{N}$  in the rotating frame, an approach that results in formulas too complicated for physical changes  $\Delta\mathbf{L}$  and  $\Delta\mathbf{A}$  to be extracted. A special solution for transitions from angular momenta state  $\ell=0$  has been recently obtained by Kazansky and Ostrovsky [13–15].

An exact analytical solution is, however, possible under the weak field and orbital adiabatic approximations for a classical projectile trajectory and when the magnitude of vectors  $\mathbf{M}$  and  $\mathbf{N}$  remains constant during the collision, as for the present case of intrashell transitions. These vectors are then obtained at any moment by orthogonal transformations from the initial values  $\mathbf{M}(t_0)$  and  $\mathbf{N}(t_0)$ . Let these transformations be  $\bar{U}_M(t, t_0)$  and  $\bar{U}_N(t, t_0)$ , respectively. Then

$\mathbf{M}(t) = \bar{U}_M(t, t_0)\mathbf{M}(t_0)$  and a similar equation holds for the time evolution of  $\mathbf{N}$ . The first equation in Eq. (22) becomes

$$\frac{d\bar{U}_{ij}}{d\Phi} = -\alpha \epsilon_{ijk} \hat{R}_n \bar{U}_{kj},$$

where  $\epsilon_{ijk}$  is the fully antisymmetric permutation symbol. Because the infinitesimal generators  $\bar{J}_k$  for the rotation group are matrices with elements  $(\bar{J}_k)_{ij} = -\epsilon_{ijk}$  (see [30] for example) and, since  $\hat{\mathbf{R}} = (0, \sin\Phi, \cos\Phi)$ , the above equation in matrix form is

$$\frac{d\bar{U}_M}{d\Phi} = -\alpha(\sin\Phi \bar{J}_2 + \cos\Phi \bar{J}_3) \bar{U}_M,$$

where  $[\bar{J}_k, \bar{J}_j] = \epsilon_{kjm} \bar{J}_m$ . This equation is the matrix representation of the group equation (7) and the solution  $\bar{U}_M$  is the matrix representation of the general solution (8). The final vector  $\mathbf{M}'$  is therefore obtained from the initial vector  $\mathbf{M}$  by three successive rotations,

$$\mathbf{M}' = \mathcal{R}[-\Phi, (1, 0, 0)] \mathcal{R}[\gamma\Delta\Phi, (1/\gamma, 0, -\alpha/\gamma)] \times \mathcal{R}[\Phi_0, (1, 0, 0)] \mathbf{M}. \quad (23)$$

The solution for  $\mathbf{N}$  has the similar form

$$\mathbf{N}' = \mathcal{R}[-\Phi, (1, 0, 0)] \mathcal{R}[\gamma\Delta\Phi, (1/\gamma, 0, +\alpha/\gamma)] \times \mathcal{R}[\Phi_0, (1, 0, 0)] \mathbf{N} \quad (24)$$

obtained simply by replacing  $\alpha$  by  $-\alpha$  in the corresponding equation for  $\mathbf{M}$ . The matrix  $\mathcal{R}[\Phi, \mathbf{n}]$  is the rotation matrix for a vector and corresponds with the representation of the abstract rotation (specified by the angle  $\Phi$  and the direction  $\mathbf{n}$  of rotation) on the three-dimensional vector space. Analytical expression for  $U_M$  and  $U_N$  can be obtained [31] as explicit functions of  $\alpha$  and  $\Delta\Phi$ . In particular, when  $\Phi=0$  and  $\Phi_0=\pi$ , the  $(3 \times 3)$  matrix  $\bar{U}_M$  is

$$\bar{U}_M = \begin{bmatrix} \gamma^{-2}[1 + \alpha^2 \cos(\pi\gamma)] & \alpha\gamma^{-1} \sin(\pi\gamma) & \alpha\gamma^{-2}[1 - \cos(\pi\gamma)] \\ \alpha\gamma^{-1} \sin(\pi\gamma) & -\cos(\pi\gamma) & -\gamma^{-1} \sin(\pi\gamma) \\ \alpha\gamma^{-2}[\cos(\pi\gamma) - 1] & \gamma^{-1} \sin(\pi\gamma) & -\gamma^{-2}[\alpha^2 + \cos(\pi\gamma)] \end{bmatrix} \quad (25)$$

and  $\bar{U}_N$  is obtained from  $\bar{U}_M$  by replacing  $\alpha$  with  $-\alpha$ .

As a result of the collision, the initial state of the target atom, specified by the vectors  $(\mathbf{L}, \mathbf{A})$ , changes to the final state  $(\mathbf{L}', \mathbf{A}')$  according to

$$\mathbf{L}' = \frac{\bar{U}_M + \bar{U}_N}{2} \mathbf{L} + \frac{\bar{U}_M - \bar{U}_N}{2} \mathbf{A}, \quad (26)$$

$$\mathbf{A}' = \frac{\bar{U}_M - \bar{U}_N}{2} \mathbf{L} + \frac{\bar{U}_M + \bar{U}_N}{2} \mathbf{A}. \quad (27)$$

For the undeflected trajectory of the projectile, when  $\Phi=0$  and  $\Phi_0=\pi$ , explicit results are:

$$\begin{aligned}
 L'_1 &= \gamma^{-2} [1 + \alpha^2 \cos(\pi \gamma)] L_1 + \alpha \gamma^{-1} \sin(\pi \gamma) A_2 + \alpha \gamma^{-2} [1 - \cos(\pi \gamma)] A_3, \\
 L'_2 &= -\cos(\pi \gamma) L_2 - \gamma^{-1} \sin(\pi \gamma) L_3 + \alpha \gamma^{-1} \sin(\pi \gamma) A_1, \\
 L'_3 &= \gamma^{-1} \sin(\pi \gamma) L_2 - \gamma^{-2} [\alpha^2 + \cos(\pi \gamma)] L_3 + \alpha \gamma^{-2} [\cos(\pi \gamma) - 1] A_1, \\
 A'_1 &= \gamma^{-2} [1 + \alpha^2 \cos(\pi \gamma)] A_1 + \alpha \gamma^{-1} \sin(\pi \gamma) L_2 + \alpha \gamma^{-2} [1 - \cos(\pi \gamma)] L_3, \\
 A'_2 &= -\cos(\pi \gamma) A_2 - \gamma^{-1} \sin(\pi \gamma) A_3 + \alpha \gamma^{-1} \sin(\pi \gamma) L_1, \\
 A'_3 &= \gamma^{-1} \sin(\pi \gamma) A_2 - \gamma^{-2} [\alpha^2 + \cos(\pi \gamma)] A_3 + \alpha \gamma^{-2} [\cos(\pi \gamma) - 1] L_1.
 \end{aligned} \tag{28}$$

Here  $\gamma = \sqrt{1 + \alpha^2}$  and the components of the initial and final vectors are defined in the fixed coordinate frame of Fig. 1. Similar expressions have also been obtained [31] for general  $\Delta\Phi$ . The above exact solutions are easily verified and satisfy the invariant relations

$$\mathbf{L}' \cdot \mathbf{A}' = \mathbf{L} \cdot \mathbf{A} = 0$$

and

$$\mathbf{L}'^2 + \mathbf{A}'^2 = \mathbf{L}^2 + \mathbf{A}^2 = n^2 \hbar^2.$$

The orbit of the final state  $(n, \mathbf{L}')$  is confined to a plane perpendicular to the final  $\mathbf{L}'$  and the energy is preserved ( $n$  is not changed).

### B. Classical transition probability

The initial state is defined by the angular momentum  $\mathbf{L}$  and Runge-Lenz  $\mathbf{A}$  vectors. Apart from the constraints that (i) the magnitude of the  $\mathbf{L}$  vector is  $\ell \hbar$ , (ii) the magnitude of the  $\mathbf{A}$  vector is  $\hbar \sqrt{n^2 - \ell^2}$  in the given state, and (iii)  $\mathbf{L}$  and  $\mathbf{A}$  are always orthogonal, the two vectors are completely random in the six-dimensional space  $\{\mathbf{L}\} \otimes \{\mathbf{A}\}$ , which is a mapping of the usual  $(\mathbf{r}, \mathbf{p})$  phase space. The initial angular momentum can have any value between 0 and  $n\hbar$ . The special case of zero initial angular momentum requires a separate analysis, presented at the end of this section. In the following discussion, the initial angular momentum is assumed strictly positive.

The hypersurface in the  $\{\mathbf{L}\} \otimes \{\mathbf{A}\}$  space on which the initial state is uniformly distributed is restricted by the above constraints and has the volume

$$V_{n,\ell} = \int \int \delta(|\mathbf{L}| - \ell \hbar) \delta(|\mathbf{A}| - \hbar \sqrt{n^2 - \ell^2}) \delta(\mathbf{L} \cdot \mathbf{A}) d\mathbf{L} d\mathbf{A}, \tag{29}$$

which, upon integration, reduces to

$$V_{n,\ell} = 8\pi^2 \hbar^2 \ell \sqrt{n^2 - \ell^2}.$$

Each point within this manifold evolves during the collision according to the rules (28), so that only a fraction of possible initial states can have the final angular momentum  $\ell'$  after

the collision. Following the definition (29), the overlap volume of accessible  $(\mathbf{L}, \mathbf{A})$  space that contains both initial and final states is

$$V_{n,\ell,\ell'} = \int \int \delta(|\mathbf{L}| - \ell \hbar) \delta(|\mathbf{L}'| - \ell' \hbar) \delta(|\mathbf{A}| - \hbar \sqrt{n^2 - \ell^2}) \times \delta(\mathbf{L} \cdot \mathbf{A}) d\mathbf{L} d\mathbf{A}. \tag{30}$$

The transition probability is then, in a geometric sense, the ratio of two volumes: the volume  $V_{n,\ell,\ell'}$  of the accessible states compatible with the required final angular momentum and the volume of the acceptable initial states  $V_{n,\ell}$ . The  $\ell \rightarrow \ell'$  transition probability is therefore defined as the ratio

$$P_{\ell,\ell'}^{(n)} = \frac{V_{n,\ell,\ell'}}{V_{n,\ell}} \tag{31}$$

of phase-space volumes. Transformation to the alternative set of vectors  $\mathbf{M}$  and  $\mathbf{N}$  defined by Eq. (2) facilitates evaluation of the integral (30). The Jacobian of this transformation is  $d\mathbf{L} d\mathbf{A} = 8 d\mathbf{M} d\mathbf{N}$ . With the aid of the identities

$$\delta(\mathbf{L} \cdot \mathbf{A}) = \delta(M^2 - N^2) = \delta(N - M)/2M,$$

$$\begin{aligned}
 \delta(|\mathbf{L}| - \ell \hbar) &= \delta(\sqrt{2M^2(1 + \cos \angle MN)} - \ell \hbar) \\
 &= \delta(\cos \angle MN - (\ell^2 \hbar^2 / 2M^2 - 1)) \ell \hbar / M^2,
 \end{aligned}$$

$$\begin{aligned}
 \delta(|\mathbf{A}| - \hbar \sqrt{n^2 - \ell^2}) &= \delta(\sqrt{2M^2(1 - \cos \angle MN)} - \hbar \sqrt{n^2 - \ell^2}) \\
 &= \delta(\sqrt{4M^2 - \ell^2 \hbar^2} - \hbar \sqrt{n^2 - \ell^2}) \\
 &= \delta(M - n\hbar/2) \hbar \sqrt{n^2 - \ell^2} / 4M,
 \end{aligned}$$

$$\begin{aligned}
 \delta(|\mathbf{L}'| - \ell' \hbar) &= \delta(\sqrt{2M'^2(1 + \cos \angle M'N')} - \ell' \hbar) \\
 &= \delta(\cos \angle M'N' - (\ell'^2 \hbar^2 / 2M'^2 - 1)) \ell' \hbar / M'^2,
 \end{aligned}$$

the accessible phase-space volume is

$$\begin{aligned}
V_{n\ell\ell'} &= \int \int 8M^2 N^2 d\Omega_M d\Omega_N dM dN \\
&\times \frac{\delta(N-M)}{2M} \frac{\sqrt{n^2-l^2}}{4M} \frac{\delta(M-n\hbar/2)}{M^2} \frac{\ell'\hbar}{M^2} \\
&\times \left[ \cos\angle MN - \left( \frac{\ell'^2\hbar^2}{2M^2} - 1 \right) \right] \frac{\ell'\hbar}{M^2} \\
&\times \left[ \cos\angle M'N' - \left( \frac{\ell'^2\hbar^2}{2M^2} - 1 \right) \right].
\end{aligned}$$

This finally reduces to the simpler form

$$\begin{aligned}
V_{n\ell\ell'} &= \frac{\sqrt{n^2-l^2}}{n^2} 4\ell'\ell'\hbar \int \int d\Omega_M d\Omega_N \\
&\times \delta(\cos\angle MN - \beta) \delta(\cos\angle M'N' - \beta')
\end{aligned}$$

where the integral is now over only the angular part of the vectors  $\mathbf{M}$  and  $\mathbf{N}$  and where the parameters  $\beta$  and  $\beta'$  are simply related to the initial and final states by

$$\beta = \frac{2\ell^2}{n^2} - 1, \quad \beta' = \frac{2\ell'^2}{n^2} - 1. \quad (32)$$

The final vectors  $\mathbf{M}' = \bar{U}_M \mathbf{M}$  and  $\mathbf{N}' = \bar{U}_N \mathbf{N}$  are given by finite rotation [Eqs. (23) and (24)] of the initial  $\mathbf{M}$  and  $\mathbf{N}$ , so that the relative angles  $\angle MN$  and  $\angle M'N'$  are independent of the specific coordinate frame chosen. Then

$$\begin{aligned}
\cos\angle M'N' &= \frac{\mathbf{M}' \cdot \mathbf{N}'}{M^2} = \frac{(\bar{U}_M \mathbf{M}) \cdot (\bar{U}_N \mathbf{N})}{M^2} \\
&= \frac{(\bar{U}_N^T \bar{U}_M \mathbf{M}) \cdot \mathbf{N}}{M^2} = \cos\angle M''N,
\end{aligned}$$

where  $\mathbf{M}''$  is obtained by rotation from  $\mathbf{M}$  using the operator  $\bar{U}_N^T \bar{U}_M$ . Being a product of two rotations, this operator is also a rotation about some direction  $\nu$  by the angle  $\chi$  determined from the trace

$$\text{Tr}[\bar{U}_N^T \bar{U}_M] = 1 + 2 \cos \chi$$

of the rotation operator. The proper rotation angle  $\chi$  depends only on the collision (Stark) parameter  $\alpha$  and the polar angle  $\Delta\Phi = \Phi - \Phi_0$  swept out during collision time interval  $(t_0, t)$  and is independent of the initial or the final state of the Kepler atom. It is determined by

$$\cos \frac{\chi}{2} = [1 + \alpha^2 \cos(\sqrt{1 + \alpha^2} \Delta\Phi)] / (1 + \alpha^2).$$

For small  $\alpha \ll 1$ ,  $\cos \chi \approx 1 - 8\alpha^2 \sin^2(\Delta\Phi/2) + O(\alpha^3)$  so that  $\chi \approx 4\alpha \sin(\Delta\Phi/2) + O(\alpha^3)$ . The plot Fig. 4 of the "universal" function  $\chi(\alpha, \Delta\Phi)$  for the case  $\Delta\Phi = -\pi$  shows that  $\chi$  has a maximum at  $\alpha \approx 0.9$  and is never greater than  $\pi$ . When

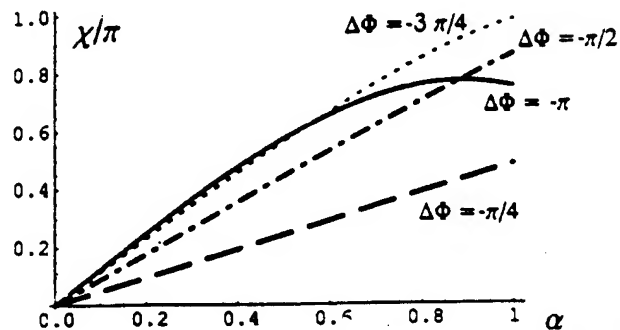


FIG. 4. The proper rotation angle  $\chi$  as a function of the Stark parameter  $\alpha$  for the net polar angle swept  $\Delta\Phi = -\pi$ ,  $-3\pi/4$ ,  $-\pi/2$ , and  $-\pi/4$ .

$\Delta\Phi \approx -3\pi/4$ , the angle  $\chi$  increases up to  $\pi$  as  $\alpha$  increases to unity. For smaller values of  $\Delta\Phi$ , the angle  $\chi$  increases monotonically with  $\alpha$ .

The classical transition probability (31) is then

$$\begin{aligned}
P_{\ell'\ell}^{(n)} &= \frac{\ell'}{2\pi^2 \hbar n^2} \int \int d\Omega_M d\Omega_N \\
&\times \delta(\cos\angle MN - \beta) \delta(\cos\angle M''N - \beta'),
\end{aligned}$$

where the angle between  $\mathbf{M}$  and  $\mathbf{M}''$  is  $\chi$ . The  $d\Omega_N$  integral can be done first if one chooses to work in spherical coordinates with the  $z$  axis along the vector  $\nu$ . In doing this, the vectors  $\mathbf{M}$  and  $\mathbf{M}''$  are fixed and have the coordinates  $(\Theta, 0)$  and  $(\Theta, \chi)$  as depicted in Fig. 5. The surface area element is  $d\Omega_N = d(\cos\theta)d\phi$ , where  $\theta$  and  $\phi$  are the spherical coordinates of the vector  $\mathbf{N}$ . Instead of the  $(\theta, \phi)$  system, a new set of coordinates can be defined by  $(u_1, u_2)$ , the angles of  $\mathbf{N}$  with  $\mathbf{M}$  and, respectively,  $\mathbf{M}''$ . The surface area element is now  $d\Omega_N = du_1 du_2 / \sin \Delta$ , where  $\Delta$  is the angle between the  $\mathbf{NM}$  and  $\mathbf{NM}''$  arcs, as in Fig. 5. A proof of this result is derived in Appendix B.

The  $d\Omega_N$  integral is now simpler to evaluate and yields

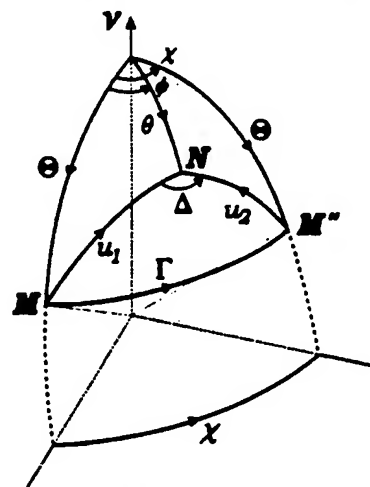


FIG. 5. The geometry and coordinates used in solving the integral (31).

$$P_{\ell',\ell}^{(n)} = \frac{2\ell'}{\pi\hbar n^2} \int_{-1}^1 d(\cos\Theta) (\sin\Delta \sin u_1 \sin u_2)^{-1},$$

where  $\cos u_1 = 2\ell^2/n^2 - 1$ ,  $\cos u_2 = 2\ell'^2/n^2 - 1$ , and the factor 2 arises because the  $(\theta, \phi) \rightarrow (u_1, u_2)$  transformation is not single-valued.

Basic trigonometry (see [32]) applied to spherical triangle MNM'' yields

$$\cos\Gamma = \cos u_1 \cos u_2 + \sin u_1 \sin u_2 \cos\Delta$$

so that

$$\sin u_1 \sin u_2 \cos\Delta = (\cos\Gamma_- - \cos\Gamma)(\cos\Gamma - \cos\Gamma_+),$$

where  $\Gamma_{\pm} = u_1 \pm u_2$  are the limits to  $\Gamma$  as  $\Delta$  rotates through  $2\pi$ . Since

$$\cos\Gamma = \cos\Theta^2 + \sin\Theta^2 \cos\chi$$

for spherical triangle MNM'', then

$$\sin u_1 \sin u_2 \sin\Delta = (1 - \cos\chi)[(\cos^2\Theta - A) \times (B - \cos^2\Theta)]^{1/2},$$

where

$$A(\ell/n, \ell'/n; \alpha) = \frac{\cos(u_1 + u_2) - \cos\chi}{1 - \cos\chi},$$

$$B(\ell/n, \ell'/n; \alpha) = \frac{\cos(u_1 - u_2) - \cos\chi}{1 - \cos\chi}. \quad (33)$$

On denoting  $\cos\Theta$  by  $z$ , the transition probability is the one-dimensional integral

$$P_{\ell',\ell}^{(n)}(\chi) = \frac{2\ell'}{\pi\hbar n^2} \frac{1}{1 - \cos\chi} \int \frac{dz}{\sqrt{(z^2 - A)(B - z^2)}},$$

where the limits of integration are defined by the condition of reality for the square-root function. The last integral can now be expressed in terms of the complete elliptic integral  $K(m) = \int_0^{\pi/2} (1 - m \sin^2 x)^{-1/2} dx$  so that

$$P_{\ell',\ell}^{(n)}(\chi) = \frac{2\ell'}{\pi\hbar n^2} \frac{1}{\sin^2\chi/2} \begin{cases} 0 & \text{if } B < 0 \\ K\left(\frac{B}{B-A}\right) / \sqrt{B-A} & \text{if } B > 0, A < 0 \\ K\left(\frac{B-A}{B}\right) / \sqrt{B} & \text{if } B > 0, A > 0 \end{cases} \quad (34)$$

provides the exact classical probability as a function of  $\ell$ ,  $\ell'$ , and  $\sin^2\chi/2$ , which combines the Stark parameter  $\alpha = (3Z_1/2)(a_n v_n/bv)$  and the net polar angle swept during the collision  $\Delta\Phi$  into one function. The probability (34) satisfies detailed balance  $2\ell P_{\ell',\ell} = 2\ell' P_{\ell,\ell'}$ , where  $2\ell$  is the classical weight of the state  $n\ell$ .

Inspecting the definitions (33) reveals more qualitative aspects. First,  $A$  and  $B$  are always less than 1, and only  $B$  can attain 1 when  $u_1 = u_2$ , i.e., for elastic collisions  $\ell = \ell'$ . The transition probability reduces, for this case, to the simpler form

$$P_{\ell,\ell}^{(n)}(\alpha \rightarrow 0) \sim \frac{1}{4\alpha\sqrt{n^2 - \ell^2}}$$

in the limit of small  $\alpha$ , thereby exhibiting the  $1/\alpha$  singularity of elastic transitions. For transitions with  $\ell' \neq \ell$  and small enough  $\alpha$ , the factor  $B$  is negative and then the transition probability is zero.  $B$  is always greater than  $A$  because  $\cos(u_1 - u_2) \geq \cos(u_1 + u_2)$ . In the limit of each  $\ell$  and  $\ell' \rightarrow 0$  or  $n$ , then  $u_{1,2} = 0$  or  $\pi$  and  $A = B = 1$ . For  $\ell \rightarrow \ell' = 0$  tran-

sitions, the probability is zero. For the important case of zero initial angular momentum, the transition probability  $P$  in the limit of  $\ell \rightarrow 0$  is

$$P_{\ell',0}^{(n)}(\alpha) = \frac{\ell'/( \hbar n^2)}{\sin(\chi/2) \sqrt{\sin^2(\chi/2) - (\ell'/n)^2}}. \quad (35)$$

This result was also obtained in [14]. When  $\ell' = n$ , the transition probability is

$$P_{n,\ell}^{(n)}(\alpha) = \frac{1/(\hbar n)}{\sin(\chi/2) \sqrt{(\ell/n)^2 - \sin^2(\chi/2)}}.$$

When the argument of the square-root function is negative, the transition probability is zero. Similarly, for maximum initial angular momentum  $\ell = n$ , the transition probability has the limit

$$P_{\ell',n}^{(n)}(\alpha) = \frac{\ell'/( \hbar n^2)}{\sin(\chi/2) \sqrt{(\ell'/n)^2 - \sin^2(\chi/2)}}.$$

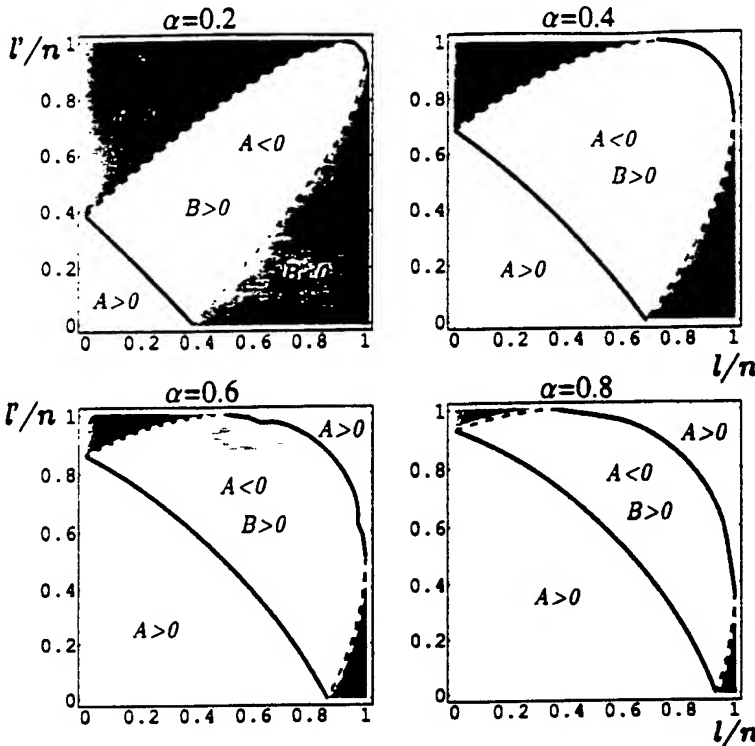


FIG. 6. Contour plots of the solutions of  $A=0$  (solid line) and  $B=0$  (dotted line) for various values of  $\alpha$ . In gray zones  $B<0$  and the transition is classically forbidden.

where, again, the transition probability is zero unless the final angular momentum  $l'$  is large enough to make the argument of the square-root function positive. If  $B>0$  and  $A$  is small, the transition probability has a singularity, typical for classical mechanics. Because the complete elliptic  $K$  function diverges logarithmically when the argument is very

close to unity, the transition probability has the following expansion for small  $A$ :

$$P \sim \frac{1}{\sqrt{B}} (2 \ln 2 - \frac{1}{2} \ln A/B).$$

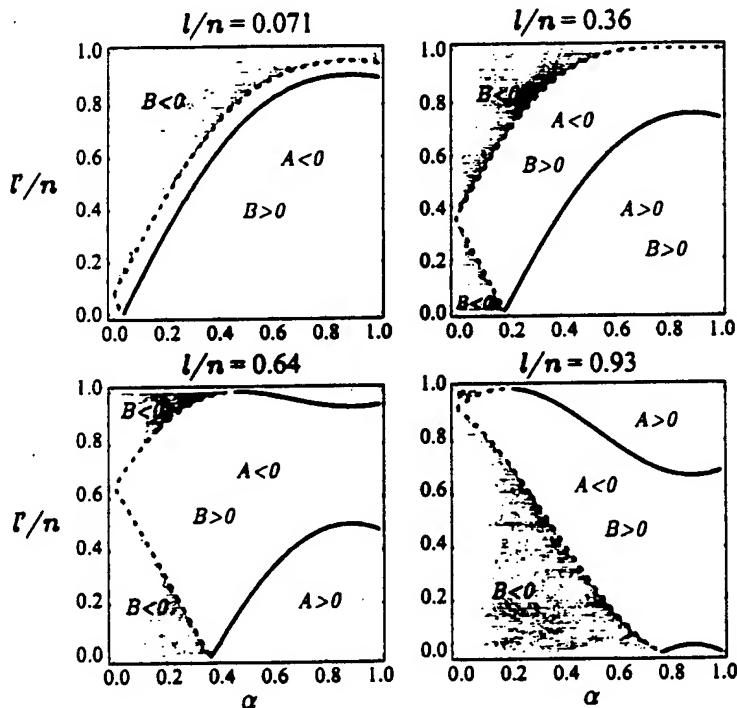


FIG. 7. Contour plots of the solutions of  $A=0$  (solid line) and  $B=0$  (dotted line) for various values of  $l/n$ . In gray zones  $B<0$  and the transition is classically forbidden.

When  $B$  has small but positive values, the transition probability has a finite limit because  $K(0) = \pi/2$ . Of course, when  $B$  approaches zero from negative values, the transition probability is zero. Thus, the singularities in the transition probability are given by the solutions of the equations  $A = 0$  and  $B = 0$ , which are  $u_2 = \pm u_1 \pm \chi$ .

A map of the various zones in the plane of reduced initial and final angular momenta ( $\ell/n, \ell'/n$ ) is displayed in Fig. 6 for the four values  $\alpha = 0.2, 0.4, 0.6$ , and  $0.8$  of the Stark parameter. In the central region,  $A$  is negative and  $B$  is positive. Within the lower left and upper right corners, both  $B$  and  $A$  are positive. The transition is classically forbidden in the upper left and lower right corners (gray zones) where  $B < 0$ . Along the solid line,  $A = 0$  lines, which represent  $\cos^{-1}(\ell/n) + \cos^{-1}(\ell'/n) = \chi/2, \pi/2 - \chi$ , the transition probability has a logarithmic (cusp) singularity. Across the dotted  $B = 0$  lines, which represent  $\cos^{-1}(\ell/n) - \cos^{-1}(\ell'/n) = \chi/2, \pi - \chi/2$ , the transition probability jumps from zero (in the gray zone) to some finite value (in the central zone). As  $\alpha \rightarrow 0$ , the two inaccessible regions (where  $B < 0$ ) increase until the central region with  $B > 0$  and  $A < 0$  becomes an elongated line strip lying along the diagonal  $\ell = \ell'$ . Only elastic collisions are therefore permitted in the limit  $\alpha \rightarrow 0$ . As  $\alpha$  increases to unity, the classically forbidden zones diminish and the collision becomes more and more effective in its ability to induce larger angular momentum changes.

Figure 7 presents corresponding maps to Fig. 6. The same characteristic regions are now displayed in the plane of final reduced angular momentum  $\ell'/n$  and the Stark parameter  $\alpha$  for four values of the initial reduced angular momentum  $\ell/n = 0.071, 0.36, 0.64$ , and  $0.93$ . Again, the classically forbidden regions (gray zones) correspond to the condition  $B < 0$  in the left upper and lower corners. The elastic  $\ell' = \ell$  transitions are always possible, even when  $\alpha \rightarrow 0$ . Again, along the solid ( $A = 0$ ) and dotted ( $B = 0$ ) lines, the transition probabilities have cusp and step singularities. When  $\alpha$  increases, the span of the possible final angular momentum, for given angular momentum, increases. Large angular momentum transfer is only possible for collisions with large Stark parameter  $\alpha \rightarrow 1$ . Both Figs. 6 and 7 are key to the interpretation of the variation of the probabilities  $P_{\ell' \ell}(\alpha)$  with both  $\ell'$  and  $\alpha$ , respectively.

The result (35) obtained from the  $\ell \rightarrow 0$  limit of the general result (34) can be also proven directly. Because  $L = 0$ , the classical orbits are characterized only by the Runge-Lenz vector  $A$ . In this case, the volume occupied by the initial state is

$$V_{n0} = \int \delta(|A| - n\hbar) dA = 4\pi n^2 \hbar^2.$$

The volume of the accessible final states  $\ell'$  is

$$V_{n0\ell'} = \int \delta(|A| - n\hbar) \delta\left(\frac{1}{2} |(\bar{U}_M - \bar{U}_N)A| - \ell' \hbar\right) dA,$$

where the orthogonal matrices  $\bar{U}_{M,N}$  depend only on the Stark parameter  $\alpha$  and are defined by Eq. (25). In a spherical

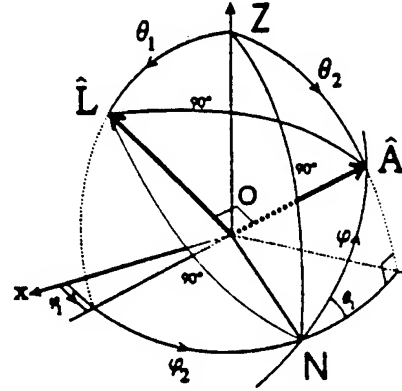


FIG. 8. The geometry of the initial state described by the directions of the angular momentum  $\hat{L}$  and Runge-Lenz  $\hat{A}$  vectors.

coordinate system where the  $z$  axis is along the principal direction  $\nu$  of the rotation matrix  $\bar{U}_N^T \bar{U}_M$  (as discussed earlier in this section), the magnitude is

$$\frac{1}{2} |\bar{U}_M A - \bar{U}_N A| = n\hbar \sin(\chi/2) \sin \theta,$$

where  $\theta$  is the angle between  $\bar{U}_M A$  (or  $\bar{U}_N A$ ) and the direction  $\nu$ . The transition probability is then

$$P_{\ell'0} = \frac{1}{2} \int_0^\pi \delta(n\hbar \sin(\chi/2) \sin \theta - \ell' \hbar) \sin \theta d\theta \\ = \frac{\ell' / (n\hbar^2)}{\sin(\chi/2) \sqrt{\sin^2(\chi/2) - (\ell'/n)^2}},$$

in agreement with the  $\ell \rightarrow 0$  limit (35) to the general classical  $\ell \rightarrow \ell'$  transition probability (34).

## V. CLASSICAL DYNAMICS SIMULATION

The present classical Monte Carlo simulations are different from the standard classical trajectory Monte Carlo simulations in that the initial state is not specified by the position and the velocity of the orbiting electron. Instead, the simulation begins with a random distribution of the initial states in the  $\{L\} \otimes \{A\}$  space, propagates each state according to the rule (28), and then performs the statistical analysis of the final distribution of states to provide, in the limit of an infinite number of trials, the probability  $P_{\ell' \ell}$  for a given transition. This section describes the correct way to generate the initial distribution of states.

The angular momentum  $L$  and the Runge-Lenz  $A$  vectors are sufficient to completely specify all characteristics of the atom's orbit, provided they are orthogonal, as for the case of pure Coulomb attraction. Only five components are therefore independent and two of them, the magnitudes  $L$  and  $A = \sqrt{n^2 - L^2}$ , characterize the shape and size of the orbit. There are then three angles that specify the orientation of the orbit in space, for a given assignment of the energy and angular momentum. The direction of the angular momentum vector  $\hat{L}$  is arbitrary. Two random numbers, the projection

$L_z = \cos \theta_1$  and its azimuthal angle  $\varphi_1$ , generate a uniform distribution of  $\hat{L}$  on the unit sphere. The direction of the Runge-Lenz vector  $\hat{A}$  is uniformly distributed in the plane perpendicular to  $\hat{L}$ , and the angle  $\varphi$  between  $\hat{A}$  and a given fixed direction  $\hat{N}$  in this plane is the third random number required to simulate an initial state. In summary, three random numbers are required: (i)  $L_z = \cos \theta_1$  uniformly distributed within the  $[-1, 1]$  interval, (ii)  $\varphi_1$  uniformly distributed within the  $[0, 2\pi]$  interval, and (iii)  $\varphi$  uniformly distributed within the  $[0, 2\pi]$  interval. The initial  $L$  and  $A$  vectors are then

$$L = \hbar \ell \begin{pmatrix} \sin \theta_1 \cos \varphi_1 \\ \sin \theta_1 \sin \varphi_1 \\ \cos \theta_1 \end{pmatrix}, \quad A = \hbar \sqrt{n^2 - \ell^2} \begin{pmatrix} \sin \theta_2 \cos \varphi_2 \\ \sin \theta_2 \sin \varphi_2 \\ \cos \theta_2 \end{pmatrix}.$$

The spherical polar angles  $\theta_2$  and  $\varphi_2$  of  $A$ , as illustrated in Fig. 8, must now be expressed in terms of the above random variables  $\theta_1$ ,  $\varphi_1$ , and  $\varphi$ . Basic trigonometry [32] applied to the spherical triangles  $Z\hat{N}\hat{A}$  and  $\hat{L}\hat{Z}\hat{A}$  yields

$$\cos \theta_2 = \sin \varphi \sin \theta_1$$

and

$$0 = \cos \theta_1 \cos \theta_2 + \sin \theta_1 \sin \theta_2 \cos(\varphi_2 - \varphi_1),$$

respectively. On solving these two equations for  $\theta_2$  and  $\varphi_2$ , the arbitrary Runge-Lenz vector

$$A(\theta_1, \varphi_1, \varphi)$$

$$= \hbar \sqrt{n^2 - \ell^2} \begin{pmatrix} -\cos \theta_1 \cos \varphi_1 \sin \varphi - \sin \varphi_1 \cos \varphi \\ -\cos \theta_1 \sin \varphi_1 \sin \varphi + \cos \varphi_1 \cos \varphi \\ \sin \theta_1 \sin \varphi \end{pmatrix}$$

is then expressed in term of the random variables. It automatically obeys the constraint requirements  $A \cdot L = 0$ ,  $A^2 + L^2 = n^2$ , and  $\hat{A} \cdot \hat{N} = \cos \varphi$ .

## VI. NUMERICAL EXAMPLES

In this section, numerical examples for calculation of the transition probability between states with given angular momentum ( $n\ell \rightarrow n\ell'$ ) are presented. There are three main methods used in this paper. The classical Monte Carlo simulation, as described in the preceding section, requires the running of a large number of trials to sample the three dimensional space of arbitrary parameters. The explicit classical mechanics expression (34) is used directly.

The quantal calculation is based on Eqs. (13) and (12). A matrix representation for the operator  $L_1 - \alpha A_3$  [where Pauli's replacement (5) was adopted] is required. Instead of the spherical basis  $|\ell m\rangle$ , which is difficult to use in this case, we define a new linear basis obtained by mapping the  $(\ell, m)$  quantum numbers to a unique index  $k = \ell^2 + \ell + m + 1$ , in such a way, for example, that  $(0, 0) \rightarrow 1$ ,  $(1, -1) \rightarrow 2$ ,  $(1, 0) \rightarrow 3$ ,  $(1, 1) \rightarrow 4$ ,  $(2, -2) \rightarrow 5$ , and so on. The inverse map-

		$\ell=0$			$\ell=1$			$\ell=2$			
$\ell$	$m$	$m'=0$	$-1$	$0$	$1$	$-2$	$-1$	$0$	$1$	$2$	
0	0	0	0	$2\alpha\sqrt{2/3}$	0	0	0	0	0	0	1
-1		0	0	$1/\sqrt{2}$	0	0	$\alpha$	0	0	0	2
1	0	$2\alpha\sqrt{2/3}$	$1/\sqrt{2}$	0	$1/\sqrt{2}$	0	0	$2\alpha/\sqrt{3}$	0	0	3
1		0	0	$1/\sqrt{2}$	0	0	0	0	$\alpha$	0	4
-2		0	0	0	0	0	1	0	0	0	5
-1		0	$\alpha$	0	0	1	0	$\sqrt{3/2}$	0	0	6
2	0	0	0	$2\alpha/\sqrt{3}$	0	0	$\sqrt{3/2}$	0	$\sqrt{3/2}$	0	7
1		0	0	0	$\alpha$	0	0	$\sqrt{3/2}$	0	1	8
2		0	0	0	0	0	0	0	1	0	9
		1	2	3	4	5	6	7	8	9	

FIG. 9. Matrix representation of  $L_1 - \alpha A_3$  for  $n=3$ .

ping is given by  $\ell = \text{floor}(\sqrt{k-1})$  and  $m = k - \ell^2 - \ell - 1$ . The index  $k$  counts the degeneracy of the energy shell, and runs from 1 to  $n^2$ . The matrix element

$$(L_1)_{\ell' m'}^{\ell m} = \frac{1}{2} \sqrt{(\ell+m)(\ell-m+1)} \delta_{\ell', \ell} \delta_{m', m-1} \\ + \frac{1}{2} \sqrt{(\ell-m)(\ell+m+1)} \delta_{\ell', \ell} \delta_{m', m+1}$$

of  $L_1$  is nonzero only for  $\Delta\ell=0$  and  $\Delta m = \pm 1$ , which reflects the fact that the cylindrical symmetry of the Rydberg atom is broken by the precession of  $L$  about the field of the projectile. These  $m$ -changing transitions are, however, conditioned by the full structure of solution (12), which shows that such transitions are only in evidence for nonzero  $\alpha$ . The matrix element

$$(A_3)_{\ell' m'}^{\ell m} = -\sqrt{\frac{(\ell^2 - m^2)(n^2 - \ell^2)}{(2\ell+1)(2\ell-1)}} \delta_{\ell', \ell-1} \delta_{m', m} \\ - \sqrt{\frac{[(\ell+1)^2 - m^2][n^2 - (\ell+1)^2]}{(2\ell+3)(2\ell+1)}} \delta_{\ell', \ell+1} \delta_{m', m}$$

of the component  $A_3 = -(2/3n)z$  along the fixed  $Z$  axis of quantization is nonzero for  $\Delta\ell = \pm 1$  and  $\Delta m = 0$  transitions. These dipole transitions only contribute for nonzero  $\alpha$ . The matrix  $L_1 - \alpha A_3$  has then a band diagonal structure, as illustrated in Fig. 9 for the special case of  $n=3$ . Explicit analytical formulas for  $P_{\ell' \ell}^{(n)}(\alpha, \Delta\Phi)$  can be directly obtained [33] for small  $n=2, 3$ .

The transition amplitude for transition  $k \rightarrow k'$  is the  $kk'$  matrix element of the exponential of the matrix  $-i\Delta\Phi(L_1 - \alpha A_3)$ , sandwiched between the rotations implied by Eq. (12). When  $\alpha=0$ , the dipole forbidden transitions are not possible, because the transition matrix  $\sim \exp i\pi L_1/\hbar$  still maintains a band diagonal structure. As  $\alpha$  increases, more and more off-diagonal elements become populated, leading to dipole forbidden transitions. Efficient algorithms, using Padé approximations, are available [27] for matrix exponentiation. The full array of transition probabilities is then obtained all at once.



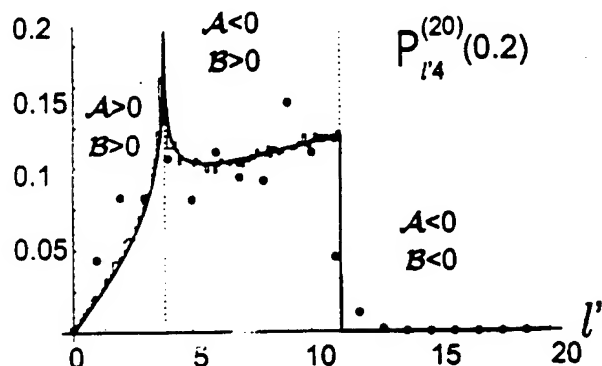


FIG. 10. The Monte Carlo simulation (steplike lines), the classical (solid line), and quantal (dots) transition probabilities  $P_{l' l}^{(20)}(\alpha)$  for given  $\alpha=0.2$  and initial  $l=4$  within the  $n=20$  shell.

The examples, provided by Figs. 10–13, demonstrate that the Monte Carlo simulation yields results identical to the classical dynamics expression (34). The transition probabilities for given Stark parameters ( $\alpha=0.2$  and  $0.6$ ) and initial angular momentum ( $l=4, 12, 14$ , and  $18$ , respectively) are represented as a function of the final angular momentum  $l'$ . This also provides the distribution over the final angular momentum states, which result from collisions, at given  $\alpha$ , from an initial population of states with the same initial angular momentum  $l$ . In this example,  $n=20$ . The present corresponding quantal results are also represented in the same graphs by dots. Vertical dotted lines indicate the positions of the singularities, corresponding to the  $A=0$  and  $B=0$  lines in Fig. 6. The  $A=0$  and  $B=0$  singularities produce cusp and step variations in  $P_{l' l}$  as  $l'$  increases through the singularity (Fig. 6). Four distinct and characteristic classes of variation of  $P_{l' l}$  with  $l'$  then emerge. These are displayed in Figs. 10–13, where the predicted (cusp, step), (step, step), (cusp, cusp), and (step, cusp) classical variations are exhibited. These results are fully representative and can be analyzed by vertical cuts through Fig. 6 appropriate to a given  $l$ . The  $l$  and  $\alpha$  parameters in Figs. 10–13 correspond to the values  $l/n=0.2$  and  $0.6$  and to  $l/n=0.7$  and  $0.9$  in the first

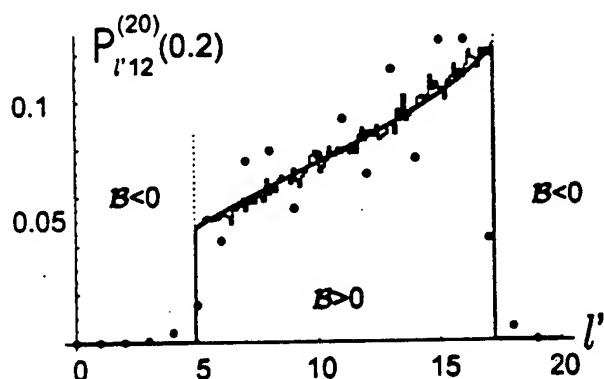


FIG. 11. The Monte Carlo simulation (steplike lines), the classical (solid line), and quantal (dots) transition probabilities  $P_{l' l}^{(20)}(\alpha)$  for given  $\alpha=0.2$  and initial  $l=12$  within the  $n=20$  shell.  $A < 0$  for all  $l'$ .

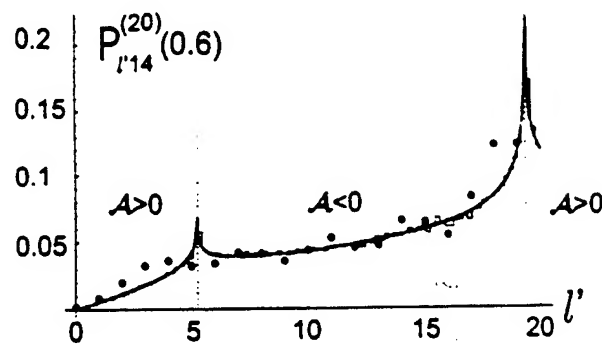


FIG. 12. The Monte Carlo simulation (steplike lines), the classical (solid line), and quantal (dots) transition probabilities  $P_{l' l}^{(20)}(\alpha)$  for given  $\alpha=0.6$  and initial  $l=14$  within the  $n=20$  shell.  $B > 0$  for all  $l'$ .

and third plots of Fig. 6, respectively. The steps indicate a classical threshold  $l'_-$  or a classical cutoff  $l'_+$  for transitions to a final value of  $l'$ . The cusp-step variation of Fig. 10 indicates that transitions to  $l' \leq l'_+$  are classically allowed and the step-step variation of Fig. 11 indicates that classically accessible  $l'$  are within the range  $l'_- \leq l' \leq l'_+$ . The cusp-cusp variation of Fig. 12 is associated with the fact that transitions to all  $l'$  are classically accessible (cf. Fig. 6, plot 3), while the step-cusp variation of Fig. 13 signifies that only transitions to  $l' \geq l'_-$  are classically possible. For a given initial angular momentum  $l$  and Stark parameter  $\alpha$ , the position of the cusp singularities, given by the solutions of the equation  $A=0$ , is

$$\left(\frac{l'}{n}\right) = \left| \left(1 - \frac{l^2}{n^2}\right)^{1/2} \sin \frac{\chi}{2} \pm \left(\frac{l}{n}\right) \cos \frac{\chi}{2} \right|. \quad (36)$$

Expressions (36) are also solutions of the equation  $B=0$  for the step singularities. The threshold value  $l'_-$  is a cusp (solution of  $A=0$ ) provided  $l < n \sin \chi/2$  and is a step (solution of  $B=0$ ) provided  $l > n \sin \chi/2$ . Similarly, the cutoff  $l'_+$  is

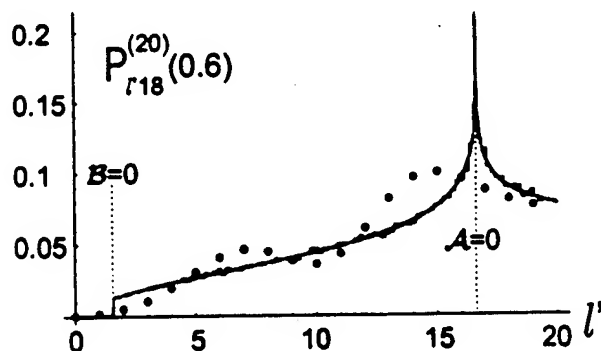


FIG. 13. The Monte Carlo simulation (steplike lines), the classical (solid line), and quantal (dots) transition probabilities  $P_{l' l}^{(20)}(\alpha)$  for given  $\alpha=0.6$  and initial  $l=18$  within the  $n=20$  shell. Across the first dotted line  $B$  changes sign and  $A$  is negative on both sides of this line.  $A$  changes sign across the second line while  $B$  remains positive.

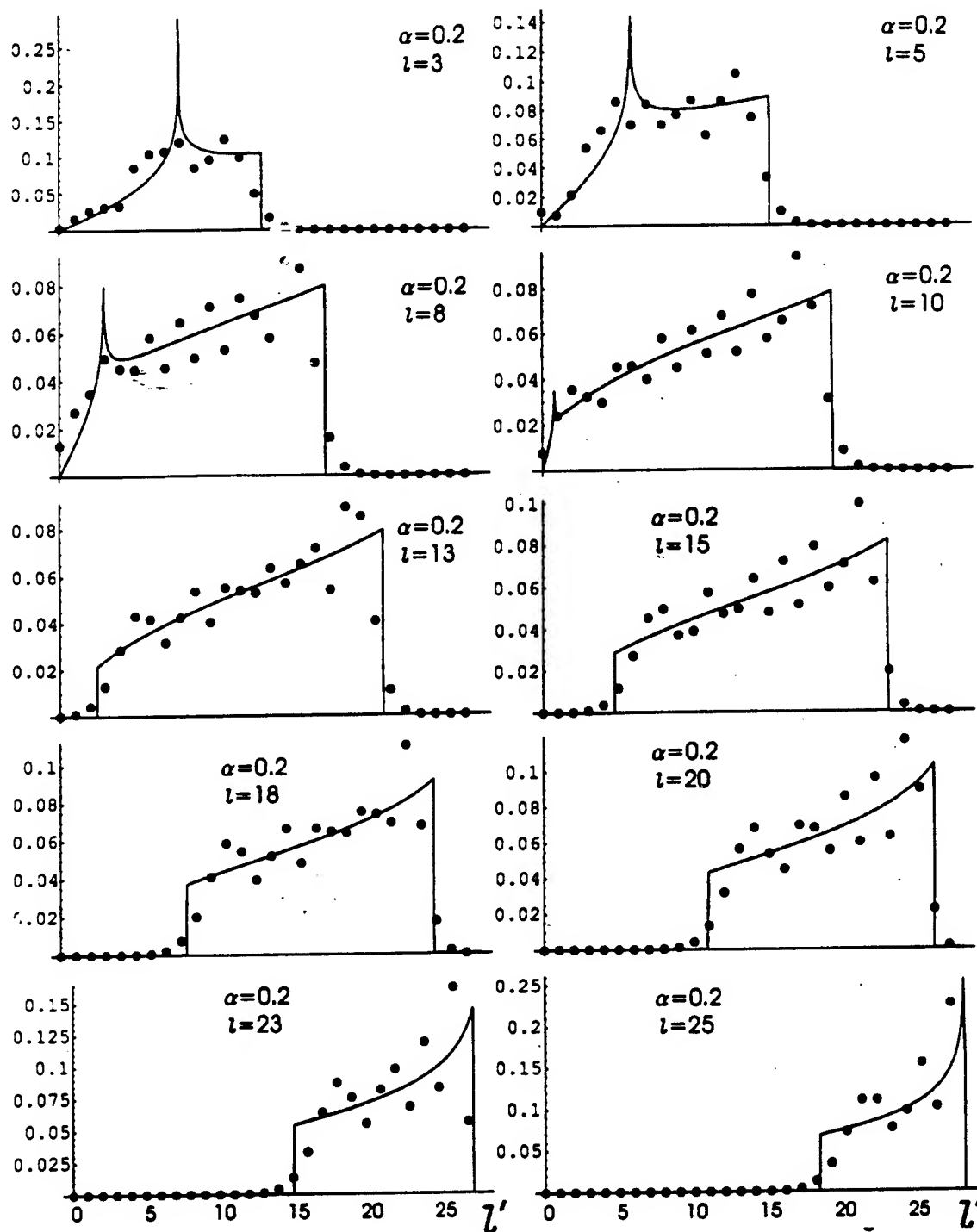


FIG. 14. The classical and quantal Stark mixing transition probabilities  $P_{l' l}(\alpha)$  within the  $n=28$  energy shell, for  $\alpha=0.2$ , as a function of the final angular momentum  $l'$  and for various initial angular momenta  $l$ .

a cusp if  $l' > n \cos \chi/2$  or a step if  $l' < n \cos \chi/2$ . The separation between the singularities is

$$\left(\frac{l'_+}{n}\right) - \left(\frac{l'_-}{n}\right) = 2 \left(1 - \frac{l'^2}{n^2}\right)^{1/2} \sin \frac{\chi}{2}$$

when  $l/n \geq \sin \chi/2$ , and is

$$\left(\frac{l'_+}{n}\right) - \left(\frac{l'_-}{n}\right) = 2 \left(\frac{l}{n}\right) \cos \frac{\chi}{2}$$

when  $l/n \leq \sin \chi/2$ . The maximum separation of  $\sin \chi$  is attained at  $l^*/n = \sin \chi/2$ . This occurs in Fig. 6 where the  $A=0$  and  $B=0$  curves both intersect the  $l/n$  axis at  $l^*/n$ . The transitions  $l \rightarrow l'$  have significant quantal probabilities

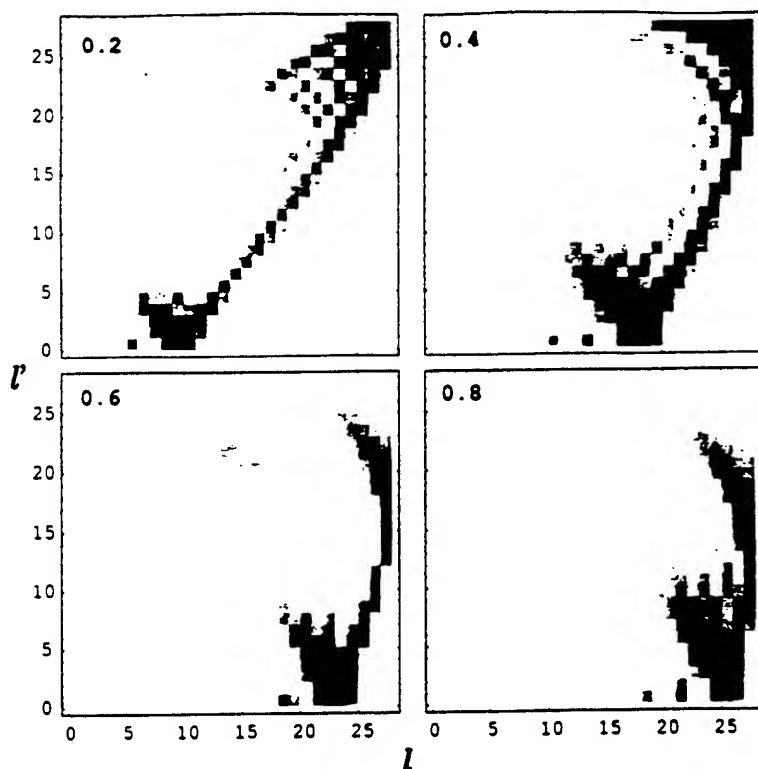


FIG. 15. Density plots of the transition probabilities, calculated within the quantal treatment, for four values of  $\alpha=0.2, 0.4, 0.6$ , and  $0.8$  in the  $(l, l')$  plane. The probability increases as the gray becomes darker.

only when  $l'$  is in the classical accessible region and exhibit the characteristic exponential decreasing behavior in the classical inaccessible regions.

The second set of examples compares between the classical and quantal transition probabilities within the  $n=28$  energy shell. A set of graphs, for various  $l$  and fixed Stark parameter  $\alpha=0.2$ , is presented in Fig. 14. The transition probability is plotted versus the final angular momentum. The cusp-step, step-step, and step-cusp variations are all apparent, together with the superimposed quantal oscillatory behavior within the classical accessible region. The oscillations possibly originate from the fact that there are two points  $N$  of intersection of the two arcs (drawn on the sphere of Fig. 5) with centers  $M$  and  $M'$  with separation  $\Gamma(\alpha)$  and radii  $u_1(l)$  and  $u_2(l')$ . Each point of intersection provides equal classical contributions to  $P_{l'l}(\alpha)$  while the different phases associated with each point produce the quantal (semi-classical) interference oscillations, exhibited in both the  $l'$  variations of  $P_{l'l}(\alpha)$  with  $l$  and  $\alpha$  fixed, as in Fig. 14, and the  $\alpha$  variation of  $P_{l'l}(\alpha)$  in Fig. 16 for  $l$  and  $l'$  fixed. Figure 14 also illustrates that the separation  $(l'_+ - l'_-)/n$  between the various discontinuities increases to  $\sin \chi$  at  $l/n = \sin \chi/2$  and then decreases as  $l$  is increased from 0 to  $n-1$ , in accord with Eq. (36). In general, Fig. 14 shows that the classical picture is complementary to the quantal in that it has the ability to explain the general overall behavior of the quantal results and to provide the general framework on which the quantal results rest. It has also provided the various regions (between cusps, steps, etc.) that remain obscured within the quantal treatment.

The set of plots in Fig. 15 is the quantal correspondent of

the similar classical set of plots presented in Fig. 6. Density maps in the  $(l, l')$  plane are shown for the same four values of Stark parameter  $\alpha$ . The first map for  $\alpha=0.2$  corresponds to the results of Fig. 14, where cuts along various values of  $l/n$  are made. The quantal transition probability increases as the gray areas becomes darker. The same zones outlined in Fig. 6 can be recognized and the boundaries between them are in exact correspondence with the classical equations  $A=0$  and  $B=0$ , as discussed at the end of Sec. V. The quantal transition probabilities are practically zero over the classical forbidden regions, occupying the upper left and lower right corners of Fig. 6. The quantal probabilities are maximum on the ridge given by the equation  $A=0$ , where the classical dynamics results in singularities.

When  $\alpha$  is very small, decreasing toward zero, only elastic transitions are allowed so that only the principal diagonal is exhibited, as in Figs. 6 and 15. The quantal calculation yields unity for the probability of elastic  $l'=l$  transitions in the  $\alpha \rightarrow 0$  limit and the classical result diverges as  $1/\alpha$  in the same limit. All other transitions have zero probability. This feature is responsible for the well known [4] divergence of the cross section (6) for elastic transitions.

Figure 16 displays the probability for transitions originating from the initial level  $l=5$  to various final levels, as a function of the Stark parameter  $\alpha$ . Again, the agreement is expectedly very good. For small  $\alpha$ , there is always a classical inaccessible region ( $B < 0$ ) for quasielastic  $l' \neq l$ , except for the fully elastic transitions  $l'=l$ . A threshold step at  $\alpha = \alpha_T$  is therefore displayed for the probability of transitions with  $l'=l$ . This property is fully explained with the

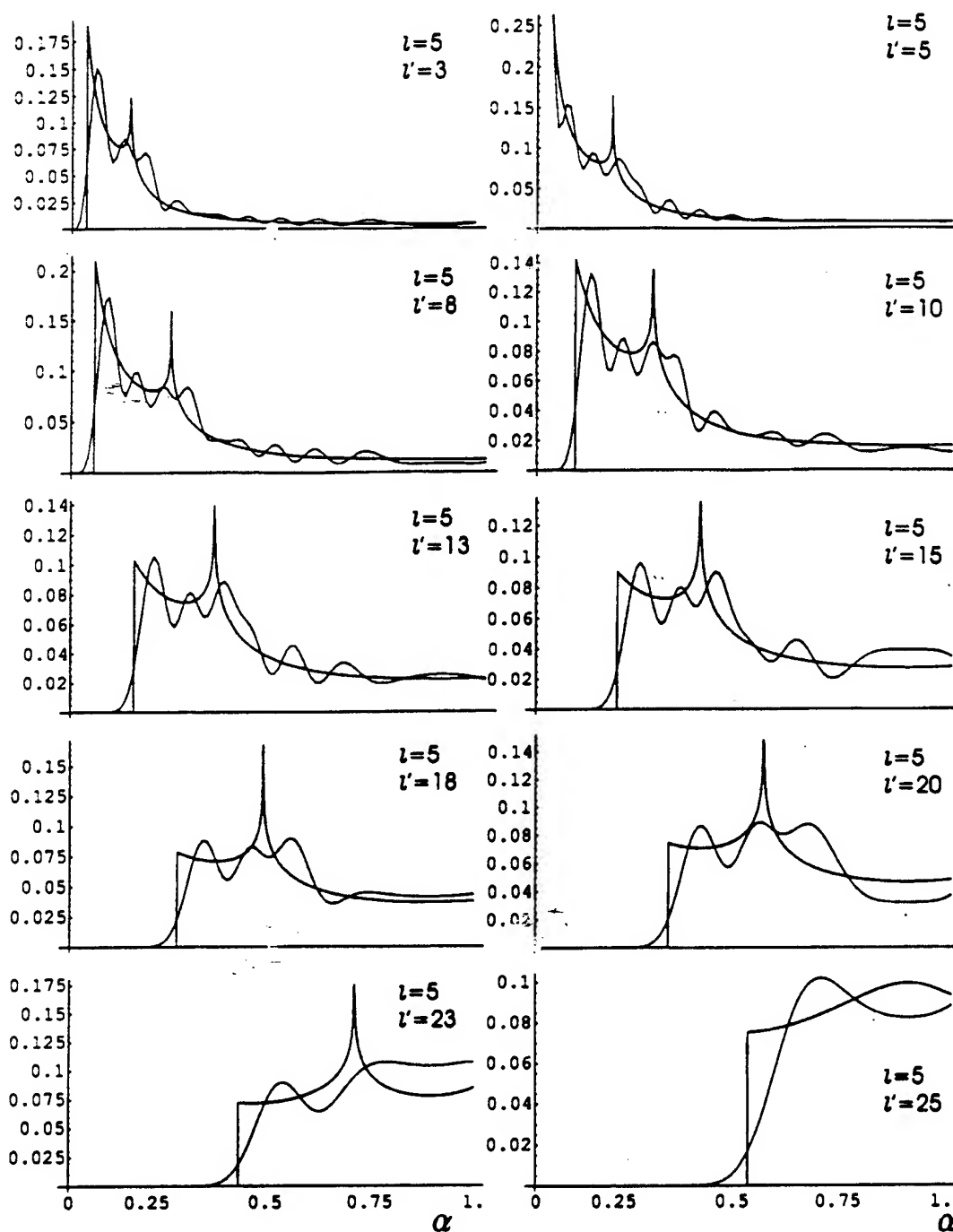


FIG. 16. The classical and quantal Stark mixing transition probabilities  $P_{l,l'}(\alpha)$  within the  $n=28$  energy shell, for  $l=5$ , as a function of the Stark parameter  $\alpha$  and for various final angular momenta  $l'$ .

aid of the plots in Fig. 7 of  $l'/n$  versus  $\alpha$  for various values of  $l'/n$ . As  $l'$  is increased,  $\alpha_T$  determined by the intersection of  $l'/n$  with the  $B=0$  curve increases and a step ( $B=0$ ) to cusp ( $A=0$ ) variation with  $\alpha$  is obtained, as exhibited in Fig. 16. For higher  $l'/n$  values, intersection with the  $A=0$  curve (and therefore the cusp) disappears. Figure 16 (for the specific  $n=28$  case considered, or in general Fig. 7) also shows that low  $l \rightarrow$  high  $l'$  and high  $l \rightarrow$  low  $l'$

transitions are precluded ( $B < 0$ ) except at high values of  $\alpha \rightarrow 1$ .

Figure 17 shows that the quantal probabilities are high in the classical accessible regions ( $B > 0$ ) of Fig. 7 and are more significant in the  $A < 0$  region than in the  $A > 0$  region. Variation of the transition probability along the horizontal line for  $l' = \text{const}$  provides plots as exhibited in Fig. 16. Figure 17 is the quantal correspondence of Fig. 7.

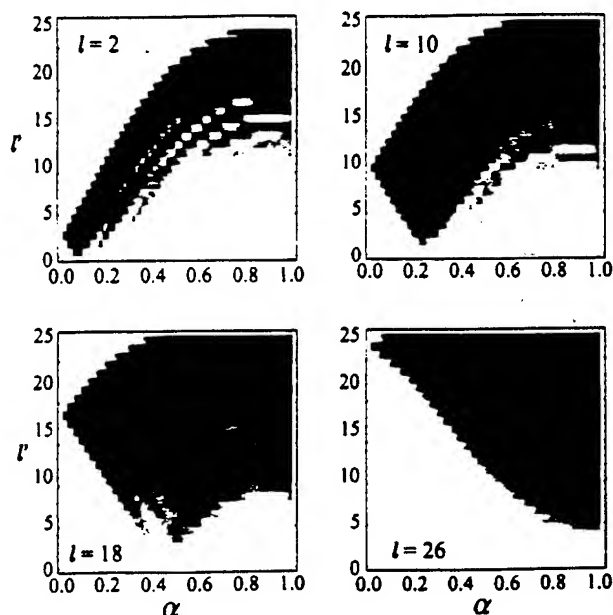


FIG. 17. Density plots of the transition probabilities, calculated within the quantal treatment, for four values of the initial angular momentum  $\ell = 2, 10, 18$ , and  $26$ , in the  $(\alpha, \ell')$  plane. The probability increases as the gray becomes darker.

Figure 18 exhibits variation of the integral factor

$$I_{\ell', \ell}^{(n)} = \int_{\alpha_{\min}}^1 P_{\ell', \ell}^{(n)} \frac{d\alpha}{\alpha^3} = \frac{\sigma_{\ell', \ell}}{\pi a_n^2} 2 \left( \frac{v}{3Z_1 v_n} \right)^2,$$

which appears in the cross section (6) as a function of the final angular momentum  $\ell'$  for various initial angular momenta  $\ell$ . It is assumed here that  $\Delta\Phi = -\pi$ . This integral does not depend on the projectile properties (velocity, impact parameter, or charge) but depends only on the initial and final state of the target. Due to the  $1/\alpha^3$  singularity, the cross sections for elastic ( $\ell = \ell'$ ) and near elastic transitions are very much enhanced. Various cutoff ( $\alpha_{\min}$ ) procedures can

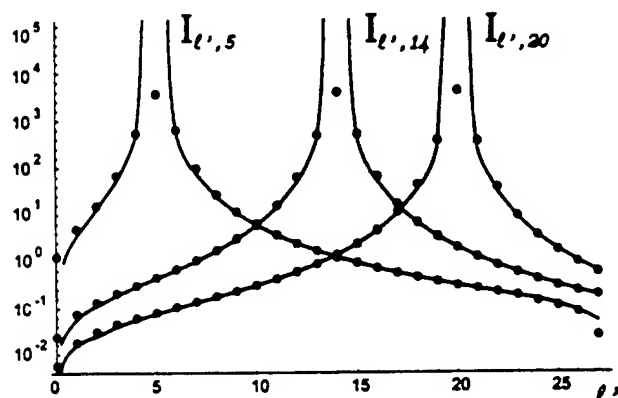


FIG. 18. Classical and quantal comparison of the integral  $I_{\ell', \ell}^{(n)}$  defining the Stark mixing cross section (6) within the  $n=28$  energy shell, for various initial angular momenta  $\ell$  as a function of the final angular momentum  $\ell'$ .

be introduced from physical considerations specific to the actual problem discussed. For the results presented in Fig. 18, an arbitrary cutoff  $\alpha_{\min}=0.01$  was introduced for both the classical and quantal calculations. With the exception of elastic transitions, where special care must be exercised since the present model fails, the agreement between quantal and classical model is much better than one would expect from the traditional correspondence principles such as Ehrenfest's theorem and Bohr's correspondence. The exceptionally rich symmetry group  $SO(4)$ , characteristic for one-electron atoms in both the quantal and classical treatments, explains the quality of the agreement obtained.

## VII. CONCLUSIONS

In conclusion, we have presented a case study of the long-standing problem of the  $n\ell \rightarrow n\ell'$  transition array in atomic hydrogen produced by distant collisions with slow heavy charged particles. Complete formulations from the quantal, classical, and Monte Carlo simulation viewpoints have been developed. The  $SO(4)$  dynamical symmetry of  $H(n)$  has been exploited to provide exact classical and quantal solutions (28) and (12), under the adiabatic, dipole and classical path assumptions. A classical expression (31) for the transition probability  $P_{\ell', \ell}^{(n)}$  is presented in a language that exploits the dynamical symmetry and is used to obtain exact analytical results (34). A new exact (fixed-frame) representation Eq. (12) of the quantal solution has also been presented and directly applied to provide exact quantal probabilities for the full array of transitions. This solution is feasible for efficient numerical calculation of probabilities for transitions involving even large  $n$  and all  $\ell$  and  $\ell'$ , in contrast to the previous quantal (rotating-frame) version [15,16], which was applied only to the  $\ell=0 \rightarrow \ell'$  transitions. Exact analytical expressions for  $P_{\ell', \ell}^{(n)}$  can also be obtained [33] for low  $n$ .

The exact quantal results for  $P_{\ell', \ell}^{(n)}$  oscillate about the classical background. By revealing essential characteristics that remain obscured within the quantal treatment, the classical results complement the quantal results. Further development would include a semiclassical analysis capable of reproducing the oscillatory structure in the quantal  $P_{\ell', \ell}^{(n)}$  without sacrificing the physical transparency of the classical model.

Although the numerical results presented here are associated with a straight line projectile path (i.e.,  $\Delta\Phi = -\pi$ ), the theory is suitable for all polar deflection angles  $\Delta\Phi$  swept out during the collision by the classical trajectory. Specific problems (nonhydrogenic atoms, stray fields, the Debye radius in plasmas, etc.) may impose further restrictions on the range of impact parameter  $b$ , which results in restrictions on  $\alpha$ . The basic theory presented can still be applied to these cases with minor adjustments. The classical trajectory appropriate to a rotating dipole can be determined to account for the influence of the target on the projectile's motion.

In summary, both classical and quantal solutions of Stark mixing have been presented in a compact form reflecting the mathematical beauty of the problem as well as their pragmatic value. It is probably one of the last remaining problems in collision physics capable of an exact solution.

*Note added in proof.* A general concise analytical expression for the quantal probabilities  $P_{j,l}^{(n)}$  for all  $n$  has since been obtained [34] in a form (a) which is easy to use for numerical evaluation, even at very high  $n \sim 100$ , (b) which yields compact analytical results for  $n=2-5$  and (c) which naturally provides the classical limit (34) obtained here.

#### ACKNOWLEDGMENTS

This work has been supported by AFOSR Grant No. 49620-99-1-0277 and NSF Grant No. 98-02622.

#### APPENDIX A: PAULI'S REPLACEMENT

Pauli's replacement [23] for the classical one-electron atom follows from the straightforward calculation of the averaged projection of the position vector on the Runge-Lenz vector,

$$\langle \mathbf{r} \cdot \hat{\mathbf{A}} \rangle = \frac{3}{2} \epsilon \frac{e^2}{2E} = -\frac{3}{2} A \frac{1}{\sqrt{-2m_e E}},$$

where  $\epsilon$  is the eccentricity of the orbit corresponding with the energy  $E$ . Because the perpendicular component of  $\mathbf{r}$  on  $\mathbf{A}$  averages to zero, the following rule is valid, *on averaging* over an orbital period:

$$\mathbf{r} \approx -\frac{3}{2} \frac{\mathbf{A}}{p_n}$$

provided  $\mathbf{A}$  does not change significantly in this time. Here  $p_n = \sqrt{\langle p^2 \rangle} = \sqrt{-2m_e E}$  is the characteristic orbital momentum.

The classical Runge-Lenz vector has the symmetrized (Pauli-Lenz) quantal form

$$\mathbf{A} = \left[ \frac{1}{2} (\mathbf{p} \times \mathbf{L} - \mathbf{L} \times \mathbf{p}) - m_e e^2 \hat{\mathbf{r}} \right] / p_n$$

alternative to the form given by Eq. (1). The operator  $\mathbf{A}$  has the following properties:

$$[A_j, H] = 0 \quad (\text{a conserved quantity}),$$

$$[L_j, A_k] = i\hbar \epsilon_{jkn} A_n \quad (\text{also a vector}),$$

$$[A_j, A_k] = i\hbar \epsilon_{jkn} L_n \quad (\text{its components do not commute}),$$

$$\mathbf{A} \cdot \mathbf{L} = \mathbf{L} \cdot \mathbf{A} = 0 \quad (\text{vector } \mathbf{A} \text{ is orthogonal on } \mathbf{L}),$$

$$A^2 + L^2 = (n^2 - 1)\hbar^2 \quad (\text{constant for intrashell transitions}).$$

These commutation relations define the  $SO(4)$  dynamic symmetry group for the restricted motion of the orbital electron to the energy shell. The Hamiltonian  $H$  is an invariant and can be used to label matrix representations for this group. The correct energy levels for the hydrogen atoms result from the symmetry without solving any differential equation. The  $SO(4)$  operators can be disentangled by intro-

ducing  $\mathbf{M} = (\mathbf{L} + \mathbf{A})/2$  and  $\mathbf{N} = (\mathbf{L} - \mathbf{A})/2$ . Each  $\mathbf{M}$  and  $\mathbf{N}$  operators generate separately a  $so(3)$  subalgebra, such that  $SO(4) = SO(3) \oplus SO(3)$ .

Following [26], it is useful to prove the following.

*Result.* The matrix elements of the operators  $\Omega$  defined by

$$\Omega = \mathbf{r} + \frac{3}{2} \frac{\mathbf{A}}{p_n}$$

are zero between any states with the same energy, i.e.,  $\Omega = 0$  within the energy shell.

*Proof.* The commutator between the Pauli-Lenz vector and the position vector can be written as

$$[A_j, r_k] = -\frac{3}{2p_n} i\hbar \epsilon_{jkn} L_n + \frac{1}{2p_n} [m_e H, r_j r_k - r^2 \delta_{jk}]. \quad (A1)$$

Because the commutator  $[H, X]$  is zero for any Hermitian operator  $X$ , when restricted to the energy shell (*the hyper-virial theorem* [35]), commutator (A1) is simply

$$[A_j, r_k] = -\frac{3}{2p_n} i\hbar \epsilon_{jkn} L_n$$

in the Hilbert subspace of degenerate states with the same energy. Thus, the vector  $\Omega$  commutes with the Pauli-Lenz vector and has the commutators

$$[M_j, \Omega_k] = [N_j, \Omega_k] = \frac{1}{2} i\hbar \epsilon_{jkn} \Omega_n$$

with the vectors  $\mathbf{M}$  and  $\mathbf{N}$  obtained by decomposition (2). With the aid of the basic Jacobi identity for commutators,

$$[A, [B, C]] + [B, [C, A]] + [C, [A, B]] = 0,$$

it follows directly that  $\Omega = 0$ . For example,  $\Omega_2 = 0$  if  $A = M_3$ ,  $B = N_2$ , and  $C = \Omega_3$ .

This result provides a concise proof that Pauli's replacement (5) is valid whenever the dynamics is constrained to the constant energy manifold (cf., [18] for a lengthier proof).

#### APPENDIX B: AREA ELEMENT FOR SPHERICAL BIFOCAL COORDINATES

The spherical bifocal coordinates are given by the angles  $u_1$  and  $u_2$  between a point ( $P$ ) and two fixed foci ( $A_1$  and  $A_2$ ) on the unit sphere. Of course, these coordinates are unique only on the half sphere.

*Theorem.* The area element in spherical bifocal coordinates is

$$dS = \frac{du_1 du_2}{\sin \Delta},$$

where  $\Delta$  is the angle between the arcs joining a given point on the sphere with the two foci:

$$\Delta = \angle A_1 P A_2.$$

*Proof.* Here are two proofs of the theorem. One is short and intuitive. The other one is longer but a bit more rigorous.

*Short Proof.* The length of the arc described by the point  $P$  on the sphere for an infinitesimal change  $u_2 \rightarrow u_2 + du_2$ , when  $u_1$  is kept fixed, is  $ds_1$ . Basic spherical triangle geometry provides

$$ds_1 = \frac{du_2}{\sin \Delta}$$

and a similar relation

$$ds_2 = \frac{du_1}{\sin \Delta}$$

for the infinitesimal arc  $ds_2$ . The elementary surface area is given by the cross product of the two arcs  $ds_1 \times ds_2$ . Since the angle between these arcs is, in the first order of approximations, again  $\Delta$ , then

$$dS = \frac{du_1 du_2}{\sin \Delta},$$

as advertised.

*Direct Proof.* A direct proof calculates by brute force the area element using

$$dS = \left| \frac{\partial \vec{P}}{\partial u_1} \times \frac{\partial \vec{P}}{\partial u_2} \right| du_1 du_2. \quad (B1)$$

The length of the calculation depends, of course, on the particular coordinate frames of choice. For example, one can choose  $A_1$  and  $A_2$  in the equatorial  $xOy$  plane, with  $A_1$  on the  $Ox$  axis. Let  $D$  be a point on the arc  $A_1 A_2$  such that the arc  $PD$  is perpendicular to  $A_1 A_2$  (like a meridian passing through  $P$ ). The coordinates of the point  $P$  are then

$$P = (\cos \theta \cos \phi, \cos \theta \sin \phi, \sin \theta),$$

where  $\theta = \angle PD$  and  $\phi = \angle A_1 D$ . Applying again spherical trigonometry to the spherical triangles  $A_1 P D$  and  $A_2 P D$ , then

$$P = (\cos u_1, \sqrt{\cos^2 \angle PD - \cos^2 u_1}, \sin \angle PD),$$

where

$$\sin \angle PD = \sin u_1 \sin u_2 \sin \Delta / \sin \Gamma,$$

where, by definition,  $u_{1,2} = \angle A_{1,2} P$ ,  $\Delta = \angle A_1 P A_2$ , and  $\Gamma = \angle A_1 A_2$ . The goal is to express all coordinates of  $P$  in terms of  $u_1$  and  $u_2$  and to do the corresponding derivatives in Eq. (B1). Spherical trigonometry yields

$$\begin{aligned} S^2 &= \sin^2 u_1 \sin^2 u_2 \sin^2 \Delta \\ &= [\cos(u_1 - u_2) - \cos \Gamma][\cos \Gamma - \cos(u_1 + u_2)]. \end{aligned}$$

On defining

$$S_{\pm} = \sin \frac{1}{2} [\Gamma \pm (u_1 + u_2)],$$

$$\tilde{S}_{\pm} = \sin \frac{1}{2} [\Gamma \pm (u_1 - u_2)],$$

the angle  $\Delta$  is then determined from

$$\sin \Delta = \frac{S}{\sin u_1 \sin u_2} = 2 \frac{\sqrt{S_+ S_- \tilde{S}_+ \tilde{S}_-}}{\sin u_1 \sin u_2}$$

and the coordinates of  $P$  are now

$$P = \left[ \cos u_1, \frac{S_+ \tilde{S}_+ - S_- \tilde{S}_-}{\sin \Gamma}, 2 \frac{\sqrt{S_+ S_- \tilde{S}_+ \tilde{S}_-}}{\sin \Gamma} \right].$$

Then Eq. (B1) finally reduces to

$$dS = \left[ \frac{\sin u_1 \sin u_2}{S} \right] du_1 du_2 = \frac{du_1 du_2}{\sin \Delta},$$

which proves directly the above theorem for spherical bifocal coordinates.

- [1] M. Leon and H.A. Bethe, *Phys. Rev.* **127**, 636 (1962).
- [2] J.E. Miraglia and J. Macek, *Phys. Rev. A* **42**, 3971 (1990).
- [3] F. Merkt and R.N. Zare, *J. Phys. Chem.* **101**, 3495 (1994).
- [4] R.M. Pengelly and M.J. Seaton, *Mon. Not. R. Astron. Soc.* **127**, 165 (1964); I. Percival, *Atoms in Astrophysics* (Plenum, New York, 1983), pp. 75–102.
- [5] L.I. Men'shikov and P.O. Fedichev, *Zh. Éksp. Teor. Fiz.* **108**, 144 (1995) [*JETP* **81**, 78 (1995)].
- [6] M.R. Flannery and D. Vranceanu, in *Atomic Processes in Plasmas: 11th APS Topical Conference*, edited by E. Oks and M. S. Pindzola (AIP, New York, 1998), pp. 317–333.
- [7] X. Sun and K.B. MacAdam, *Phys. Rev. A* **47**, 3913 (1993).
- [8] V.S. Lebedev and I.L. Beigman, *Physics of Highly Excited Atoms and Ions* (Springer-Verlag, Berlin, 1998); I.L. Beigman and M.I. Syrkin, *Zh. Éksp. Teor. Fiz.* **89**, 400 (1985) [*Sov. Phys. JETP* **62**, 226 (1985)].
- [9] M. Born, *The Mechanics of the Atom* (Ungar, New York, 1960), p. 235.
- [10] Yu.N. Demkov, B.S. Monozon, and V.N. Ostrovskii, *Zh. Éksp. Teor. Fiz.* **57**, 1431 (1969) [*Sov. Phys. JETP* **30**, 775 (1970)].
- [11] A.K. Kazansky and V.N. Ostrovsky, *J. Phys. B* **29**, L855 (1996).
- [12] Yu.N. Demkov, V.N. Ostrovskii, and E.A. Solov'ev, *Zh. Éksp. Teor. Fiz.* **66**, 125 (1974) [*Sov. Phys. JETP* **39**, 57 (1974)].
- [13] A.K. Kazansky and V.N. Ostrovsky, *Phys. Rev. A* **52**, R1811 (1995).
- [14] A.K. Kazansky and V.N. Ostrovsky, *J. Phys. B* **29**, 3651 (1996).

- [15] A.K. Kazansky and V.N. Ostrovsky, Zh. Éksp. Teor. Fiz. 110, 49 (1996) [Sov. Phys. JETP 83, 1095 (1996)].
- [16] A.K. Kazansky and V.N. Ostrovsky, Phys. Rev. Lett. 77, 3094 (1996).
- [17] P. Bellomo, D. Farrelly, and T. Uzer, J. Chem. Phys. 107, 2499 (1995).
- [18] P. Bellomo, C.R. Stroud, D. Farrelly, and T. Uzer, Phys. Rev. A 58, 3896 (1998).
- [19] C.E. Wulfman, in *Group Theory and its Applications*, edited by E.M. Loebl (Academic, New York, 1977), p. 146; B.G. Wybourne, *Classical Groups for Physicists* (Wiley, New York, 1974).
- [20] H.A. Bethe and E.E. Salpeter, *Quantum Mechanics of One- and Two-electron Atoms* (Plenum, New York, 1977), p. 83.
- [21] T.P. Hezel *et al.*, Am. J. Phys. 60, 329 (1992).
- [22] I.C. Percival and D. Richards, J. Phys. B 12, 2051 (1979).
- [23] W. Pauli, Z. Phys. 36, 336 (1926).
- [24] J.D. Louck, in *Atomic, Molecular, and Optical Physics Handbook*, edited by G.W.F. Drake (AIP, New York, 1996), p. 15.
- [25] C.B. Tarter, J. Math. Phys. 11, 3192 (1970).
- [26] G. Flamand, J. Math. Phys. 7, 1924 (1964).
- [27] G.H. Golub and C.F.V. Loan, *Matrix Computation* (Johns Hopkins University, Baltimore, 1983), p. 384.
- [28] M.R. Flannery, Phys. Rev. A 22, 2408 (1980).
- [29] D. Vrinceanu and M.R. Flannery, Phys. Rev. Lett. 82, 3412 (1999).
- [30] H. Goldstein, *Classical Mechanics* (Addison-Wesley, Reading, MA, 1980), p. 173.
- [31] D. Vrinceanu and M.R. Flannery (unpublished).
- [32] *Handbook of Mathematical Functions* edited by M. Abramowitz and I.A. Stegun (Dover Publications, New York, 1972), p. 79.
- [33] D. Vrinceanu and M.R. Flannery, J. Phys. B 33, L721 (2000).
- [34] D. Vrinceanu and M.R. Flannery, J. Phys. B 34, L1 (2001).
- [35] J.O. Hirschfelder, J. Phys. Chem. 33, 1460 (1960).



# REPORT DOCUMENTATION PAGE

AFRL-SR-BL-TR-01-

18  
maintaining the  
is for reducing  
VA 22202-  
play a currently

Public reporting burden for this collection of information is estimated to average 1 hour per response, including the time for data needed, and completing and reviewing this collection of information. Send comments regarding this burden estimate or this burden to Department of Defense, Washington Headquarters Services, Directorate for Information Operations and Rep 4302. Respondents should be aware that notwithstanding any other provision of law, no person shall be subject to any penalty for not providing information if it does not have an OMB control number. PLEASE DO NOT RETURN YOUR FORM TO THE ABOVE ADDRESS.

0363

1. REPORT DATE (DD-MM-YYYY) 23-04-01		2. REPORT TYPE FINAL		3. DATES COVERED (From - To) 01/06/99-11/30/01	
4. TITLE AND SUBTITLE Collision Dynamics of Stretched Atoms				5a. CONTRACT NUMBER	
				5b. GRANT NUMBER F49620-99-1-0277	
				5c. PROGRAM ELEMENT NUMBER 61102F	
6. AUTHOR(S) M. R. Flannery				5d. PROJECT NUMBER 2301	
				5e. TASK NUMBER DX	
				5f. WORK UNIT NUMBER	
7. PERFORMING ORGANIZATION NAME(S) AND ADDRESS(ES) Dr. M. R. Flannery School of Physics Georgia Institute of Technology Atlanta, GA 30332-0430				8. PERFORMING ORGANIZATION REPORT NUMBER Dennis Farmer Georgia Tech Research Corporation Centennial Research Bldg, Rm 246 Atlanta, GA 30332-0420	
9. SPONSORING / MONITORING AGENCY NAME(S) AND ADDRESS(ES) Dr. Ralph Kelley AFOSR, Physics Directorate 801, North Randolph Street Room 732 Arlington VA 22203-1977				10. SPONSOR/MONITOR'S ACRONYM(S) Michael E. Yocum AFORR/PK1 801, North Randolph Street Room 732 Arlington VA 22203-1977	
				11. SPONSOR/MONITOR'S REPORT NUMBER(S)	
12. DISTRIBUTION / AVAILABILITY STATEMENT Unlimited					
13. SUPPLEMENTARY NOTES AIR FORCE OFFICE OF SCIENTIFIC RESEARCH (AFOSR) NOTICE OF TRANSMITTAL DTC. THIS TECHNICAL REPORT HAS BEEN REVIEWED AND IS APPROVED FOR PUBLIC RELEASE LAW AFR 100-12. DISTRIBUTION IS UNLIMITED.					
14. ABSTRACT: A detailed account of the progress achieved under the present AFOSR grant is provided, with full documentation of the results and papers published. The Collision Dynamics of Stretched Atoms was investigated within the processes of (a) electron- ion recombination at ultralow temperatures $T \sim 5\text{mK}$ and (b) three body recombination between positrons and antiprotons at 4K to form antihydrogen. The long outstanding problem ( $\sim 40$ years) of collisional Stark Mixing in Rydberg Atoms was solved exactly in both classical and quantal formulations of the problem. Here analytical expressions are provided for the probabilities for the full array $n \rightarrow n'$ of transitions in a Rydberg atom in state $n$ , induced by the time-dependent (dipole) electric field generated by adiabatic collisions with an ion at ultralow energies. In addition, the classical form factor for $n \rightarrow n'$ transitions was defined. This permitted a detailed investigation of classical / quantal transition probabilities arising from any external sudden perturbation (whether due to collisions with particles or to pulses of electromagnetic radiation) on Rydberg systems.					
15. SUBJECT TERMS Stark Mixing, Recombination, Antihydrogen Production, Rydberg Collisions, Ultracold Collisions, Classical Form Factors, Quantal-Classical Correspondence					
16. SECURITY CLASSIFICATION OF:			17. LIMITATION OF ABSTRACT	18. NUMBER OF PAGES 84	19a. NAME OF RESPONSIBLE PERSON M. R. Flannery
a. REPORT Unclassified	b. ABSTRACT	c. THIS PAGE			19b. TELEPHONE NUMBER (include area code) 404-894-5263